

SURFACE MAPPING BASED ON THE CORRELATED EMISSION OF IONS AND
ELECTRONS FROM HYPERVELOCITY C₆₀ IMPACTS

A Dissertation

by

MICHAEL J. ELLER

Submitted to the Office of Graduate Studies of
Texas A&M University
in partial fulfillment of the requirements for the degree of

DOCTOR OF PHILOSOPHY

Approved by:

Chair of Committee,	Emile Schweikert
Committee Members,	Robert Burghardt
	Paul Cremer
	Dong Hee Son
Head of Department,	David Russell

December 2012

Major Subject: Chemistry

Copyright 2012 Michael J. Eller

ABSTRACT

High resolution mapping of molecular species, specifically sub-micrometer spatial resolution mapping, is at the forefront of recent interest in Secondary Ion Mass Spectrometry (SIMS). Large projectiles, e.g. C_{60} , Au_{400} , display high quasi-molecular ion yields with reduced fragment ion yields compared to atomic or polyatomic projectiles. However, the application of large projectiles in a sub-micrometer beam is hampered by limitations in source brightness and angular emission characteristics which are incompatible with tight focusing. An alternate approach to a focused beam is to reduce the beam intensity to less than 1000 impacts per second (referred to as the event-by-event mode) and localize each projectile impact via an electron emission microscope. The characterization and performance of such an instrument for localizing individual projectile impacts of 15-75keV C_{60} with sub-micrometer spatial resolution are described here.

The quest for localizing single cluster impacts requires an understanding of the relationship between SI and electron emissions. It was found that electron emission is observed independently of the number or type of secondary ion emitted for flat homogeneous samples. The independence of ion and electron emission confirms the rationale for using the emitted electrons to localize individual projectile impacts. Further investigation of electron emission revealed that the electron yield is characteristic of the class of sample investigated (e.g. metal, organic, semiconductor). The electron yield

was found to depend on the size and topology of the sample. Additionally, the electron yield increases with increasing projectile velocity.

The use of the novel instrumentation presented here, necessitated the development of custom acquisition and analysis software. The analysis of co-emitted species from nano-metric dimensions is enhanced with the ability to perform multiple coincidence/anti-coincidence calculations. New concepts were implemented for integrating localization and mass spectrometry via software solutions for image analysis and localization and subsequently correlation between emitted ions and electrons. The result is software and instrumentation capable of generating ion maps with sub-micrometer spatial resolution.

NOMENCLATURE

CFD	Constant Fraction Discriminator
COM	Center of Mass
CMOS	Complementary Metal-Oxide Semiconductor
EEM	Electron Emission Microscope
PSD	Position Sensitive Detector
ROI	Region of Interest
SEM	Scanning Electron Microscopy
SI	Secondary Ion
SIMS	Secondary Ion Mass Spectrometry
TDC	Time to Digital Converter
ToF	Time-of-Flight

TABLE OF CONTENTS

	Page
ABSTRACT	ii
NOMENCLATURE.....	iv
TABLE OF CONTENTS	v
LIST OF FIGURES.....	vii
LIST OF TABLES	xiv
1. INTRODUCTION.....	1
2. ELECTRON EMISSION MICROSCOPE.....	7
2.1 Introduction	7
2.2 Design and Operation.....	9
2.3 Electron Emission from C ₆₀ Impacts on Flat Homogeneous Samples.	16
2.4 Electron Emission from C ₆₀ Impacts on Nano-Objects.....	37
3. SECONDARY ION MASS SPECTROMETER COUPLED TO AN ELECTRON EMISSION MICROSCOPE.....	71
3.1 Introduction	71
3.2 C ₆₀ Source and Mass Spectrometer	74
3.3 Hardware Integration.....	78
3.4 Software Integration.....	83
4. LOCALIZATION	85
4.1 Introduction	85
4.2 Software Methodologies	86
4.3 Resolution.....	117
5. DATA ANALYSIS SOFTWARE	122
5.1 Introduction	122
5.2 Diagnostic Tools and Acquisition.....	122

5.3	Advanced Analysis Techniques	132
5.4	Eight Anode Mass Resolution.....	149
5.5	Anode Distribution.....	166
6.	CONCLUSIONS.....	179
	REFERENCES.....	186
	APPENDIX A	194
	APPENDIX B	195
	APPENDIX C	197
	APPENDIX D.....	202

LIST OF FIGURES

FIGURE	Page
1.1 Analytical Resolution	2
2.1 Electron Emission Microscope.....	11
2.2 Position Sensitive Detector	12
2.3 Exposure Times for IDT M3 Camera	13
2.4 Electron Distribution from Center of Mass.....	15
2.5 Measured Electron Distribution from 15keV C ₆₀ Impacts on Flat Homogenous Targets.....	18
2.6 Measured Electron Distribution from 30keV C ₆₀ Impacts on Flat Homogenous Targets.....	20
2.7 Mass Spectrum of 500nm Thick Au Layer Deposited on Si.....	22
2.8 Measured Ion Specific Electron Distributions from 30keV C ₆₀ Impacts on Au Target.....	23
2.9 Measured Ion Specific Electron Distributions from 30keV C ₆₀ Impacts on Guanine Target.....	25
2.10 Measured Ion Specific Electron Distributions from 30keV C ₆₀ Impacts on Gramicidin S Target	26
2.11 Measured Ion Specific Electron Distributions from 15keV C ₆₀ Impacts on Glycine Target.....	27
2.12 Measured Ion Specific Electron Distributions from 30keV C ₆₀ Impacts on Glycine Target.....	28
2.13 Measured Electron Distributions from 15keV C ₆₀ Impacts on Au Target for a Selected Number of Detected Secondary Ions	29
2.14 Measured Electron Distributions from 30keV C ₆₀ Impacts on Au Target for a Selected Number of Detected Secondary Ions	30

FIGURE	Page
2.15 Measured Electron Distributions from 15keV C ₆₀ Impacts on Gramicidin S Target for a Selected Number of Detected Secondary Ions	31
2.16 Measured Electron Distributions from 30keV C ₆₀ Impacts on Gramicidin S Target for a Selected Number of Detected Secondary Ions	32
2.17 Measured Electron Distributions from 15keV C ₆₀ Impacts on Guanine Target for a Selected Number of Detected Secondary Ions	33
2.18 Measured Electron Distributions from 30keV C ₆₀ Impacts on Guanine Target for a Selected Number of Detected Secondary Ions	34
2.19 Two Ion Selected Electron Distribution from 30keV C ₆₀ Impacts on CsI	36
2.20 Electron Probability Distributions from the Three Aluminum Oxide Samples Bombarded by C ₆₀ at 30keV	40
2.21 Measured Ion Specific Electron Distributions from 30keV C ₆₀ Impacts on a Flat Aluminum Oxide Coated Si Wafer	46
2.22 Measured Ion Specific Electron Distributions from 30keV C ₆₀ Impacts on Aluminum Boehmite Whiskers	47
2.23 Measured Ion Specific Electron Distributions from 30keV C ₆₀ Impacts on 50nm Nano-Particles	48
2.24 Measured Total Electron Distributions from 15keV C ₆₀ Impacts on a Gold Coated Si Wafer and 5nm Gold Nano-Particles	51
2.25 Measured Total Electron Distributions from 30keV C ₆₀ Impacts on a Gold Coated Si Wafer and 5nm Gold Nano-Particles	52
2.26 Measured Ion Specific Electron Distributions from 30keV C ₆₀ Impacts on a Gold Coated Si Wafer	53
2.27 Measured Ion Specific Electron Distributions from 30keV C ₆₀ Impacts on 5nm Gold Nano-Particles as a Multi-Layer	54

FIGURE	Page
2.28 Measured Total Electron Distributions from 15 and 30keV C ₆₀ Impacts on 5nm Au Nano-Particles Deposited as a Multi-Layer and a Single Layer	59
2.29 Measured Ion Specific Electron Distributions from a Multi-Layer and Single Layer of 5 nm Au NPs Bombarded by C ₆₀ at 30 keV	60
2.30 Measured Ion Specific Electron Distributions from a Single Layer of 5 nm Au NPs on Glycine Bombarded by C ₆₀ at 30 keV	62
2.31 Comparison of Measured Ion Selected Electron Distributions from 30keV C ₆₀ Impacts on 5nm Au Nano-Particles Deposited as a Single Layer on Glycine and a Neat Glycine Target.....	63
2.32 Mass Spectrum of 5nm Gold Nano-Particles Deposited on an Aluminum Foil Bombarded by 43keV C ₆₀	64
2.33 Coincidental Mass Spectrum of 5nm Gold Nano-Particles Deposited on an Aluminum Foil Bombarded by 43keV C ₆₀	66
2.34 Measured Total Electron Distributions from 30keV C ₆₀ Impacts on a Multi-Layer of 5nm Au Nano-Particles and Aluminum Oxide Coated Si Wafer	67
2.35 Measured Ion Selected Electron Distributions from 43keV C ₆₀ Impacts on a Multi-Layer of 5nm Au Nano-Particles and Aluminum Oxide Coated Si Wafer	68
3.1 Schematic of the Custom Built Secondary Ion Mass Spectrometer.....	72
3.2 Data Analysis Examples.....	73
3.3 Picture of C ₆₀ Effusion Source	76
3.4 Wien Filter Separation of C ₆₀ Projectiles.....	77
3.5 Timing Sequence.....	80
3.6 Pulse Sequence.....	81
4.1 Raw Image.....	88

FIGURE	Page
4.2 Processed Image	89
4.3 Processed Image with Center of Mass	90
4.4 Processed Image Center of Mass with Region of Interest	91
4.5 Processed Image with Impact Coordinates	93
4.6 Ion Selected Electron Distribution Logic Tree	98
4.7 Ion Selected Electron Map Logic Tree.....	99
4.8 Two Ion Electron Distribution Logic Tree Part 1 of 2.....	101
4.9 Two Ion Electron Distribution Logic Tree Part 2 of 2.....	102
4.10 Double Coincidence Map Logic Tree Part 1 of 2	103
4.11 Double Coincidence Map Logic Tree Part 2 of 2	104
4.12 Total Ion Map for 400 Line Per Inch CsI Coated Grid Bombarded by C ₆₀ at 30keV	106
4.13 Line Scan of 400 Line Per Inch CsI Coated Grid Bombarded by C ₆₀ at 30keV	107
4.14 Total Ion Density Plot of 400 Line Per Inch CsI Coated Grid Bombarded by C ₆₀ at 30keV	108
4.15 Mass Spectrum of CsI Bombarded by C ₆₀ at 30keV.....	110
4.16 One Ion Density Plot	111
4.17 Coincidental Mass Spectrum of Impacts Where I ⁻ was Detected	112
4.18 Double Coincidence Density Plot of I ⁻ and CsI ₂ ⁻	113
4.19 SEM Image of 500 Line Per Inch Copper Grid	114
4.20 SEM Image of 500 Line Per Inch Copper Grid Coated by Cholesterol.....	115
4.21 Total Ion Map.....	116

FIGURE	Page
4.22 Total Ion Density Plot	118
4.23 One Ion Density Plot	119
5.1 Logic Tree Key.....	124
5.2 Yield Calculation Logic Tree	125
5.3 Example Ion Selection	126
5.4 Idea Anode Distribution	128
5.5 Monitor Ion Yield Logic Tree	129
5.6 Monitor Ion Yield Example	131
5.7 Single Ion Multiplicity Logic Tree.....	133
5.8 Single Ion Coincidence Logic Tree.....	135
5.9 Double Coincidence Logic Tree Part 1 of 2.....	137
5.10 Double Coincidence Logic Tree Part 2 of 2.....	138
5.11 One-Ion Coincidence One-Ion Anti-Coincidence Logic Tree Part 1 of 2 .	139
5.12 One-Ion Coincidence One-Ion Anti-Coincidence Logic Tree Part 2 of 2 .	140
5.13 Mass Spectrum from Phage Deposited on NALDI Plate: One-Ion Coincidence One-Ion Anti-Coincidence 0-100m/z.....	142
5.14 Mass Spectrum from Phage Deposited on NALDI Plate: One-Ion Coincidence One-Ion Anti-Coincidence 100-200m/z.....	143
5.15 Mass Spectrum from Phage Deposited on NALDI Plate: One-Ion Coincidence One-Ion Anti-Coincidence 200-300m/z.....	144
5.16 Double Coincidence One-Ion Anti-Coincidence Logic Tree Part 1 of 3 ...	146
5.17 Double Coincidence One-Ion Anti-Coincidence Logic Tree Part 2 of 3 ...	147
5.18 Double Coincidence One-Ion Anti-Coincidence Logic Tree Part 3 of 3 ...	148

FIGURE	Page
5.19 Mass Spectrum from Phage Deposited on NALDI Plate: Double Coincidence One-Ion Anti-Coincidence 0-100m/z.....	150
5.20 Mass Spectrum from Phage Deposited on NALDI Plate: Double Coincidence One-Ion Anti-Coincidence 100-200m/z.....	151
5.21 Load Mass Spectrum Logic Tree Part 1 of 4	152
5.22 Load Mass Spectrum Logic Tree Part 2 of 4	153
5.23 Load Mass Spectrum Logic Tree Part 3 of 4	154
5.24 Load Mass Spectrum Logic Tree Part 4 of 4	155
5.25 Total Ion Distribution for 200 Arrays	158
5.26 Total Ion Distribution for 50 Arrays	161
5.27 Uncorrected Mass Spectrum with Mass Resolution	163
5.28 Corrected Mass Spectrum with Mass Resolution	164
5.29 Overlay of Corrected and Uncorrected Mass Spectra.....	165
5.30 Overlay of Corrected Mass Spectra from Each Anode	167
5.31 Overlay of Uncorrected Mass Spectra from Each Anode.....	168
5.32 One Ion Polar Plot	169
5.33 One Ion Polar Plot Logic Tree	171
5.34 Ion Coincidence Anode Polar Plot Part 1 of 2	172
5.35 Ion Coincidence Anode Polar Plot Part 2 of 2	173
5.36 Polar Plot for $\text{Au}(\text{CN})_2^-$ from All Impacts	175
5.37 Polar Plot for $\text{Au}(\text{CN})_2^-$ in Coincidence with Au_3^-	176
5.38 Polar Plot for $\text{Au}(\text{CN})_2^-$ in Coincidence with SiO_3^-	177

FIGURE	Page
6.1 Measured Electron Distributions from Impacts of C_{60} and Au_{400} on Glycine	183

LIST OF TABLES

TABLE	Page
2.1 Yields of Electrons from Individual C_{60}^+ and C_{60}^{2+} Impacts at 15 and 30keV	19
2.2 Electron Yields from 30keV C_{60} Impacts on CsI.....	38
2.3 Electron Yields: Total and SI Specific for Different Aluminum Oxide Samples Bombarded by C_{60} at 30keV	41
2.4 Secondary Ion Yields from Aluminum Oxide Samples Bombarded by C_{60} at 30keV	43
2.5 Ratio of SI Yields of AlO^- and AlO_2^- from the Aluminum Oxide Samples Bombarded by C_{60} at 30 keV.....	45
2.6 Total and Ion Specific Electron Yields from Au Samples Bombarded by C_{60} at 15 or 30keV.....	55
2.7 Secondary Ion Yields from Au Samples Bombarded by C_{60} at 15 or 30keV	57
2.8 Calculated Correlation Co-efficients from Impacts of 30keV C_{60} on 5nm Gold Nano-Particles Deposited on Glycine	58
4.1 Cirstat File	94
4.2 Allcircles File	95
4.3 Center of Mass File	96
5.1 Example 1-D Mass Spectrum Array	156
5.2 14 Ion Array with Channel Numbers	159
5.3 14 Ion Array with Anode Number	160

1. INTRODUCTION

Analysis of surfaces is an important issue in many areas of science and technology (e.g. corrosion, catalysis, friction, adhesion, diffusion).^[1-3] In response numerous physical and chemical analytical tools have been and continue to be developed (figure 1.1). Each has characteristic features and offers distinct information about a surface. High spatial resolution molecular imaging or mapping is at the forefront of recent interest.^[4-9] Surface mass spectrometry, more precisely, SIMS, with its intrinsic versatile information is among the methods of choice. The technique involves scanning a surface with a focused primary ion beam, its impact on a solid causes, via sputtering, emission of neutral and ionized atoms, molecular fragments and molecules. The secondary ions, SIs, are identified with a mass spectrometer. Atomic ion beams, in particular Ga⁺ and Cs⁺ can be focused to diameters of a few tens of nanometers ^[10]. However, such beams produce mostly atomic ion and low mass molecular fragments. Desorption of intact molecules of a few 100 Da occurs with low efficiency.^[11]

The low efficiency for ionizing molecular ions by atomic SIMS, prompted a search for different projectiles. Atomic projectiles sputter molecules and atoms by a linear collision cascade.^[12] With molecular or cluster projectiles the mechanism is described as a non-linear collision cascade, in which many collision cascades overlap.^[13] The initial observation of this effect showed an increase by an order of magnitude increase in secondary ion yield for quasi molecular ions by bombarding the surface with

Analytical Resolution versus Detection Limit

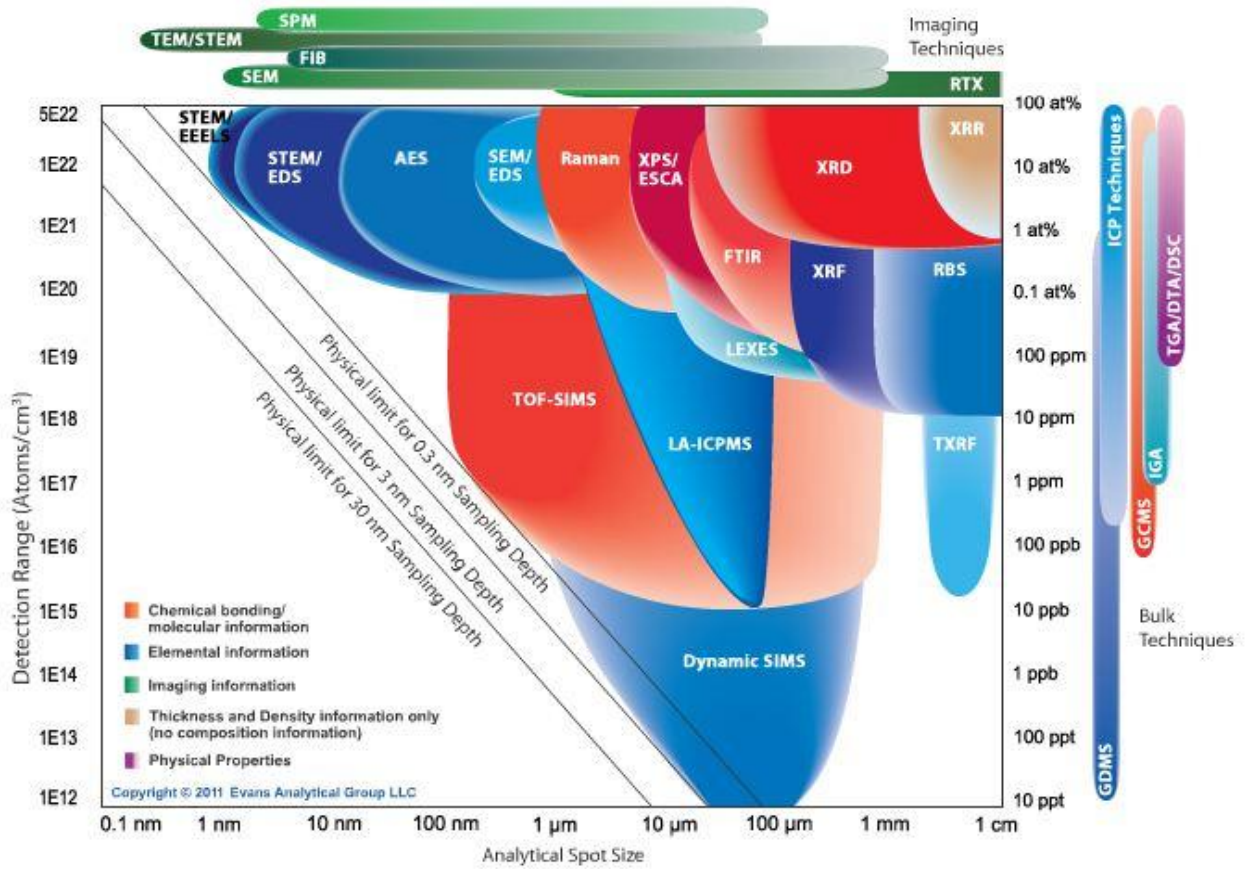


Figure 1.1 Analytical Resolution. A chart of the analytical resolution versus detection limit for a selected set of surface analytical techniques. Copyright 2012 Evans Analytical.

a cluster compared to an atomic projectile.^[14] It was later shown that this effect depends on the number of constituent atoms in the projectile and their mass.^[15] As the number of constituent increases the yield increases this effect can be described by equation 1.1. The equation indicates that the SI yield from impacts of Au₃ is greater than or equal to three times the yield from impacts of Au. This equation holds true up to ~9 constituent atoms.^[16] The effect of this enhancement was also shown for a series of polyatomic projectiles including SF₆, CsI clusters, and Bi oxide clusters.^[15, 17-21]

$$\frac{Y_{A_n}(E)}{n \cdot Y_A\left(\frac{E}{n}\right)} \geq 1 \quad \text{Equation 1.1: Yield Enhancement. } A_n \text{ is a homonuclear projectile with } n$$

atoms. $Y(E)$ is the yield of ions at energy E . $Y(E/n)$ is the yield at equal velocity.

Yet still higher SI yields can be obtained with larger cluster projectiles: e.g. C₆₀, Au₄₀₀. Their interaction occurs by a different mechanism, referred to as a fluid-flow like process.^[22] From which intact molecular ions are emitted from the periphery of the impact site. The increase in SI yield from C₆₀⁺ impacts has been shown to be up to 80x larger than Cs⁺ at the same impact energy.^[23] SI ion yields can be further enhanced by the use of massive projectiles such as Au₄₀₀. Recent studies indicate that 500 keV Au₄₀₀⁺ generates SI yields which are one to two orders of magnitude greater than those obtained with 130 keV Au₃⁺ and 50 keV C₆₀⁺ projectiles.^[24]

It has been shown that the detection of molecular species can be achieved efficiently with cluster projectiles, specifically massive ones such as, C₆₀ or Au₄₀₀.^[25]

^{26]} SIs produced from these impacts display high quasi-molecular ion yields with reduced fragment ion yields.^[27]

It is tempting to apply the efficient massive projectiles in a similar mode to focused atomic ion beams, i.e. to complement nanoscale isotopic analysis with spatially resolved molecular analysis. The application of massive projectiles in a sub-micrometer beam is hampered though by limitations in source brightness in the case of C₆₀. Massive clusters e.g. Au₄₀₀ which are produced with liquid metal ion sources have energy and angular emission characteristics which are incompatible with tight focusing. This dissertation explores an alternate approach for achieving molecular analysis with sub-micrometer resolution. The idea is to reduce the intensity of the nanoparticle beam to where single projectiles are resolved in time and space ^[28]. The individual impact will set the limit for spatial resolution. The diameter of the corresponding area from which SIs are emitted is ~10-20nm.^[25] In practice the validity of the approach depends on efficient SI information from an individual nanoparticle impact. Co-emission of several SIs is readily obtained with C₆₀⁺²⁺ or Au₄₀₀⁴⁺ accelerated to impact energies ≥ 300 eV/atom.^[28] In practice such “nano-probe” experiments are run in the event-by-event bombardment-detection mode: single projectiles are spaced ~10-3s apart, the SIs resulting from each impact are recorded individually. When biasing the surface negatively, electrons co-emitted with the SIs can provide the start for SI identification via time-of-flight (ToF) measurement. To be complete, the nano-analysis scheme must include the locations of the individual projectile impacts. This may be accomplished by imaging the electrons with an electron emission microscope, EEM. Initial experiments

with such a device have shown notable electron yields (number of electrons per impact) from 15-75 keV C60 impacts. Surprisingly the phenomenon cannot be explained with conventional electron emission models.^[29-31] The few reports on electron emission from massive projectile impact invoke “quasimolecular auto-ionization” or introduce a new parameter related to electron diffusion into the conventional theory.^[32]

We present here results from a set of experiments designed to assess the concept of “positional mass spectrometry”. The first task was to devise the hardware and software for the localization-identification of SIs from single projectile impacts. The ability to localize single cluster impacts allows for the investigation of fundamental questions about the relationship between SI and electron emissions. Is the coemission of negative SIs and electrons correlated, or are SIs and electrons emitted independently? What is the electron yield when there is co-emission of multiple SIs? How does the electron yield vary with projectile energy? What is the mechanism for electron emission from large projectiles? Ultimately the application of such an instrument for localizing individual projectile impacts is shown.

The software issues faced with implementing such an instrument are complex. In mass spectrometry the amount of data can be staggering, especially in an imaging application where each pixel will have its own mass spectrum. The result are data sets in excess of 10gb of raw data. Therefore, the need for sophisticated data analysis software for mass spectrometry is a prevalent issue.^[33-35] Custom designed instruments operating in novel modes face compounded data analysis issues. An event-by-event data analysis program for SIs with the ability to identify coincidental emission was operational at the

outset of the present study.^[36] A much expanded data analysis capability is described in this document, including multi-anode mass spectrometry and multiple coincidence/anti-coincidence data processing. New concepts were implemented for integrating localization and mass spectrometry, including software for image analysis and localization, and correlation between detected ions and electrons. The performance of the software solutions are described in sections 3.4, 4.2, 5.2-5.5, and is illustrated with sub-micrometer resolution ion maps in sections 4.2-4.3.

2. ELECTRON EMISSION MICROSCOPE^{*+#}

2.1 INTRODUCTION

Electron emission from low velocity ion impacts is a long standing topic of interest, particularly in connection with detection of large biomolecules. Several authors have examined electron emission from large molecular ions colliding with solids.^[32, 37-41] The development of ionization techniques capable of desorbing molecules in excess of 60 kilodaltons, matrix assisted laser desorption ionization, MALDI, and plasma desorption mass spectrometry, PDMS, benefited from detection of large molecules via the emitted electrons.^[42, 43]

The detection of large molecules prompted the issue of a threshold for electron emission. An electron emission threshold has been mentioned for large water clusters impacting Cu at a velocity of ~ 18 km/s, corresponding to an energy per unit mass of ~ 1.7 eV/amu.^[44] Electron emission was observed from stainless steel and CsI for incident projectiles velocities as low as 3.5 km/s or ~ 0.06 eV/amu.^[41, 45] The electron emission observed from hypervelocity $C_{60}^{1,2+}$ impacts on solid surfaces occurs where kinetic electron emission from comparable velocity atomic projectiles does not take place.^[32, 41]

* Part of this section is reprinted with permission from “Single Impacts of C_{60} on Solids: Emission of Electrons, Ions and Prospects for Surface Mapping” S. V. Verkhoturov, M. J. Eller, R. D. Rickman, S. Della-Negra, E. A. Schweikert, 2010. *Journal of Physical Chemistry C*, Copyright [2012] by American Chemical Society.

+ Part of this section is reprinted with permission from “Simultaneous detection and localization of secondary ions and electrons from single large cluster impacts” by M. J. Eller, S. V. Verkhoturov, F. A. Fernandez-Lima, J. D. DeBord, E. A. Schweikert, S. Della-Negra, 2012. *Surface and Interface Analysis*, Copyright [2012] by John Wiley and Sons.

Part of this section is reprinted with permission from “Electron Emission from Hypervelocity C_{60} Impacts” M. J. Eller, S. V. Verkhoturov, S. Della-Negra, E. A. Schweikert, 2010. *Journal of Physical Chemistry C*, Copyright [2012] by American Chemical Society.

The phenomenon cannot be attributed to potential electron emission given $C_{60}^{1,2+}$ characteristics.

The present study focuses on impacts with C_{60}^{q+} ($q = 1, 2$) at velocities of 63 to 115 km/s. There are very few observations with C_{60} in this velocity range. They report electron emission from Au and CsI targets “well below the classical kinetic emission threshold”.^[40] In one case the emission was explained as a result of “quasimolecular autoionization”.^[39] Others have accounted for the deviation from conventional electron emission models by introducing parameters related to the diffusion of electrons and their probable “escape” from the surface.^[41] A more nuanced understanding may emerge from larger sets of experimental data. However, the yet to be explained mechanism of emission must arise from a projectile-related collective effect.

The goal of this study is to expand the previous data on electron emission from large cluster impacts, by measuring over a range of samples, and projectile energies. The electron emission is measured by an electron emission microscope, EEM, which is detailed in section 2.1. This EEM is coupled to a custom built cluster SIMS instrument described in section 3. The projectile used was $C_{60}^{+,2+}$ with energy ranging from 15-50keV. The electron emission from a series of homogeneous samples (Section 2.3) was measured and the correlation between ion and electron emission was studied. Additionally, the electron emission from a series of nano objects was measured and is detailed in section 2.4.

It has been shown that there can be prolific electron emission (>7 electrons) from a single projectile.^[39] Our findings on electron emission can be summarized by the

following statements. The electron emission follows a Poisson distribution,^[46] which increases linearly with increasing projectile energy in the range measured (15-50keV). Additionally the electron emission depends on the composition, topology and morphology of the surface.^[47] The electron emission has also been found to be independent from the type and number of co-emitted negative SIs for a range of organic, inorganic and metallic targets.^[46]

2.2 DESIGN AND OPERATION

The electron emission microscope, EEM, is part of a custom built ToF-SIMS instrument comprised of the following: C₆₀ effusion source, analysis chamber, and ToF mass analyzer. In this section the EEM will be discussed the remainder of the instrument is detailed in section 3.

The EEM (figure 2.1) uses the emitted electrons generated in a C₆₀ impact to determine the impact site of the C₆₀. The EEM is comprised of five einzel lenses and a position sensitive detector, PSD. A description of the operation of the lens system follows. First the secondary electrons generated from an impact are accelerated by a potential difference (+10kV) between the sample and grounded extraction plate of the first einzel lens. The Lens I forms the first intermediate image of the electrons in the deflection center of the magnetic prism ($\sim 10^{-3}$ tesla) with a demagnification of 0.5X. Lens II accepts the image and forms a second intermediate image with a magnification of 2X. The rationale for forming the image in the center of the magnetic prism is to eliminate the second-order angular aberration and first-order transverse chromatic

aberration. The second intermediate image is accepted by three consecutive lenses which form the magnified image ($\leq 1000X$ magnification) onto the PSD.

The PSD consists of a pair of microchannel plates, MCPs, in the chevron configuration, aluminized P43 phosphor screen, and fast CMOS camera (figure 2.2). The MCP assembly multiplies the electron signal by a factor of $\sim 10^6X$.^[48] After multiplication the electrons are accelerated by a potential difference of +4.7kV. The accelerated electrons strike an aluminized P43 phosphor screen which is coated by a 500Å thick layer of Al. The flux of electrons through the Al is observed as a voltage spike that is sent to a constant fraction discriminator, CFD, and counted. After passing through the Al the electrons reach the phosphor and excite the phosphorescent material which emits light at 545nm. The luminance from the electron impacts can be detected by the camera system from $t = 0-200\mu s$ after the initial voltage pulse is detected (figure 2.3). The phosphor is deposited on a pellet of fiber optic wires each 10µm in diameter. The fiber optic wires transfer the light to a glass window, where a fast CMOS camera (M3, Integrated Design Tools) equipped with a high-precision (1:1) optical lens (Schneider Optics) and takes a picture of the luminance.

The camera characteristics are essential to the performance of the instrument. The camera uses a 1.3Mp CMOS sensor and operates in the master-slave configuration (Section 3). In the CMOS sensor each pixel is an individual detector. This gives the camera a large active range and allows it to detect all the electrons from a single impact. The master slave configuration allows for synchronization of the camera with the time to

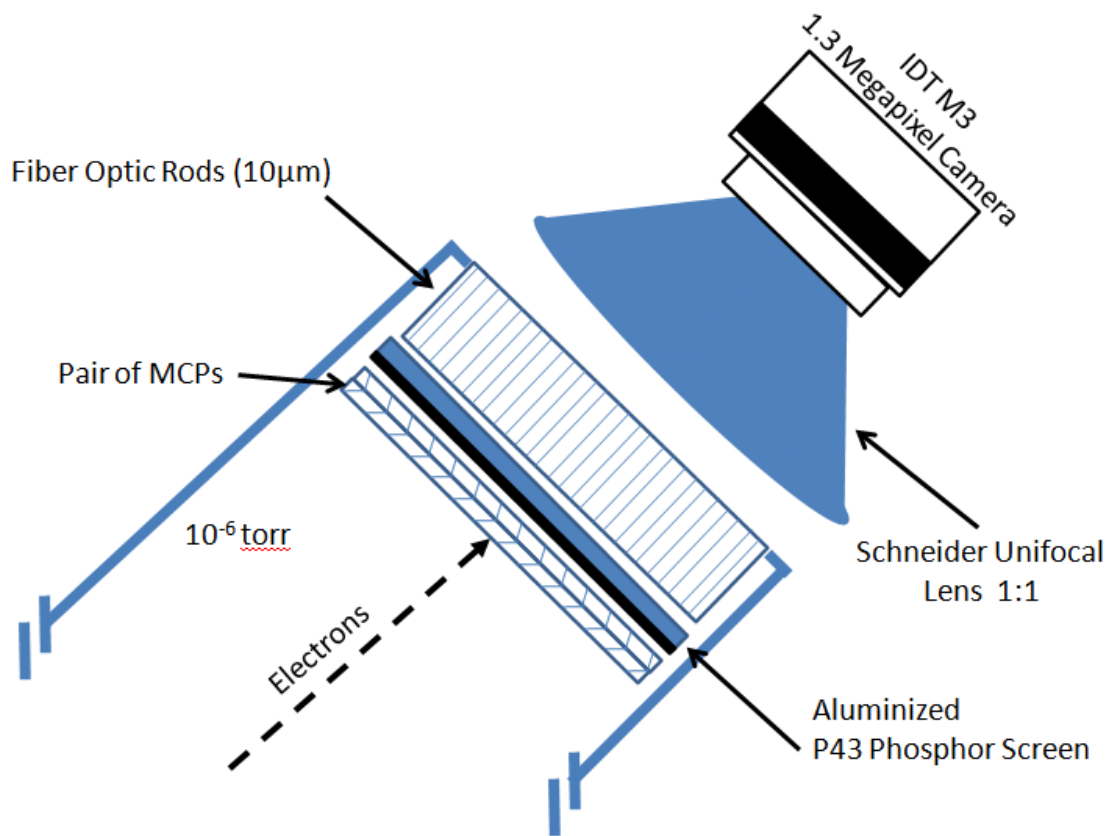


Figure 2.2 Position Sensitive Detector. A schematic of the PSD with MCPs, aluminized phosphor screen, fiber optic rods and camera. Not to scale.

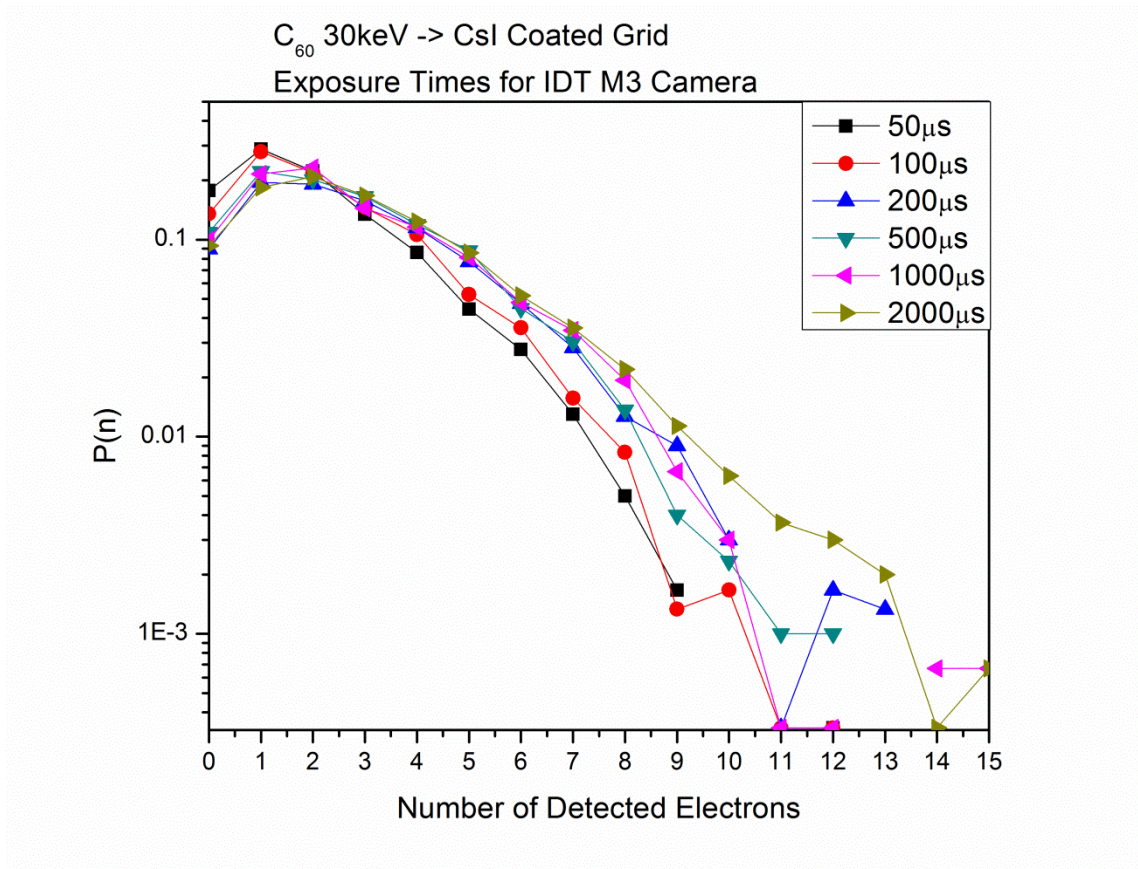


Figure 2.3 Exposure Times for IDT M3 Camera. The exposure time from 50µs to 2ms for a CsI target bombarded by C₆₀ at 30keV

digital converter, TDC. This ensures concurrent detection of ions and electrons from a single impact. To maintain a high rate of collection, on the order of a few hundred impacts per second, the camera is equipped with a CameraLink (National Instruments, Austin, TX USA) connection and can acquire up to 500 frames per second. This allows for rapid collection of the desired number of impacts (100-500,000).

The EEM is designed to handle electrons with low kinetic energy (less than 10eV). Low energy electrons are inherently better for localization and they can be handled with a simplified microscope. The energy of emitted electrons affects the ability to localize the impact. The translational energy of the emitted electrons can be estimated from the distance of the electron from the center of mass (figure 2.4). All measured translation energies are below 1eV with an average energy lower than 1/40eV. With thermal electron emission, the electron energies are expected to be low $\sim 1/40$ eV. This result suggests that thermal electron emission is a likely possibility for the mechanism of electron emission observed here.

For high kinetic energy electrons, >10 eV, we can expect large angular velocities. Electrons with large energies will have non-ideal trajectories through the electro static lenses in the microscope. These electrons will experience additional aberrations and may no longer be imaged properly. As was noted earlier, there are no apertures or collimators in the electron microscope or ToF region, other than the lenses themselves ~ 9 mm in diameter. The absence of collimation allows for nearly all electrons emitted to be detected. Therefore, one can count the number of electrons per impact which is target

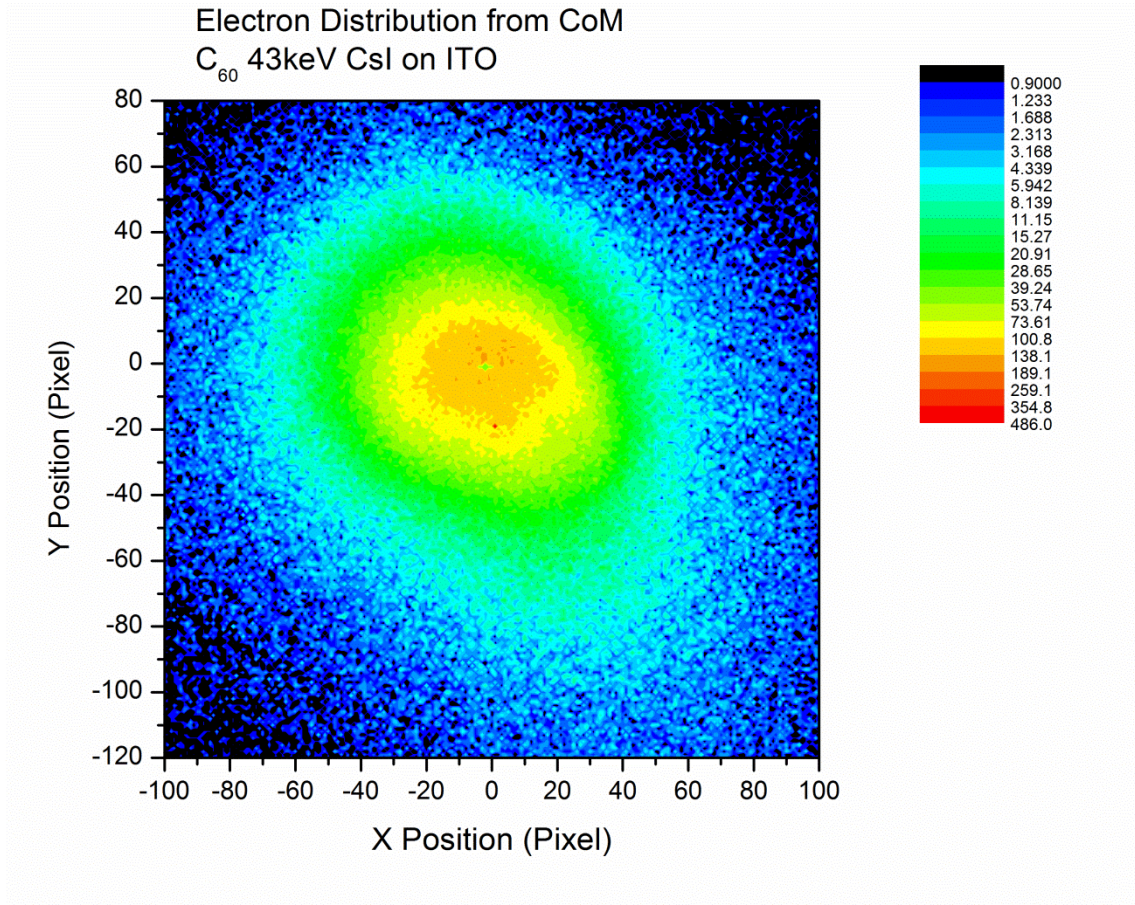


Figure 2.4 Electron Distribution from Center of Mass. The distribution of all detected electrons from the center of mass for each impact.

specific. However, collecting all electrons includes those electrons experiencing aberrations. The latter are detrimental to high resolution localization and must be removed by software collimation (discussed in sections 4 and 5).

2.3 ELECTRON EMISSION FROM C₆₀ IMPACTS ON FLAT HOMOGENEOUS SAMPLES

Samples examined include, organic (glycine, guanine), ionic salts (CsI), metals (Cu, Au and Al), peptides (gramicidin). Each of these samples provides insights into the properties of electron emission from large cluster impacts. We show below that electron yields provide target characteristic data.

The electron emission from homogeneous samples was studied, due to the simplicity of data analysis and to ensure consistent samples. The homogeneous samples were either purchased, or made in house. The following samples were used: glycine, guanine, gramicidin S, aluminum oxide, gold, CsI, silicon. These samples were chosen to cover a range of target characteristics. Additionally, several have been measured previously^[39] and could be used to compare with previous results. All samples had a silicon substrate and a layer of analyte of 500nm to several microns. The glycine, guanine, gramicidin S and CsI were prepared in the laboratory by vapor deposition resulting in a layer of a few micrometers.^[49] The aluminum oxide and gold bulk samples consist of a 5000Å thick layer deposited on a silicon wafer. The silicon sample was purchased from Silicon Valley Manufacturing. The mass spectrum and electron

emission from each sample was measured using C₆₀ at 15 and 30keV total impact energy.

Figure 2.5 shows the measured electron distributions from single impacts of C₆₀ at 15 and 30 keV for a suite of samples. A first observation is that, the electron emission follows a Poisson distribution (Figure 2.5-2.6). Secondly, the electron emission is similar for samples of the same classes, with glycine and guanine (amino acids) having similar electron emission, the two metals (aluminum oxide, gold) also have similar electron emission. The different classes have different electron emission from one another, amino acids having the lowest electron emission, followed by silicon, the metals, and CsI having the largest electron emission. This can be seen in table 2.1, which contains the electron yield for each sample. The electron yields are calculated from the electron distribution, using equation 2.1, where Y_{exp} is the measured yield, n is the number of emitted electrons, $P(n)$ is the probability of emitting n electrons, τ is the detection efficiency, which is equal to 0.6 for these experiments, and Y is the electron yield corrected for the detection efficiency. The experimentally measured electron yield, uncorrected for detection efficiency, is the value reported here.

$$\text{Equation 2.1: } Y_{exp} = \sum n * P(n) = \tau Y$$

The effect of the projectile energy is illustrated by comparing figure 2.6 to figure 2.5. The samples measured with 15keV C₆₀ all have smaller electron emission compared

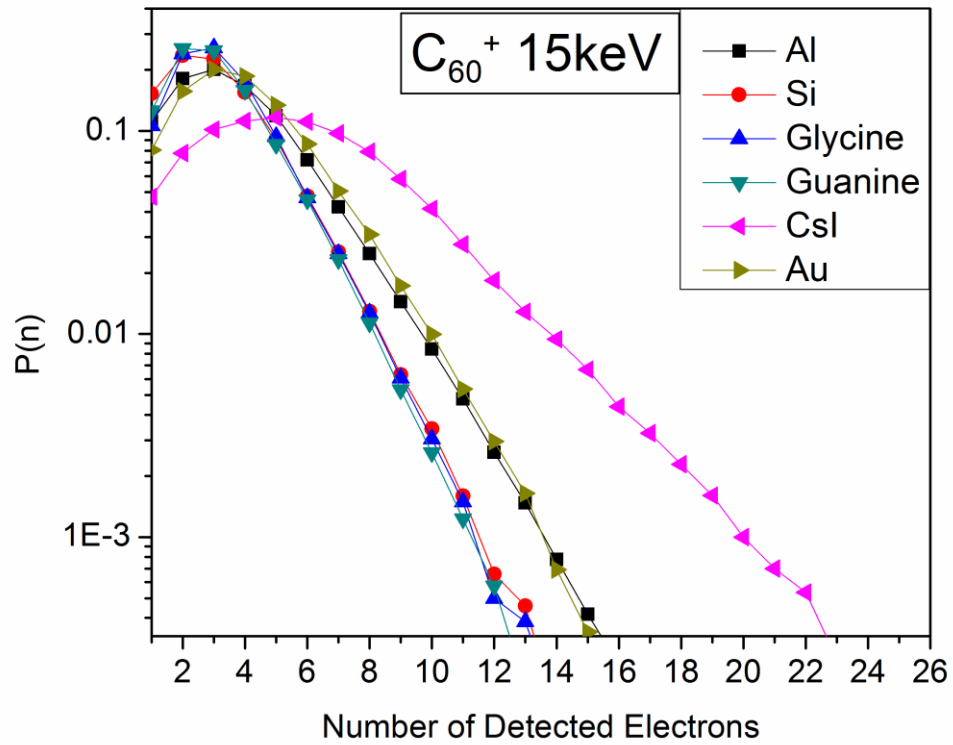


Figure 2.5 Measured Electron Distribution from 15keV C_{60} Impacts on Flat Homogenous Targets. In this figure the electron distribution from 15keV C_{60} impacts a series of homogenous targets is shown. The electron emission is larger for metals and CsI compared to the organic targets and silicon wafer.

Table 2.1 Yields of Electrons from Individual C_{60}^+ and C_{60}^{2+} Impacts at 15 and 30 keV.

	e^- yield	e^- yield
Analyte	C_{60}^+	C_{60}^{2+}
Glycine	3.2	3.9
Guanine	3.1	3.6
Si wafer	3.1	4.1
Al Oxide (bulk)	3.6	5.7
Au (bulk)	3.9	5.9
CsI on 400 mesh grid	5.6	7.8

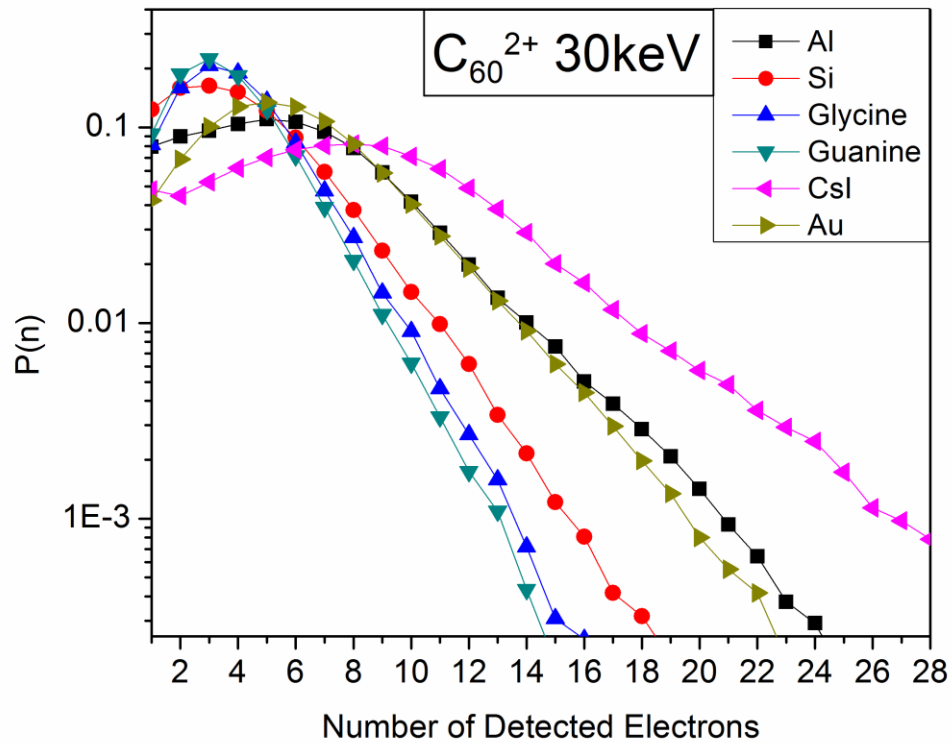


Figure 2.6 Measured Electron Distribution from 30keV C_{60}^{2+} Impacts on Flat Homogenous Targets. In this figure the electron distribution from 30keV C_{60}^{2+} impacts a series of homogenous targets is shown. The electron emission is larger for metals and CsI compared to the organic targets and silicon wafer, the difference is more pronounced than the data in figure 2.5.

to samples measured with 30keV C_{60} . A second observation is that the electron distributions a higher mean, and the differences in electron emission between samples is more pronounced. In the 15keV data, silicon and the two amino acids have very similar electron emission distributions, however in the 30keV data the distributions are separated, especially for emission of more than 8 electrons.

In these experiments the secondary ions were measured concurrently with the electrons. This unique measurement allows for the investigation of the effect of electron emission on the measured ions. To be specific the correlation or anti-correlation of secondary ion emission and electron emission can be studied. This was accomplished using the electron analysis software discussed in section 5. The correlation or anti-correlation was investigated for two different cases: a) the correlation between electron emission and the emission of an ion of interest, b) the correlation between the electron emission and the number of secondary ions emitted.

The correlation or anti-correlation of electron emission with an ion of interest was investigated for impacts on the 500nm gold layer deposited on a Si wafer (discussed previously). The emission of H^- , Au^- and Au_2^- were selected for analysis, Au^- and Au_2^- both originate from the sample and H^- is due to contamination on the surface from hydrocarbon pump oil or absorbed hydrogen on the surface, the mass spectrum can be found in figure 2.7. The concurrently measured electron emissions from impacts which generated H^- , Au^- and Au_2^- are shown in figure 2.8. The electron emission from the selected impacts has an identical distribution as the total electron distribution from

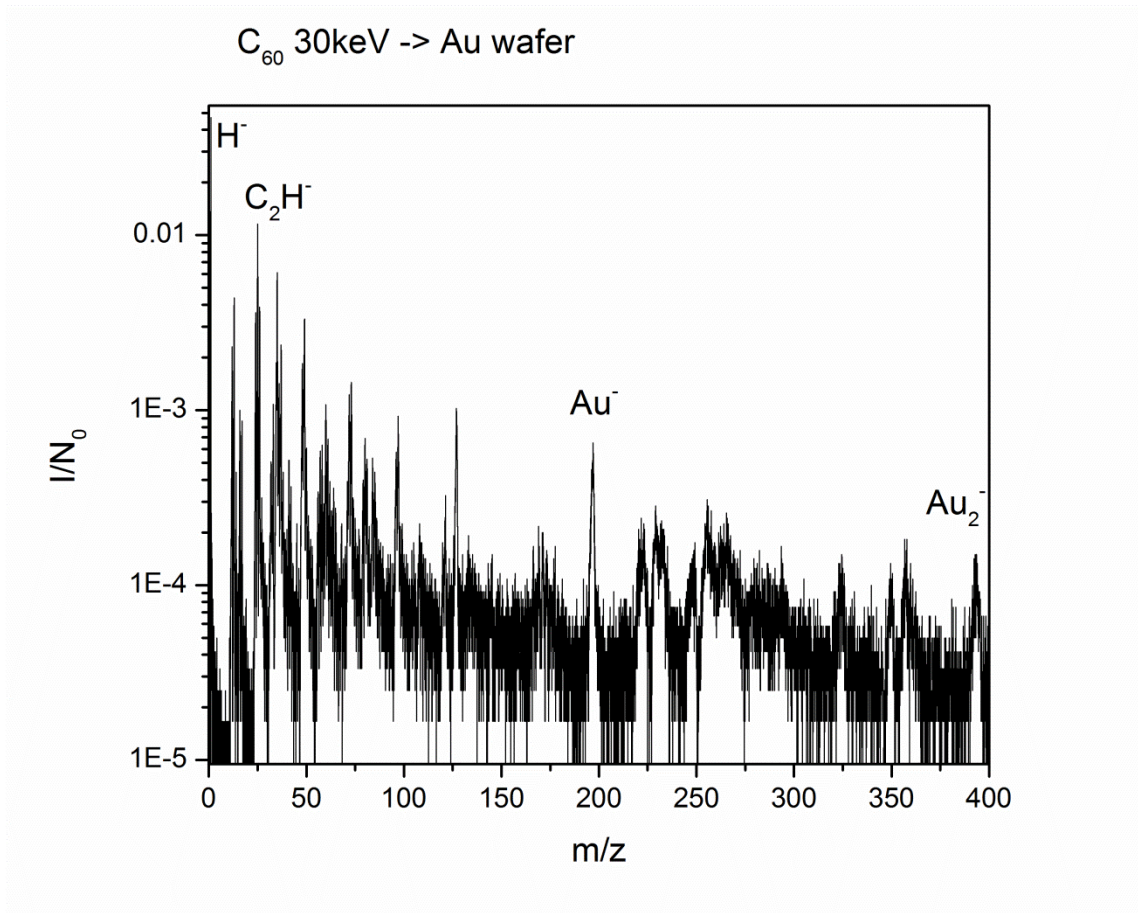


Figure 2.7 Mass Spectrum of 500nm Thick Au Layer Deposited on Si. Au target bombarded by 30keV C_{60} .

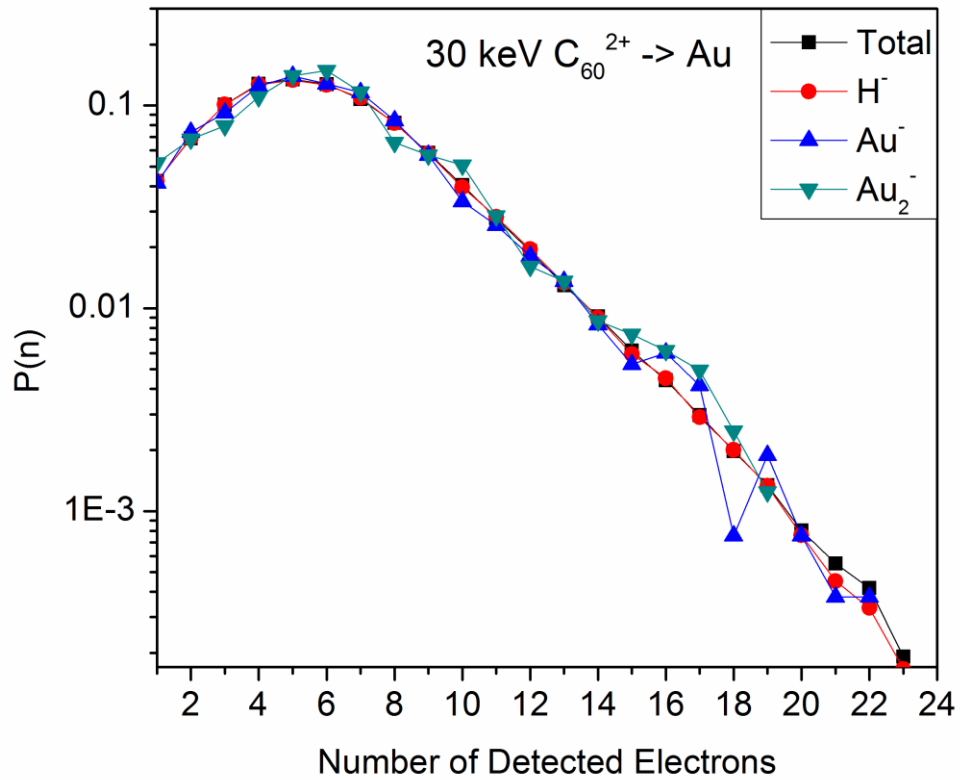


Figure 2.8 Measured Ion Specific Electron Distributions from 30keV C_{60} Impacts on Au Target. In this figure the ion specific electron distribution from 30keV C_{60} impacts, for the selected ions H^- , Au^- and Au_2^- are compared to the total measured electron distribution.

impacts on this sample. Therefore, electrons are emitted independently from the type of ion emitted for the ions examined.

The correlation or anti-correlation of electron emission with an ion interest was further investigated for all the samples described above: glycine, guanine, aluminum oxide, CsI and silicon. For each case the electron emission was independent of secondary ion emission for any ion of interest chosen, examples for guanine, glycine, and gramicidin S can be found in figures 2.9-2.12. CsI is an exception and is discussed in more detail below (CsI is not a homogeneous target).

The correlation or anti-correlation of electron emission versus the number of ions emitted was investigated for impacts on the 500nm thick Au layer deposited on a silicon wafer (described previously). Events where the number of ions detected varied from zero, to five ions were selected and the corresponding electron emission distribution is plotted for each case and overlaid in figures 2.13 and 2.14. Additionally the total electron distribution (from all 120,000 impacts) was plotted for comparison. Figure 2.13 corresponds to C₆₀ with 15keV total impact energy and figure 2.14 corresponds to C₆₀ with 30keV total impact energy. The electron distribution for events where a specific number of ions were detected (0-5) is identical to the total distribution for both the 15 and 30keV. This means that equation 2.2, where m and n are, respectively, the number of ions and electrons detected per projectile impact, holds true and the electron emission is independent from the number of secondary ions detected. The absence of relationship between the number of secondary ions and the number of emitted electrons is further illustrated in the cases of guanine, and gramicidin S (figures 2.15-2.18).

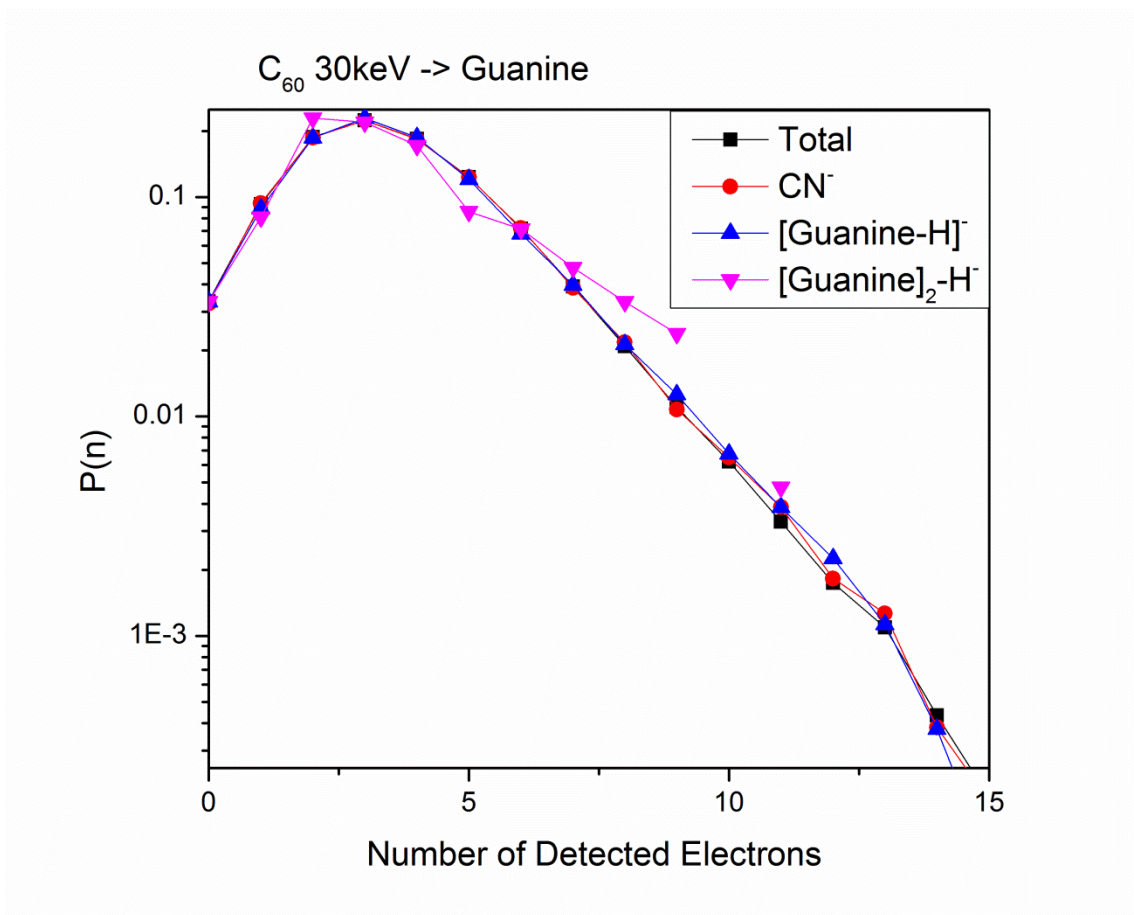


Figure 2.9 Measured Ion Specific Electron Distributions from 30keV C₆₀ Impacts on Guanine Target. In this figure the ion specific electron distribution from 30keV C₆₀ impacts, for the selected ions CN⁻, [Guanine-H]⁻ and [Guanine]₂-H⁻ are compared to the total measured electron distribution.

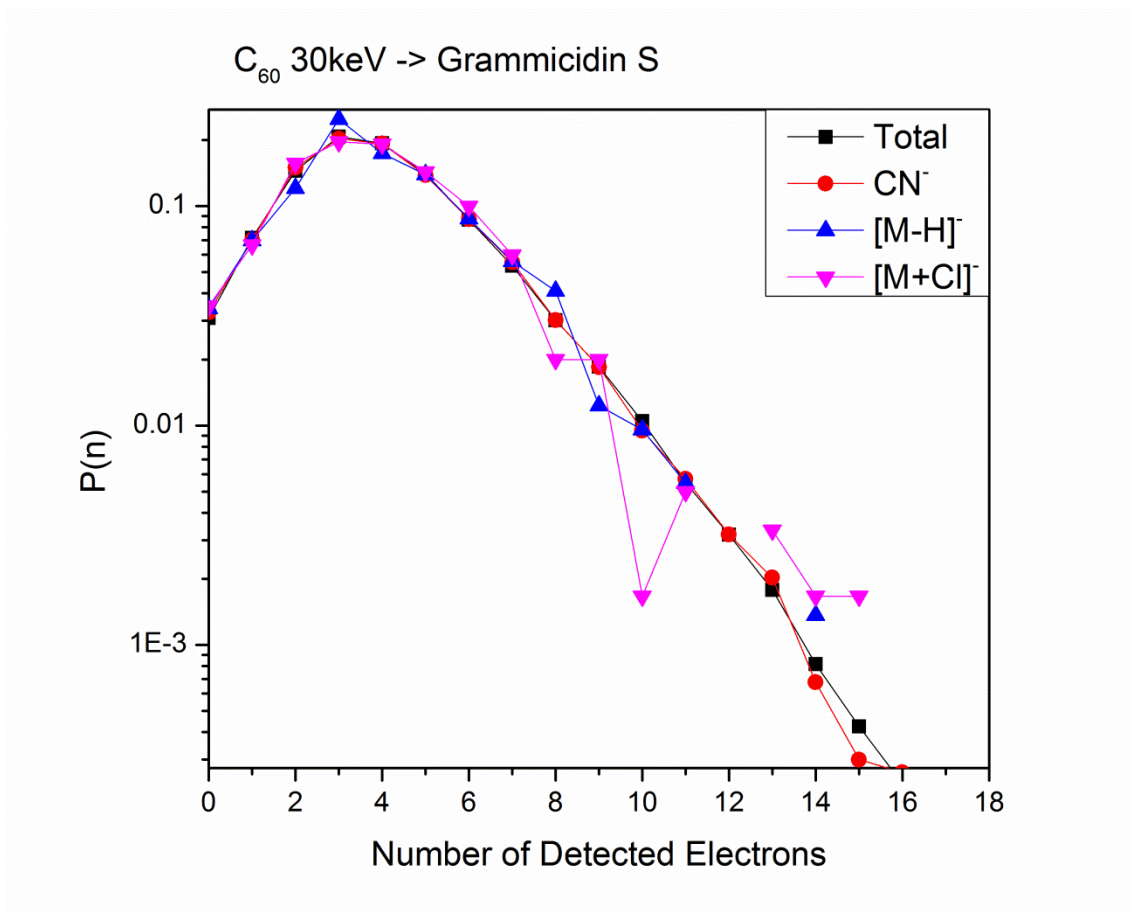


Figure 2.10 Measured Ion Specific Electron Distributions from 30keV C_{60} Impacts on Gramicidin S Target. In this figure the ion specific electron distribution from 30keV C_{60} impacts, for the selected ions CN^- , $[M-H]^-$ and $[M+Cl]^-$ are compared to the total measured electron distribution.

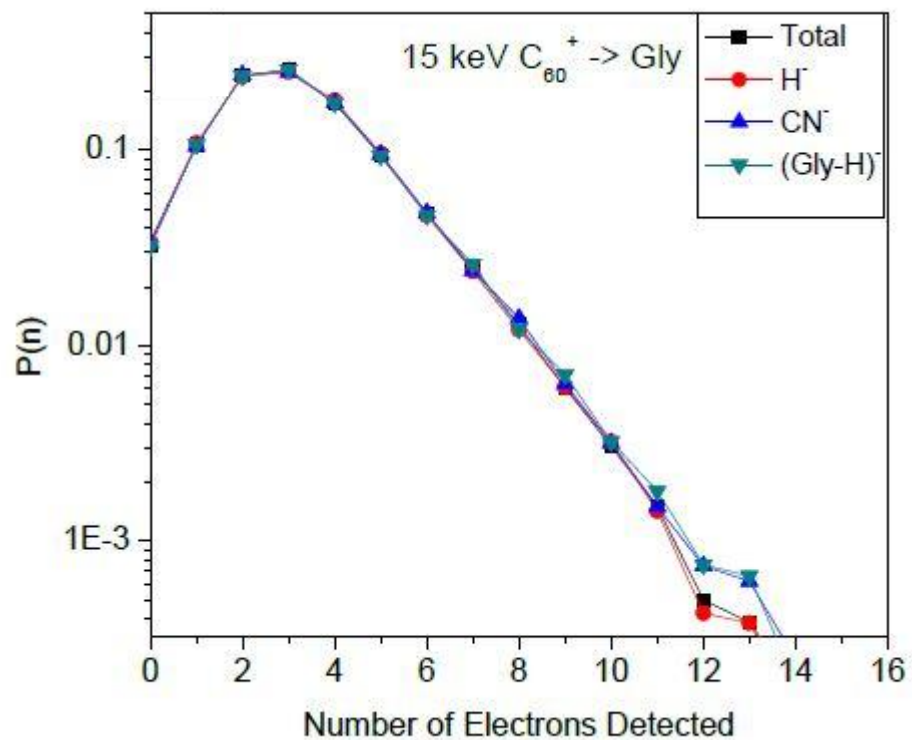


Figure 2.11 Measured Ion Specific Electron Distributions from 15keV C_{60} Impacts on Glycine Target. In this figure the ion specific electron distribution from 15keV C_{60} impacts, for the selected ions H^+ , CN^- and $[M-H]^-$ are compared to the total measured electron distribution.

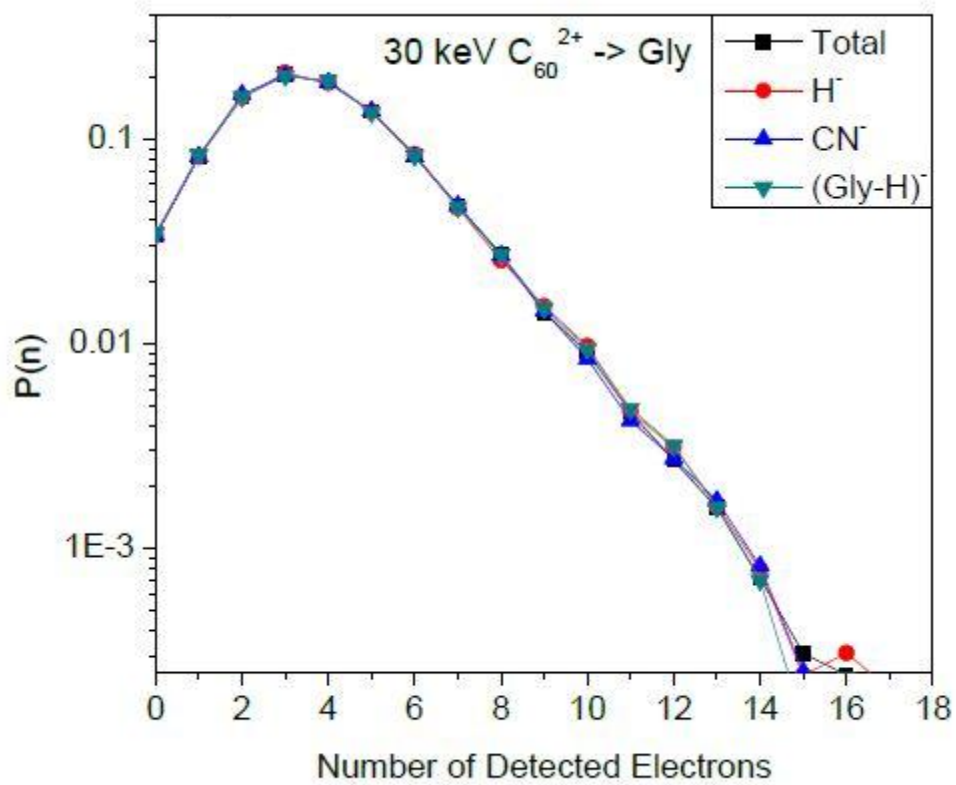


Figure 2.12 Measured Ion Specific Electron Distributions from 30keV C_{60} Impacts on Glycine Target. In this figure the ion specific electron distribution from 30keV C_{60} impacts, for the selected ions H^- , CN^- and $[M-H]^-$ are compared to the total measured electron distribution.

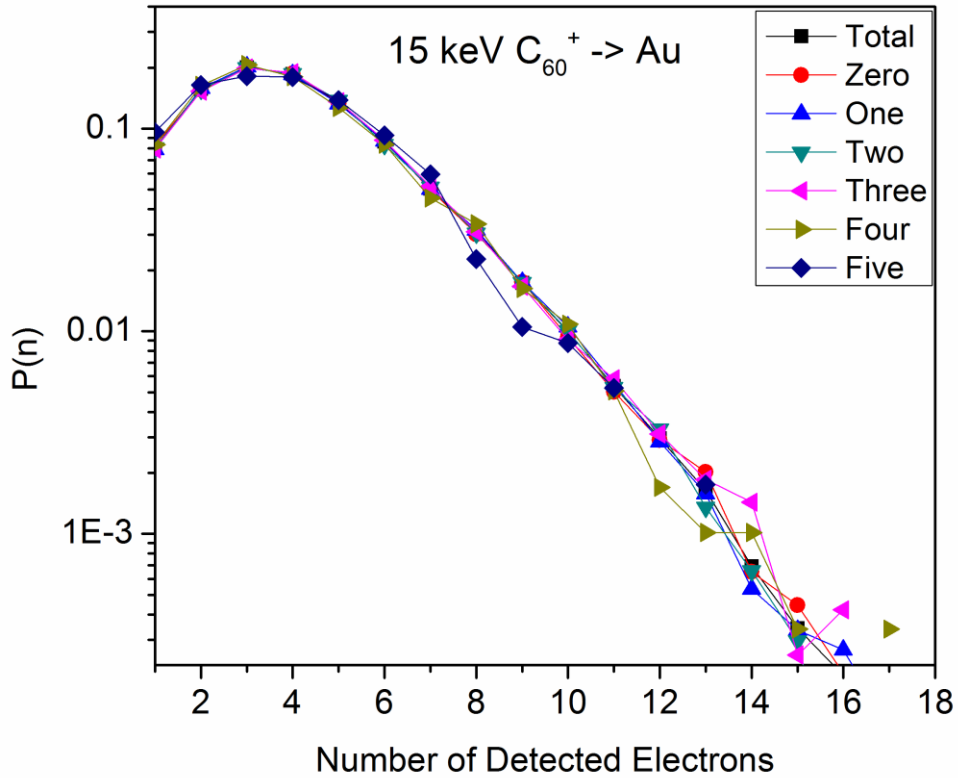


Figure 2.13 Measured Electron Distributions from 15keV C_{60} Impacts on Au Target for a Selected Number of Detected Secondary Ions. Total electron distribution (black square), electron distribution when no (red circle), one (blue triangle), two (green triangle), three (pink triangle), four (brown triangle), and five (purple diamond) ions were detected for electron probability distribution $P(n)$ from a Au target bombarded by C_{60}^+ at 15 keV total impact energy .

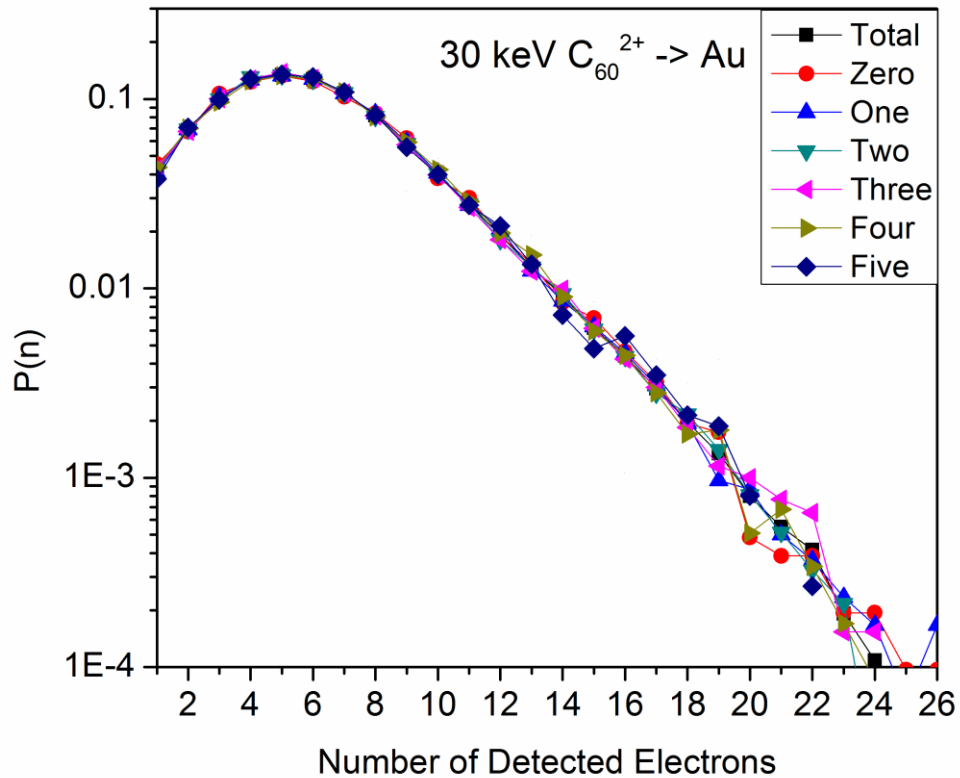


Figure 2.14 Measured Electron Distributions from 30keV C_{60} Impacts on Au Target for a Selected Number of Detected Secondary Ions. Total electron distribution (black square), electron distribution when no (red circle), one (blue triangle), two (green triangle), three (pink triangle), four (brown triangle), and five (purple diamond) ions were detected for electron probability distribution $P(n)$ from a Au target bombarded by C_{60}^{2+} at 15 keV total impact energy .

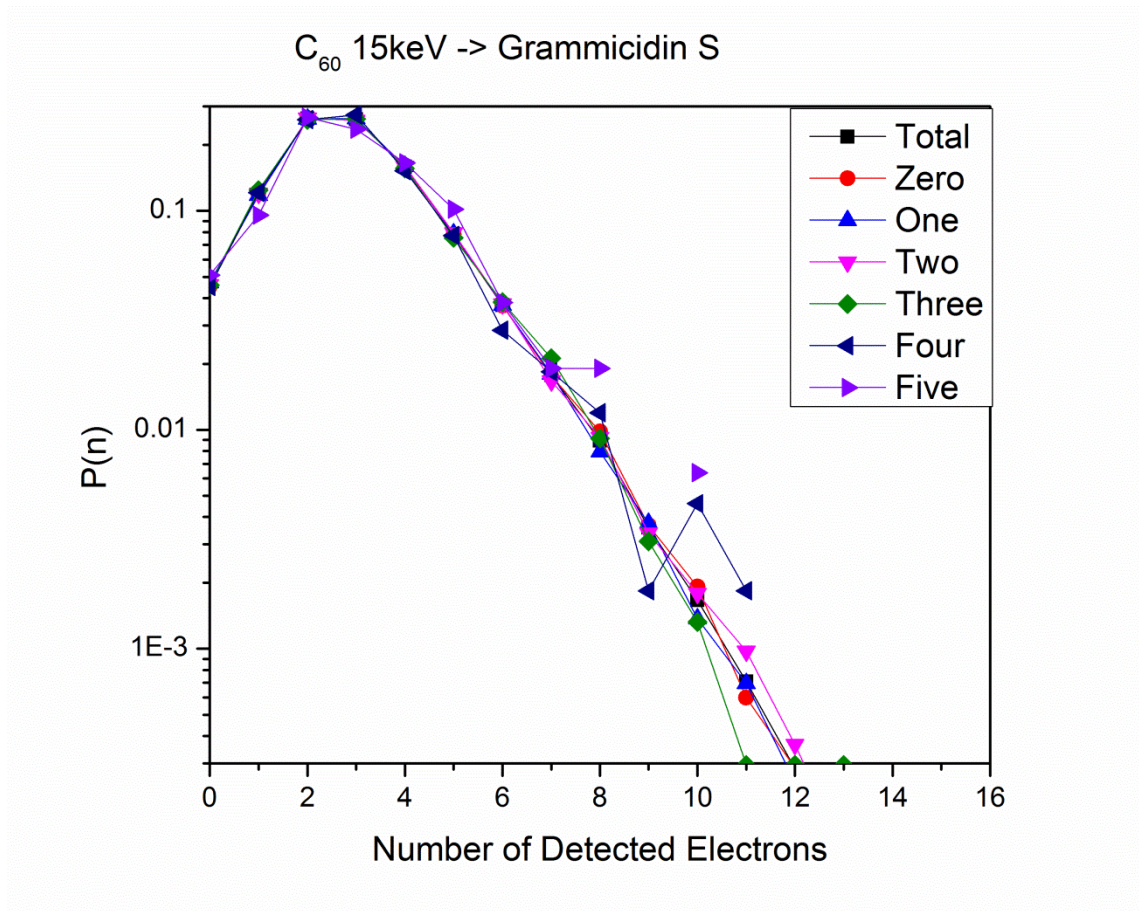


Figure 2.15 Measured Electron Distributions from 15keV C_{60} Impacts on Grammicidin S Target for a Selected Number of Detected Secondary Ions. Total electron distribution (black square), electron distribution when no (red circle), one (blue triangle), two (green triangle), three (pink triangle), four (brown triangle), and five (purple diamond) ions were detected for electron probability distribution $P(n)$ from a gramicidin S target bombarded by C_{60}^+ at 15 keV total impact energy .

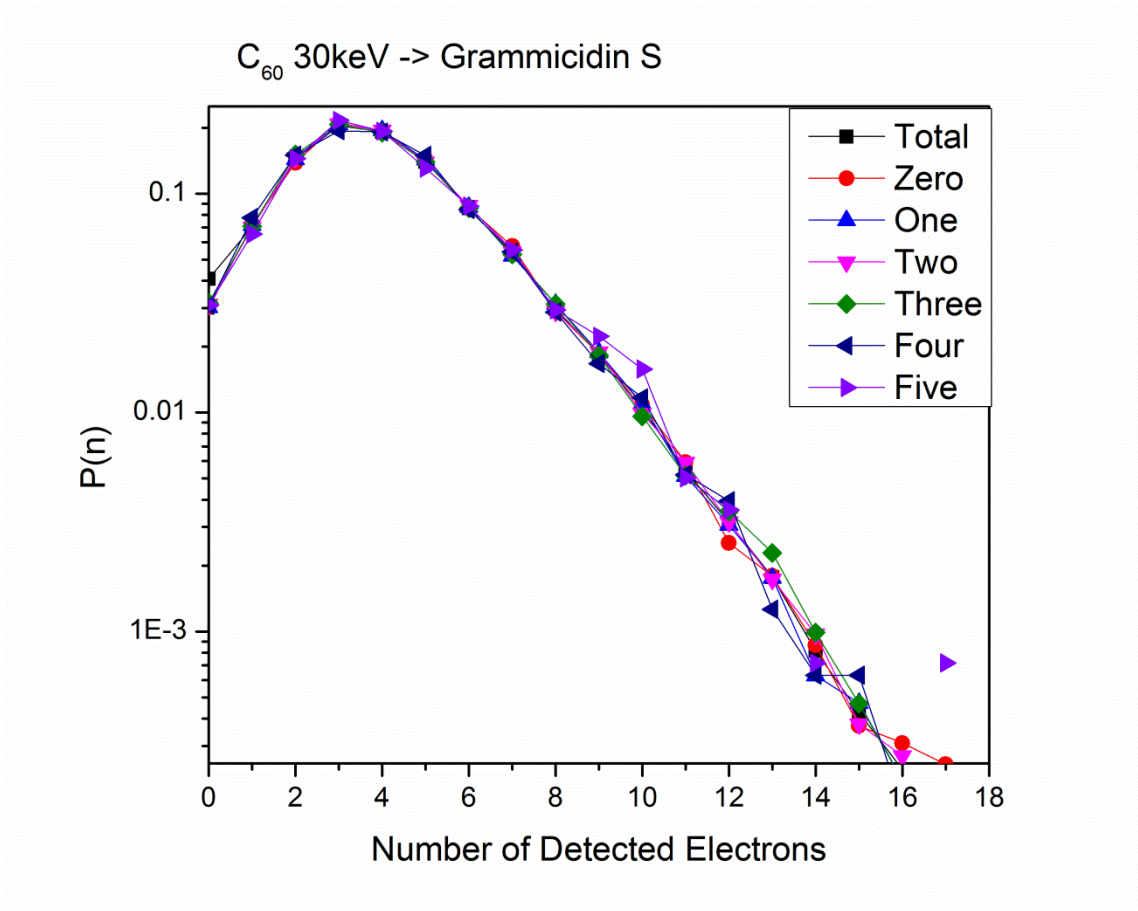


Figure 2.16 Measured Electron Distributions from 30keV C_{60} Impacts on Grammicidin S Target for a Selected Number of Detected Secondary Ions. Total electron distribution (black square), electron distribution when no (red circle), one (blue triangle), two (green triangle), three (pink triangle), four (brown triangle), and five (purple diamond) ions were detected for electron probability distribution $P(n)$ from a grammicidin S target bombarded by C_{60}^{2+} at 30 keV total impact energy .

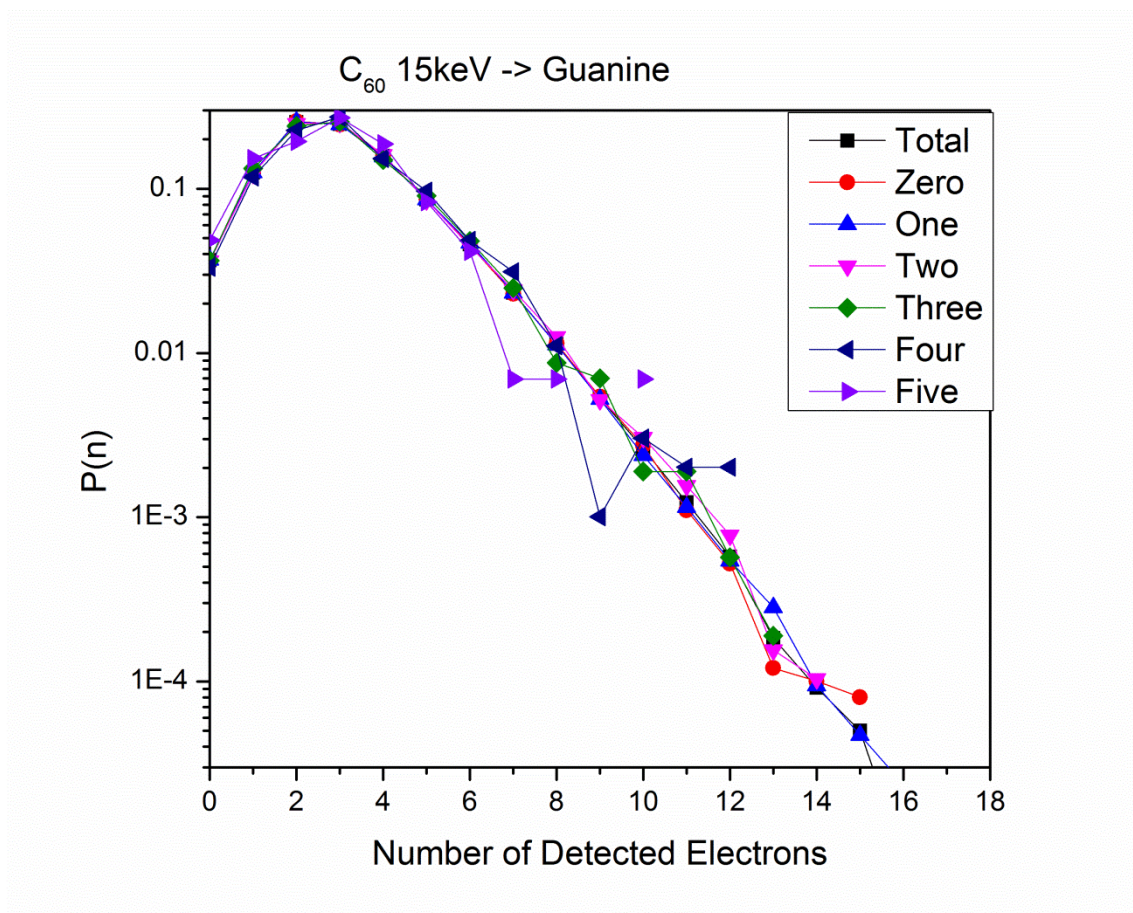


Figure 2.17 Measured Electron Distributions from 15keV C_{60} Impacts on Guanine Target for a Selected Number of Detected Secondary Ions. Total electron distribution (black square), electron distribution when no (red circle), one (blue triangle), two (green triangle), three (pink triangle), four (brown triangle), and five (purple diamond) ions were detected for electron probability distribution $P(n)$ from a guanine target bombarded by C_{60}^+ at 15 keV total impact energy .

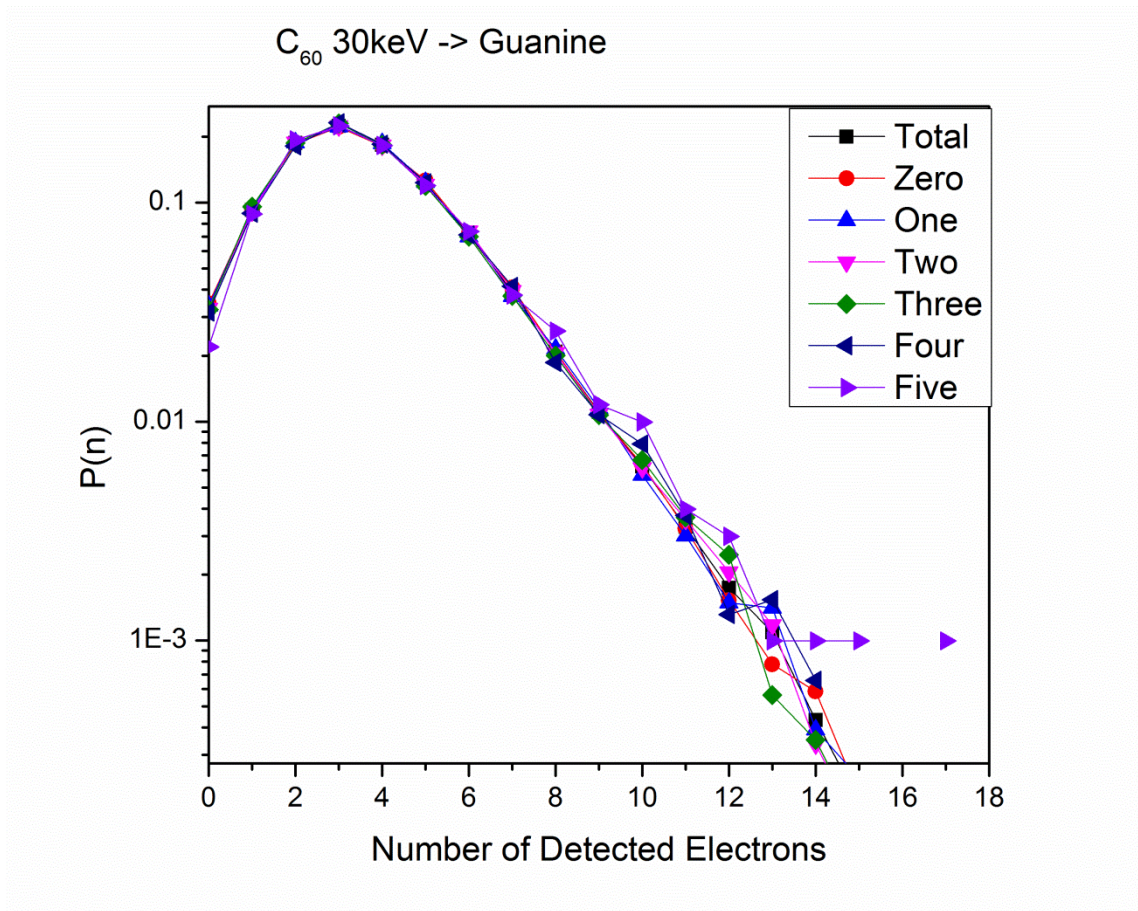


Figure 2.18 Measured Electron Distributions from 30keV C_{60} Impacts on Guanine Target for a Selected Number of Detected Secondary Ions. Total electron distribution (black square), electron distribution when no (red circle), one (blue triangle), two (green triangle), three (pink triangle), four (brown triangle), and five (purple diamond) ions were detected for electron probability distribution $P(n)$ from a guanine target bombarded by C_{60}^{2+} at 30 keV total impact energy .

Equation 2.2: $P(m|n) = P(n)$

The implications of independent emission of electrons from the type and number of secondary ions detected are crucial for the mapping experiment. The mapping of one ion on a surface will have the same parameters as the mapping of another ion from the surface, for flat homogeneous samples. Additionally, impacts which generate a large number of secondary ions will also have the same parameters for localization as impacts which generate fewer secondary ions. Together, these two consequences allows for the mapping/localization of flat homogeneous samples without concerns that one impact would be unequal to another impact.

Returning briefly to CsI, it has been shown that CsI can be deposited as polycrystal.^[50, 51] This polycrystalline structure can change the quantum yield of the CsI and this quantum yield will vary laterally on the surface as different crystal structures are sampled.^[50, 51] In our experiments, the polycrystalline structure also incorporated water into the surface. This can be observed in the mass spectrum, presence of OH⁻ in negative ion mode. Additionally, the effect can be observed in the electron emission. By selecting the ion specific electron emission, from the CsI the differences in the electron emission from areas where water has been incorporated can be observed (figure 2.19). The ion specific electron emission shown is a double coincidence selection (detailed in section 5), where two ions are selected and the electron emission from impacts where those two ions were detected is plotted.

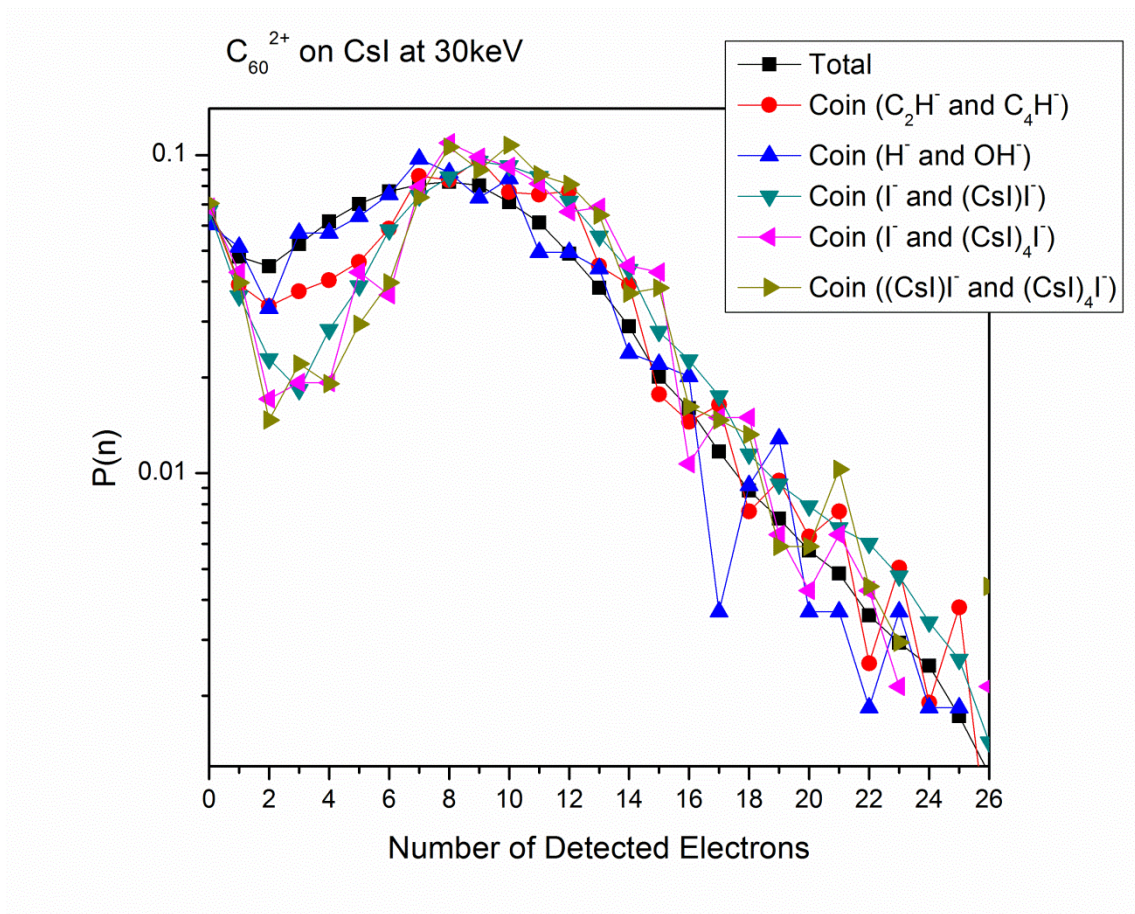


Figure 2.19 Two Ion Selected Electron Distribution from 30keV C_{60} Impacts on CsI. The two ion selected electron distribution from 30keV impacts on CsI for a series of ion pairs. The total electron yield (all impacts) is included for comparison.

As can be seen in the figure the electron emission from impacts where OH^- and H^- are emitted is drastically different from impacts where $(\text{CsI})^-$ and I^- are both emitted. This can be seen quantitatively in table 2.2 where the electron yields for these selected impacts are tabulated. The electron yield from the areas incorporated with water is lower than areas with abundant CsI emission. This example demonstrates how the electron emission can be used to examine complex surfaces.

The insights gained from homogeneous flat samples are important for mapping of projectile impacts. However, many applications of mapping or localizing species are on non-flat inhomogeneous surfaces. The applicability of the mapping methodology for complex samples is demonstrated and studied in section 2.4.

2.4 ELECTRON EMISSION FROM C_{60} IMPACTS ON NANO-OBJECTS

Pinnick has reported a size effect in secondary ion emission when a massive cluster impacts a nano-object too small for full projectile energy deposition.^[52] We examine here electron emission from nano-scale objects. Several questions arise in this context. Does the size and shape of the nano-object affect the electron emission? Is the co-emission of electrons and negative SIs correlated from nano-objects? Does the electron yield vary with the co-emission of multiple SIs?

The analysis of nano-objects was first investigated with a series of aluminum oxide samples. Three samples were produced, 50nm aluminum oxide nano-particles^[53], 2x200nm boehmite whiskers, and a flat aluminum oxide sample, which consists of a

Table 2.2 Electron Yields from 30keV C_{60} Impacts on CsI. The two ion selected electron yields from 30keV impacts on CsI for a series of ion pairs. The total electron yield (all impacts) is included for comparison.

	e^- yield
Ions	30 keV C_{60}^+
Total	7.8
OH^- and H^-	7.9
C_2H^- and C_4H^-	8.5
I^- and $(CsI)I^-$	9.2
I^- and $(CsI)_4I^-$	9.1
$(CsI)I^-$ and $(CsI)_4I^-$	9.2

500nm Al oxide layer deposited on a silicon wafer. The 500nm Al oxide layer acts as the bulk Al oxide sample. The 50 nm Al oxide particles were obtained from Argonide (Sanford, Florida, USA) and were suspended in acetone at 25 mg/mL and sonicated. Then, 10 μ L of the aluminum solution was deposited onto a silicon wafer; the thickness of this layer is a few micrometers, which is much larger than the depth of emission for this experiment, \sim 10 nm. The boehmite whiskers were prepared by a process described elsewhere and are 2 nm wide and 200 nm long.^[52]

Three gold samples were also prepared; a 500 nm thick gold layer was deposited on a silicon wafer. Second, a multilayer of 5 nm gold nano-particles (NPs) functionalized with dodecanethiol (Sigma Aldrich) was prepared by suspending Au NPs in hexane at 10mg/mL and depositing 15 μ L of this solution onto a silicon wafer. Similar to the 50 nm Al particles, this produced a few micrometers thick layer of Au NPs on the silicon surface. A third sample consisting of the Au NPs dispersed as a single layer on glycine was prepared.^[54] This was performed by vapor-depositing glycine in a several micrometers thick layer (Sigma Aldrich) onto a Si wafer, then suspending the Au NP in hexane, in which glycine is insoluble, at 0.5 mg/mL and depositing 5 μ L of this solution onto the glycine surface.

Total electron probability distributions for the three aluminum samples bombarded by C₆₀²⁺ at 30 keV total impact energy are presented in Figure 2.20. From these electron distributions, the electron yields can be calculated for the three samples using equation 2.1. The data are tabulated in Table 2.3.

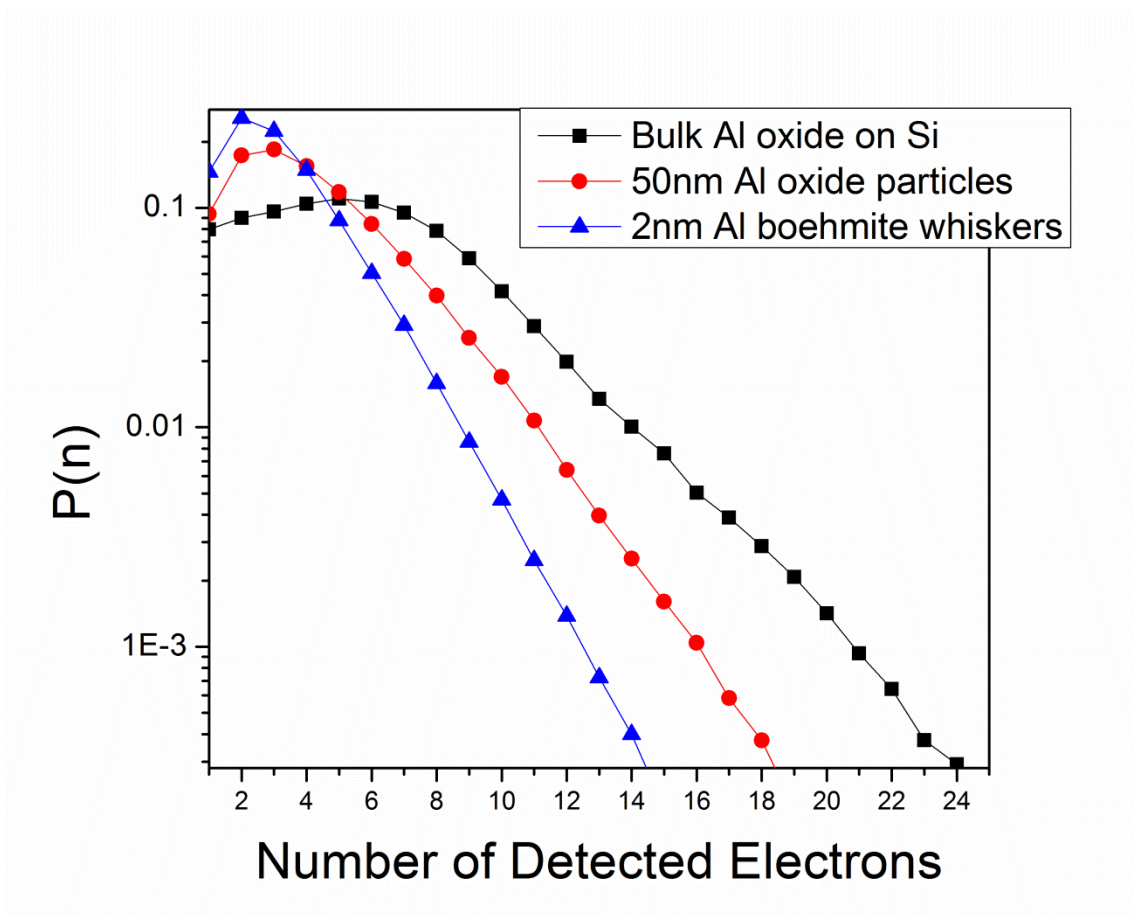


Figure 2.20 Electron Probability Distributions from the Three Aluminum Oxide Samples Bombarded by C_{60} at 30 keV.

Table 2.3 Electron Yields: Total and SI Specific for Different Aluminum Oxide Samples

Bombarded by C_{60} at 30keV

e^-/impact	Total Ave	AlO^-	AlO_2^-
Al wafer	5.7	5.8	5.7
Al 50 nm	4.2	4.2	4.2
Al whiskers	3.2	3.2	3.2

The measured electron yields are ≥ 3.2 electrons per impact for the aluminum samples investigated. The highest electron yield was observed for the bulk Al oxide (500 nm Al oxide layer on silicon) with a value of 5.7 electrons per impact. The electron yield is reduced to 4.2 electrons per impact in the case of the 50 nm Al oxide particles. For still smaller objects, specifically the 2 nm in diameter Al boehmite whiskers, the electron yield decreased to 3.2 electrons per impact. The calculated ion-specific electron yields are computed by selecting the impacts that yielded an ion(s) of interest using equation 2.1. Ion-specific electron yields for AlO^- and AlO_2^- for all three Al oxide samples investigated are shown in table 2.3. Interestingly, the ion-specific electron yields are nearly identical to the total electron yield for each sample.

The decreasing electron yield from smaller objects is evidenced by the altered electron distributions. As seen in figure 2.20, the total electron distribution for 50 nm Al oxide is narrower and shifted to the left (smaller number of electrons emitted) compared to bulk aluminum oxide. This trend continues as the size of the object decreases to 2 nm in diameter for the Al boehmite whiskers.

SI yields from the three aluminum oxide samples are shown in table 2.4. The SI yields were calculated using equation 2.3.

Equation 2.3 $Y_z = \frac{N_z}{N_t}$ where Y_z is the yield of a specified ion, N_z is the number of impacts where that ion was detected, and N_t is the total number of detected impacts.

Table 2.4 Secondary Ion Yields from Aluminum Oxide Samples Bombarded by C₆₀ at 30 keV.

Ion	Al wafer	50 nm Al	Al whisker
AlO ⁻	2.0×10^{-2}	1.3×10^{-2}	2.7×10^{-2}
AlO ₂ ⁻	3.5×10^{-2}	3.3×10^{-2}	1.3×10^{-2}
AlO ₃ OH ⁻	2.8×10^{-2}	1.6×10^{-2}	1.0×10^{-2}
AlO ₂ (AlO) ₂ (OH) ₂ ⁻	1.4×10^{-2}	5.9×10^{-3}	3.4×10^{-3}
Al ₂ O ₃ (AlO) ₃ (OH) ₃ ⁻	2.4×10^{-2}	5.7×10^{-3}	1.0×10^{-3}
(Al ₂ O ₃) ₃ AlO ₂ ⁻	1.3×10^{-2}	4.3×10^{-3}	5.0×10^{-4}
(Al ₂ O ₃) ₅ OH ⁻	1.3×10^{-2}	2.9×10^{-3}	
(Al ₂ O ₃) ₆ OH ⁻	8.6×10^{-3}	1.8×10^{-3}	
(Al ₂ O ₃) ₇ (AlO ₂) ⁻	4.1×10^{-3}	2.3×10^{-3}	

As noted already, when the size of an isolated object is below the size of the desorption volume (estimated $\sim 10^3 \text{ nm}^3$), fragmentation of the object occurs with shifted mass distribution of the SIs.^[52] This case is illustrated with the ratio of AlO^- to AlO_2^- in the whisker sample (Table 2.5). The ratio of $\text{AlO}^-/\text{AlO}_2^-$ is <1 for the 50 nm Al NP and the bulk Al oxide; however, for the whiskers, it is >2 , showing that for object volumes below the impact volume smaller SIs are preferentially generated. Additionally, the whiskers show a significantly reduced production of AlO clusters (Table 2.4) compared with the Al oxide wafer or the 50 nm NP. The predominance of atomic and diatomic SIs from a confined volume “suggests the ejection of energetic chunks of matter that (in turn) undergo extensive fragmentation”.^[52]

The SI yields in the range of a few percent (Table 2.4) make it practical to run SIMS in the event-by-event bombardment/detection mode. This approach allows us to identify co-emitted SIs from individual projectile impacts, that is, to identify chemical species colocated within an emission area of $10\text{--}20 \text{ nm}^2$.^[25] The concurrent electron emission can, after magnification, be used to pinpoint the coordinates of the impact site. Ultimately, location and SIs recorded from such enable one to construct a map of chemical species.^[46, 55] The performance of “positional mass spectrometry” depends on the relationship between ion and electron emission. Figure 2.21 shows that they are independent from one another when originating from homogeneous Al oxides. The same result was observed for a range of flat homogeneous samples, section 2.2. The independence of ion-electron emission holds for nano-objects (figures 2.22-2.23). However, in the case investigated here, objects where one dimension is $\leq 50 \text{ nm}$, the

Table 2.5 Ratio of SI Yields of AlO^- and AlO_2^- from the Aluminum Oxide Samples Bombarded by C_{60} at 30 keV.

Sample	$\text{AlO}^-/\text{AlO}_2^-$
Al wafer	0.6
Al 50 nm	0.4
Al whiskers	2.1

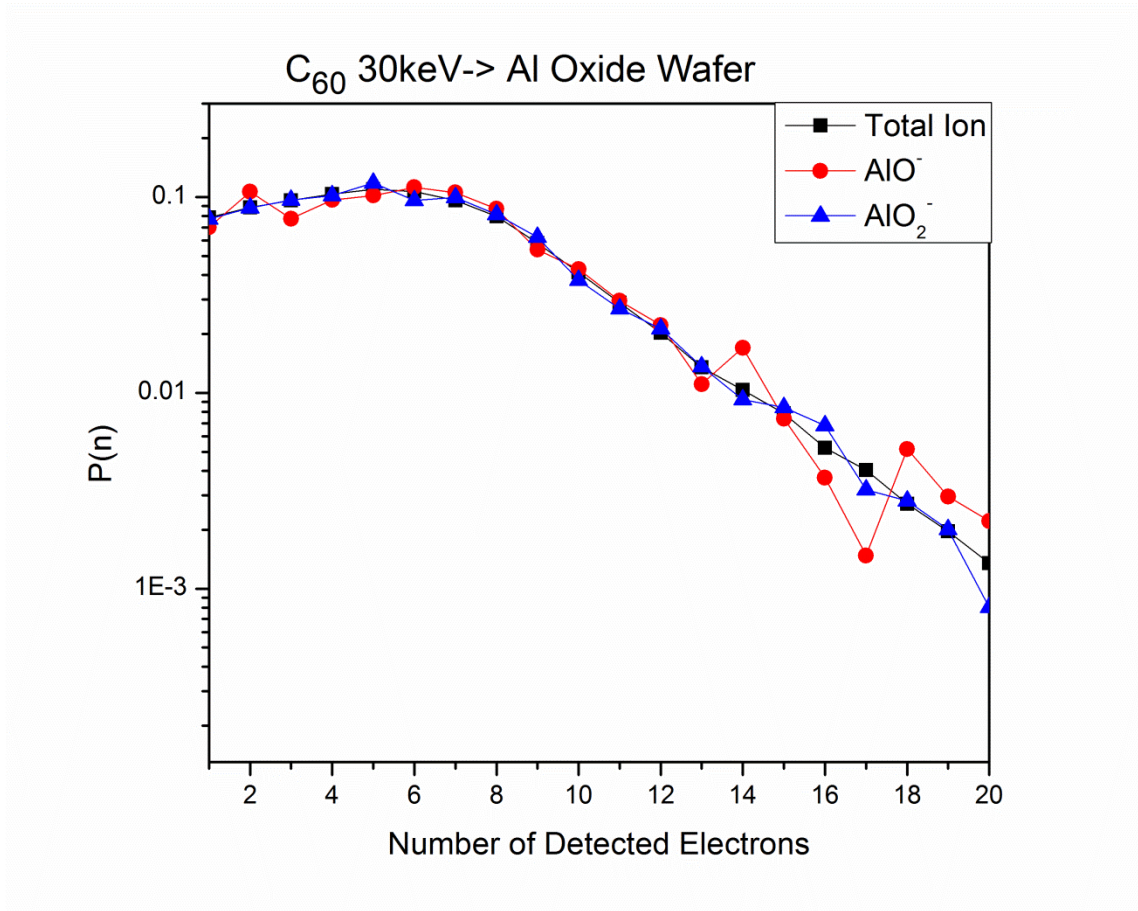


Figure 2.21 Measured Ion Specific Electron Distributions from 30keV C₆₀ Impacts on a Flat Aluminum Oxide Coated Si Wafer. In this figure the ion specific electron distribution from 30keV C₆₀ impacts, for the selected ions, AlO⁻ and AlO₂⁻ are compared to the total measured electron distribution.

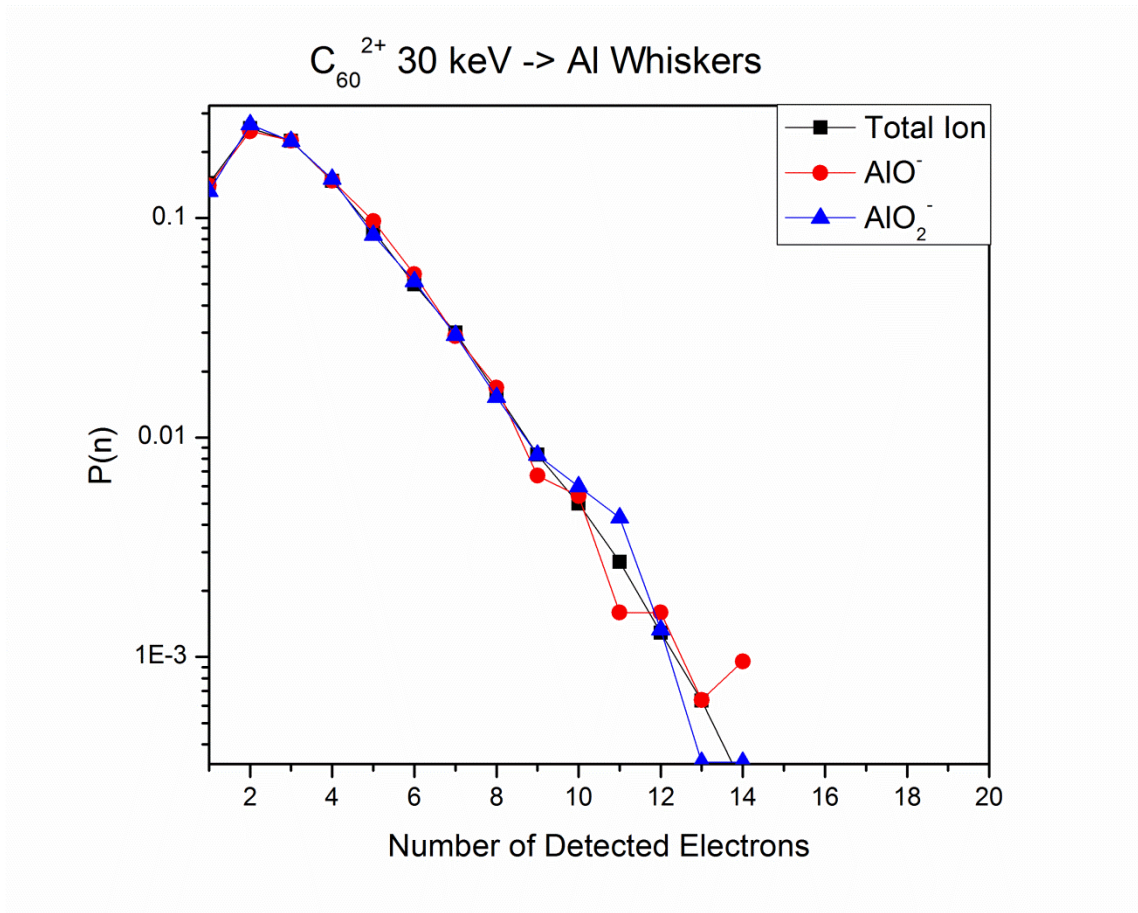


Figure 2.22 Measured Ion Specific Electron Distributions from 30keV C_{60} Impacts on Aluminum Boehmite Whiskers. In this figure the ion specific electron distribution from 30keV C_{60} impacts, for the selected ions, AlO^- and AlO_2^- are compared to the total measured electron distribution.

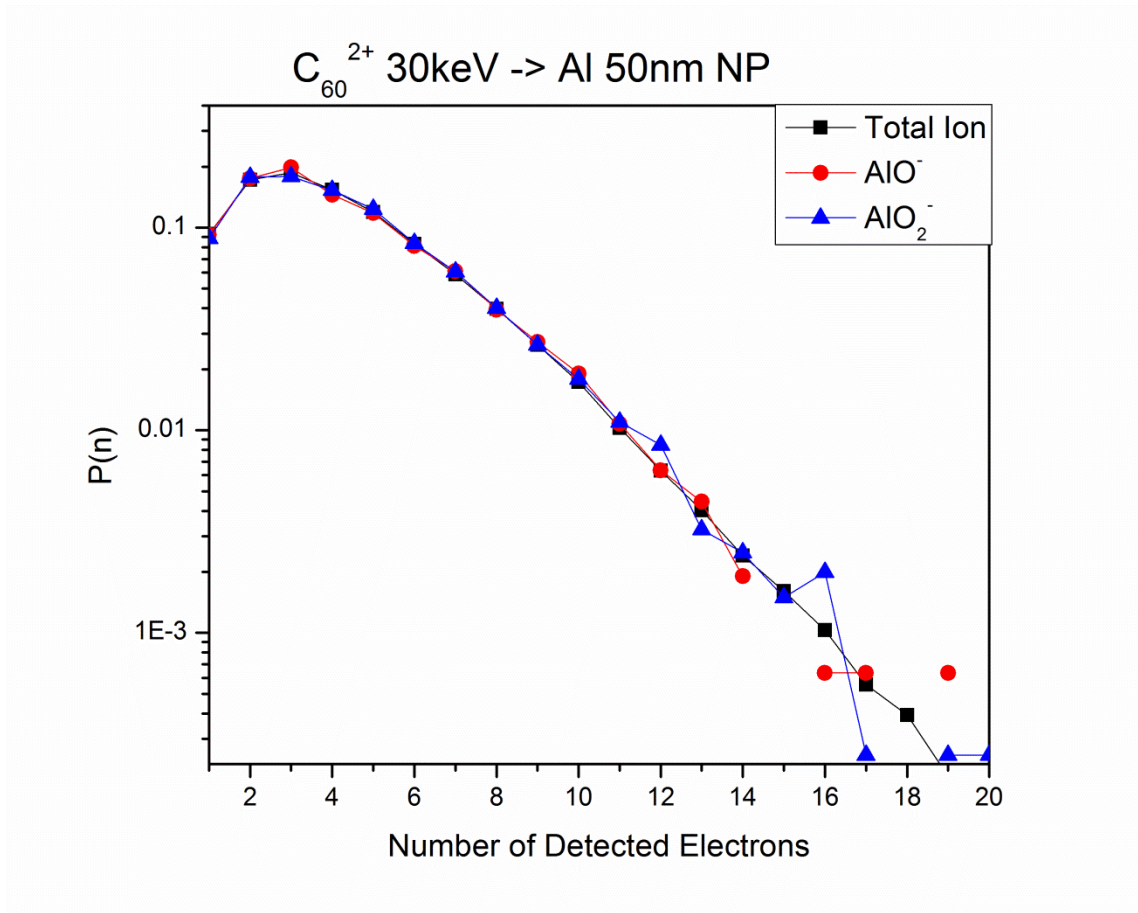


Figure 2.23 Measured Ion Specific Electron Distributions from 30keV C_{60} Impacts on 50nm Nano-Particles. In this figure the ion specific electron distribution from 30keV C_{60} impacts, for the selected ions, AlO^- and AlO_2^- are compared to the total measured electron distribution.

electron and SI yields and distributions become size-dependent. These trends are readily apparent in figures 2.21-2.23 and in the yield data listed in Tables 2.2-2.5.

The occurrence and characteristics of the electron emission are tied to the vibrational and electronic excited nano-volume generated by a C₆₀ impact. The nano-volume's characteristics (energy density, size, emission area, sputter rate) and its temporal evolution have been explored with molecular dynamic simulations.^[56] It has been shown that the excited nano-volume, which contains atoms, clusters, molecular fragments, and molecules, expands within a few tens of picoseconds.^[57, 58] The vibrationally and electronically excited species move upward and undergo charge exchange processes that result in positive ionization and emission of electrons. The mechanism of positive ionization should be similar (with some restrictions) to the ionization mechanism of dense gases via heavy projectile impacts.^[58] It has been proposed that the free electrons ejected in these ionizations are responsible for the high electron yields and the broad distributions of the number of electrons per massive projectile impact.^[59] This hypothesis is supported by the results presented in section 2.3 and here is section 2.4. The classic kinetic electron emission mechanism requires the emission of electrons after the energy is deposited in the first surface layers. The latter do not depend on the morphology and size of the impacted nano-objects, which in the present case are larger than the size of the incoming projectile. For isolated nano-objects, the electron yield depends on the projectile energy deposited, that is, the characteristics of the expanding collision volume, which in turn depend on the object size and morphology. The low electron yields from nano-objects that shatter after

impact suggest that electron exchange between initial fragments from shattering is reduced.

The suppressed electron emission from shattered objects was also observed in the case of gold NPs. The total electron probability distributions for a multilayer layer of 5 nm Au NP and, for comparison, from a flat 500 nm thick layer of Au on a silicon wafer are presented in figure 2.24 and 2.25. As with the Al oxide samples, the distribution is shifted toward lower electron emission, and the distribution becomes narrower with shrinking object size. The differences in electron distribution are enhanced at higher impact energy (figure 2.25) because of more prolific electron emission at higher energies.^[32, 41, 46] Electron yields calculated using equation 2.1 are tabulated in table 2.6 for bulk gold and the multilayer of 5 nm Au NPs.

The ion-specific electron distributions and yields were also investigated. The data are shown in figures 2.26 and 2.27. The ion-specific electron probability distributions are the same as the total distributions, indicating that electrons and ions are emitted independently from these two samples (equation 2.2). A comparison of the ion specific electron yields in table 2.6 further confirms this observation.

Regarding the SI emission, there are notable differences for the Au-coated wafer and the multilayer of Au NPs. The yields of Au^- and Au_n^- are larger from the 5 nm Au NPs compared to the Au coated Si wafer (table 2.7). A C_{60} impact on a Au NP will result in forward and lateral emission of fragments.^[54, 60] However, when the Au NPs are deposited onto glycine as a single layer, the fragments emitted forward implant into the

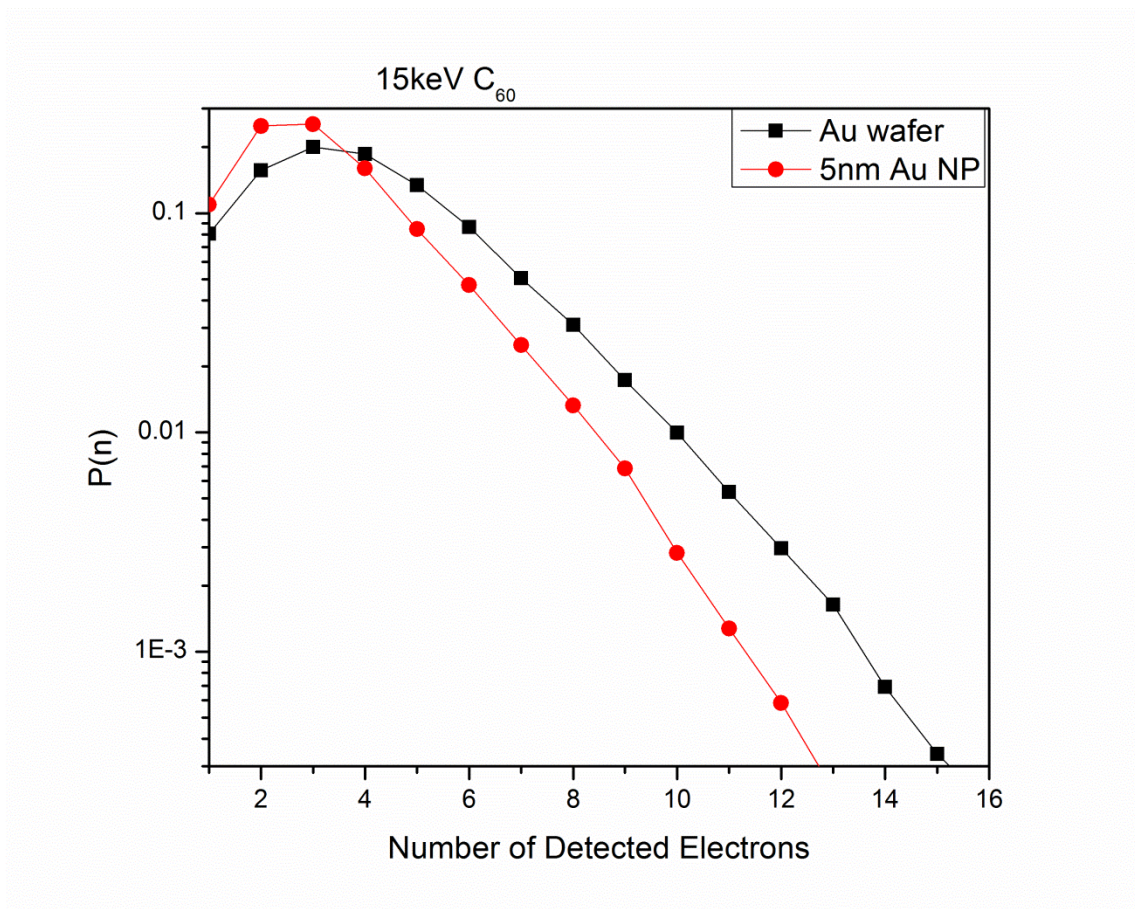


Figure 2.24 Measured Total Electron Distributions from 15keV C₆₀ Impacts on a Gold Coated Si Wafer and 5nm Gold Nano-Particles. In this figure the total electron distribution from 15keV C₆₀ impacts on the gold wafer are compared to the 5nm coated gold nano-particles.

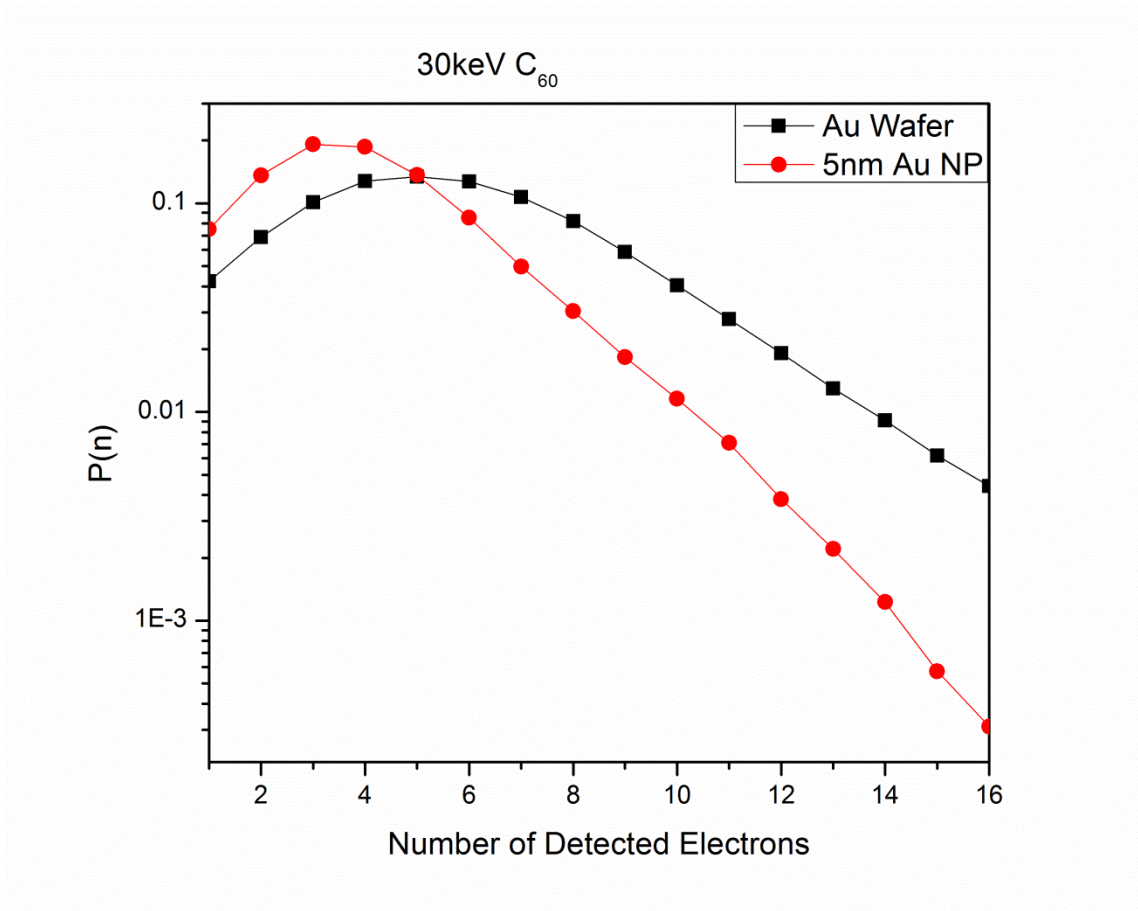


Figure 2.25 Measured Total Electron Distributions from 30keV C_{60} Impacts on a Gold Coated Si Wafer and 5nm Gold Nano-Particles. In this figure the total electron distribution from 30keV C_{60} impacts on the gold wafer are compared to the 5nm coated gold nano-particles.

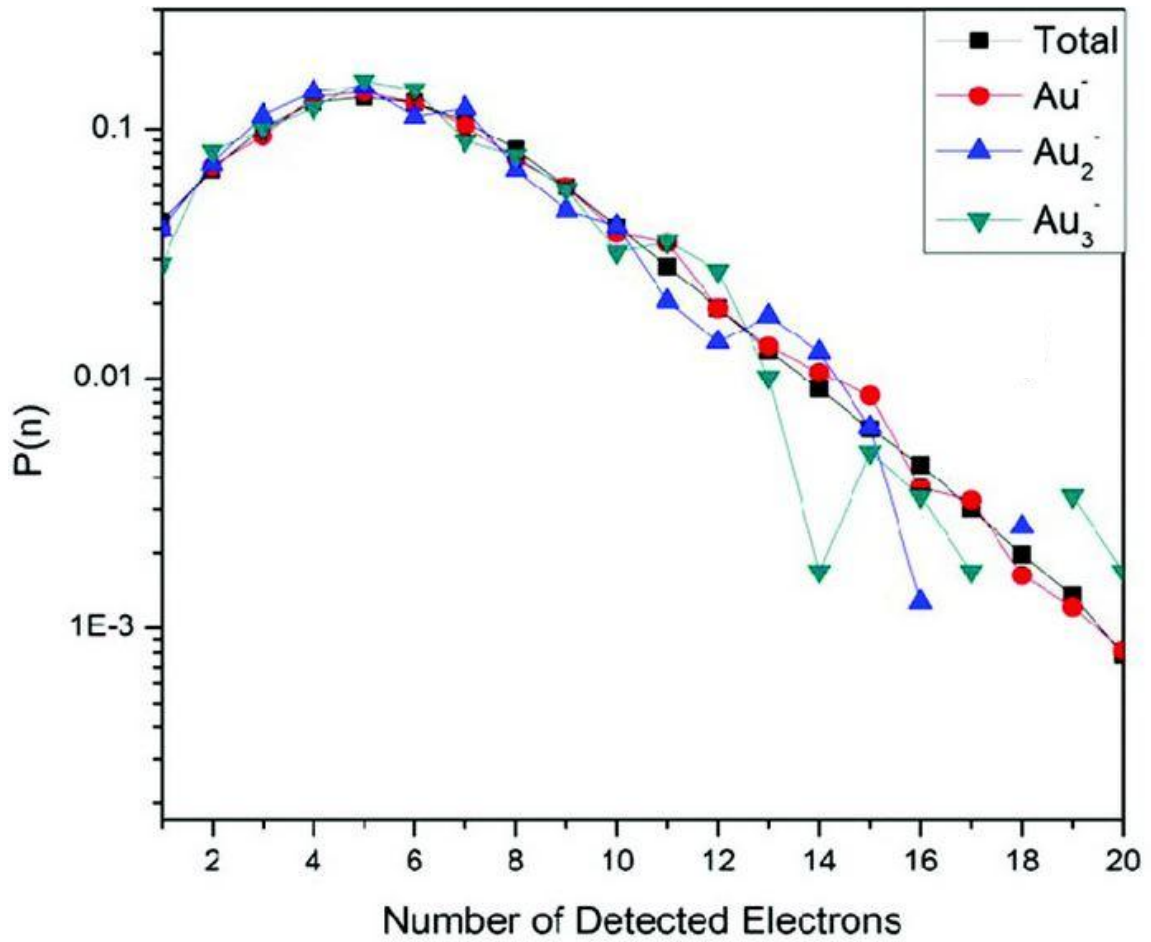


Figure 2.26 Measured Ion Specific Electron Distributions from 30keV C₆₀ Impacts on a Gold Coated Si Wafer. In this figure the ion specific electron distribution from 30keV C₆₀ impacts, for the selected ions Au⁻, Au₂⁻ and Au₃⁻ are compared to the total measured electron distribution.

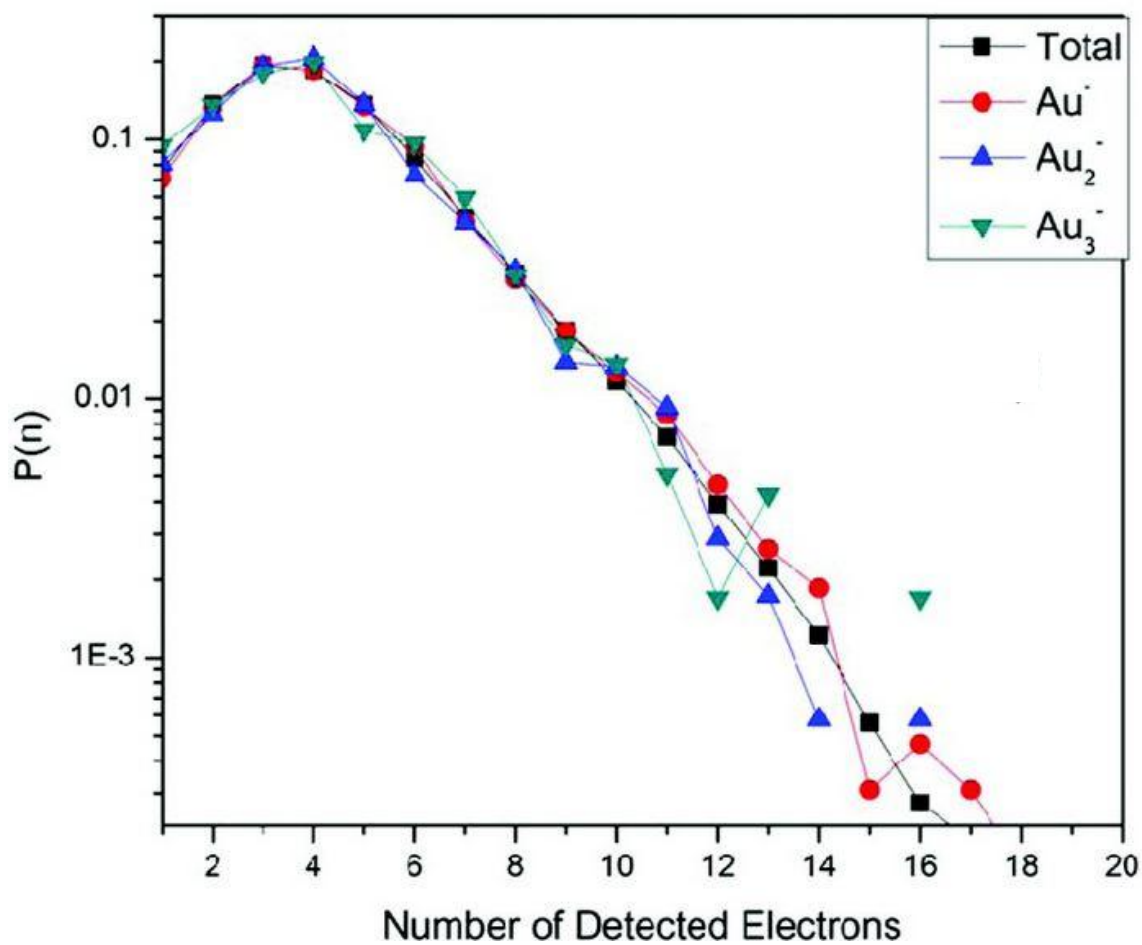


Figure 2.27 Measured Ion Specific Electron Distributions from 30keV C_{60} Impacts on 5 nm Gold Nano-Particles as a Multi-Layer. In this figure the ion specific electron distribution from 30keV C_{60} impacts, for the selected ions Au^- , Au_2^- and Au_3^- are compared to the total measured electron distribution.

Table 2.6 Total and Ion Specific Electron Yields from Au Samples Bombarded by C₆₀ at 15 or 30 keV.

e ⁻ /impact								
Sample	total	Au ⁻	Au ₂ ⁻	Au ₃ ⁻	CN ⁻	Au(CN) ₂ ⁻	(Gly-H) ⁻	(Gly ₂ -H) ⁻
Au Wafer 30 keV	5.9	6	5.7	5.9	NA	NA	NA	NA
5 nm Au NP 30 keV	3.9	4	3.9	3.9	NA	NA	NA	NA
Au Wafer 15 keV	3.9	3.9	4	4.1	NA	NA	NA	NA
5 nm Au NP 15 keV	3.1	3.2	3.1	3.1	NA	NA	NA	NA
5 nm Au NP on Gly 30 keV	3.9	3.9	4	3.9	3.9	3.9	3.9	3.9
5 nm Au NP on Gly 15 keV	3.1	3.1	3.2	NA	3.1	3.2	3.1	3.3

Table 2.7 Secondary Ion Yields from the Au Samples Bombarded by C₆₀ at 15 or 30 keV.

Yield						
Sample	Au ⁻	Au ₂ ⁻	Au ₃ ⁻	Au ₄ ⁻	Au ₅ ⁻	Au(CN) ₂ ⁻
Au wafer 30 keV	2.0×10^{-2}	9.0×10^{-3}	4.0×10^{-3}	-	-	-
5 nm Au NP 30 keV	5.4×10^{-2}	1.5×10^{-2}	9.0×10^{-3}	2.0×10^{-3}	2.0×10^{-3}	-
Au wafer 15 keV	1.0×10^{-2}	3.0×10^{-3}	1.0×10^{-3}	-	-	-
5 nm Au NP 15 keV	3.2×10^{-2}	8.0×10^{-3}	5.0×10^{-3}	1.0×10^{-3}	1.0×10^{-3}	-
5 nm Au NP on Gly 30 keV	8.0×10^{-3}	1.0×10^{-3}	1.0×10^{-3}	-	-	2.1×10^{-2}
5 nm Au NP on Gly 15 keV	3.0×10^{-3}	1.0×10^{-3}	-	-	-	1.2×10^{-2}

substrate. As a result, there is a lower emission of the Au^- and Au_n^- with the appearance of gold glycine adducts, $\text{Au}(\text{CN})_2^-$ (table 2.7).^[49, 54, 61]

Returning to the electron emission, we can examine its occurrence as a function of different types of impacts on Au NPs in multi-layers or in a single layer on glycine. In the latter case, we had a ~40% coverage of 5 nm Au NPs on glycine. The compilation of SIs in the event-by-event bombardment-detection mode allows us to identify “bulls-eye” impacts (emission of Au^- , Au_n^- , $\text{Au}(\text{CN})_2^-$), grazing impacts (emission of Au^- and AuS^- ; sulfur from the dodecanethiol), and impacts on open areas of glycine (emission of CN^- , molecular ions, and dimers of glycine). We tested the distinction of different types of impacts by computing a correlation coefficient.^[62] The parameter was calculated using equation 2.4.

Equation 2.4. $Q = \frac{Y_a * Y_b}{Y_{ab}}$ where Y_a is the yield of ion a, Y_b is the yield of ion b, and Y_{ab} is the coincidental yield of ion a with ion b

The correlation coefficient for coincidental emission of Au_n^- with AuS^- is ≤ 1 , confirming the distinction of direct projectile impacts on NPs versus grazing impacts (table 2.8).

The ion-specific electron distributions from the multilayer and the single-layer Au NPs show no differences. The effect of the projectile energy on the electron emission is shown for the two types of Au NP targets in figure 2.28. A more detailed examination of the electrons co-emitted with selected SIs is presented in figure 2.29. For

Table 2.8 Calculated Correlation Co-efficients from Impacts of 30keV C₆₀ on 5nm Gold Nano-Particles Deposited on Glycine.

Q	w/Au ⁻	w/AuS ⁻	w/Au ₂ ⁻
Au	1	0.96	0.55
AuS ⁻	0.96	1	0.64
Au ₂ ⁻	0.55	0.64	1
Au ₃ ⁻	0.63	0.84	0.53

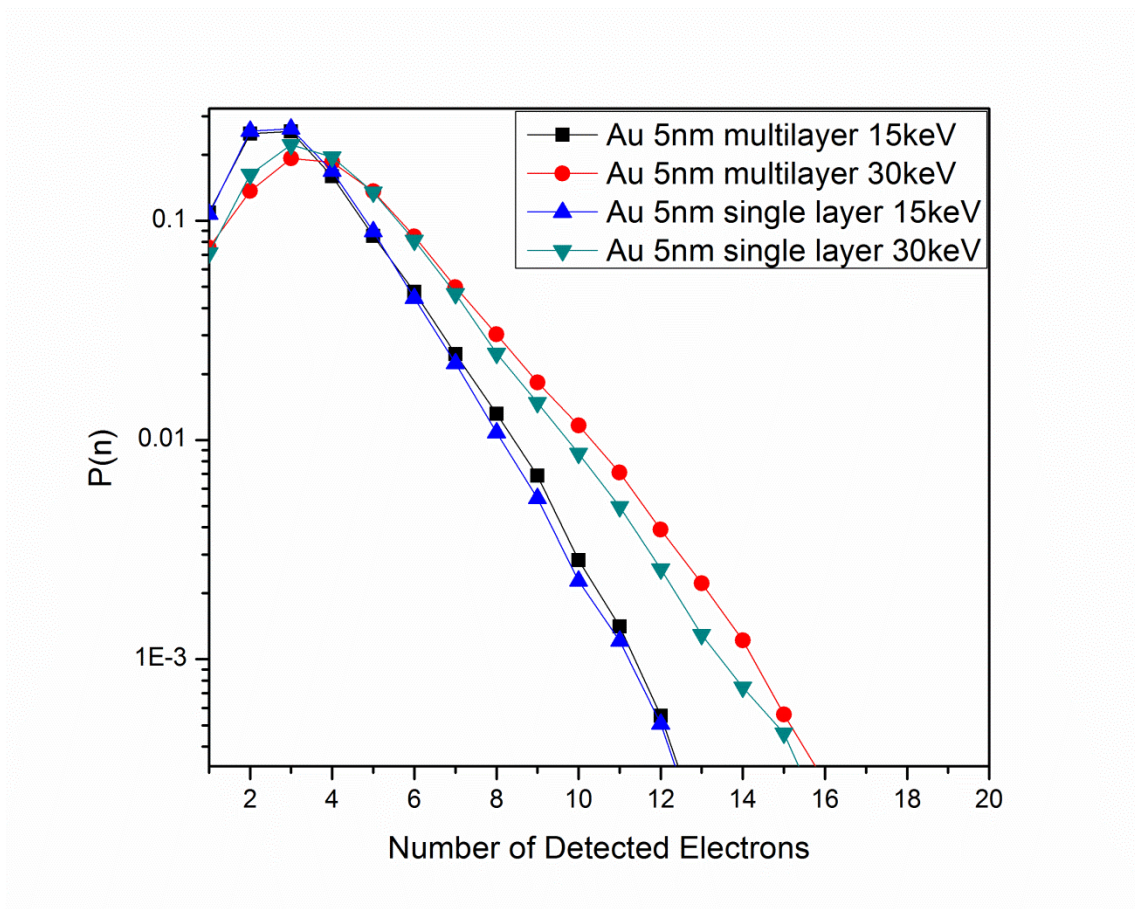


Figure 2.28 Measured Total Electron Distributions from 15 and 30keV C₆₀ Impacts on 5 nm Au NP as a Multi-Layer and a Single Layer. In this figure the total electron probability distributions from 5 nm Au NP as a multilayer and a single layer bombarded by C₆₀ at 15 and 30 keV. There are no significant differences between the single layer and the multilayer.

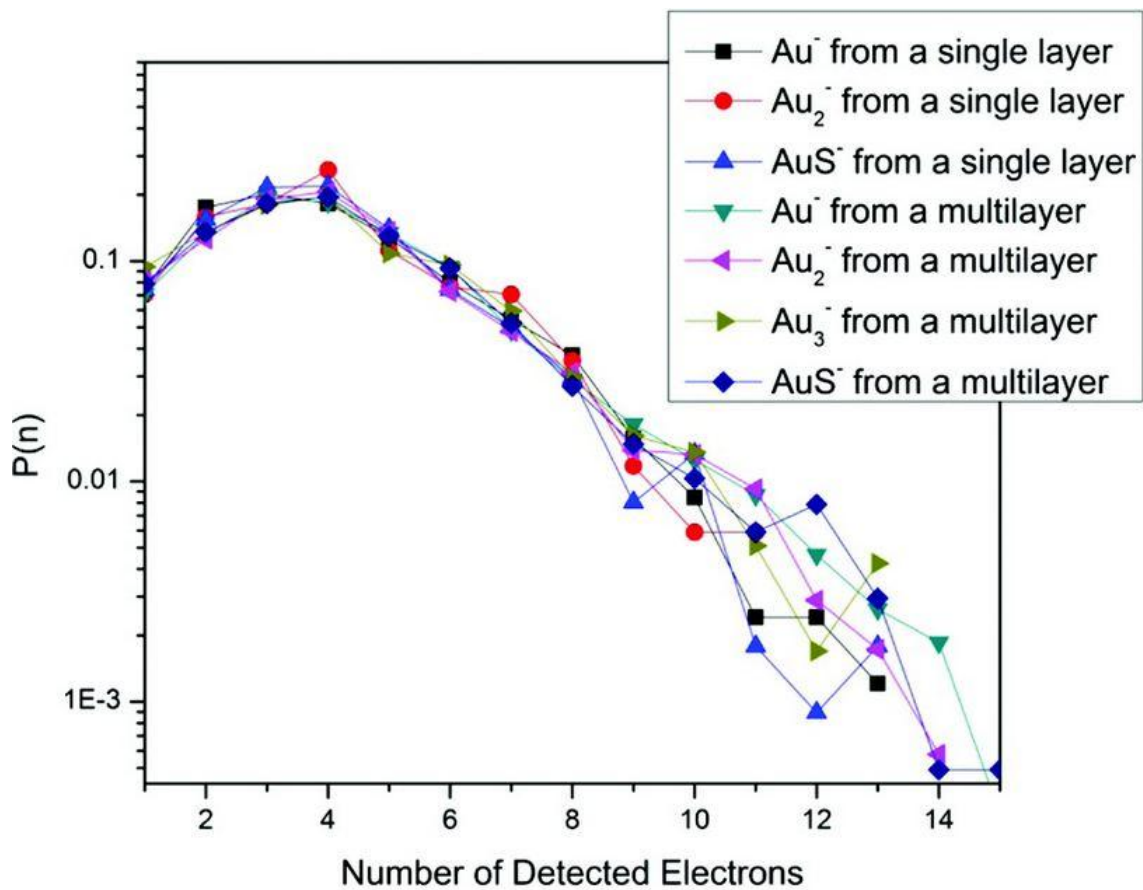


Figure 2.29 Measured Ion Specific Electron Distributions from a Multi-Layer and Single Layer of 5 nm Au NPs Bombarded by C_{60} at 30 keV. In this figure the ion specific electron distribution from 30keV C_{60} impacts, for the selected ions Au^- , Au_2^- and AuS^- are compared for a multilayer and a single layer.

both targets and for all cases, the electron probability distributions are identical. Indicating, the electron and ion emission from the nano particles are independent.

In Figure 2.30, a compilation of ion-specific electron probability distributions from the single layer of Au NPs on glycine. Each distribution is nearly identical to the total distribution. The electron distribution from neat glycine happens to be coincidentally identical to that from the 5 nm Au NPs, as indicated when comparing the data from neat glycine (figure 2.31) with that from Au NPs in a single or multilayer (Figure 2.29).

There is a notable difference in the electron emission yields from a flat bulk Au layer and multilayer of Au NPs. We attribute the lower yield from the Au NPs to fragmentation on impact and to their coverage with a monolayer of dodecanethiol. Indeed electron emission from organic surfaces is less abundant than emission from Au. A surprising observation concerns the electron emission from the single layer of Au NPs on glycine. Here the electron probability distributions correlated with Au_n^- emission resemble those from impacts on neat glycine.

Given the coincidentally similar electron yields from glycine and the 5 nm Au NPs, a new sample was prepared with an aluminum substrate. This sample was prepared similarly to the layer deposited on glycine. A solution of Au NPs was prepared with 0.5 mg/mL and 5 μ L of this solution was deposited onto an aluminum foil. The coverage of the nano-particles was determined to be ~30% using a coverage calculation.^[63] A mass spectrum from this sample can be found in figure 2.32. In the mass spectrum, emission from the aluminum foil (aluminum oxide clusters) and the Au NPs (Au_n^- and

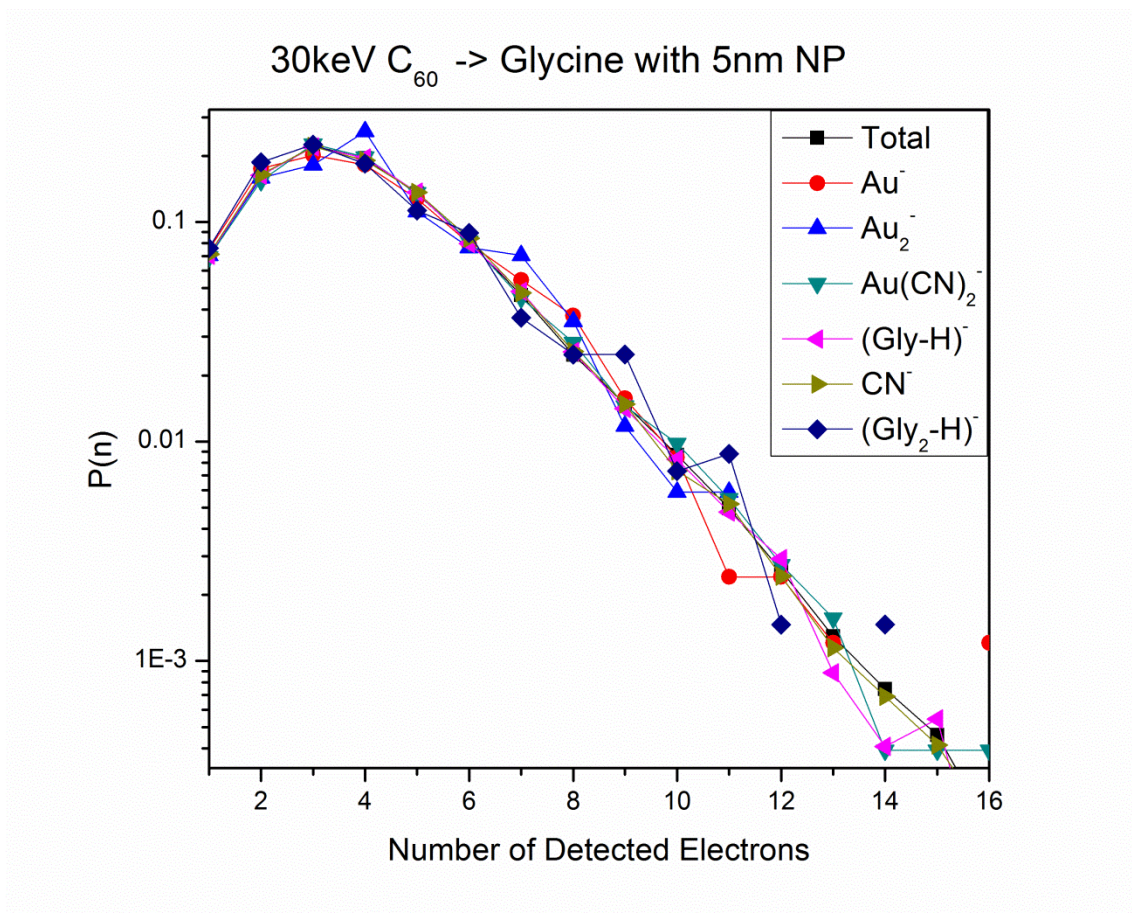


Figure 2.30 Measured Ion Specific Electron Distributions from a Single Layer of 5 nm Au NPs on Glycine Bombarded by C₆₀ at 30 keV. In this figure the ion specific electron distribution from 30keV C₆₀ impacts, for the selected ions Au⁻, Au₂⁻, Au(CN)₂⁻, (Gly-H)⁻, CN⁻ and (Gly₂-H)⁻ are compared to the total electron distribution measured.

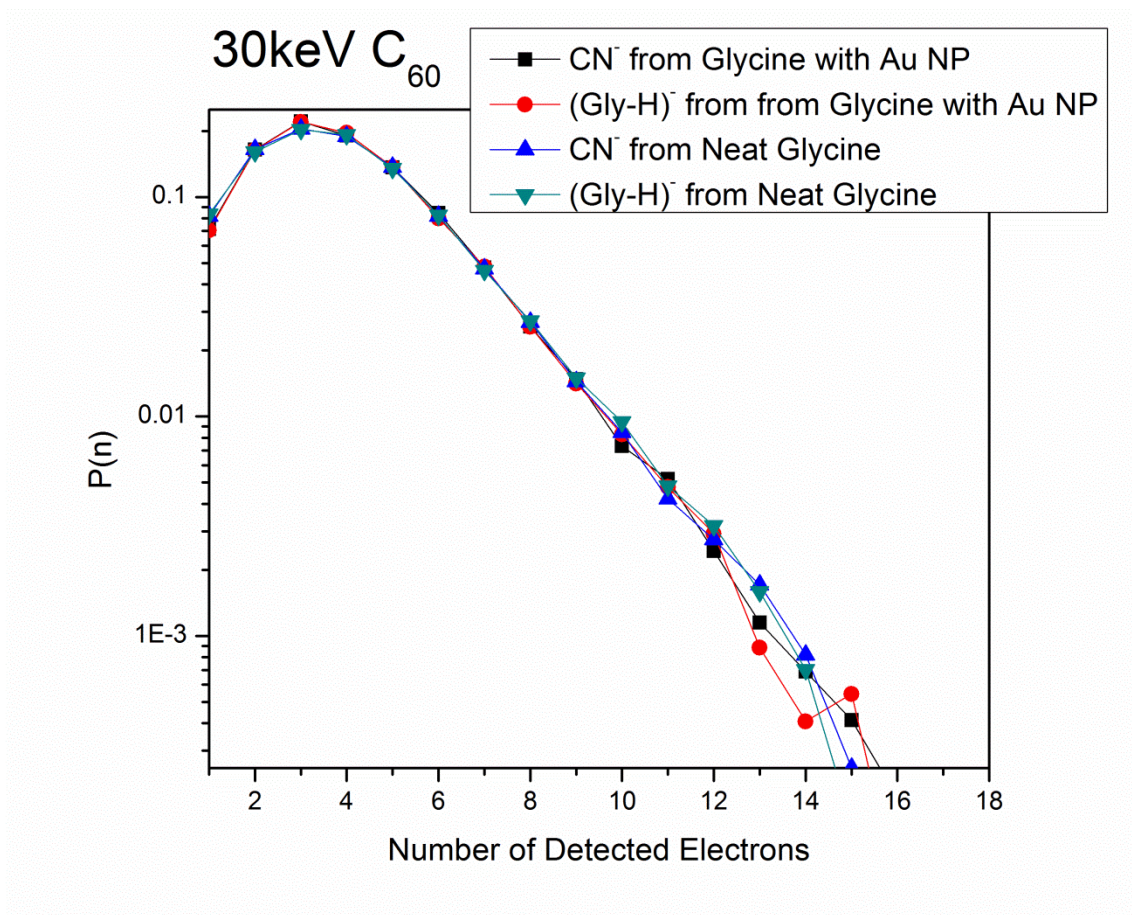


Figure 2.31 Comparison of Measured Ion Selected Electron Distributions from 30keV C₆₀ Impacts on 5nm Au Nano-Particles Deposited as a Single Layer on Glycine and a Neat Glycine Target. In this figure the ion specific electron distribution from 30keV C₆₀ impacts, for the selected ions CN⁻, (Gly-H)⁻ and AuS⁻ are compared for 5 nm Au NPs on glycine and a neat glycine sample bombarded by C₆₀ at 30 keV.

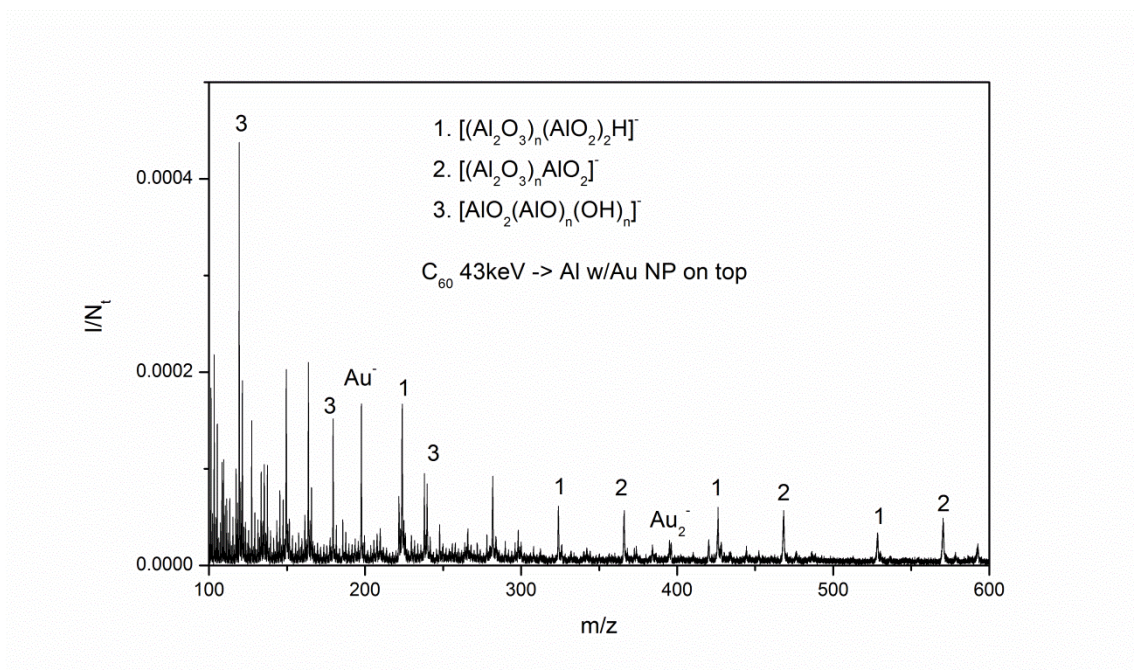


Figure 2.32 Mass Spectrum of 5nm Gold Nano-Particles Deposited on an Aluminum Foil Bombarded by 43keV C_{60} . Mass spectrum of aluminum foil with 5nm Au NPs deposited as a single layer bombarded by 43keV C_{60} .

Au_nS^-) can be observed. If a coincidence window is placed on Au^- , shown in figure 2.33, impacts on the Au particles only are selected. In figure 2.33 the emission of aluminum clusters can be observed. Indicating there are impacts where the SIs specific to the aluminum are emitted from impacts on Au NPs. Demonstrating there are Au NPs distributed as a single layer on the aluminum oxide surface.

In figure 2.34 the total electron probability distributions from 30keV C_{60} impacts on the multilayer of 5 nm Au NPs and the aluminum oxide are shown. The two have significantly different electron emissions. Therefore, impacts on the Au NPs may have different electron emission from impacts on the open aluminum oxide.

The ion selected probability distributions from the aluminum foil and 5nm NP assembly can be found in figure 2.35. The electron emission from impacts where aluminum clusters are detected has the same electron emission from impacts where Au^- and AuS^- are detected. Surprisingly, the electron emission from impacts on Au NPs is enhanced and as large as impacts on the aluminum foil. The aluminum foil electron emission dominates the observed electron emission. Kinetic electron emission is not the mechanism of electron emission observed here because, kinetic electrons emission arises from the initial atom-atom collisions between the projectile and the atoms on the surface. As Au atoms would be impacted first in the collision with Au NPs. The electron emission for those impacts would be similar to the electron emission observed from the multilayer of Au NPs. Instead, the electron emission observed is identical to that of the aluminum foil, indicating the substrate is involved in the electron emission.

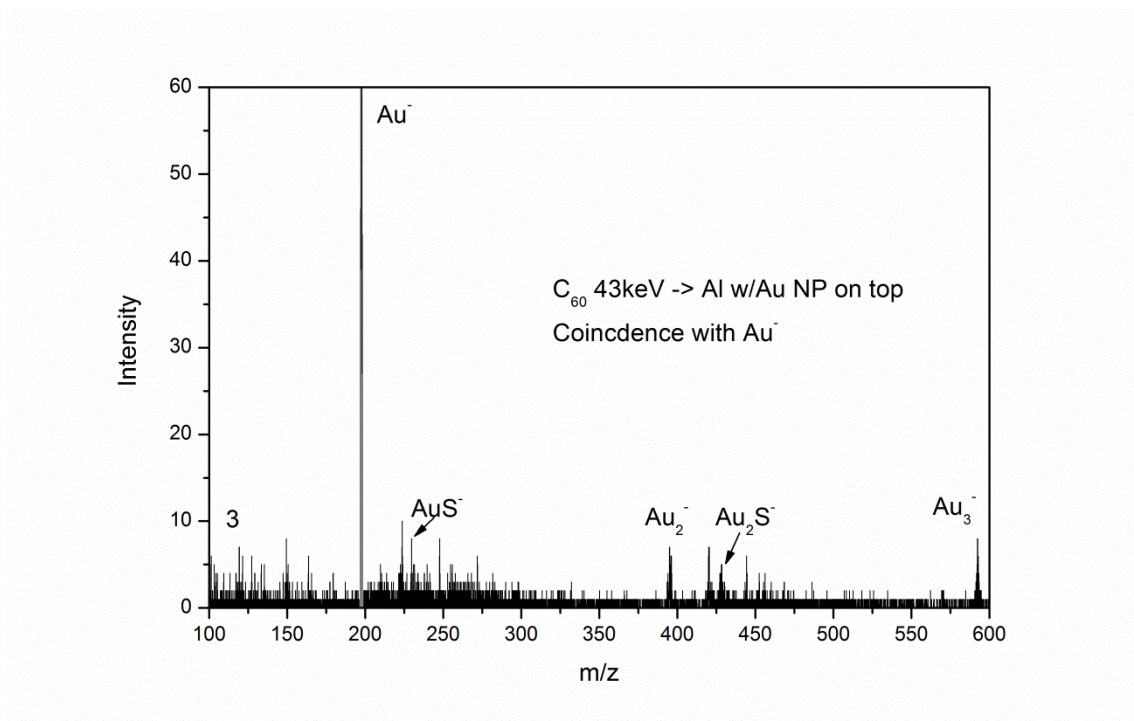


Figure 2.33 Coincidental Mass Spectrum of 5nm Gold Nano-Particles Deposited on an Aluminum Foil Bombarded by 43keV C₆₀. Mass spectrum of aluminum foil with 5nm Au NPs deposited as a single layer bombarded by 43keV C₆₀ where impacts on the Au NPs have been selected.

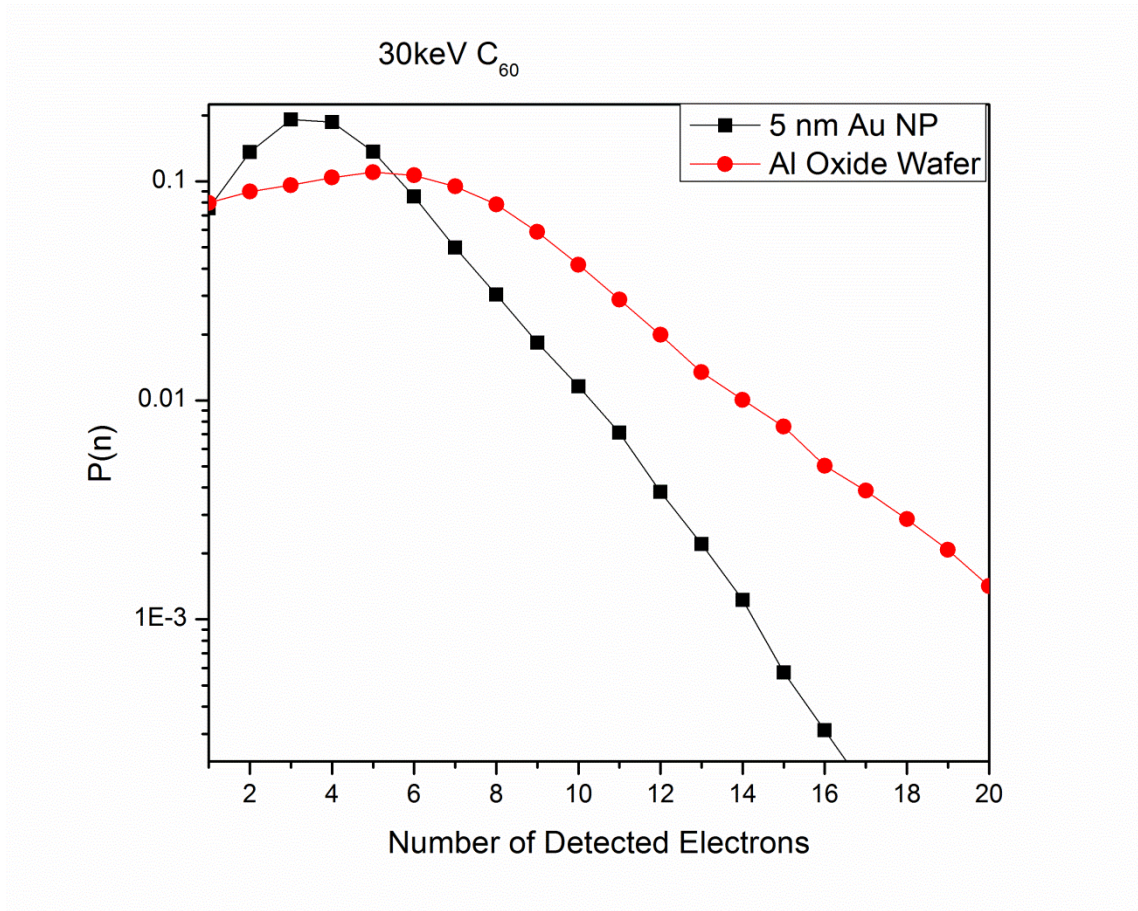


Figure 2.34 Measured Total Electron Distributions from 30keV C₆₀ Impacts on a Multi-Layer of 5nm Au Nano-Particles and Aluminum Oxide Coated Si Wafer. In this figure the total electron probability distributions from 5 nm Au NP as a multilayer and an aluminum oxide wafer by C₆₀ at 30 keV.

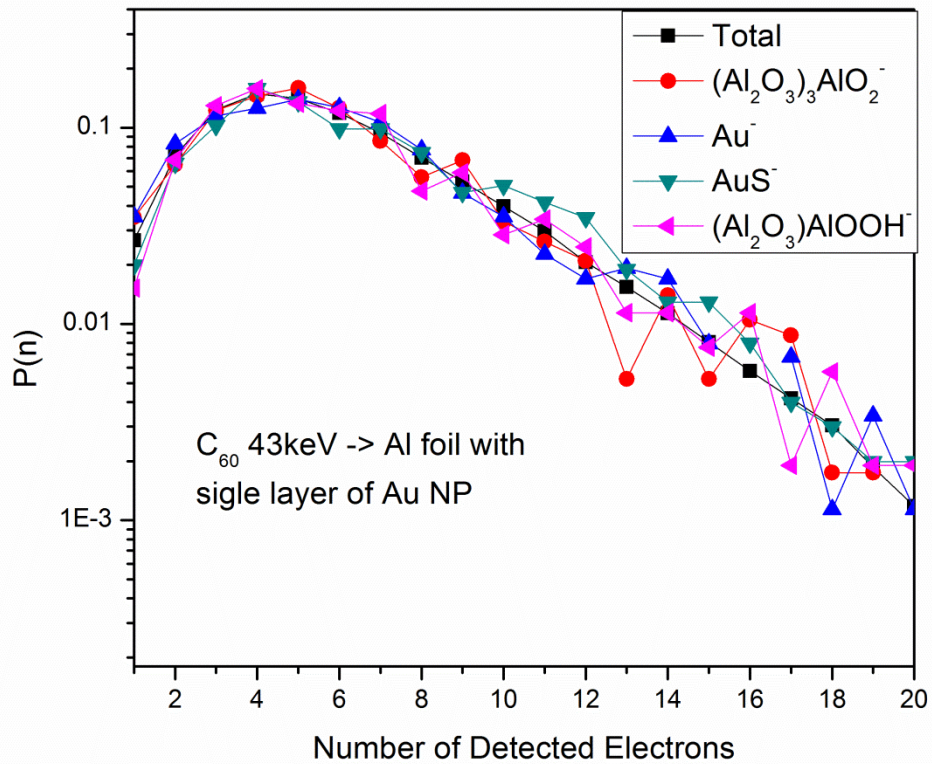


Figure 2.35 Measured Ion Selected Electron Distributions from 43keV C_{60} Impacts on a Multi-Layer of 5nm Au Nano-Particles and Aluminum Oxide Coated Si Wafer. In this figure the ion specific electron distribution from 43keV C_{60} impacts, for the selected ions Au^- , AuS^- , $(Al_2O_3)(AlO)OH^-$ and $(Al_2O_3)AlO_2^-$ are compared.

Electron emission from nano-objects is independent of the ion emitted but is dependent on the size and morphology of the sample. The electron emission decreases as the size of the nano-object decreases. In the case of C_{60} impacts on Au NPs deposited as a single layer, fragmentation of the NP takes place and energy is deposited into the substrate.^[60, 64, 65] In the case of a single layer of particles where the nano-object cannot fully contain the projectile impact, the electron emission observed is identical to that of the substrate. Indicating, that the electron emission may not originate from the initial atom-atom collisions on the surface, but a later time in the evolution of the collision cascade. What is the source of the electrons that are observed? At least a portion of the electrons observed may be the result of thermal electron emission.

Thermal electron emission from surfaces is a phenomenon which was first described by Richardson and Dushman.^[66-68] The thermal electron emission current can be calculated using the Richardson-Dushman equation. Thermal electron emission has been observed from a series of surfaces at or above $\sim 1000\text{K}$.^[69-72] These cases all exhibit electron emission from a bulk surface which is heated to high temperatures. In the case of ion bombardment in SIMS, a non-equilibrium situation occurs, where local excitation takes place. In SIMS a “thermal spike” is referred to for cluster bombardment on surfaces.^[73, 74] The thermal spike is calculated to be as high as $26,000\text{K}$, for cluster bombardment in SIMS, and the length of excitation is on the order of 10s of picoseconds.^[74, 75] Excitation of surfaces by a femtosecond laser pulse, which has a temperature of $\sim 11,000\text{K}$, has shown to generate thermionic electron emission.^[76] It is

therefore reasonable to deduce that the electron emission observed by bombardment of C_{60} at 15-50keV total impact energy is due, in part, to thermal electron emission.

3. SECONDARY ION MASS SPECTROMETER COUPLED TO AN ELECTRON EMISSION MICROSCOPE*

3.1 INTRODUCTION

The use of cluster projectiles in SIMS has been shown to greatly increase the yield of quasi-molecular ions.^[14, 15, 17-19, 77, 78] As mentioned in section 1, polyatomic projectiles display the “cluster effect”. Larger projectiles such as, coronene, SF₆, C₆₀, and Au₄₀₀ while not displaying super linear enhancement, still generate ion yields proportional to the number of projectile constituents. In the case of C₆₀ the simplicity of vaporization via an effusion source, as well as large mass, 720 daltons, has made it an ideal candidate for use as a primary ion.^[79] A SIMS instrument equipped with a C₆₀ effusion source coupled to an EEM operating in the bombardment detection mode is presented (figure 3.1).

Utilizing the event-by-event bombardment detection mode and synchronization method described in section 3.3 the data collected are collected concurrently. With this scheme the ions detected from a nano-metric volume can be related to a specific point on surface using the detected electrons. Matching the events (impacts) from both data sets results in a matrix of data that contains the position, electron and ion information from each impact. The data can then be investigated to generate ion specific maps, where

* Part of this section is reprinted with permission from “Real-time localization of single C₆₀ impacts with correlated secondary ion detection” by M. J. Eller, S. V. Verkhoturov, S. Della-Negra, R. D. Rickman, E. A. Schweikert, 2010. *Surface and Interface Analysis*, Copyright [2012] by John Wiley and Sons.

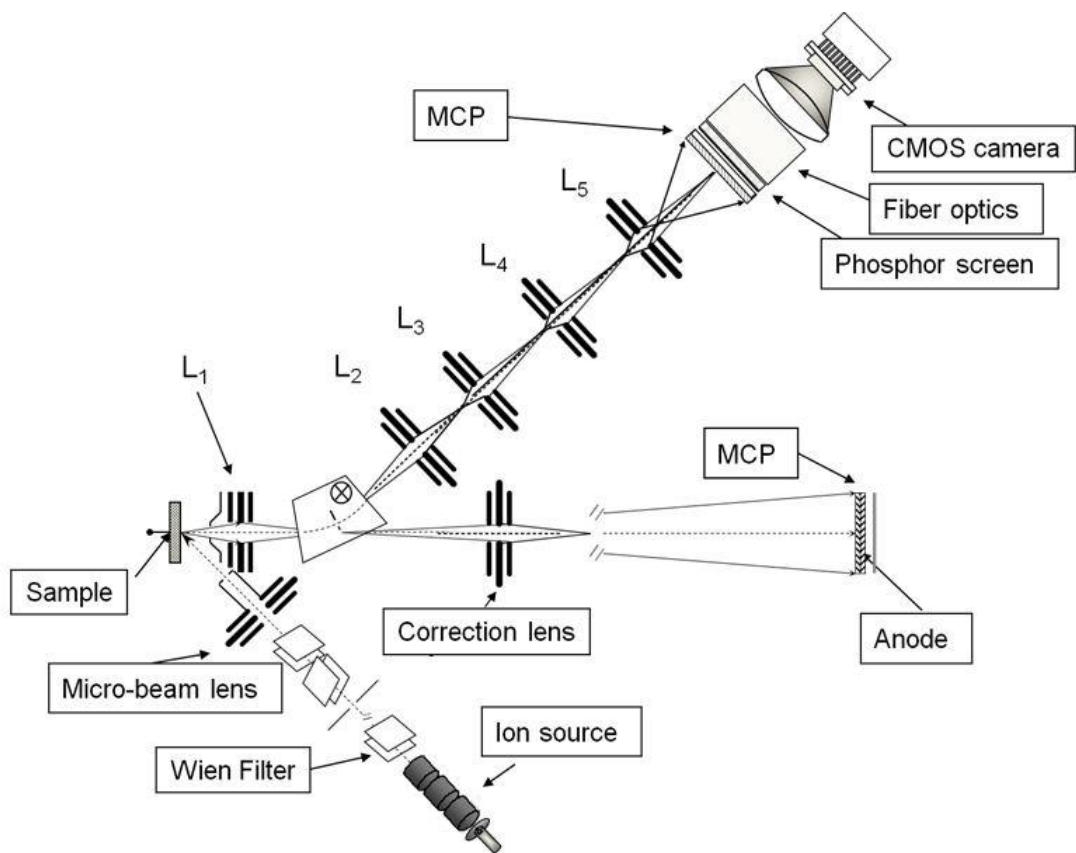


Figure 3.1 Schematic of the Custom Built Secondary Ion Mass Spectrometer. In this schematic, the source, the analysis, ToF and EEM regions can all be seen.

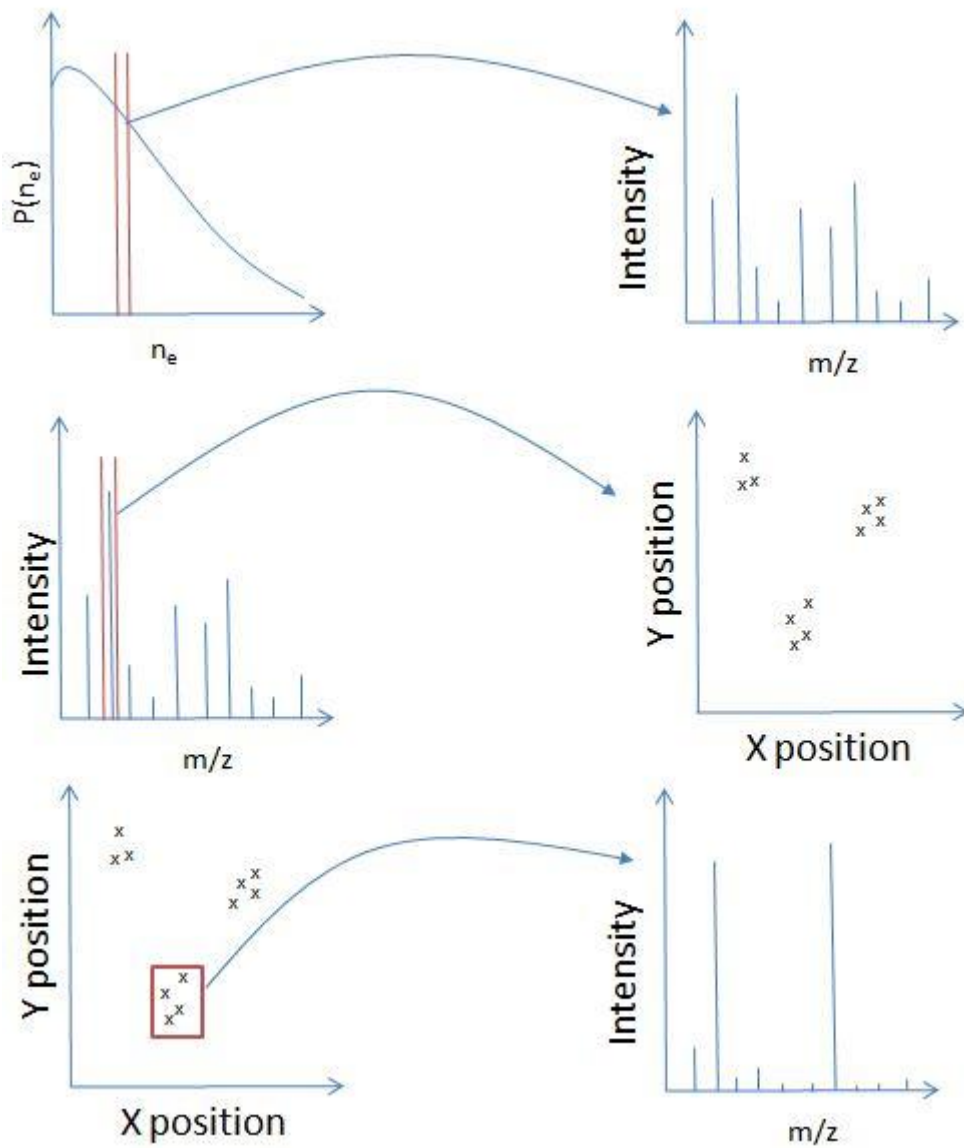


Figure 3.2 Data Analysis Examples. A cartoon of different types of data analysis which can be performed. The selection of data is shown on the left, the resulting data are shown on the right.

positions of events containing an ion of interest can be plotted (figure 3.2). The relationship between electron emission and ion emission can be investigated (discussed in sections 2.3 and 2.4) by selecting an ion of interest and graphing the number of emitted electrons. The reverse case can be studied where a particular number of electrons can be selected and the corresponding mass spectrum for those impacts spectrum can be graphed. The section below describes the hardware synchronization, and software setup for acquisition.

3.2 C₆₀ SOURCE AND MASS SPECTROMETER

The C₆₀ source is a custom built device which contains a C₆₀ effusion source, electrostatic lens, two pairs of deflector plates, and a Wien filter. The effusion source, (seen in figure 3.3) is composed of a Cu reservoir that can hold up to 0.5g of C₆₀ powder. The reservoir is heated to above 600K (the sublimation temperature of C₆₀) the resulting sublimated C₆₀ escapes the reservoir through a small nozzle (~500μm in diameter). The escaping C₆₀ enters the ionization region of the source which is comprised of a heated Ta disc, and repelling electrode. The Ta disc emits electrons that are accelerated to 150eV. The repelling electrode is biased to -153V which repels any electrons which do not interact with a C₆₀ molecule, and directs them back towards the nozzle. The use of this repelling electrode increases the cross section for ionization of the C₆₀. The 150eV electrons strike the C₆₀ and ionize it to C₆₀^{+,2+,3+} by electron impact ionization. The resulting ionized C₆₀ is accelerated toward an electrostatic lens by a potential difference of -7kV applied between the heater and an extraction plate. The C₆₀^{q+} is further

accelerated up to 15qkeV before reaching the electrostatic lens. A procedure for setting up and shutting down the C₆₀ effusion source can be found in appendix A.

The electrostatic lens and pair of deflectors focuses and steers the beam of C₆₀ from the source into the Wien filter. The Wien filter is comprised of a magnetic field, electric field, and small aperture which function as a velocity filter for the primary ions generated by the source (see equation 3.1).^[80] The Wien filter acts as a mass analyzer, because all projectiles will have the same acceleration energy (15qkeV), but different velocities. The Wien filter has a base line mass resolution of ~10 which is sufficient to resolve C₆₀⁺ from C₆₀²⁺(see figure 3.4). After mass selection the beam of C₆₀ is focused to an area ranging 20µm-0.2mm by an electrostatic lens and steered toward the target using a pair of deflectors. By using the source described a beam of C₆₀⁺²⁺ with ~100,000 impacts per second can be generated with a spot size of ~20µm. Typically, the instrument is operated in the event by event bombardment detection mode at a bombardment rate of <1000 impacts per second.

Equation 3.1: $V = k * \sqrt{\frac{K_e}{M}}$, where V is the potential in volts applied to the

Wien filter, k is an empirically determined constant, and M is the mass of the projectile and K_e is the kinetic energy of the projectile.

The mass analysis of emitted negative SIs from a C₆₀ impact is accomplished using a linear ToF mass spectrometer. The ions generated from an impact are accelerated by a potential difference of +10kV. The 10keV ions are accepted and focused by an einzel lens into the center of a magnetic prism which steers the emitted

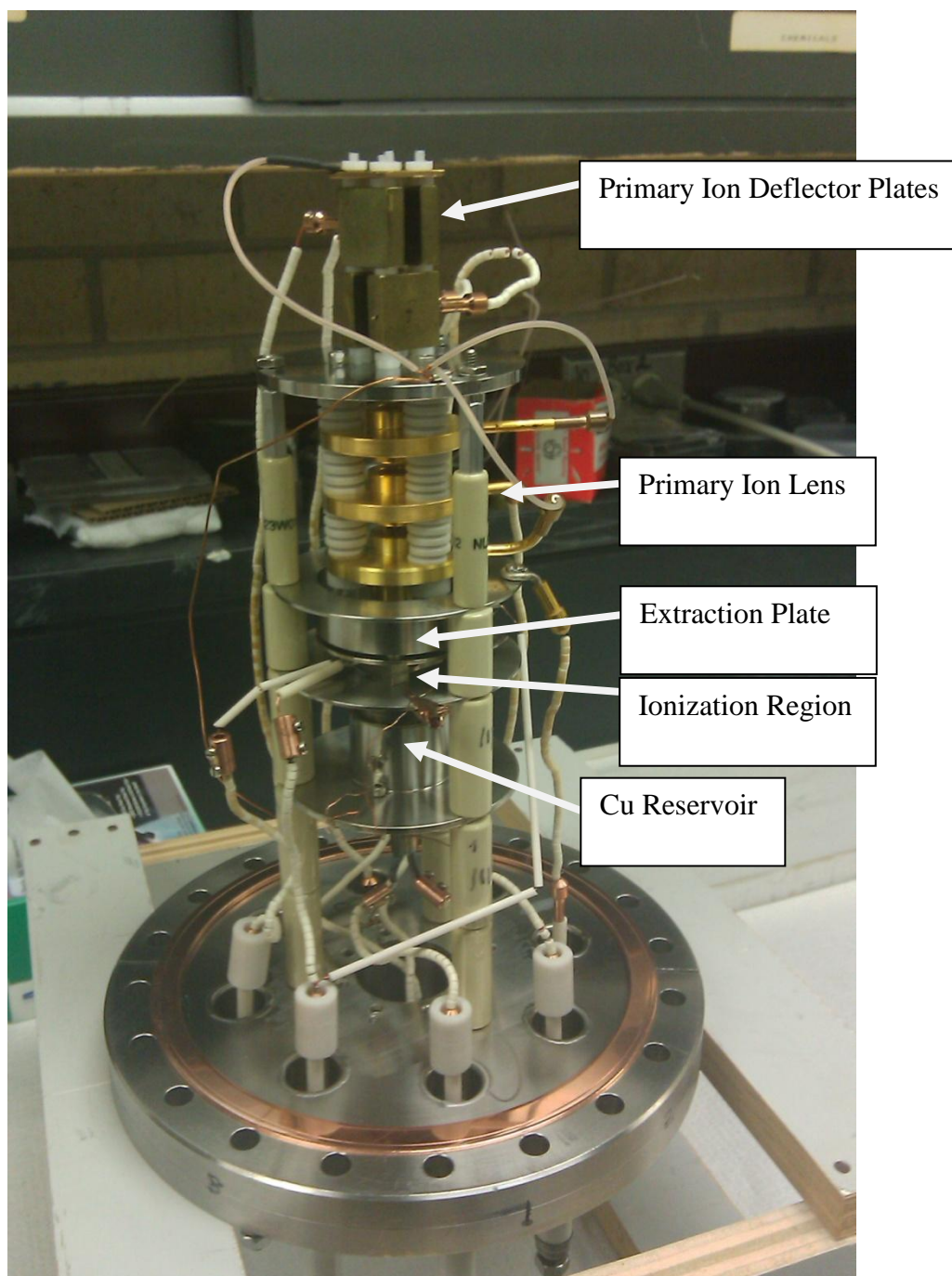


Figure 3.3 Picture of C₆₀ Effusion Source. A picture of the C₆₀ effusion source used in these studies. The entire length of the source is ~27cm.

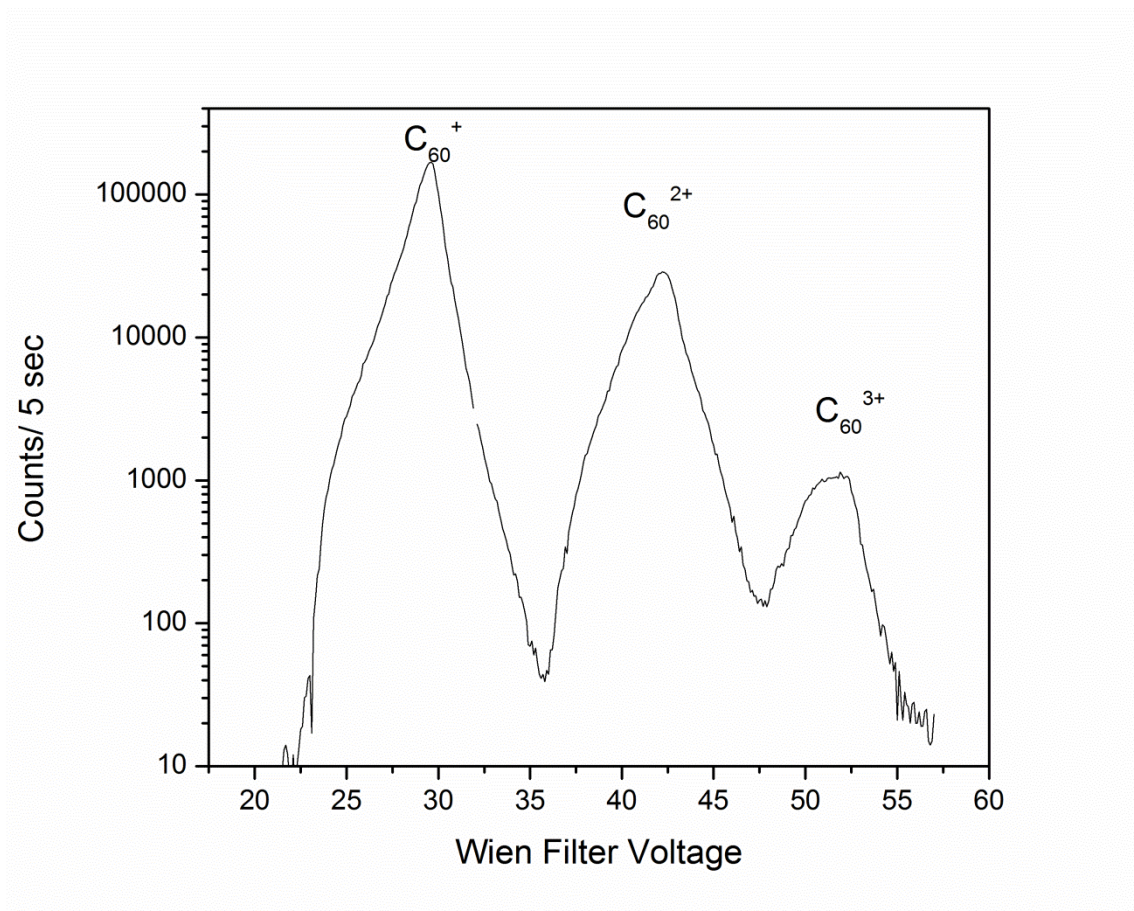


Figure 3.4 Wien Filter Separation of C₆₀ Projectiles. The counts per second as a function of the voltage applied in the Wien filter, shows clear separation of C₆₀⁺, C₆₀²⁺ and C₆₀³⁺.

electrons toward the EEM detector. The magnetic field is weak, $\sim 10^{-3}$ tesla, thus the 10keV SIs are relatively unperturbed as they pass by through the magnet. The intermediate image of secondary ions is accepted by a second lens, which is used for correcting the angle of the ions (non-imaging mode). The ions pass the secondary ion optics and enter the ToF region (1m) and are detected by the 8 anode MCP detector.^[28]

The detector is composed of a pair of microchannel plates, MCP, from Photonis (Merignac, France) in the chevron configuration and an 8 anode detector. The resulting voltage spike from the burst of electrons striking an anode is sent to a constant fraction discriminator, CFD, CF 8000 from Ortec (Oak Ridge, TN, USA) and recorded by a time-to-digital converter, TDC, CTNM4 from Institut de Physique Nucléaire d'Orsay (Orsay, France).

3.3 HARDWARE INTEGRATION

The methodology for coupling the EEM to a SIMS instrument is accomplished with an original scheme. The scheme involves a suite of hardware and software solutions, in this section the techniques used for hardware integration are detailed, the software solutions are detailed in section 3.4.

As previously described the SIs and electrons are detected in separate detectors. The emitted electrons are detected with the EEM, while the SIs are collected by a ToF mass spectrometer equipped with a MCP based detector. All mass spectra obtained with the integrated EEM and SIMS instrument are collected in negative ion mode. As the

emitted electrons have much larger velocities, their detection is used as the start of the ToF measurement and camera collection.

In this section different types of logic signals are employed. Nuclear Instrumentation Module, NIM, is one such example. The pulse logic for NIM is defined as a pulse of -0.8V or more negative is logical “true”, while -0.7V and more positive is logical “false”. A second logic used is Transistor Transistor Logic, TTL. The pulse logic for TTL is defined as a pulse of +2.2V to +5.0V is logical “true”, and 0 to 0.8V is considered logical “false”.

A description of the timing and pulse sequence for the measurement follows and a graphical depiction can be found in figures 3.5-3.6. Upon exiting the MCP assembly, the multiplied electrons strike the aluminized phosphor screen. The resulting voltage pulse is discriminated by a CFD and which outputs a NIM pulse of -0.8V with a length of 100ns. This NIM pulse is sent to a pulse generator which outputs a TTL pulse of +3.0V with a length of 4ms. The TTL pulse is split with one pulse sent to a second pulse generator (referred to as the timing pulse generator) and the second to the fast CMOS camera. The fast CMOS camera operating in master mode begins acquiring the frame ~1.6 μ s after receiving the TTL pulse. Once the acquisition of the frame is started, the camera outputs a TTL pulse of +3.0V with a length of 1ms (corresponding to the camera exposure time) which triggers slave modules (TDC, timing pulse generator). The exposure time of the frame is 1ms to allow for collection of light from the phosphor. The timing pulse generator, outputs a TTL pulse of +3.0V with a length of 100ns which is delayed 1.7 μ s.

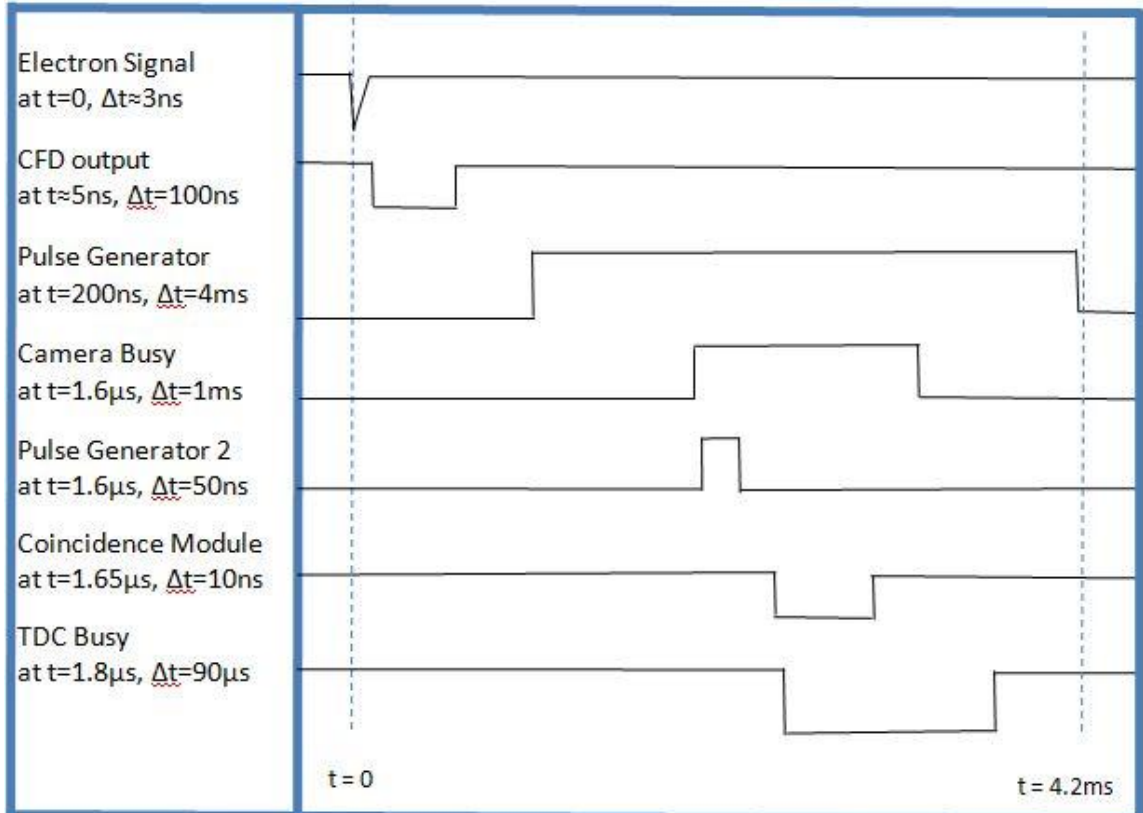


Figure 3.5 Timing Sequence. The timing sequence for synchronizing electron and ion collection in the event-by-event mode.

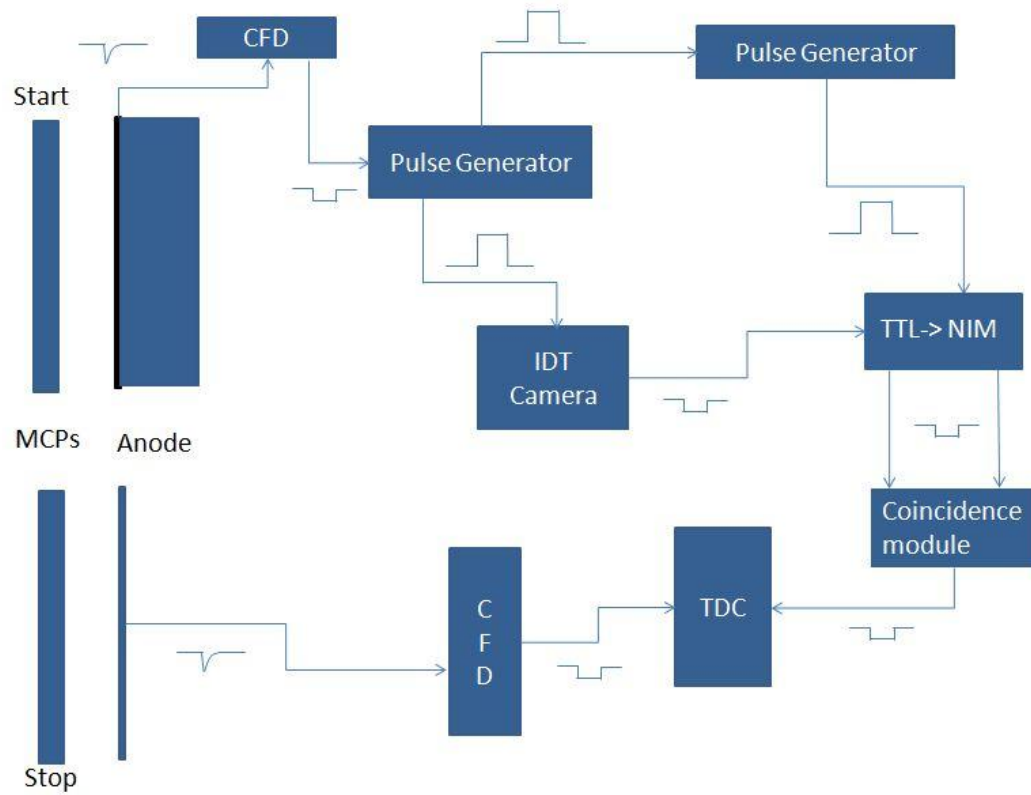


Figure 3.6 Pulse Sequence. A pictorial depiction of the pulse sequence for hardware triggering in the event-by-event mode.

After the camera and timing pulse generator have each generated a TTL pulse, the two pulses are sent to a TTL->NIM level logic translator model 688AL, LeCroy Corporation (Chestnut Ridge, NY, USA). This module converts the TTL pulses to NIM pulses. The resulting NIM signals are inputted into a coincidence module, model 465 triple 4-fold logic unit from the LeCroy Corporation. If both pulses arrive within a given time window the coincidence module outputs a NIM signal. The time window is defined by the length of the first pulse accepted by the module. The coincidence module is used to ensure that the camera has successfully initialized before starting the TDC, as well as removing the jitter of the camera output. The jitter in the camera output arises from differences in the initiation time of the pixels (~40ns). The TDC is then initialized with a variable time window (ranging from .6 μ s to 13ms) and a fixed time resolution of 400ps/channel, for the experiments described here the time window was set to ~90 μ s.

To acquire, analyze, and process the data in the experiment an overall software solution was developed comprising custom routines and a fast camera program provided by IDT. The latter (Motion Studio 2.10.04) operated the camera, the acquisition of frames and the saving of images. The TDC acquisition software was written in house using National Instruments Lab Windows Version 7.5 (National Instruments Inc.).

The acquisition software interfaces with the TDC module through a high speed digital IO card, NI PCI-6533 from National Instruments Inc. The images collected by the camera are saved through a Camera Link® frame grabber, NI PCI-1428 from National Instruments Inc.

3.4 SOFTWARE INTEGRATION

The integration of EEM with the SIMS instrument is achieved in the most part by hardware integration, discussed in section 3.3. However, essential features for the integrated operation are accomplished via a series of software solutions. Particularly the acquisition of both the EEM and SIMS data are done by the software.

As is mentioned in section 3.3 the camera operates as the master, in the master-slave configuration, and the TDC operates in the slave mode. This is not the case for the software integration. Instead each module (camera and TDC) operates independently of each other. Additionally, each module is collected by a separate computer.

The rationale for keeping the software acquisition separate is to reduce jitter in data collection. Jitter is described as uncertainty in the initiation time. Our tests have shown that the jitter can be as high as 200ns for the computer setup employed here. A jitter of 200ns could significantly harm the mass resolution of the system, by increasing the width of peaks by up to 10X, with a proportional decrease (1/10) in mass resolution. The issue of jitter and simplicity of independent software solutions for each module prompted the use of separate software.

The software for acquisition with the TDC is described in section 5.2. An identical acquisition system for collecting the mass spectrum is used for experiments with the EEM. The software for saving images collected by the camera is accomplished with a complete software kit (Motion Studio 2.10.04) provided by Integrated Design Tools INC. (Tallahassee, FL. USA). The Motion Studio software has a wide range of camera controls including, background correction, exposure time, triggering mode, gain,

contrast, pixel binning, recording tools (number of frames collected), gamma correction, filters (sharpening, smoothing), and region of interest (ROI).

As discussed in the hardware integration section (3.3), the camera is triggered by a 4ms TTL pulse. To ensure the camera is triggered properly specific settings in the software must be enabled. In the triggering mode setup, the camera is set to external triggering. The pulse type accepted is set to “edge high”, which is a positive pulse and ensures the camera is triggered on the leading edge of the pulse. The exposure is configured for “internal exposure”, this allows the exposure time to be set by the software instead of being defined by the trigger pulse length (4ms).

The procedure for properly setting up the camera can be found in appendix B. This appendix includes the settings for the various camera controls as well as a troubleshooting guide.

During the acquisition images are saved as an uncompressed AVI file containing up to 100,000 individual frames. If more than 100,000 frames need to be collected, the software saves the acquired frames and begins acquiring the next 100,000 frames. The collected frames are processed off-line using an in-house written program utilizing image processing functions Vision Assistant version 8.2.1 (National Instruments Inc), a full description of which can be found in the localization section (section 4.1).

4. LOCALIZATION^{*+}

4.1 INTRODUCTION

In SIMS there are different methodologies for generating maps or images of surfaces. The most common approach is the microprobe approach, which employs a focused ion beam and scans the focused beam across the surface.^[81] In the microprobe method, the resolution of the image is constrained by the size of the beam. In some cases the resolution that can be achieved is on the order of tens of nms.^[5, 10, 82] Those cases employ a beam of atoms which given the source characteristics, can be focused to very small diameters. However, given the low SI yields generated by atomic projectiles, the focused beams must be applied in high intensity resulting in emission limited to atomic ions and small molecular fragments (e.g. CN). Alternatively, a polyatomic ion such as Bi_3^+ can be used to increase SI yields. However, polyatomic sources cannot be focused as tightly as an atomic beam, in this case (Au_3^+ or Bi_3^+) spatial resolutions of $\sim 100\text{nm}$ have been reported.^[83, 84] The use of large clusters, e.g. C_{60} , has increased SI yields significantly over atomic and polyatomic projectiles. The application of such large clusters to the microprobe methodology has yielded spatial resolutions at $\sim 1\mu\text{m}$.^[85]

* Part of this section is reprinted with permission from “Simultaneous detection and localization of secondary ions and electrons from single large cluster impacts” by M. J. Eller, S. V. Verkhoturov, F. A. Fernandez-Lima, J. D. DeBord, E. A. Schweikert, S. Della-Negra, 2012. *Surface and Interface Analysis*, Copyright [2012] by John Wiley and Sons.

+ Part of this section is reprinted with permission from “Real-time localization of single C_{60} impacts with correlated secondary ion detection” by M. J. Eller, S. V. Verkhoturov, S. Della-Negra, R. D. Rickman, E. A. Schweikert, 2010. *Surface and Interface Analysis*, Copyright [2012] by John Wiley and Sons.

An alternate approach is the ion microscope method. In the ion microscope mode ions from the impact are imaged and assigned locations. The intrinsic advantage of the ion microscope mode is that the resolution of the image is no longer tied to the size of the analysis beam. The resolution is instead determined by the properties of the emitted species, (e.g. radial velocities, energies) and the performance of the microscope. There are multiple approaches for detection, including delay line detectors and pixilated detectors. One application with a delay line detector using C_{60} at the primary ion showed a spatial resolution of $\sim 4\mu\text{m}$.^[86] The use of a “TimePix” detector is an alternative approach for obtaining the location and arrival times of a detected ion.^[87] In this case a resolution of $\sim 8\mu\text{m}$ has been observed. A different approach is presented in section 4.2 in which the emitted electrons are used to localize the projectile impact. The use of electrons to localize MeV atomic projectiles has been shown previously.^[88] The work presented here, demonstrates for the first time, the ability to localize the impact sites of individual cluster ions via electron emission microscopy.

4.2 SOFTWARE METHODOLOGIES

Each projectile impact is localized using the image of simultaneously emitted/detected electrons. As discussed in section 3.4 each electron image is collected by the camera. Collected images are stored sequentially on a PC in the form of an audio video interleave, avi, file. This avi file is investigated one frame at a time using image recognition software. The image recognition software was developed in house. This

software is part of the SAMPI analysis software and utilizes functions provided by National Instruments Inc. and is written in C.

The image recognition software processes the frames by first converting the image to a logical image using the “local threshold with background correction” function, this function assigns bright areas of the frame as a logical 1 and dark areas as a 0. A raw image can be found in figure 4.1. The border of the frame is then removed using the “remove border objects” function, this often the edges of the frame tend to be brighter than the center of the frame and thus may lead to false signals. A processed image is shown in figure 4.2 in this figure the detected electrons can be clearly seen. The frame is then analyzed for the detected electrons by the “Find Circles” function, which identifies circles of radii greater than three pixels. The “Find Circles” function also records the (X,Y) positions of the detected circles. From these circle coordinates the impact can be localized using a custom algorithm; a description follows.

Initially, if a frame shows at least 5 electrons, a provisional center of mass is computed from the emitted electrons. An example of the provisional center of mass can be seen in figure 4.3. Electrons whose distance from the center of mass is greater than the limit set in the software collimation, are excluded from the center of mass calculation by an iterative process. An initial region of interest, ROI, is placed 200 pixels from the center of mass, any electrons detected outside of this area are removed. In the example in figure 4.4 an ROI is represented by a red circle and an electron impact to be removed is seen. After the electrons outside the ROI are removed, a center of mass is recalculated

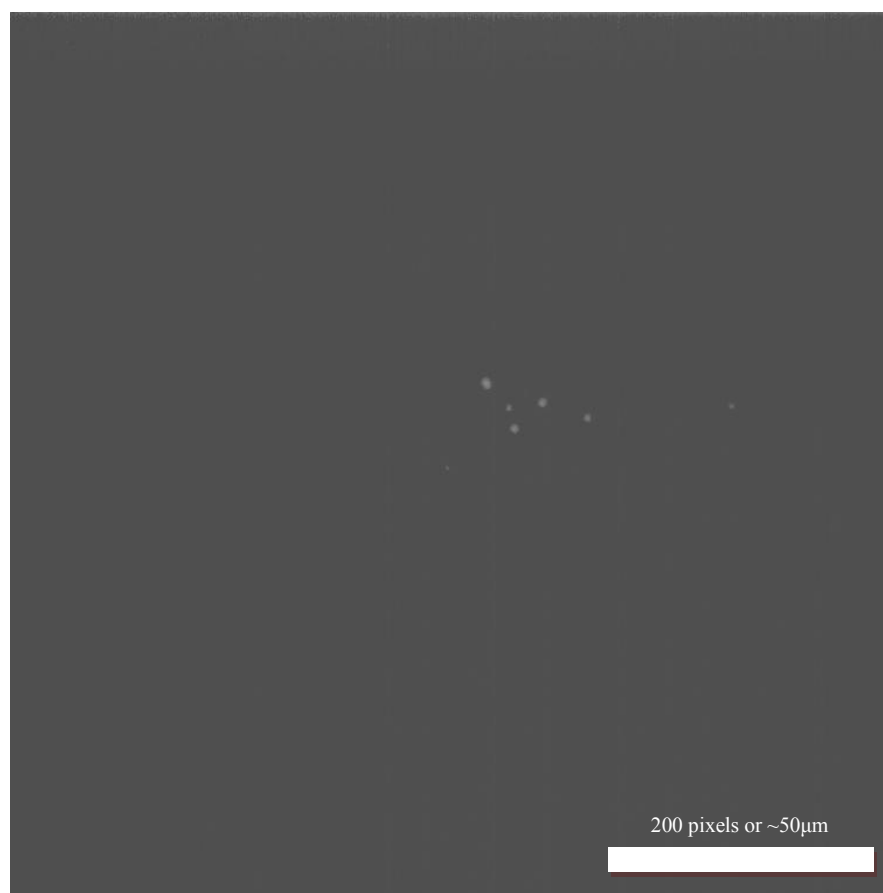


Figure 4.1 Raw Image. The raw image of the detected electrons from a single 30keV C_{60}^{2+} impact on CsI. Magnification $\sim 100x$.

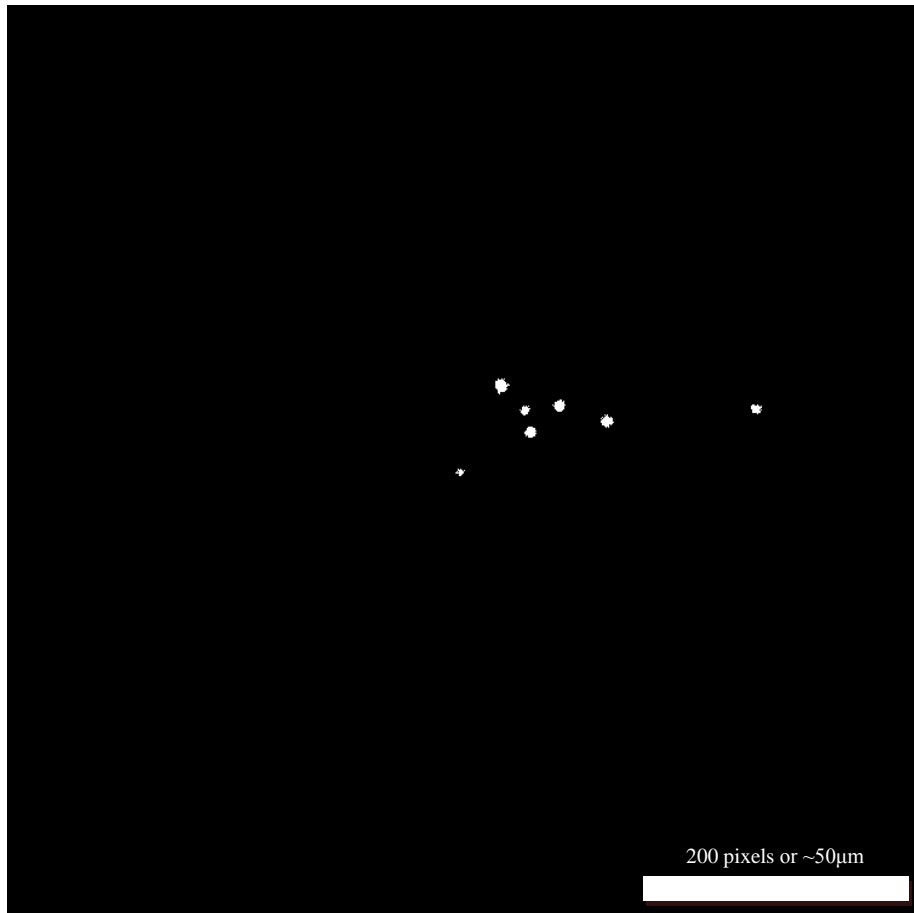


Figure 4.2 Processed Image. The processed image of the detected electrons from a single 30keV C_{60}^{2+} impact on CsI. Magnification $\sim 100x$.

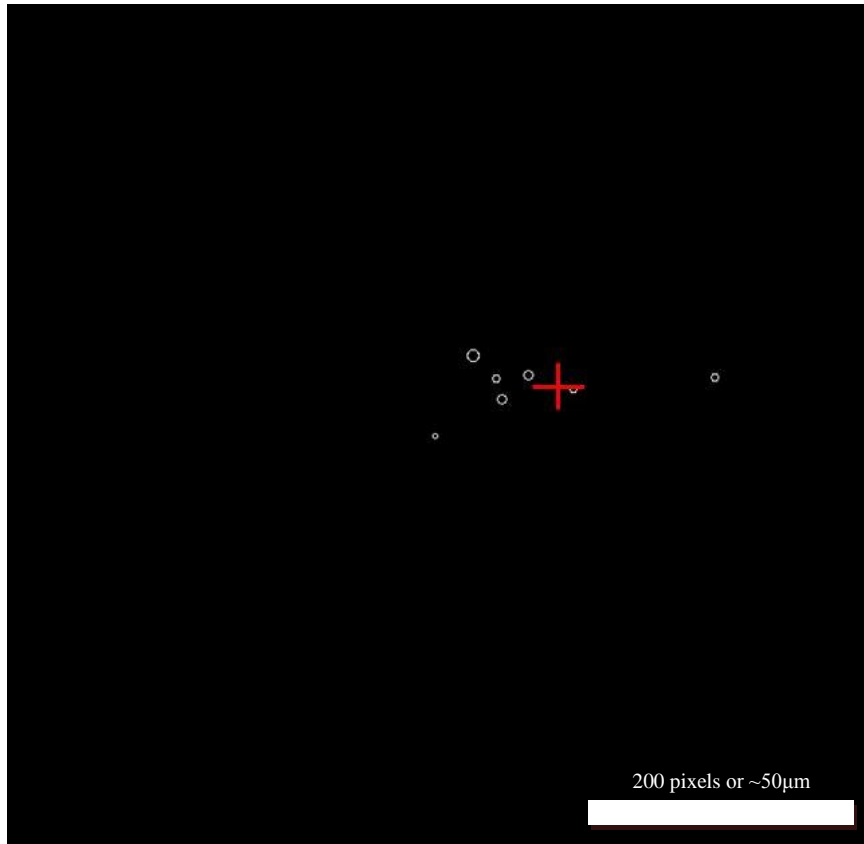


Figure 4.3 Processed Image with Center of Mass. The processed image of the detected electrons from a single 30keV C_{60}^{2+} impact on CsI with corresponding provincial center of mass, shown by a red cross. Magnification $\sim 100x$.

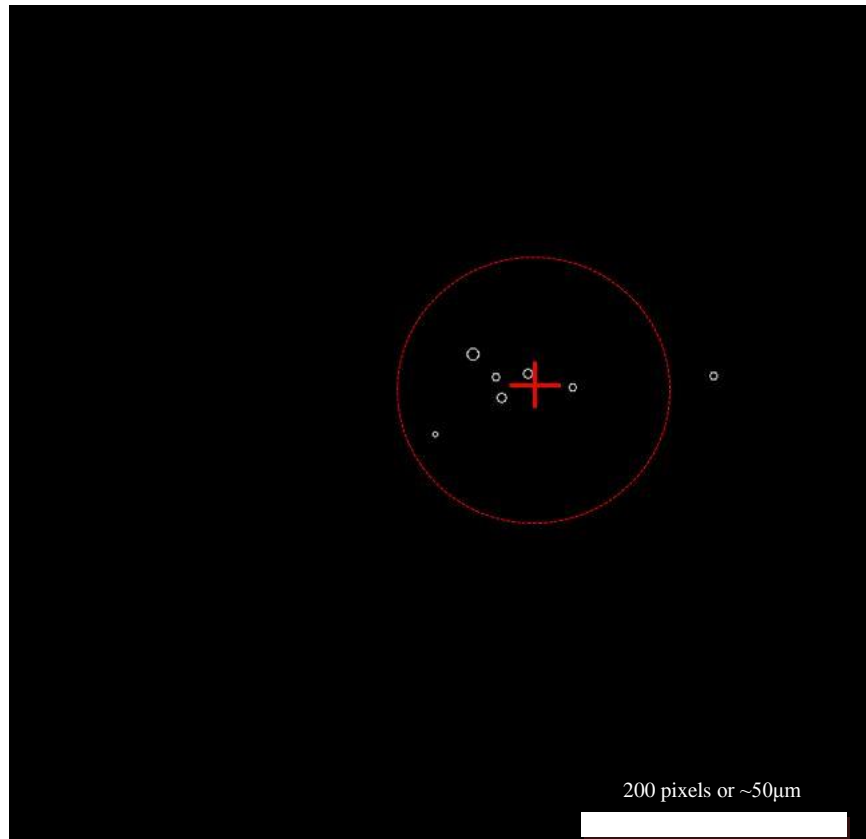


Figure 4.4 Processed Image Center of Mass with Region Of Interest. The processed image of the detected electrons from a single 30keV C_{60}^{2+} impact on CsI with corresponding center of mass, shown by a red cross, and region of interest (red circle). Magnification $\sim 100x$.

using the remaining electrons. A second collimation is performed with the ROI placed 100 pixels from the second center of mass. Electrons outside of the ROI are removed, and if after this final collimation ≥ 4 electrons remain within the ROI, a new center of mass is calculated with the remaining electrons (figure 4.5). The coordinates of the center of mass calculation were used to assign the site of a C_{60} projectile impact. By removing dispersed electrons, a reduction in the error of localization was observed which is further discussed in the resolution section (section 4.4).

To generate ion selected maps, and calculate ion selected electron distributions, the data are loaded by the SAMPI software in several steps. First, a list of events with the number of electrons detected in each impact are loaded, referred to as the “cirstat” data, an example can be found in table 4.1. Second, the “allcircles (including more than 1 cir)” data are loaded, these data contain the (X,Y) coordinates of each electron, along with the area and radius of the spot on the detector (table 4.2). Third, the calculated center of masses (centroid file) are loaded see table 4.3. After all the electron data have been loaded, the mass spectrum which was concurrently collected is loaded by the software (see section 3.1-3). The impact position, number of electrons, electron positions and mass spectrum all are paired to the event number. Therefore by selecting an ion of interest, the position and number of electrons detected along with that ion are known.

Ion selected electron distributions are covered more in sections 2.3-2.4, they consist of a histogram of the number of electrons detected when an ion of interest is



Figure 4.5 Processed Image with Impact Coordinates. The processed image of the detected electrons from a single 30keV C_{60}^{2+} impact on CsI with corresponding impact coordinates shown by a red cross. Magnification $\sim 100x$.

Table 4.1 Cirstat File. This shows the file structure of the “cirstat” file, which contains the frame, and number of detected electrons.

Frame	Number of Detected Electrons
0	3
1	0
2	3
3	3
4	1
5	0
6	0
7	1
8	2
9	3
10	3
11	2
12	1
13	2
14	3
15	0
16	2
17	0

Table 4.2 Allcircles File. This shows the file structure of the “allcircles (including more than 1 cir)” file, which contains the frame and coordinates of each electron.

Frame	X Position	Y Position
0	152	473
0	246	564
0	377	657
2	331	537
2	327	540
2	215	687
3	350	277
3	378	368
3	345	376
4	254	282
7	695	404
8	123	342
8	427	398
9	198	419
9	185	431
9	566	576
10	398	391
10	277	429
10	453	555
11	247	262
11	470	343
12	215	219

Table 4.3 Center of Mass File. This shows the file structure of the “centroid” file, which contains, the frame, number of detected electrons and the (X,Y) position the impact was detected at in pixels.

Frame	X Position	Y Position	Number of Detected Electrons
34	240	265	6
38	206	376	6
44	448	330	5
45	382	378	6
48	476	313	6
65	645	550	5
68	637	551	11
78	480	339	9
107	353	607	10
116	371	343	5
118	505	413	5
132	398	351	5
133	83	510	11
149	339	148	6
162	209	427	5
165	544	343	8
169	218	332	5
186	577	524	5
224	539	595	6

presented in figure 4.6, a brief written explanation follows. From the main mass spectrum, an ion of interest is selected (the procedure can be found in appendix C). As mentioned in section 5.1, the data are stored as individual events. Each event is examined for the ion of interest. A scan is performed with a series of “if clauses” which investigates each ion detected in an event and determines if it was detected in the time window selected. If the ion desired is found, that corresponding event is located in the cirstat file, and the number of detected electrons are recorded. This process is repeated until all events have been investigated.

Ion Selected Maps (single ion): Ion selected maps show the location (X,Y) an ion of interest. A logic chart of how ion selected maps are calculated is presented in figure 4.7, a brief written explanation follows. From the main mass spectrum, an ion of interest is selected. If the ion desired is found, that corresponding event is located in the centroid file, and the position of the impact site is recorded. This process is repeated until all events have been investigated.

Two-Ion Selected Electron Distributions are plots which show the number of detected electrons when two selected ions are detected in the same event. The calculation is essentially a double coincidence (section 5.3) where the number of electrons is investigated rather than the co-emitted ions. Two ion selected electron distributions can give additional information for surface characterization, such as surface inhomogenities discussed in section 2.3.

Ion Selected Electron Distribution

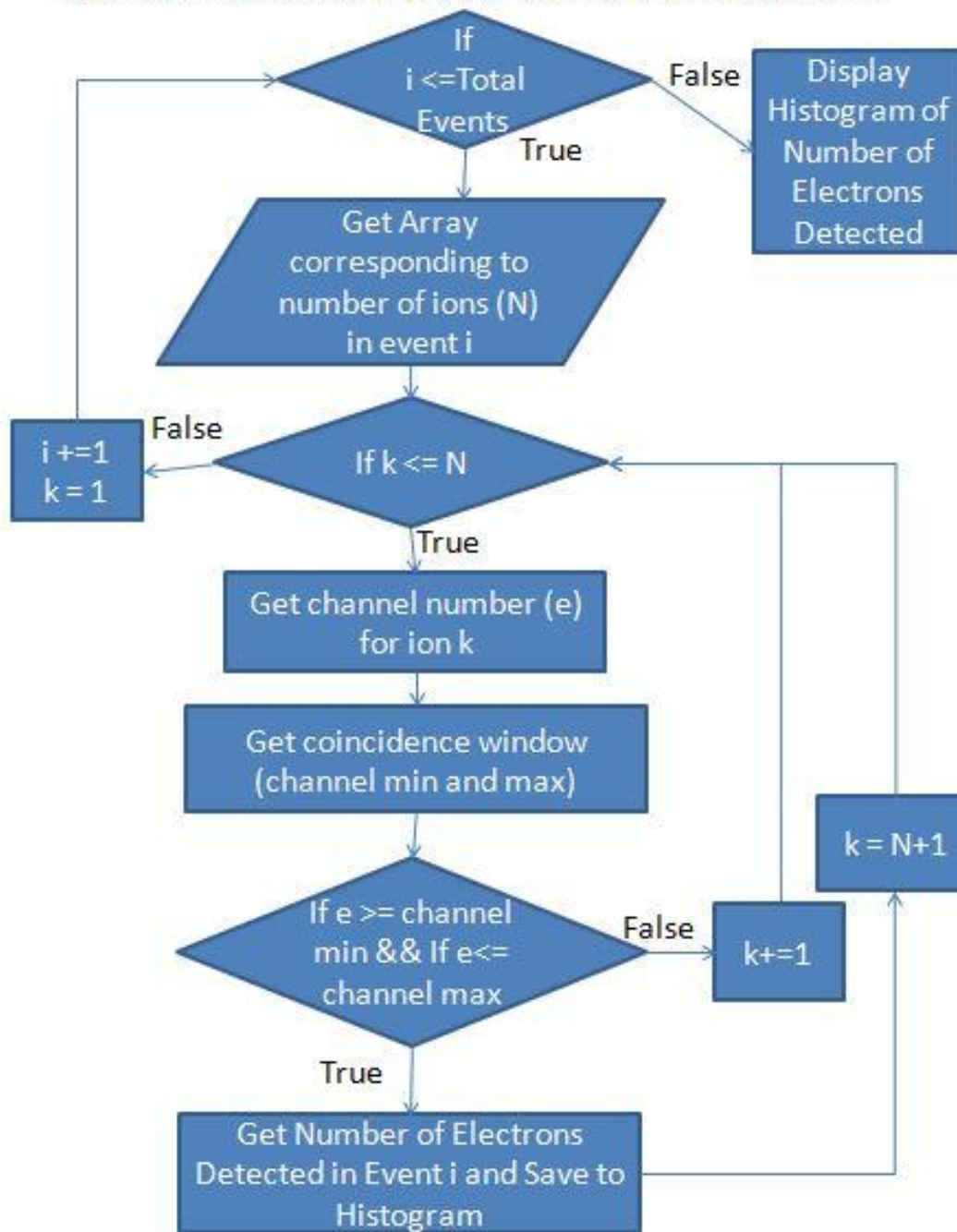


Figure 4.6 Ion Selected Electron Distribution Logic Tree. Logic tree for the ion selected electron distribution calculation.

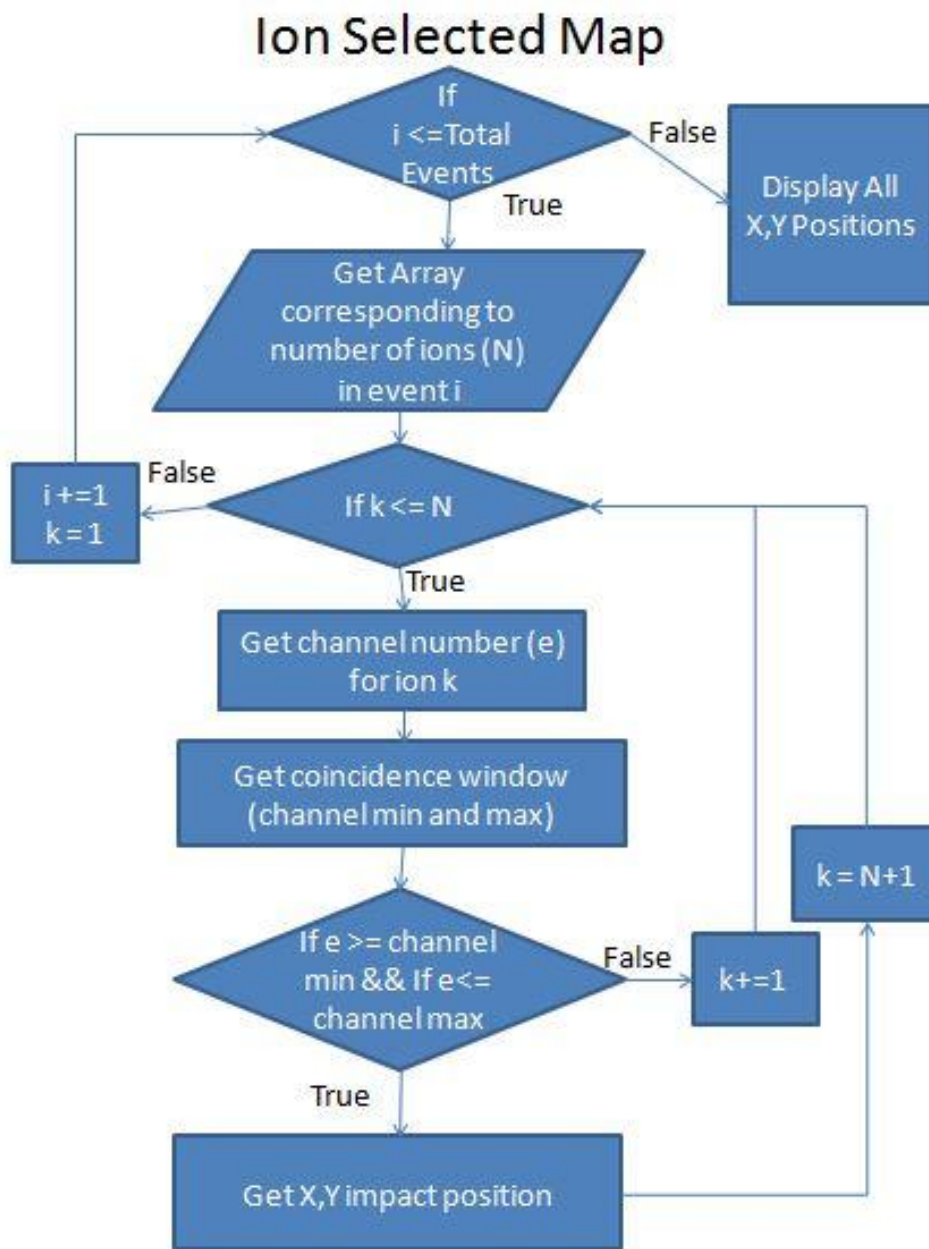


Figure 4.7 Ion Selected Electron Map Logic Tree. Logic tree for the ion selected electron map calculation.

The two ion selected electron distribution logic tree can be found in figures 4.8-4.9. A brief description of this calculation follows, from the main mass spectrum two ions of interest are selected. If the spectrum is mass scaled, the masses of the ions of interest are converted to channel numbers. Using the channel numbers the events can be examined to see if an event contains both ions of interest. First, each event is examined to determine if the first ion of interest is the event, if the first ion is present then the event is examined to determine if the second ion of interest was detected in the event. If both ions are detected in the same event, then the number of detected electrons in that event (found in the “cirstat” file) is recorded. The data are subsequently displayed as a histogram

Double Coincidence Maps: Double coincidence maps are plots which show where two co-emitted ions originated from. This calculation is similar to the two ion electron distribution. The use of double coincidence maps allows for the localization of co-emitted ions, which is a unique ability of the event-by-event methodology. A logic trees for this calculation can be found in figures 4.10-11.

Density plots are an alternate method of displaying the data instead of the map version. By showing a total ion map or ion selected map, in the magnification range here each pixel corresponds to $\sim 250 \times 250 \text{nm}$, therefore many impacts could occur within a single pixel. If there are multiple impacts in a single pixel, this information is “lost” by only plotting the points at which each impact was detected. Therefore, by using a color scale the intensity as well as the position is shown. However, this is often not sufficient to get a full picture of the surface. One of the key advantages of operating in the event

Two Ion Electron Distribution

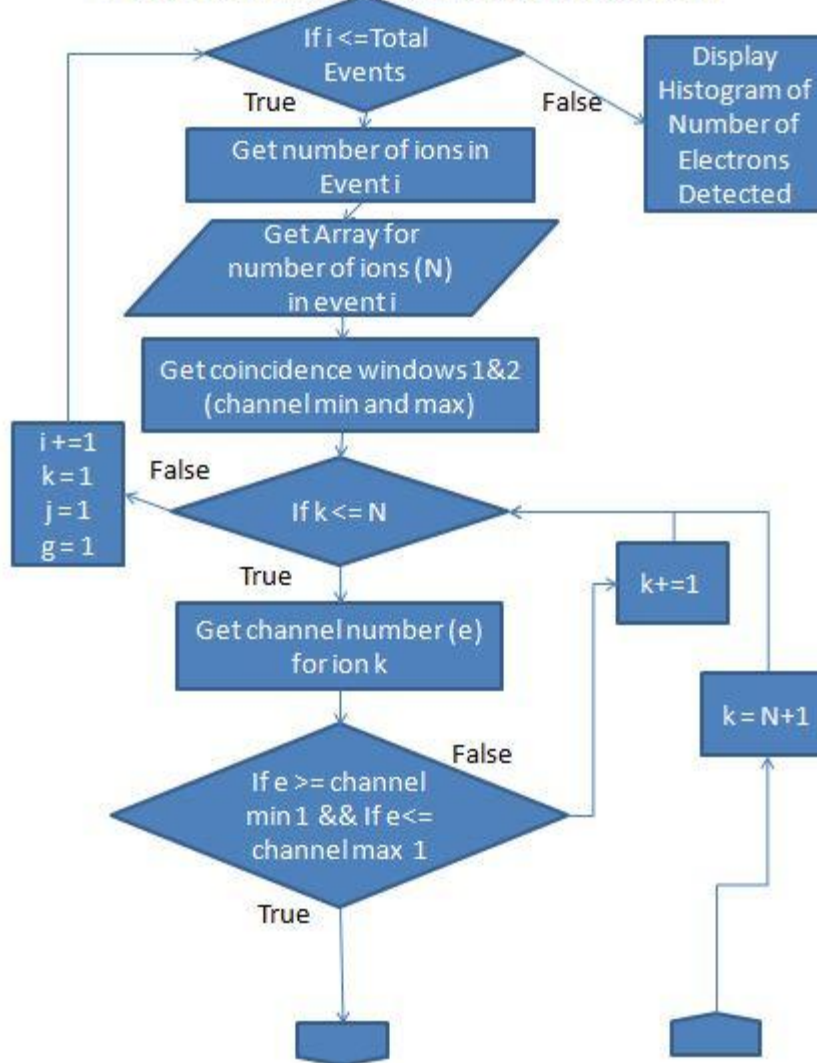


Figure 4.8 Two Ion Electron Distribution Logic Tree Part 1 of 2. The logic tree for two ion electron distribution calculation part 1 of 2 (figures 4.8-4.9).

Two Ion Electron Distribution Cont.

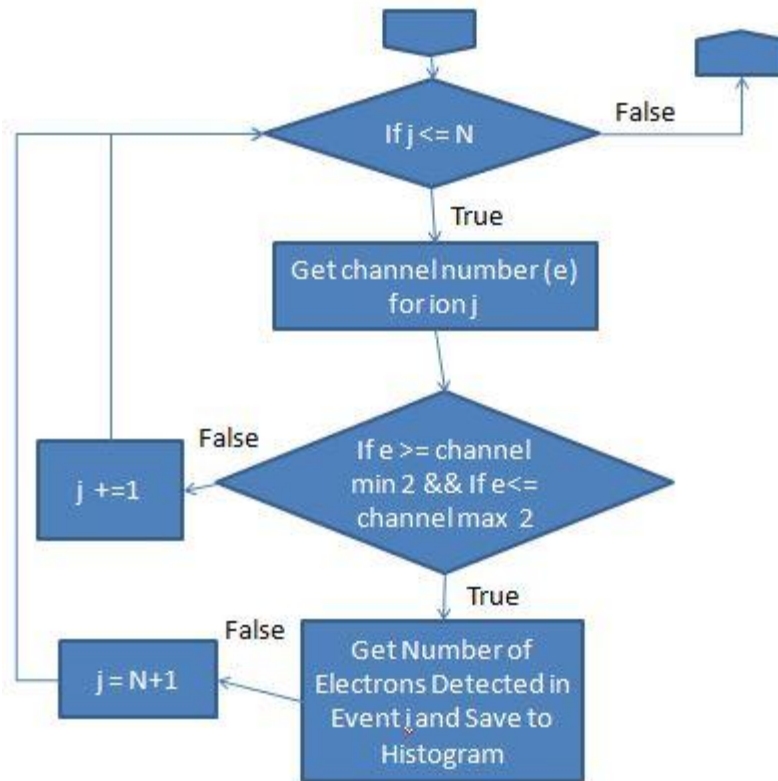


Figure 4.9 Two Ion Electron Distribution Logic Tree Part 2 of 2. The logic tree for two ion electron distribution calculation part 2 of 2 (figures 4.8-4.9).

Double Coincidence Map

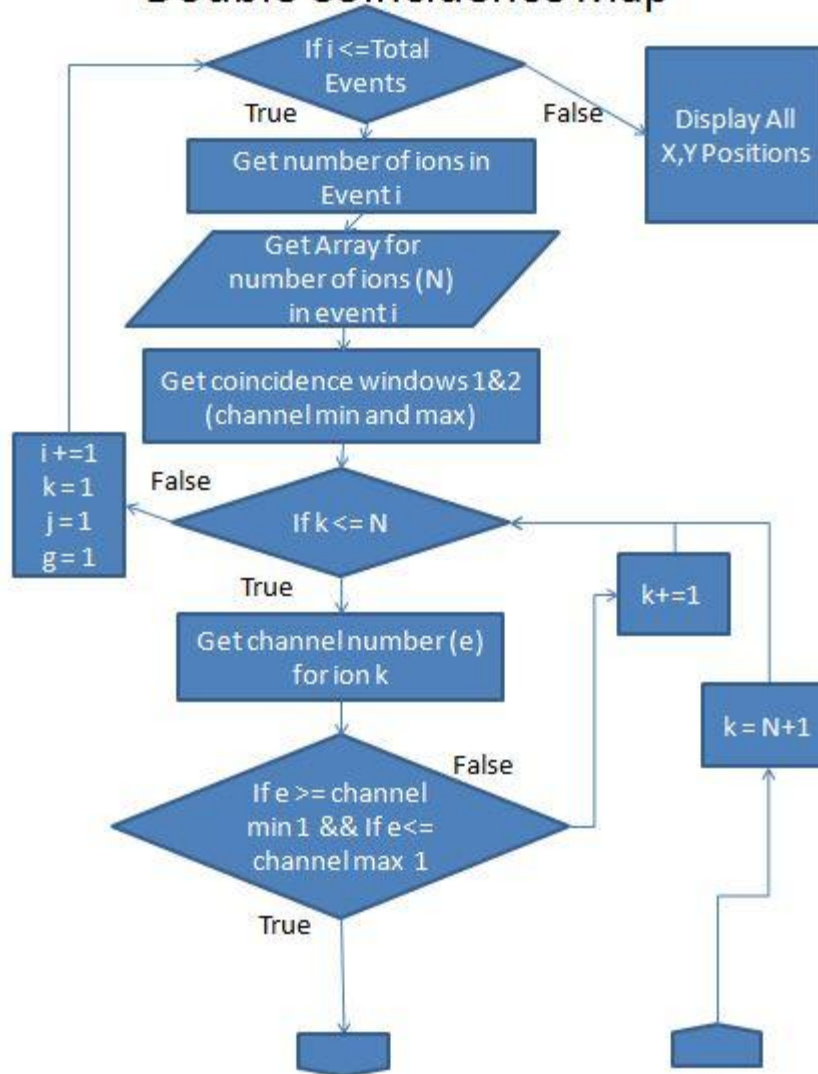


Figure 4.10 Double Coincidence Map Logic Tree Part 1 of 2. The logic tree for the double coincidence map calculation part 1 of 2 (figures 4.10-4.11).

Double Coincidence Map Cont.

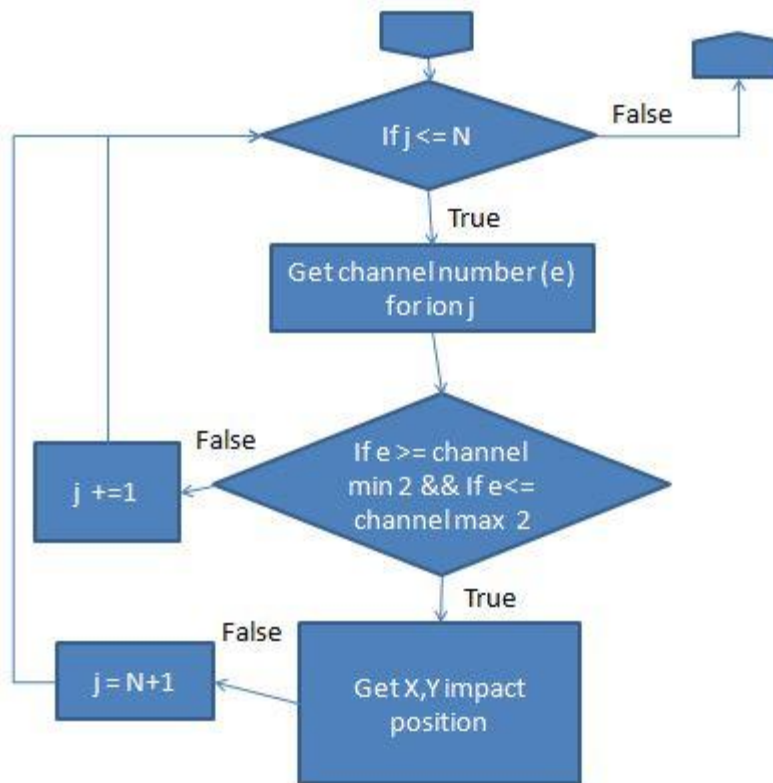


Figure 4.11 Double Coincidence Map Logic Tree Part 2 of 2. The logic tree for the double coincidence map calculation part 2 of 2 (figures 4.10-4.11).

by event bombardment mode of operation is that an unperturbed surface is sampled each time, however, this also means that not every point on the surface is analyzed. Thus, when an ion selected map or non-binned density plot is shown, many points on the map/plot will not contain information. To improve this pixels are binned and averaged to give a fuller picture of the surface. Binning decreases the resolution of the image, but as is shown in section 4.3 the current resolution of the microscope is $\sim 600\text{nm}$ and therefore larger than the binned pixels.

One of the main goals of the localization method presented is to generate ion selected maps or density plots. These ion selected density plots are a visualization of the distribution of an ion(s) of interest on the surface. The software method for generating these maps/density plots was discussed previously. A series of standard samples were generated to test the resolution of the microscope and to confirm the methodology. In this case a 400 line per inch nickel grid was coated by CsI by vapor deposition. The 400 line per inch square grid was purchased from Precision Eforming (Cortland, NY, USA). The dimensions of the grid are $63.5\mu\text{m}$ wire center to center, and the wires are $14.2\mu\text{m}$ wide. The total electron map can be found in figure 4.12. A line scan across the horizontal lines can be performed, and the measured wire thickness and center to center distances can be measured (see figure 4.13). The line scan is in good agreement with the reported wire thicknesses and center-to-center distance. The density plot is presented in figure 4.14. In the density plot, each 4×4 pixel area on the map is summed and divided by 16 and re-plotted with a color scale. Interestingly, the image shows that the sample is probed unevenly by the C_{60} , indicating the uneven density of the C_{60} beam.

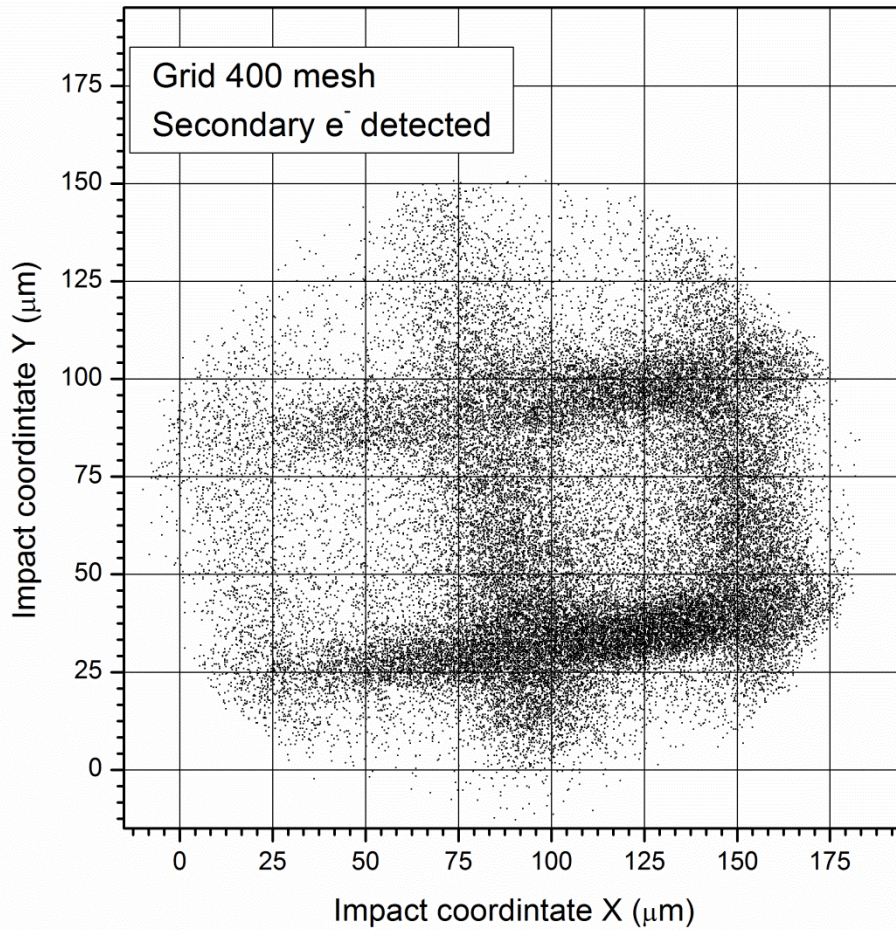


Figure 4.12 Total Ion Map for 400 Line Per Inch CsI Coated Grid Bombarded by C_{60} at 30keV. The total ion map plot of C_{60}^{2+} at 30keV bombarding CsI coating a 400 line per inch grid. Magnification $\sim 100x$.

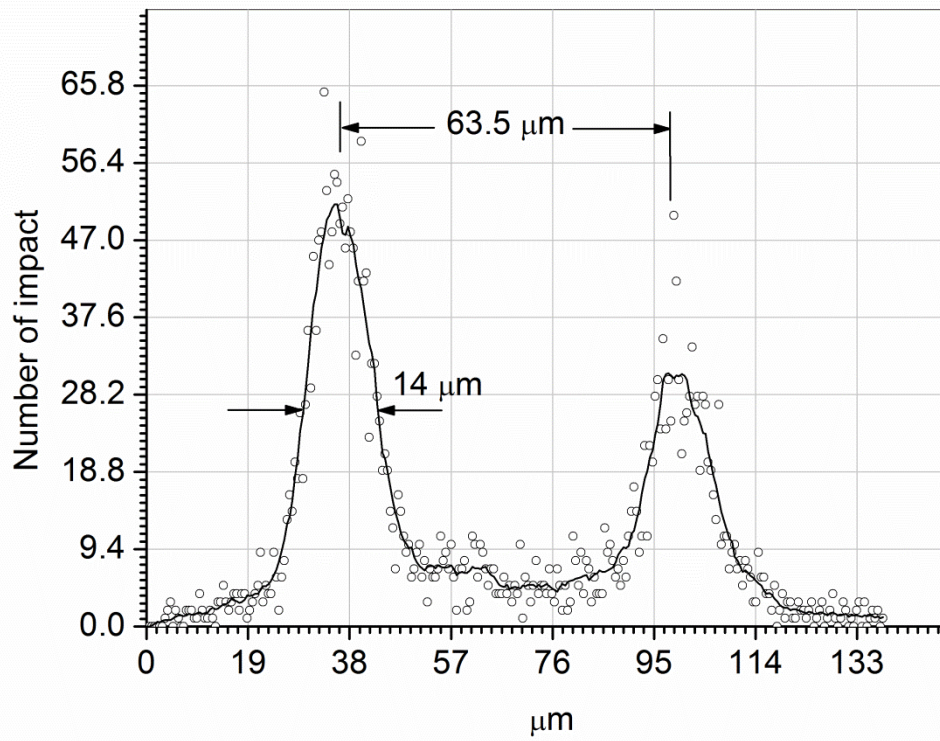


Figure 4.13 Line Scan of 400 Line Per Inch CsI Coated Grid Bombarded by C_{60} at 30keV. The line scan across the horizontal lines in figure 4.15.

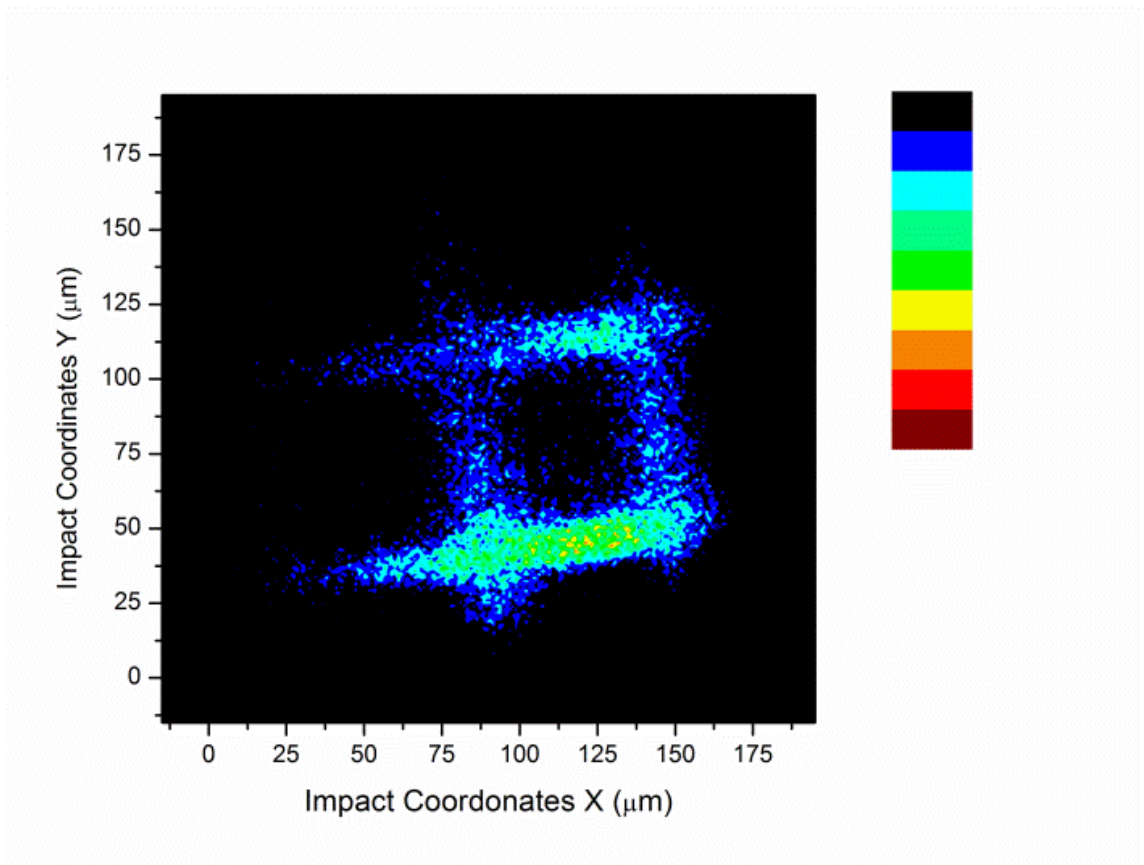


Figure 4.14 Total Ion Density Plot of 400 Line Per Inch CsI Coated Grid Bombarded by C_{60} at 30keV. The total ion density plot of C_{60}^{2+} at 30keV bombarding CsI coating a 400 line per inch grid. Magnification ~100x.

From the total electron map the impacts when Γ^- was emitted can be selected (figure 4.15). These impacts can be binned 4x4, in this way each 4x4 area on the map is summed and divided by 16 then re-plotted. The resulting density plot is shown in figure 4.16. A one ion density plot is similar to a conventional SIMS image, in which the location of a detected molecule is displayed.^[89]

A distinct advantage of the coincidence methodology is the ability to analyze co-emitted ions. In this case (CsI deposited on a 400 line per inch nickel grid) the co-emission of Γ^- with CsI_2^- can be investigated. First a coincidence mass spectrum is calculated for Γ^- , then from this mass spectrum a second ion of interest is selected (CsI_2^-), see figure 4.17. The detected impact coordinates for impacts when the two ions were co-emitted are mapped. Similar to the single ion map, the double coincidence map can be displayed as a density plot. Again the impacts are binned 4x4 and the resulting density plot can be found in figure 4.18. In this figure the power of displaying the coordinates from which two co-emitted secondary ions can be seen.

A second test sample had cholesterol vapor deposited onto a 500 line per inch copper grid. The rationale for a second sample was to show the ability to map a bio-relevant molecule, and made for a good comparison to a previously published example.^[90, 91] The dimensions, 500 line per inch square grid are $50.8\mu\text{m}$ between wire centers and the wire is $11.8\mu\text{m}$ wide (figure 4.19). After deposition the grid lines are broadened due to the deposited cholesterol (figure 4.20). A total ion map can be calculated from the impacts on the grid sample, see figure 4.21. As can be seen in the figure, the map is very similar to the image obtained by scanning electron microscopy,

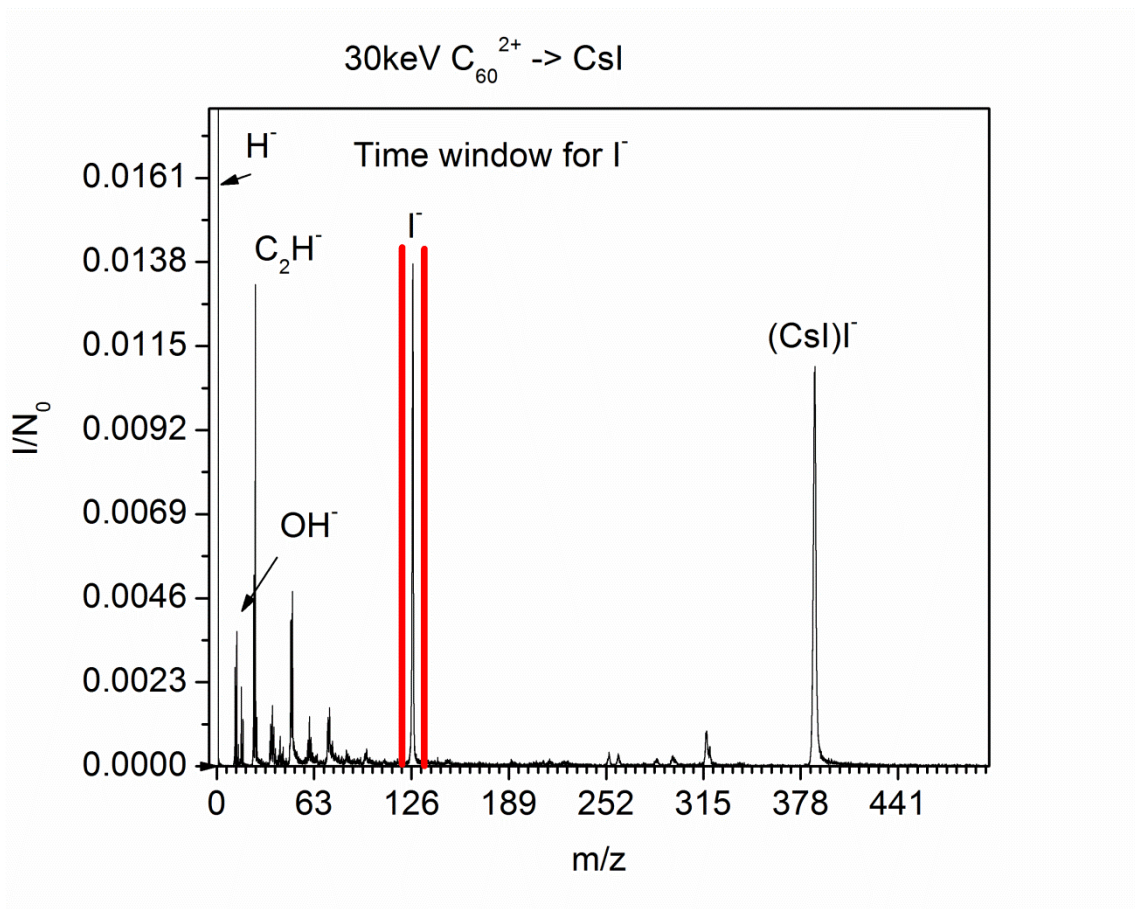


Figure 4.15 Mass Spectrum of CsI Bombarded by C₆₀ at 30keV. From this mass spectrum the impacts where I⁻ was detected can be selected (red lines).

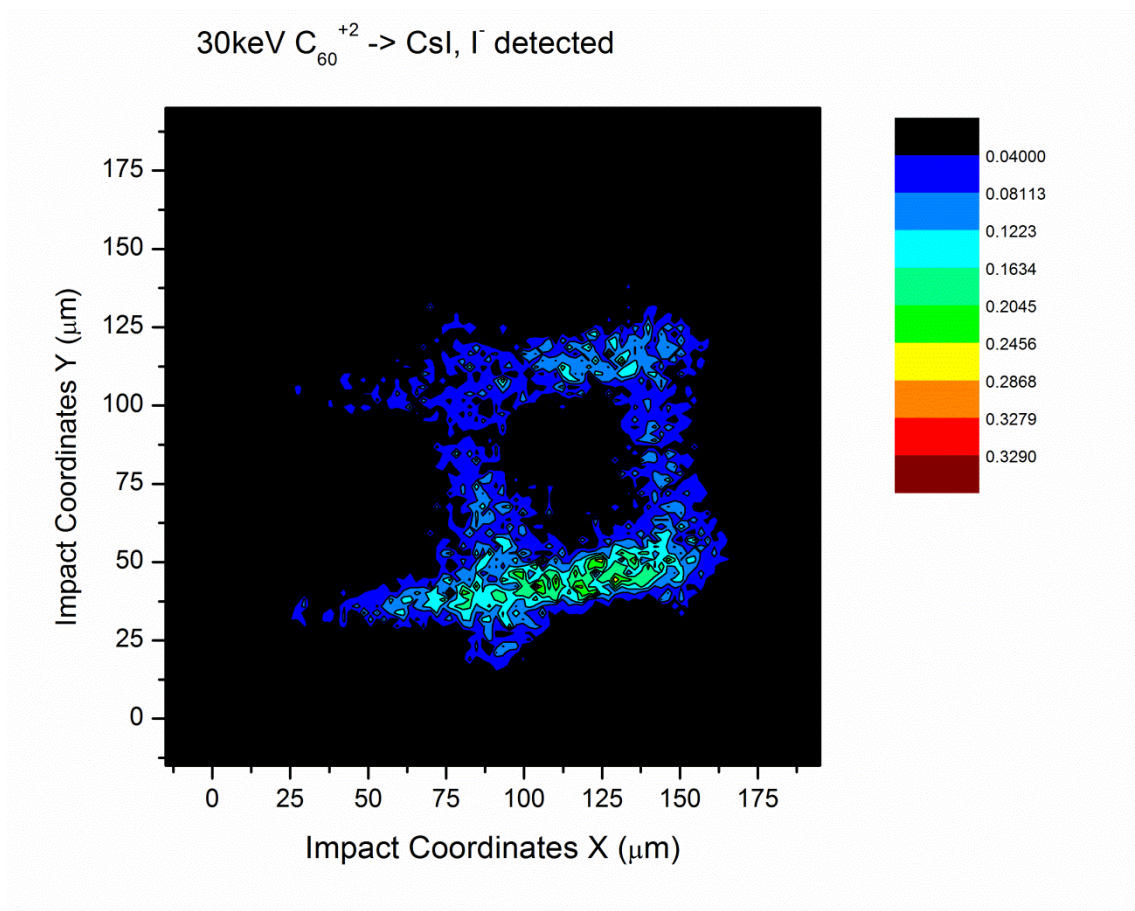


Figure 4.16 One Ion Density Plot. The one ion density plot of I^- , which was detected from impacts of C_{60}^{2+} at 30keV bombarding CsI coating a 400 line per inch grid. Magnification $\sim 100x$.

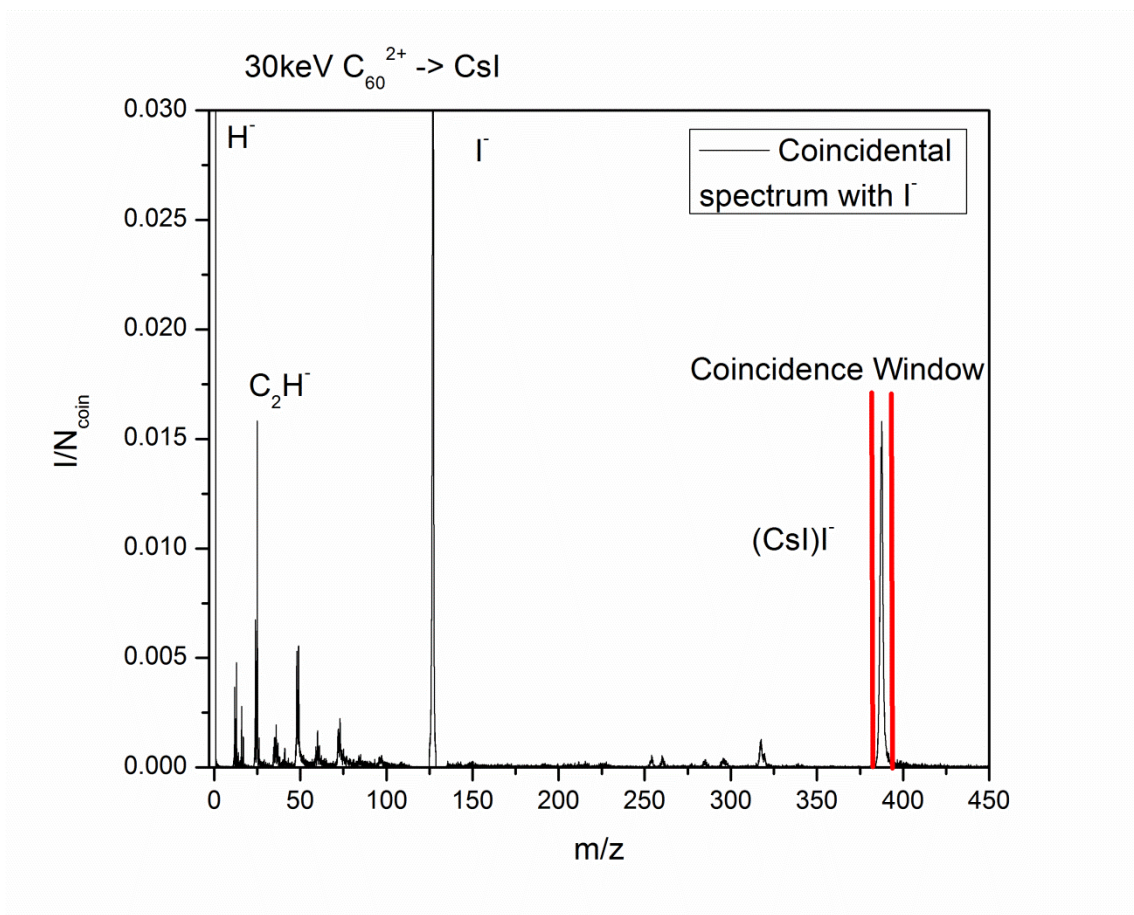


Figure 4.17 Coincidental Mass Spectrum of Impacts Where I^- was Detected. From this coincidental mass spectrum the impacts where $(CsI)I^-$ was co-emitted (red lines) are selected.

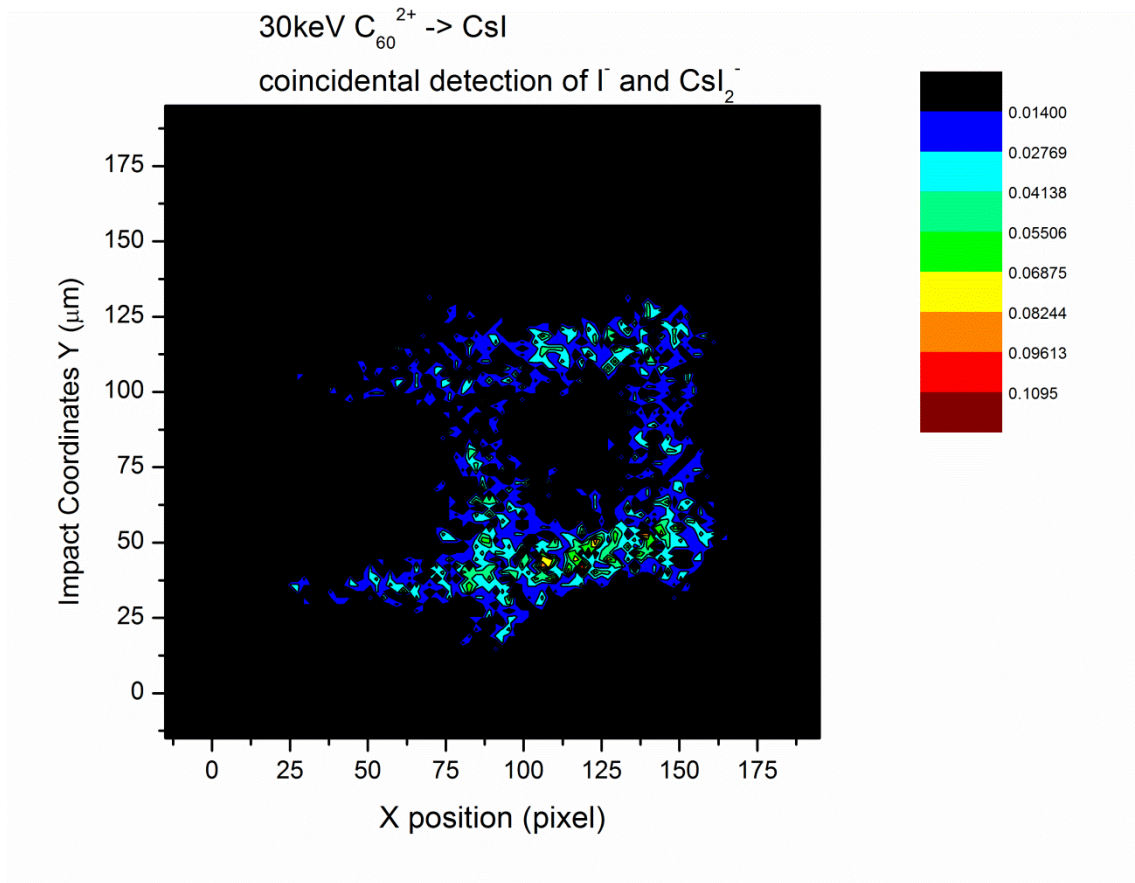


Figure 4.18 Double Coincidence Density Plot of Γ^- and CsI_2^- . The density plot of the impacts from which Γ^- and CsI_2^- were co-emitted. Magnification $\sim 100x$.

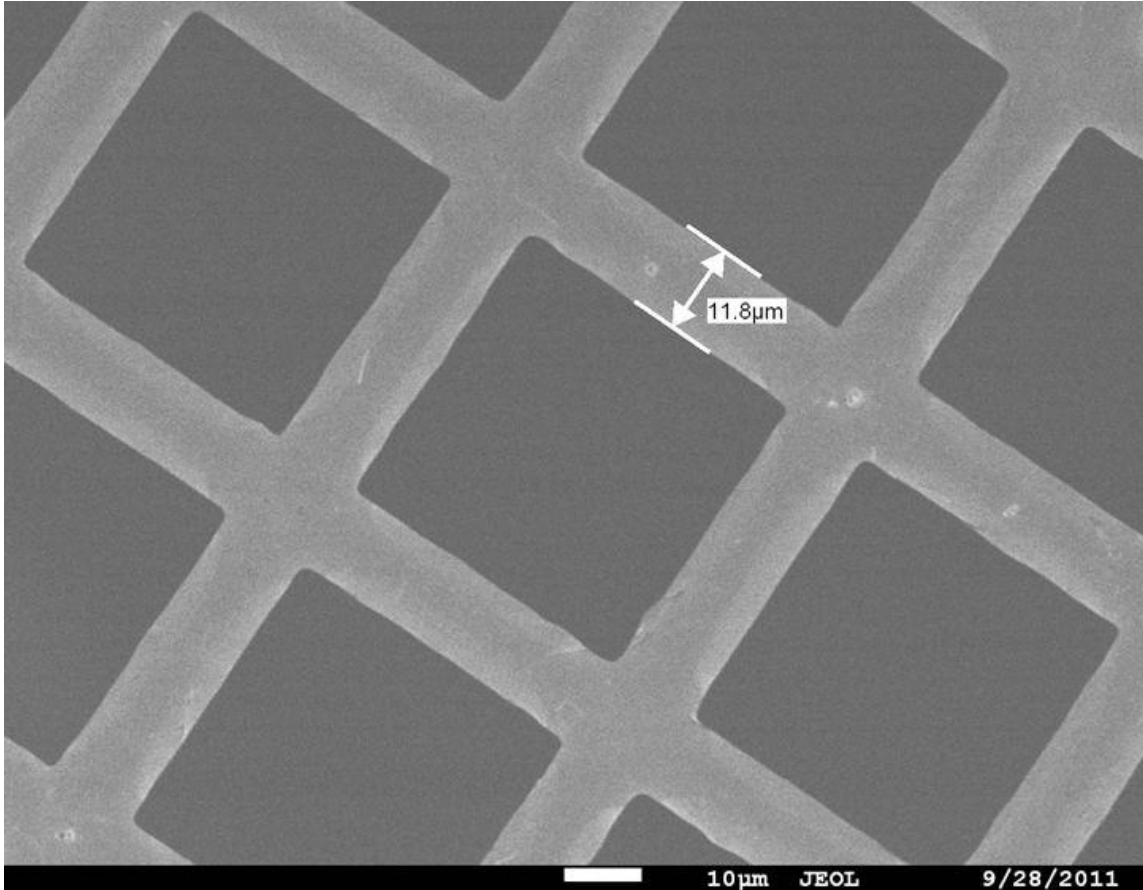


Figure 4.19 SEM Image of 500 Line Per Inch Copper Grid.

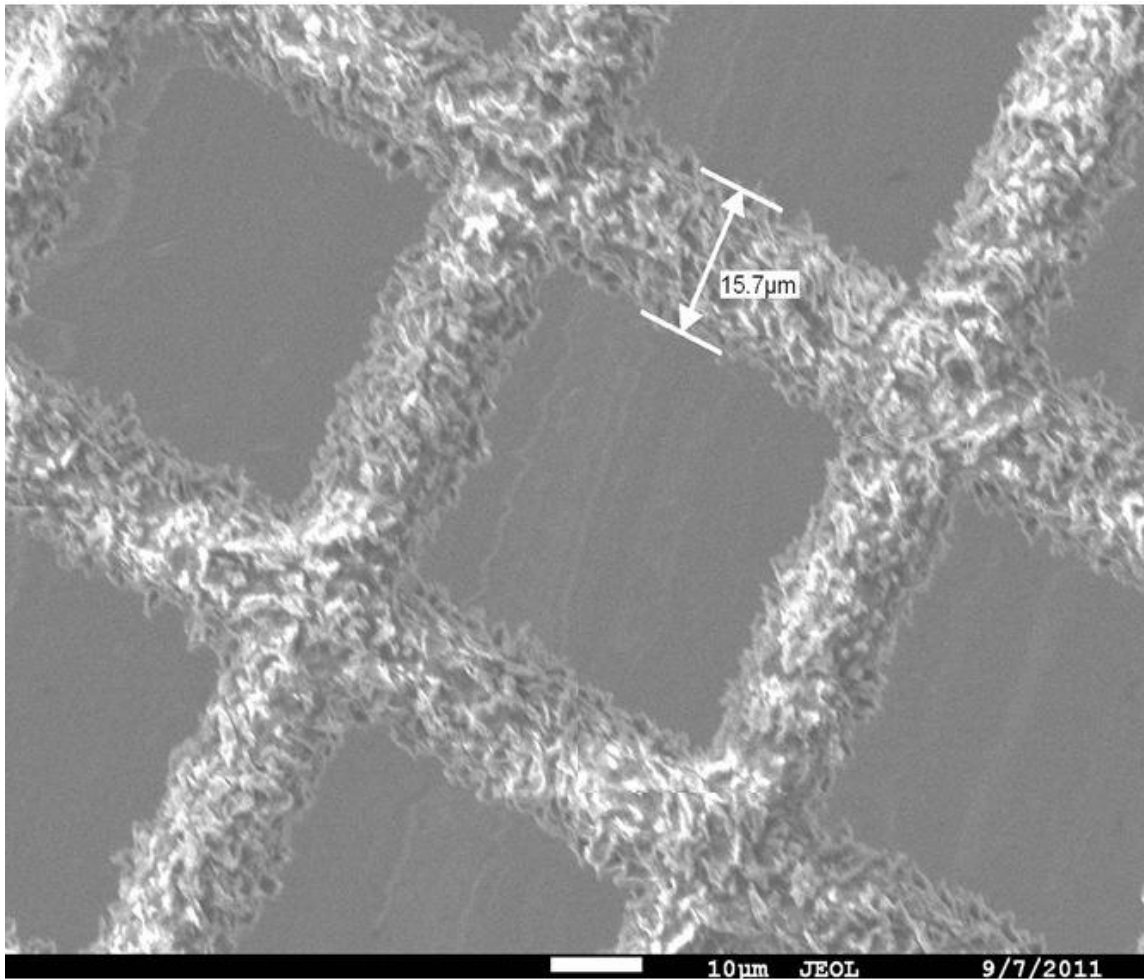


Figure 4.20 SEM Image of 500 Line Per Inch Copper Grid Coated by Cholesterol.

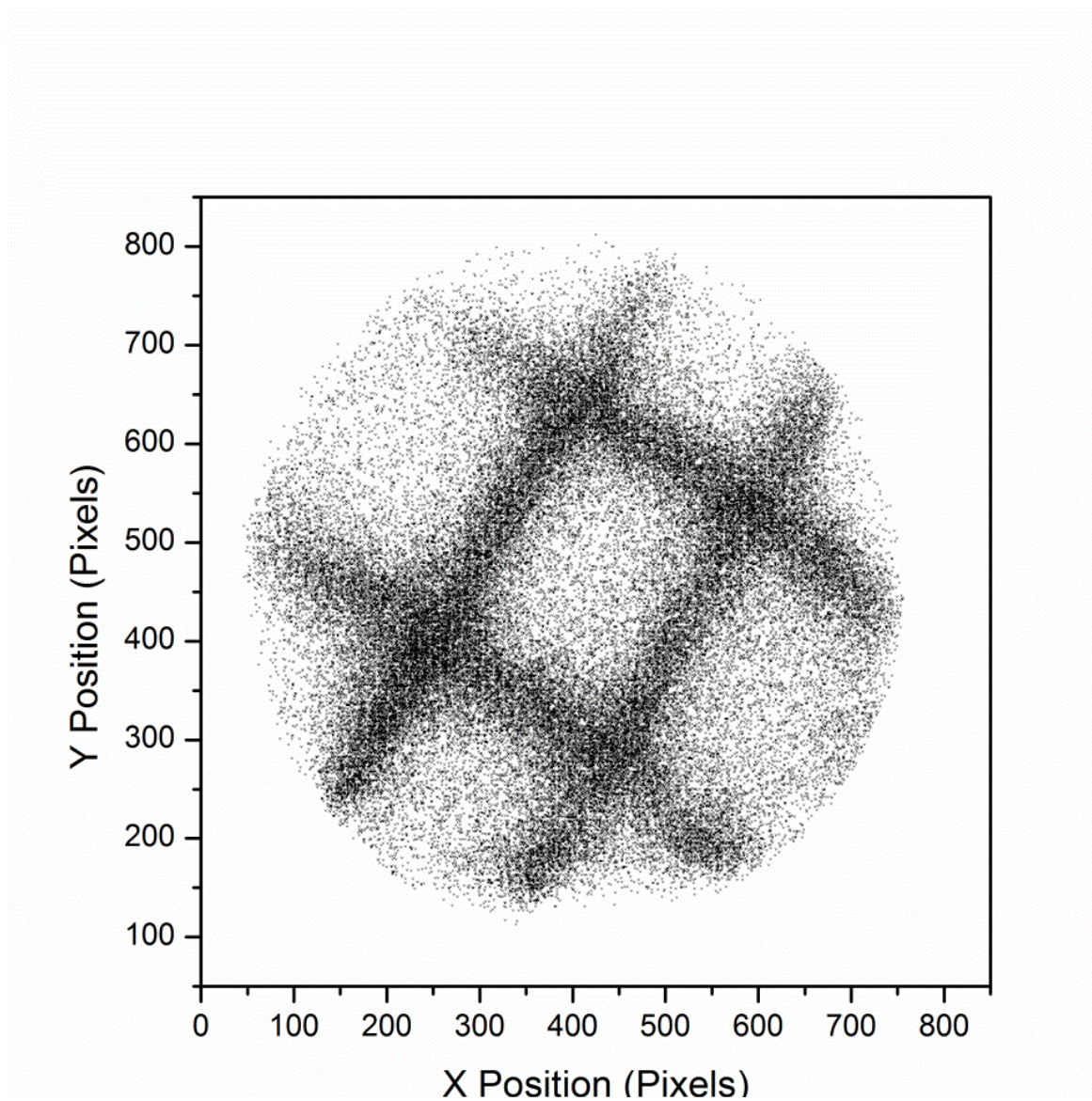


Figure 4.21 Total Ion Map. Total ion from impacts of C_{60}^{2+} at 30keV on a 500 line per inch grid coated by cholesterol. Magnification ~150x.

SEM. An ion selected map can be calculated by selecting the impacts when the cholesterol [M-H]⁺ was detected, figure 4.22. The one ion density plot can be calculated by binning 4x4, figure 4.23. The density plot of cholesterol is in good agreement with the SEM image. This sample is used to calculate the resolution of the EEM and PSD, section 4.3.

4.3 RESOLUTION

As noted earlier, we limit localization to impacts from which at least 5 electrons were emitted/detected and where, additionally, at least 4 electrons remain after software collimation. The error of this localization calculation will define the effective probing diameter of the projectile impact. To calculate the error in localization equation 4.1 shown below was used.^[92] Where Δx is the error in localization, S_d is the standard deviation of the spread of the electrons, and N is the number of electrons used for localization.

$$\langle (\Delta x)^2 \rangle = \frac{S_d^2}{N} \text{ Equation 4.1 Error in localization.}$$

The percent of impacts from which an impact site could be determined with the instrumental and software boundaries noted above is ~10% for 50keV C₆₀ impacts on cholesterol. Most of the non-localized impacts were from events where less than 5 electrons were detected (~50% of all impacts).

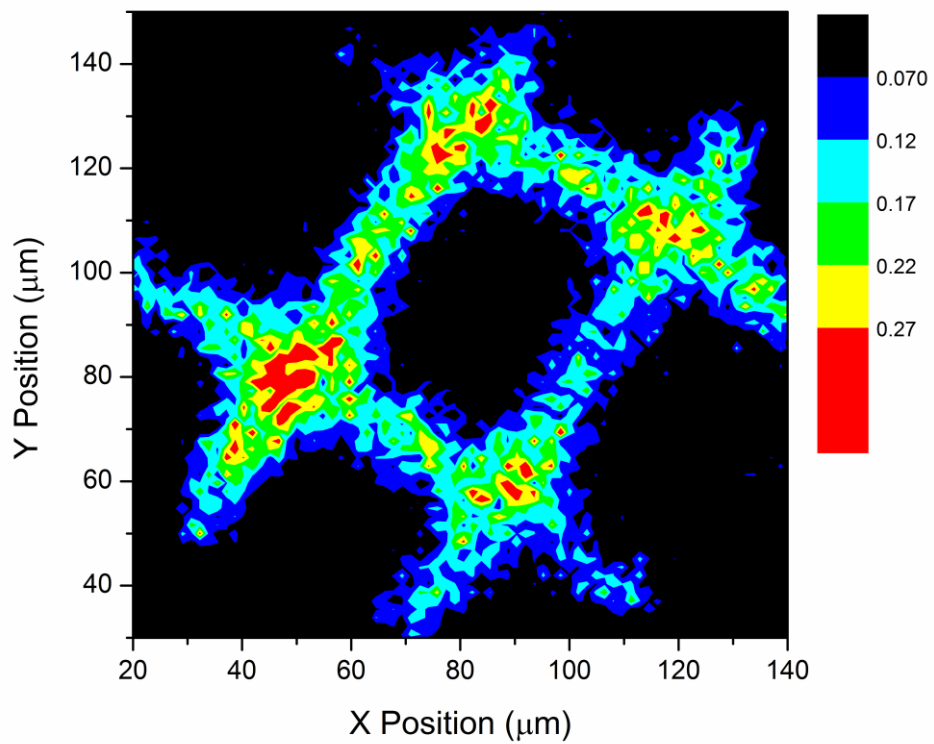


Figure 4.22 Total Ion Density Plot. Total ion density plot from impacts of C_{60}^{2+} at 30keV on a 500 line per inch grid coated by cholesterol. Magnification $\sim 150x$.

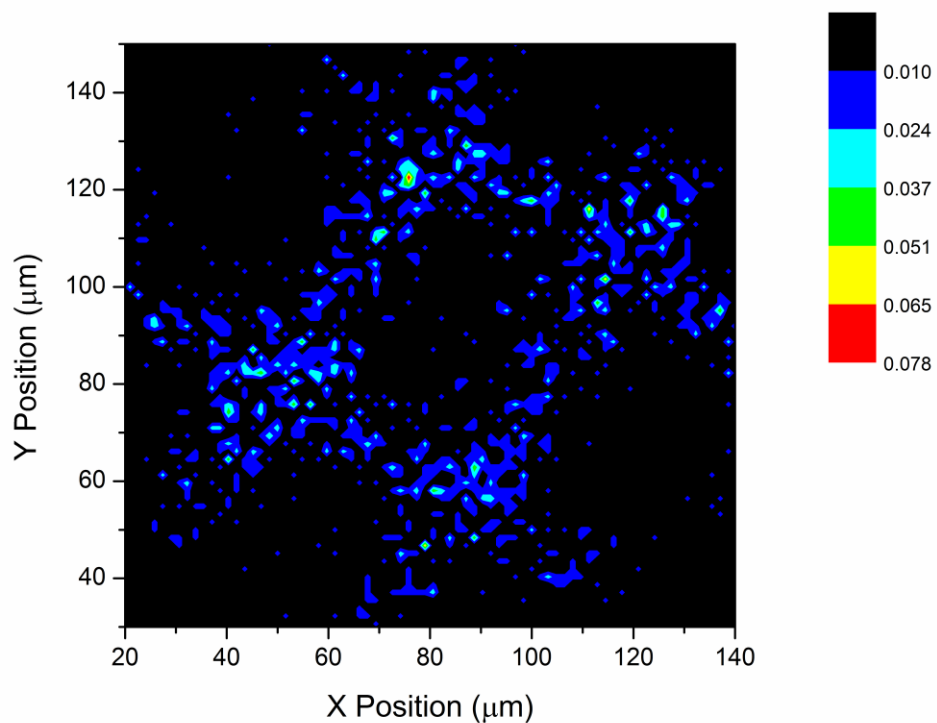


Figure 4.23 One Ion Density Plot. One ion density plot of [cholesterol-H]⁻ from impacts of C₆₀²⁺ at 30keV on a 500 line per inch grid coated by cholesterol. Magnification ~150x.

The error in localization was tested on a model target in which cholesterol was vapor deposited onto a 500 mesh Cu grid (Precision Eforming). The 500 mesh Cu grid dimensions are 50.8 μm wire center to center with a wire thickness of 11.8 μm . After vapor depositing cholesterol the wire width was measured at $\sim 15.7\mu\text{m}$ by SEM (figure 4-22).

The cholesterol sample was investigated with C_{60} at 50keV total impact energy. The error in localization, Δx , without software collimation was determined to be 1.90 μm with a corresponding S_d of 5.1 μm . The preceding data are mean values from a set of individual impacts ($\sim 80\text{k}$) where $N \geq 5$. After software collimation (selection of events where $N \geq 4$ in the ROI), we obtain a mean Δx of 600nm (from $\sim 30\text{k}$ impacts) with a S_d of 1.4 μm . This Δx was obtained with a low magnification of $\sim 150\times$. A total ion density plot corresponding to Δx of 600nm is obtained and shown in figure 4.22. The lack of definition around the edges is attributed to electron scattering and/or local electric field distortion. In this figure the map of impacts are averaged over a 4x4 pixel area, ($\sim 500 \times 500\text{nm}$). An ion-selected density plot can be generated by selecting the impacts in which an ion(s) of interest was detected, in figure 4.23 an ion-selected density plot is presented corresponding to impacts where m/z 384, [cholesterol-H] $^+$, was detected. Both density plots, total ion and [cholesterol-H] $^+$, correspond well with the SEM image obtained.

The resolution obtained with the instrument presented here ($\sim 600\text{nm}$) compares well with the 300nm resolution obtained with an In^+ beam on a similar sample.^[90] The advantage to this approach is using C_{60} which generate significantly higher SI yields

than atomic projectiles. The 600nm spatial resolution reported here is lower than the $\sim 1\mu\text{m}$ previously obtained with C_{60} using the micro-beam approach.^[85]

5. DATA ANALYSIS SOFTWARE

5.1 INTRODUCTION

Advanced data analysis solutions for mass spectrometry have been developed to meet a myriad of applications including: acquisition, 2-D and 3-D imaging solutions, data base searching, high resolution mass spectrometry, and many other challenging tasks.^[7, 93-98] In many of these cases, the instrument manufacture provides the software. In the Schweikert laboratory, custom built instrumentation is utilized, which in turn requires custom software. SAMPI (Surface Analysis and Mapping of Projectile Impacts) is a software solution written to work with these custom built instruments operating in the event-by-event bombardment detection mode. In sections (5.2-5.5) the data analysis portion of this software package is described. The mapping portion of the software is detailed in sections 4.2 and 4.3. The SAMPI software is written in C, and uses functions provided by National Instruments Inc. (Austin, TX).

SAMPI uses the Total Matrix of Events© (TME) file format for creating and loading mass spectra.^[99] In the TME file format, ions from a single event are collected and saved. Therefore, analysis of co-emitted ions can be performed. In the following sections (5.2-5.5) the versatility of this file format is detailed.

5.2 DIAGNOSTIC TOOLS AND ACQUISITION

In the event by event methodology the data are collected using the TDC setup described in the instrumentation section. This TDC is interfaced to the computer

through a National Instrument card (Austin, TX, USA). The acquisition software (Appendix D) has been modified from previous work by Rickman.^[36] A key improvement is the ability monitor the collection more effectively through the addition of online diagnostic tools. Their purpose is to analyze the collection of an ion if interest, including yield calculation, anode distribution, and anode specific mass spectra. The rate of instrument optimization has been improved greatly through automation in file creation.

A key for the logic trees presented in sections 5.2-5.5 can be found in figure 5.1. A short algorithm found in lines 958-1040 of appendix D, details the acquisition of a single event. The operation of the acquisition software follows. Each time an ion is recorded by the TDC, the channel number (time) the ion was detected at is saved and the anode on where the ion was detected is saved. All ions emitted in a single event are saved sequentially until the end of the acquisition (typically tens of microseconds). At the end of the acquisition the end of event marker is saved. These values (channel numbers, anode number, and end of event) are written to an array, after 8000 elements are collected, the array is appended to a file and the array begins to fill again.

For meaningful feedback the diagnostic tools require a minimum of ~30,000 events. First, the yield of an ion of interest is calculated by summing the number of counts in a selected area on the mass spectrum (figure 5.2-3) and dividing by the number of events collected. This yield is compared to previously collected data to assure the user that the detection system is operating correctly. Second, the distribution of the ion of interest on the eight anode detector is calculated. As was noted previously each time an

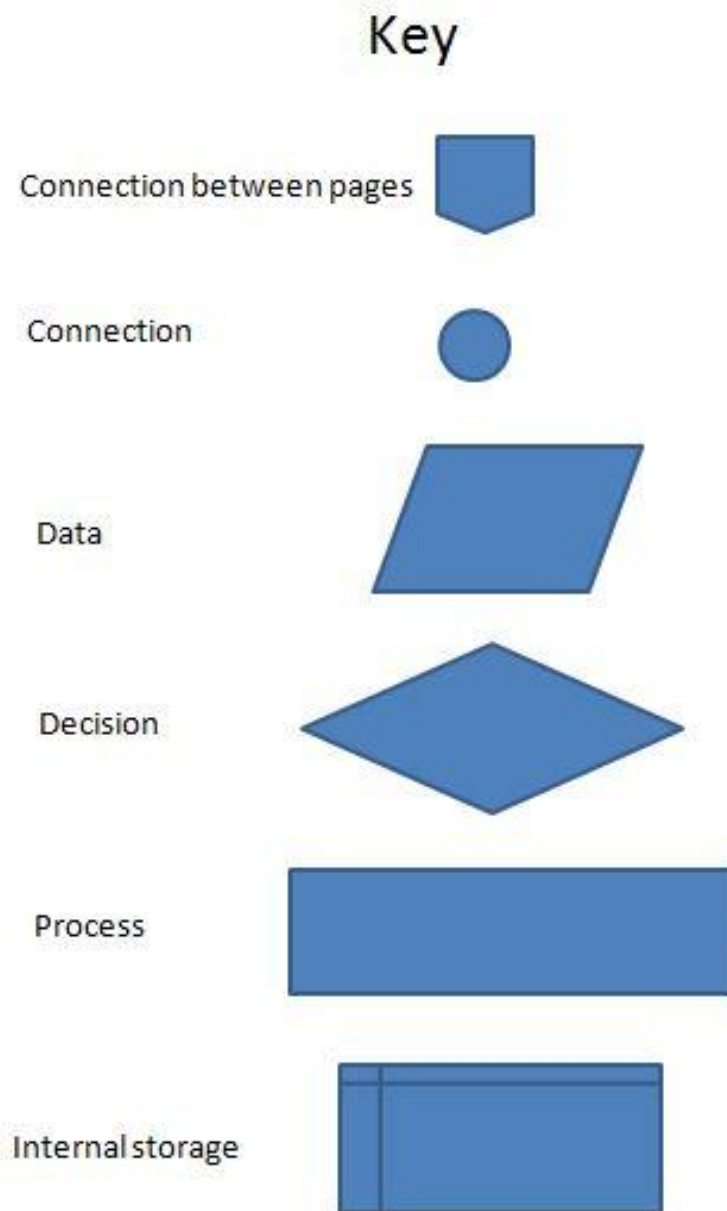


Figure 5.1 Logic Tree Key. This is the key for the shapes used in the logic trees found in sections 4.2 and 5.2-5.5.

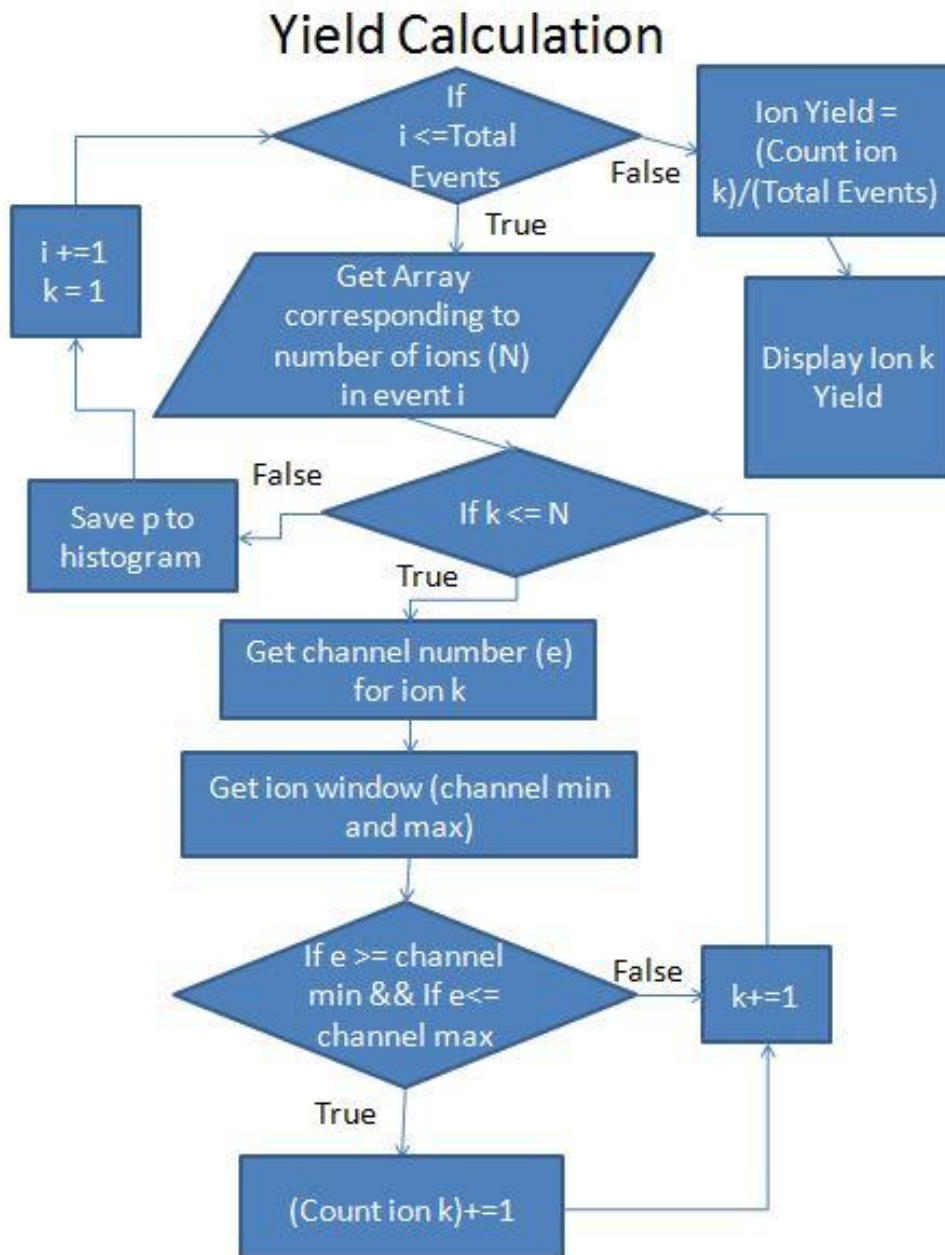


Figure 5.2 Yield Calculation Logic Tree. Logic Tree for calculating the ion yield.

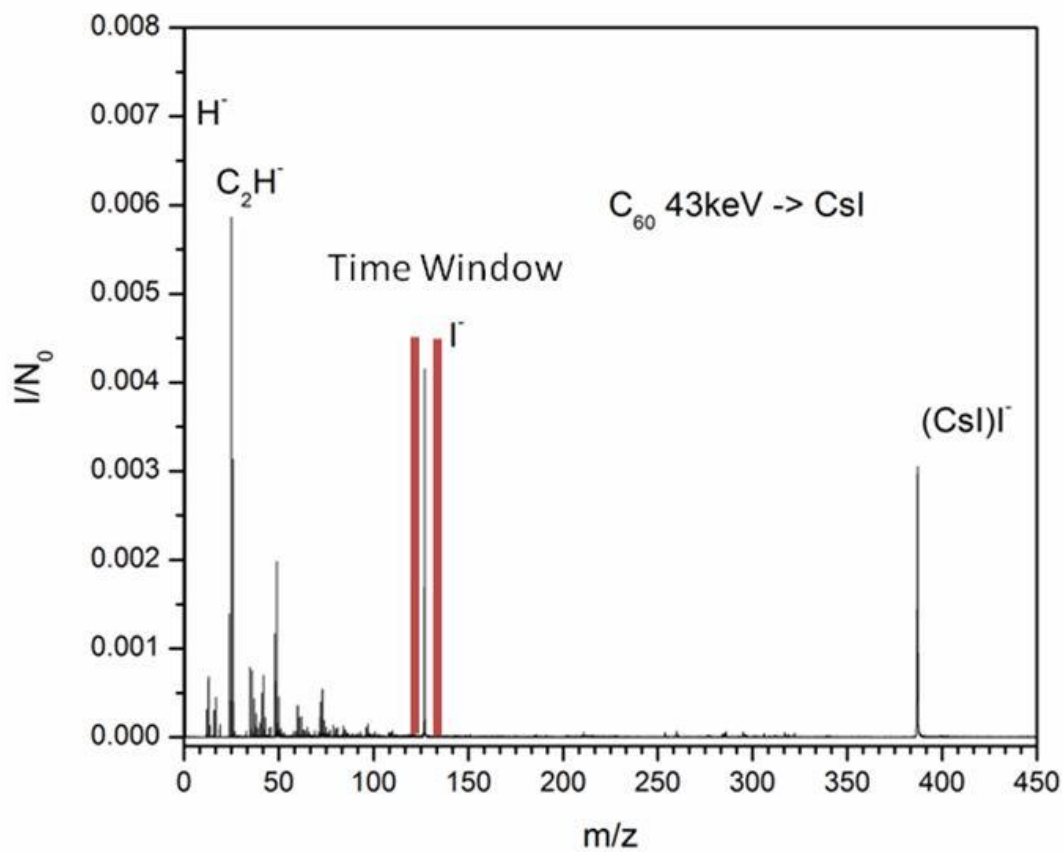


Figure 5.3 Example Ion Selection. Red lines: the selection of impacts generating I^- from 43keV C_{60} impacting a CsI target.

ion is detected the channel number and the pertinent anode are recorded, therefore the data can be sorted by the ion of interest and by the anode it was detected on. The ion distribution is optimized such that the ion which is emitted normal to the surface^[100] has approximately 1/8 of the total signal on each anode (Figure 5.4). By optimizing for an ion known to be emitted normal to the surface, the radial distributions of ions can be measured. The measurement of radial distributions can give insights into the mechanism of an ions formation.^[100] In our case up to eight of the same ion to be detected in a single event.^[101] Third, the mass spectrum from each anode is investigated to ensure that the peak shapes are similar. Lastly, if any of the above diagnostic tools indicates a problem, the proper adjustments to the instrument can be made and a new mass spectrum can be quickly collected without reopening the software. The software automatically creates a file with a new name each time a collection is performed, allowing for rapid adjustments.

Ion Yield Monitor: This calculation is an offline diagnostic tool. This analysis feature displays the number of counts of an ion of interest as the experiment progresses. An example can be found in figure 5.5, which shows the number of counts of CN^- for every 1,000 events collected (~1s for this experiment). The number of counts will have statistical fluctuations, however the counts are steady, upwards or downwards trends are not observed. This absence of up or down trend is a sign that the data are being collected consistently. A downward trend may indicate that the surface is being damaged by the beam and fewer intact ions are available for desorption.^[102] A upward trend may also indicate sample damage and creation of preformed ions, depending on

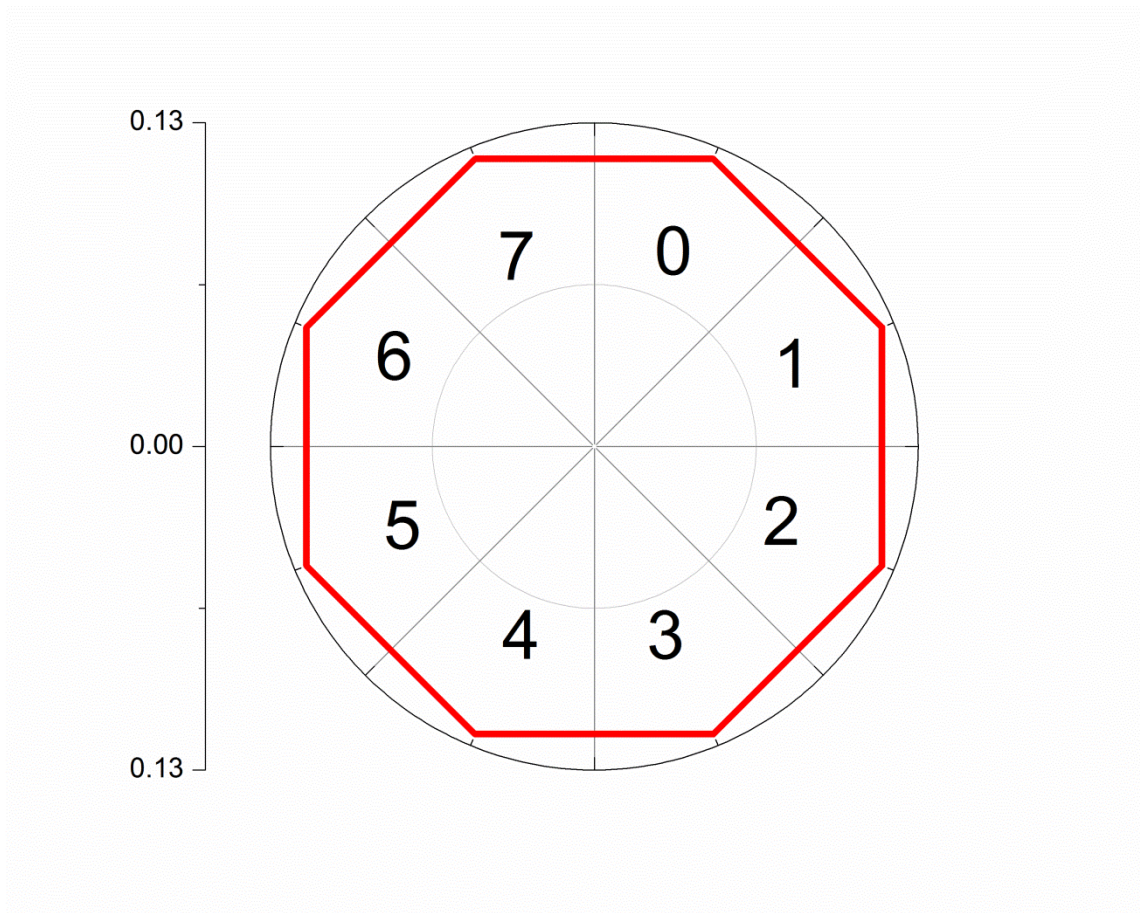


Figure 5.4 Ideal Anode Distribution. The ideal distribution on the eight anode detector with $1/8^{\text{th}}$ of the total signal on each anode.

Monitor Ion Yield

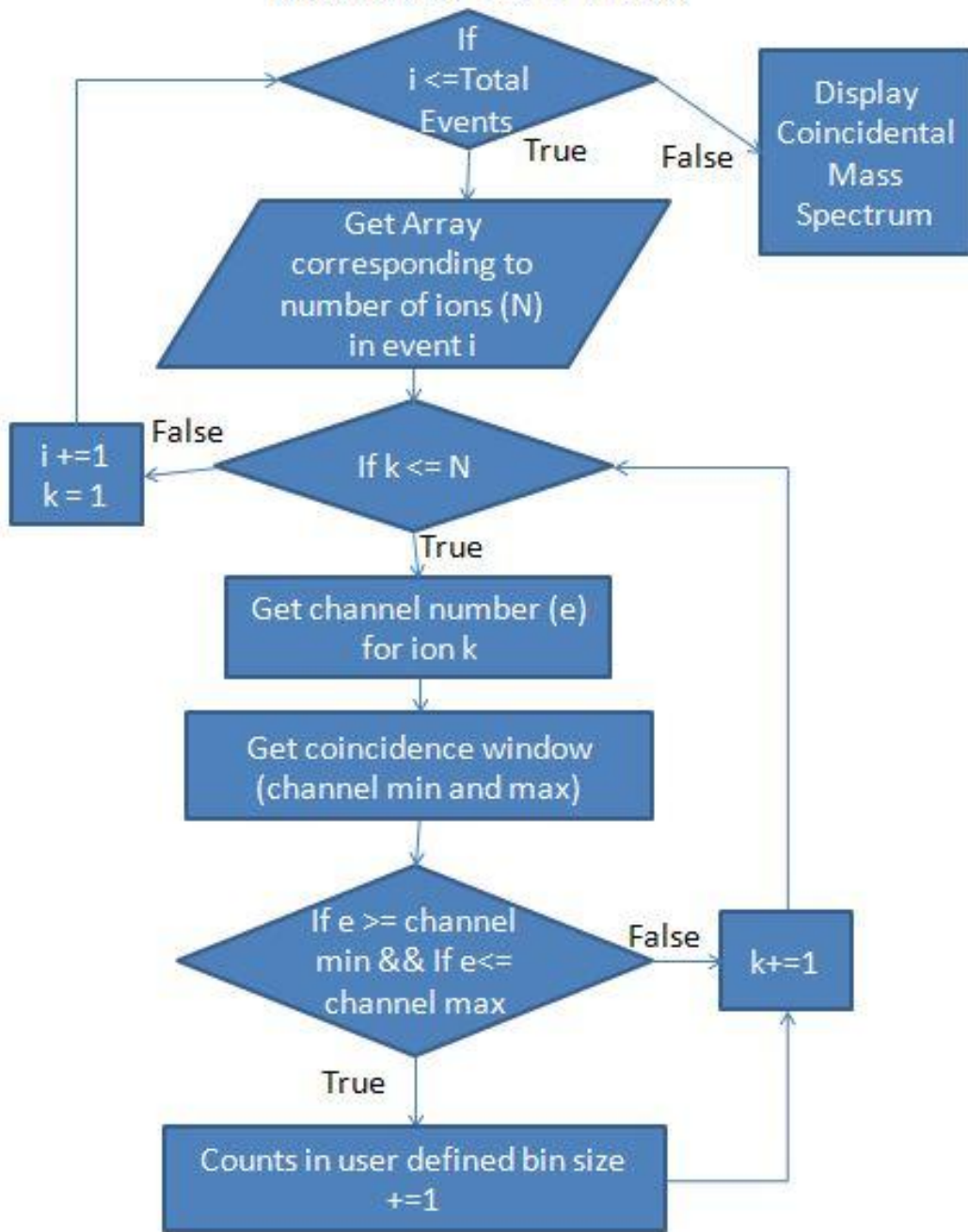


Figure 5.5 Monitor Ion Yield Logic Tree. Logic tree for the monitor ion yield calculation.

the ion monitored.^[103] A trend upwards or downwards in the number of counts could also indicate movement in the bombardment region; and this new part of the sample may have a different composition to the area previously being analyzed. These are a few examples of possible issues revealed by monitoring the number of counts as a function of analysis time. Monitoring ion yield is a useful offline diagnostic feature which can diagnose a variety of instrument complications. Complications, such as the loss of a power supply, loss of vacuum, fluctuations in bombardment rate, and any shift in the region being analyzed.

Monitor Yield Calculation: A logic chart can be found in figure 5.6 and an example is presented in 5.6. A written explanation of how this calculation is performed follows. From the main mass spectrum, a single ion of interest is chosen. The first event is examined for the ion of interest and each time it is found in the event (up to 8 times for 8 anode detector), a counter is increased by 1. This is repeated for the number of events specified, 1,000 for example. In this example the counts in the first 1,000 events are summed. This is repeated for the next 1,000 events until the end of the collection is reached. After all events have been investigated the number of counts in each bin (1,000 events) is plotted.

Single Ion Multiplicity: Single ion multiplicity is the measurement of the number of times an ion of interest was detected in every event. A plot of single ion multiplicity is shown as the probability of detecting an ion of interest 0-8 times. The number of ions generated per projectile will differ for different projectiles.^[99, 104] The direct comparison between projectiles can be done.^[101, 104, 105] In DeBord et al., the ion multiplicities from

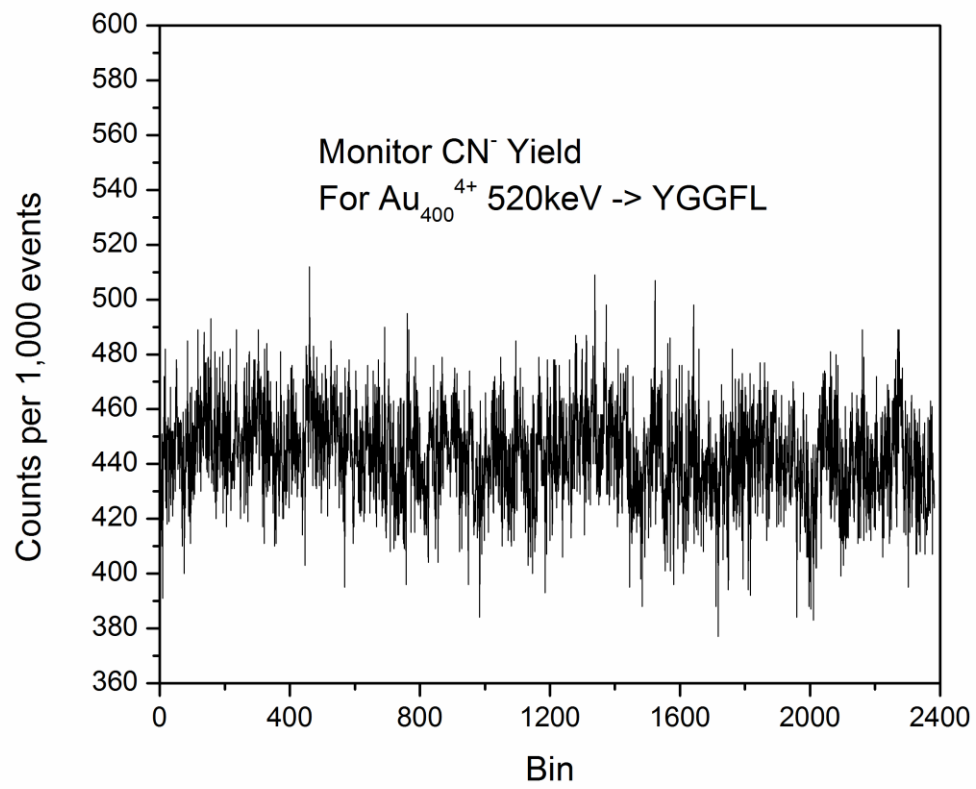


Figure 5.6 Monitor Ion Yield Example. The counts per 1,000 events of CN⁻, for 520keV Au₄₀₀⁴⁺ impacts on YGGFL.

Au_{400}^{4+} and Au_3^+ projectile impacts on leu-enkephalin are compared. It was found that with Au_{400}^{4+} , up to 7 leu-enkephalin quasi-molecular ions can be detected in a single event. However for Au_3^+ , the most prolific impacts only generated three leu-enkephalin quasi-molecular ions.

Single Ion Multiplicity Calculation: The logic chart for this calculation can be found in figure 5.7. A brief written description of how this calculation is performed follows. In the main mass spectrum a single ion of interest is chosen. First, an event is examined to determine the number of times the ion of interest was detected in the event, the number of times the ion was detected in the event is recorded (0-8). Every event in the mass spectrum is examined for the number of times the ion of interest was detected and this is recorded. Multiplicity data are then displayed as a histogram, normalized to the total number of events.

5.3 ADVANCED ANALYSIS TECHNIQUES

Coincidence mass spectrometry is a key advantage of the event-by-event methodology.^[54] It allows for the analysis of the co-emission of two or more ions of interest, specifically the colocalization of ions, as these ions originate from a nanometric volume. The analysis of individual nano-particles can be performed, examples of this can be found in section 2.4. Additionally, the coincidence methodology can be used in meta-stability studies.^[104, 106] To perform these analyses, dedicated software

Single Ion Multiplicity

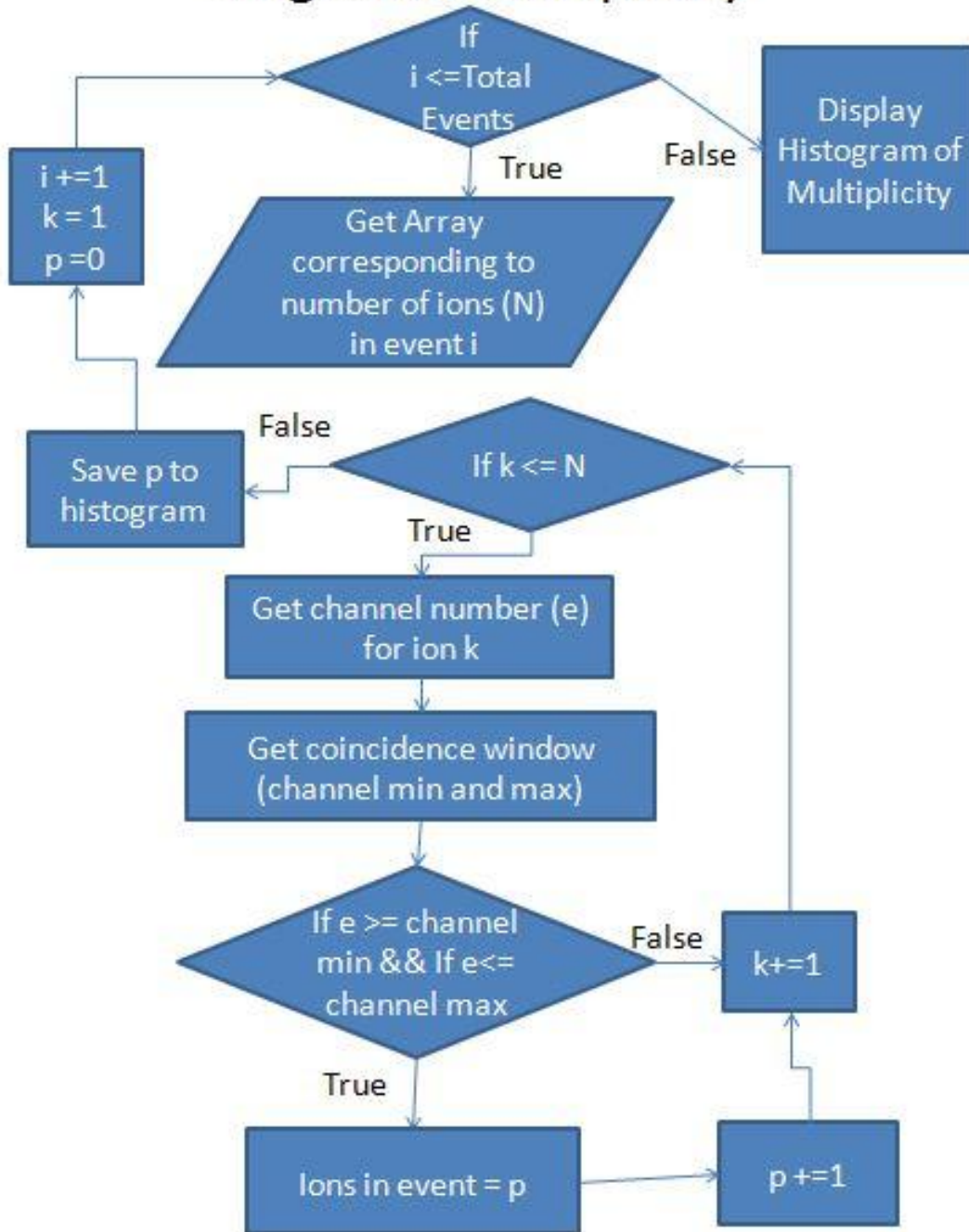


Figure 5.7 Single Ion Multiplicity Logic Tree. Logic tree for single ion multiplicity calculation.

tools are required. Descriptions of coincidental mass spectrometry tools for analysis, with logic trees, are presented in this section.

A single coincidence calculation is diagrammed in the logic chart found in figure 5.8, a brief text description follows. From the main mass spectrum, an ion of interest is selected (a procedure can be found in Appendix C). As was mentioned in section 5.1 the data are stored as individual events. Each event is examined to see if it contains the ion of interest. The scan is performed with a series of if clauses which determine if a detected ion is in the desired range. If the ion desired is found, all the ions detected in that event are written to a coincidental mass spectrum. This process is repeated until all events have been investigated. The coincidental mass spectrum can then be further investigated.

Double coincidence is a methodology in which two ions of interest are be selected. The resulting mass spectrum will contain all co-emitted secondary ions. The double coincidence selection is a tool to investigate complex samples. For example, the relationship between two nanometric layers, or surface segregated molecules.^[107] In reference 107, several different layers and combination of layers created an inhomogeneous surface due to partial attachment of some layers. In that case a three layer system was generated, layer one was silane (acryl silane or NH₂ silane), layer two was NHS biotin linker, and the third layer was neutravidin. Partial attachment of the biotin or neutravidin resulted in a complex surface. Some areas had all three layers present, while others had one or two of the layers. Double coincidence between a peak

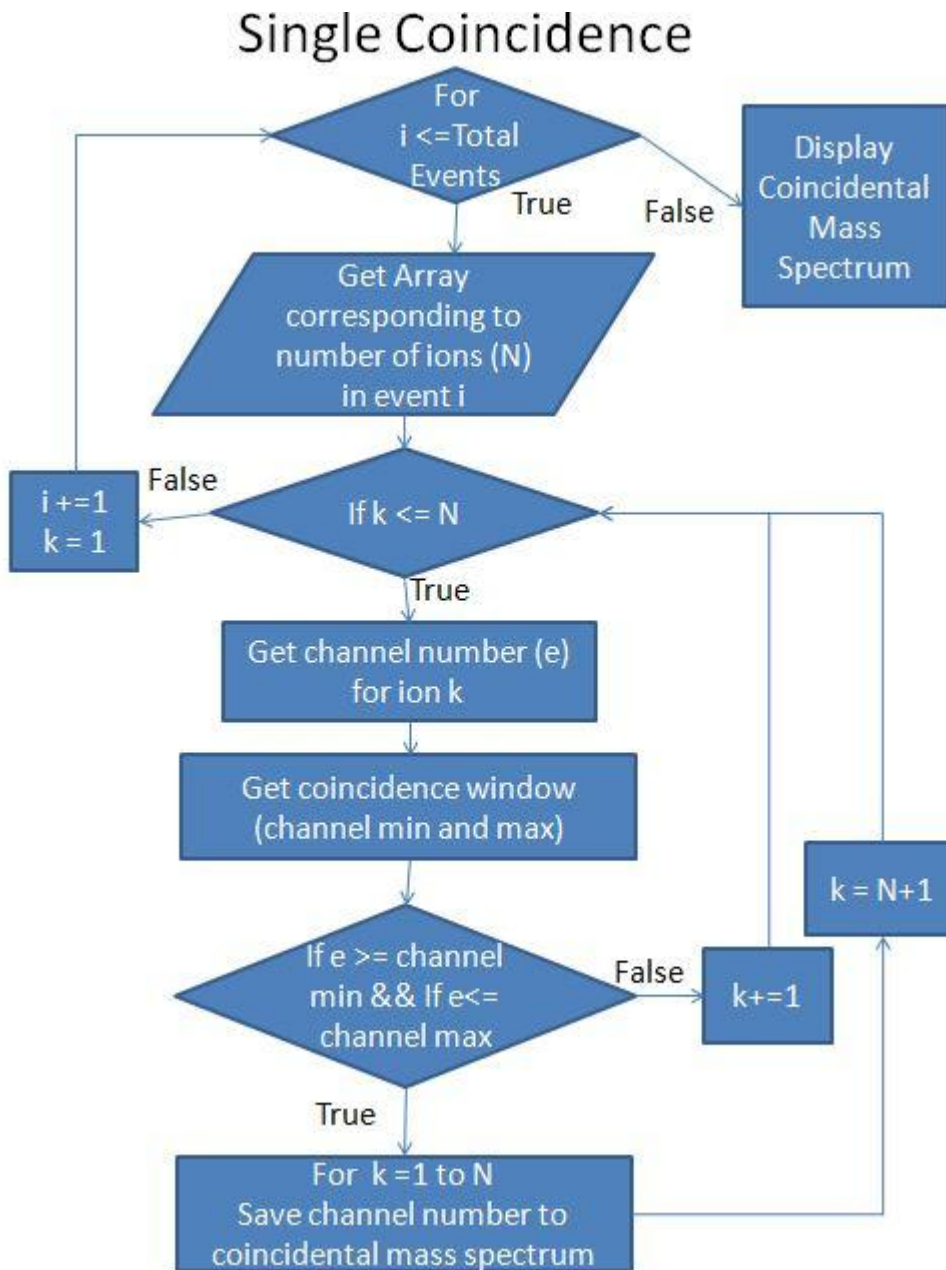


Figure 5.8 Single Ion Coincidence Logic Tree. Logic tree for single ion coincidence calculation.

specific to avidin and a peak specific to the linker identified areas of properly assembled layers and hence determine the perspective of integral versus incomplete assembly.

Double Coincidence: A double coincidence calculation can be performed with the SAMPI software, a logic chart can be found in figure 5.9-5.10. A brief written description follows: From the main mass spectrum two ions of interest are selected. If the spectrum is mass scaled, the masses of the ions of interest are converted to channel numbers. Using the channel numbers the events can be examined to see if an event contains both ions of interest. First, each event is examined to determine if the first ion of interest is the event, if the first ion is present then the event is examined to determine if the second ion of interest was detected in the event. If both ions are detected in the same event, then all the ions detected in the event are written to a double coincidence mass spectrum. After all events are investigated, the double coincidence mass spectrum is displayed.

One-Ion Coincidence and One-Ion Anti-Coincidence is a methodology in which two ions of interest are selected, much like double coincidence, however in this case one will be in coincidence with other ions while the other will be in anti-coincidence. Anti-coincidence events are characterized by the absence of a specific ion.

One-ion coincidence and one-ion anti-coincidence calculation logic charts can be found in figures 5.11-5.12, a brief written description follows. From the main mass spectrum, two ions are designated. The first is the species that will be in coincidence

Double Coincidence

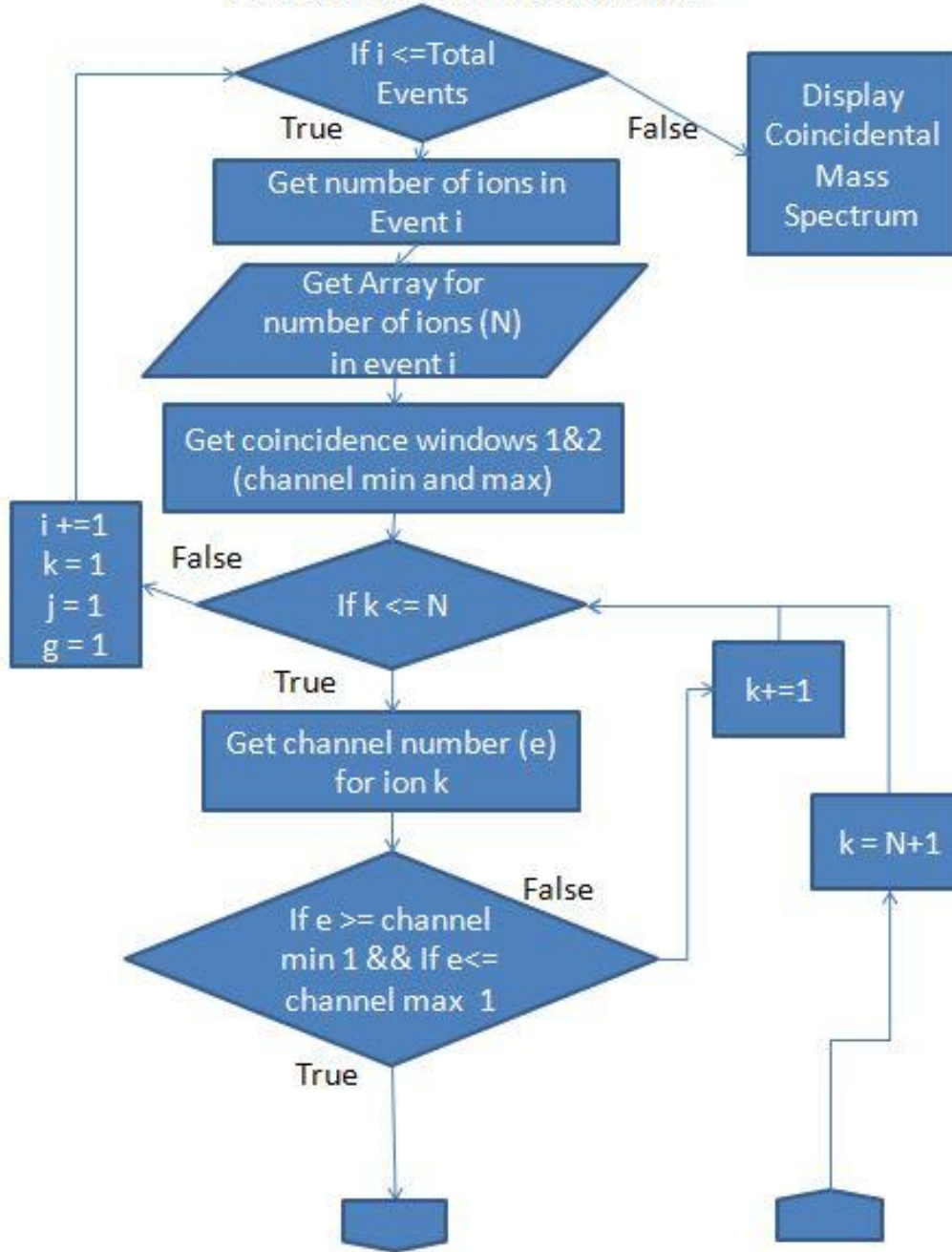


Figure 5.9 Double Coincidence Logic Tree Part 1 of 2. Logic tree for double ion coincidence calculation part 1 of 2 (figures 5.9-5.10).

Double Coincidence Continued

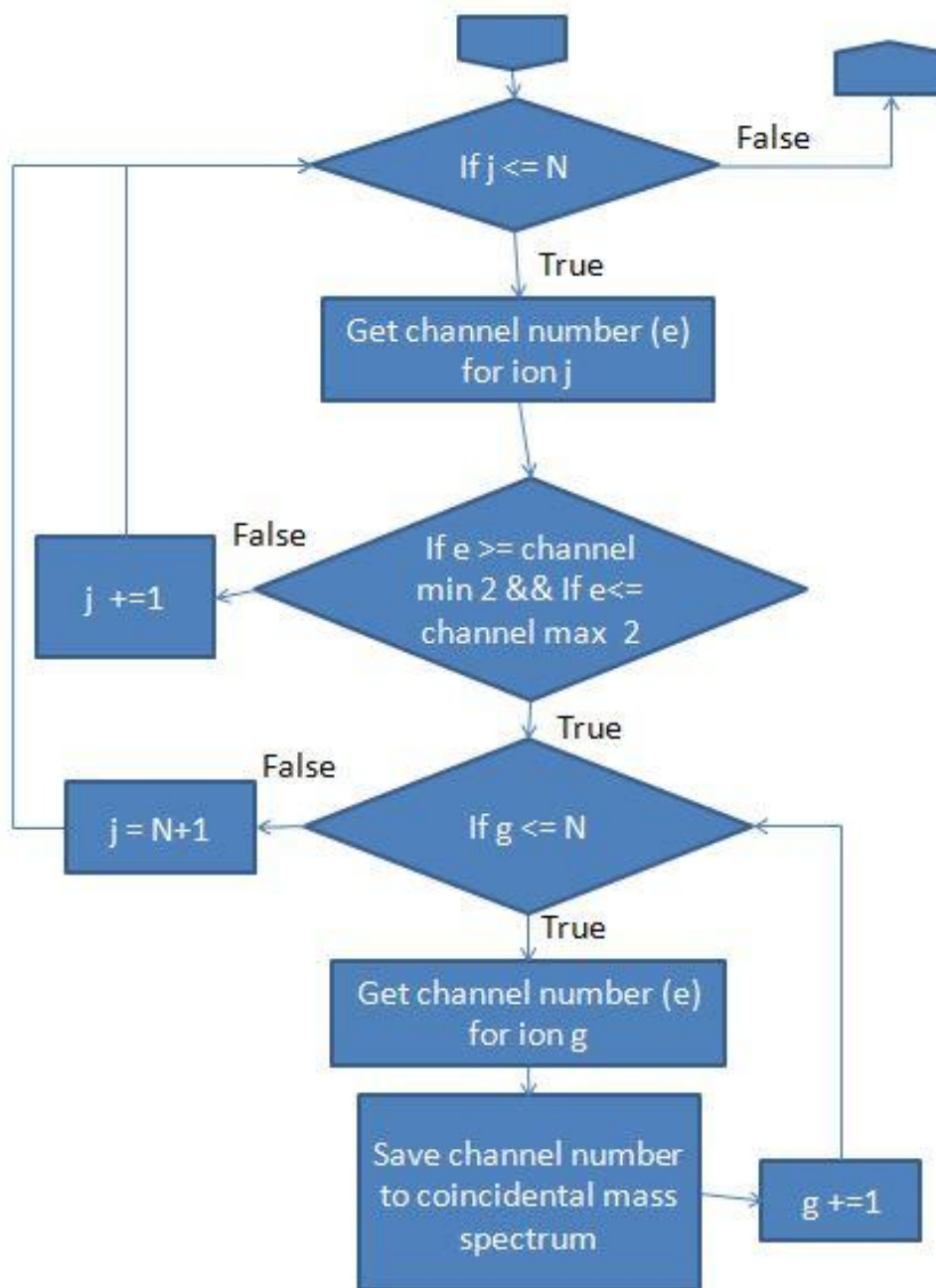


Figure 5.10 Double Coincidence Logic Tree Part 2 of 2. Logic tree for double ion coincidence calculation part 2 of 2 (figures 5.9-5.10).

One Coincidence One Anti-Coincidence

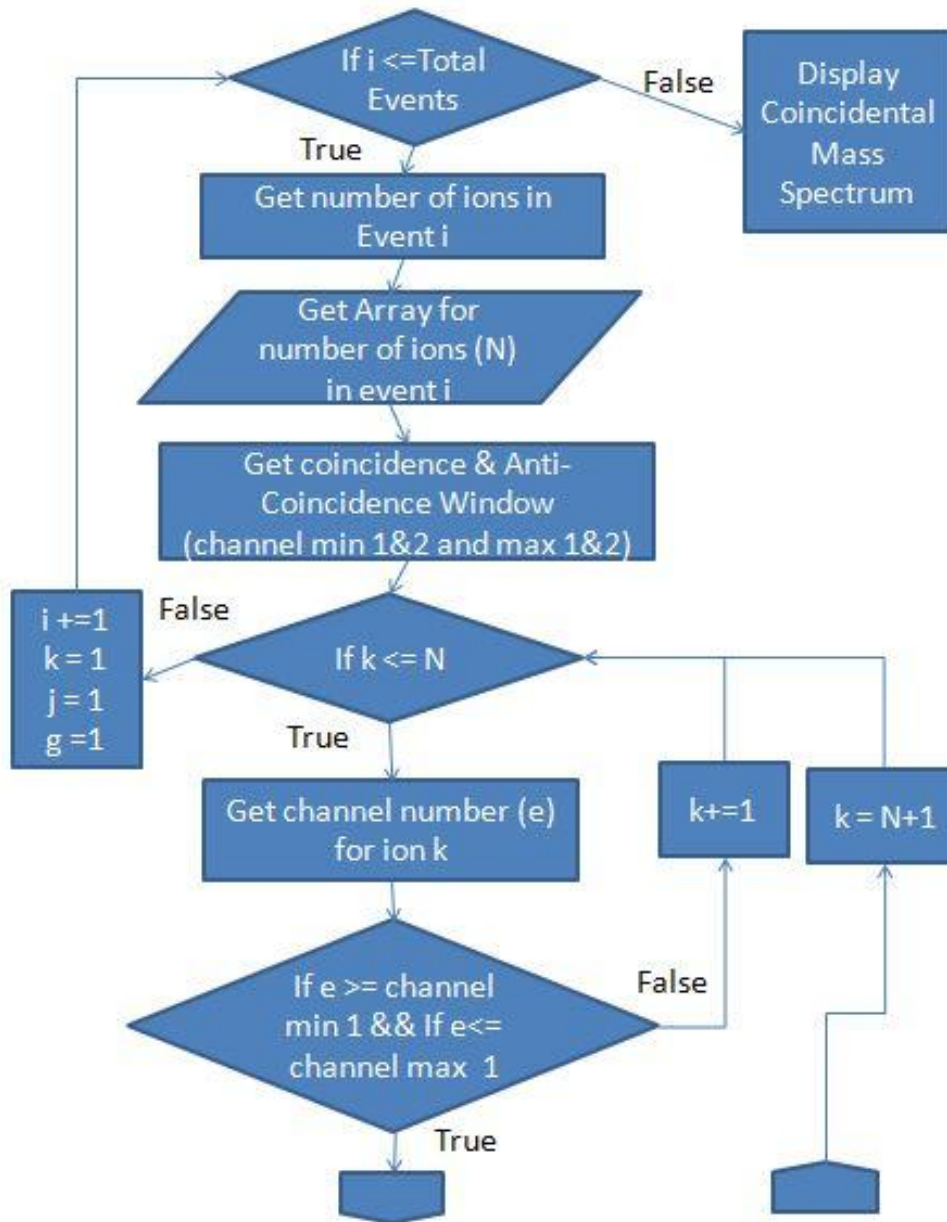


Figure 5.11 One-Ion Coincidence One-Ion Anti-Coincidence Logic Tree Part 1 of 2.

Logic tree for one-ion coincidence one-ion anti-coincidence calculation part 1 of 2

(figures 5.11-5.12).

One Coincidence One Anti-Coincidence

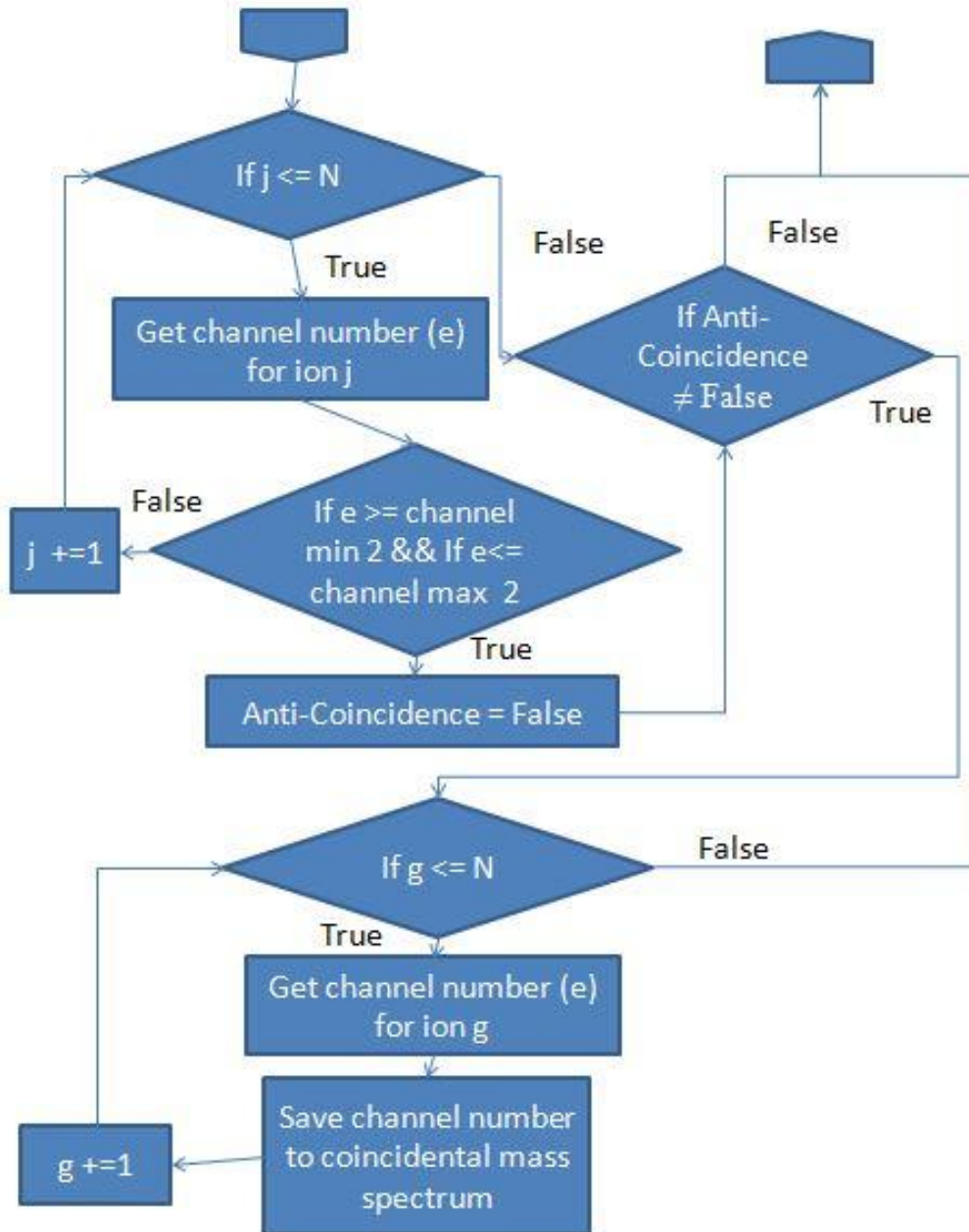


Figure 5.12 One-Ion Coincidence One-Ion Anti-Coincidence Logic Tree Part 2 of 2.

Logic tree for one-ion coincidence one-ion anti-coincidence calculation part 2 of 2 (figures 5.11-5.12).

with the co-emitted ions and the second will have an anti-coincidence relationship. Each event is examined for the first ion of interest. In the affirmative the event is further examined for the second ion. In the affirmative, then the event is excluded from the one ion coincidence and one ion anti-coincidence mass spectrum. In the negative, then all ions detected in that event will be included in the one ion coincidence and one ion anti-coincidence mass spectrum. This process is repeated for all events in the mass spectrum. After this has been completed the mass spectrum can be investigated further.

Systems with nanometric inhomogeneities are a case where one-ion coincidence and one-ion anti-coincidence is relevant.^[108] In the citation the nano-objects (phage) were placed on a NALDI substrate. This substrate has characteristic secondary ion emission such as, F⁻ and other fluorine containing molecules which only originate from the substrate. Impacts of C₆₀ or Au₄₀₀ on large nano-particles can be entirely contained within the nano particle, if the nano-particle is large enough.^[53] However, there will be some grazing impacts at the interface between the nano-particle and the substrate.^[54] Most important for analysis are “bulls-eye” impacts which strike only the nano-object. In this case considered here, the latter is of such reduced dimensions that emission from the substrate is observed. To obtain a mass spectrum from the nano-objects which does not contain the grazing impacts, a one-ion coincidence and one-ion anti-coincidence calculation needs to be performed. An ion specific to the phage is Adenine-H⁺ which is an amino acid residue from the protein shell and will serve as the coincidental ion of interest, and the anti-coincidence ion of interest is F⁻ which is from the substrate. The resulting mass spectrum is only from bulls-eye impacts on the phage (figure 5.13-5.15).

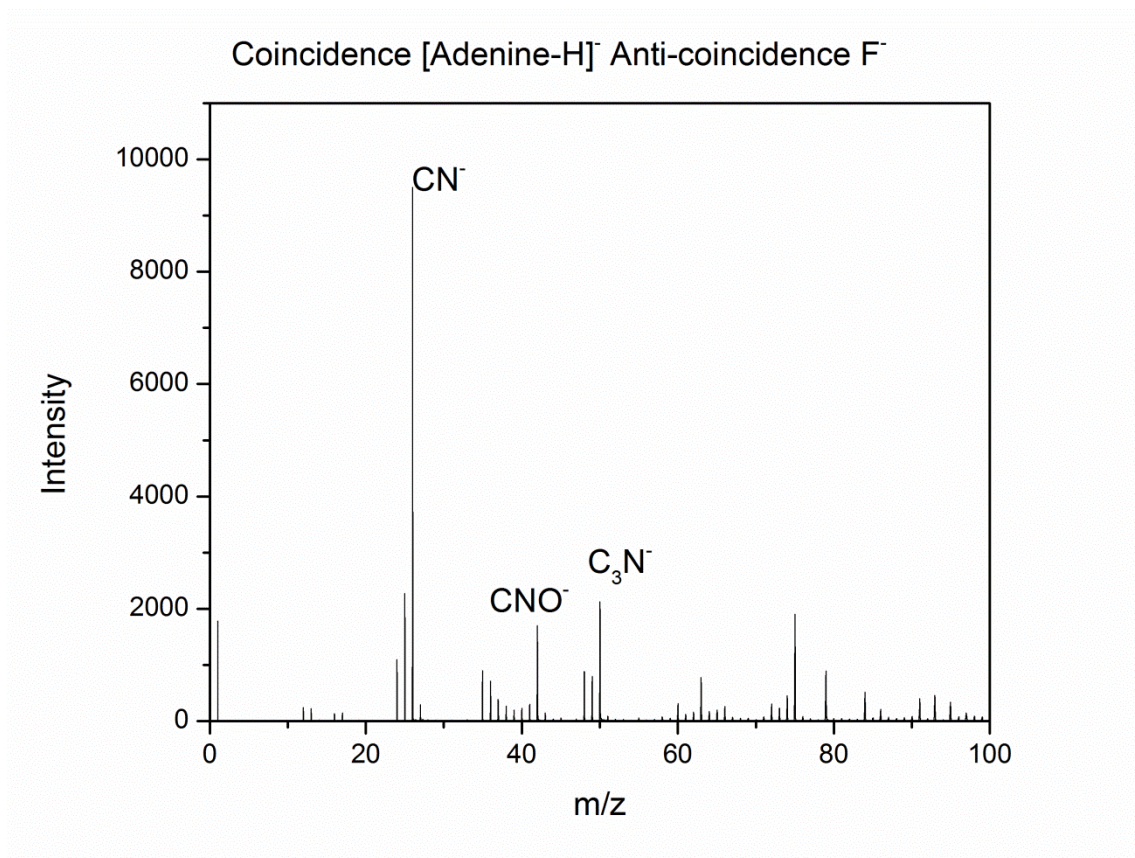


Figure 5.13 Mass Spectrum from Phage Deposited on NALDI Plate: One-Ion Coincidence One-Ion Anti-Coincidence 0-100m/z. One-ion coincidence one-ion anti coincidence [Adenine-H]⁻ and F⁻ for impacts on phage and NALDI plate.

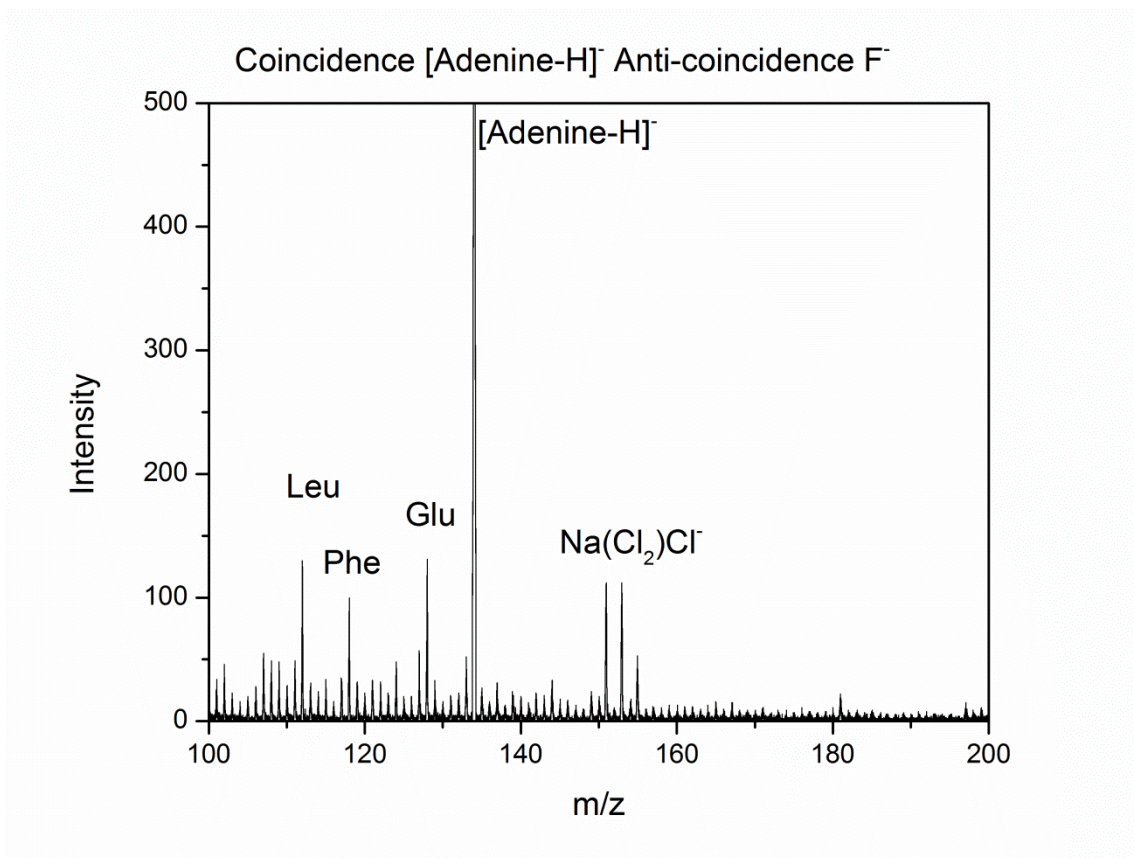


Figure 5.14 Mass Spectrum from Phage Deposited on NALDI Plate: One-Ion Coincidence One-Ion Anti-Coincidence 100-200m/z. One-ion coincidence one-ion anti coincidence [Adenine-H]⁻ and F⁻ for impacts on phage and NALDI plate.

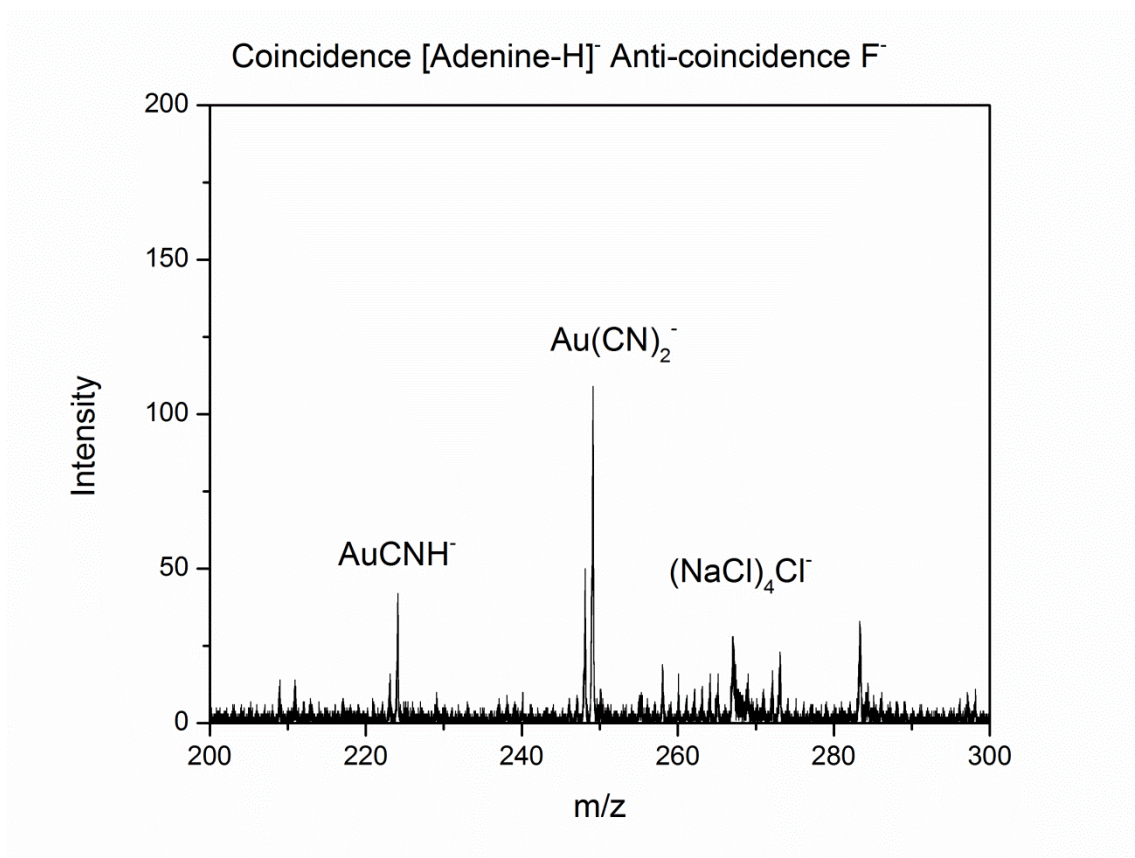


Figure 5.15 Mass Spectrum from Phage Deposited on NALDI Plate: One-Ion Coincidence One-Ion Anti-Coincidence 200-300m/z. One-ion coincidence one-ion anti coincidence [Adenine-H]⁻ and F⁻ for impacts on phage and NALDI plate.

Double Coincidence and One Ion Anti-Coincidence: Here three ions of interest are selected. Two will be in coincidence while the other will be in anti-coincidence. In this case a three component system can be investigated similarly to the one ion coincidence and one ion anti-coincidence calculation. The calculation logic chart can be found in figure 5.16-5.18. A brief written description follows, from the main mass spectrum three ions are selected, the first two are coincidental ions and the third is an anti-coincidence ion. The masses recorded from each impact are examined of for these three ions. First, an event is examined to determine if one of the coincidence ions is present in the event, if true then the event is examined to determine if the second coincidence ion is in the event. In the affirmative, the event is examined further and if the third ion is in the event, in the affirmative the event is excluded from the coincidental mass spectrum. In the negative, all the ions detected in the event are written to the coincidence mass spectrum. This process is repeated for all events in the mass spectrum. After all events have been examined then the coincidental mass spectrum is displayed for further investigation.

An example of double coincidence and one-ion anti-coincidence is presented in figure 5.19-5.20 for the case of the phage on a NALDI plate.

A one-ion coincidence and one-ion anti-coincidence mass spectrum contains peaks that do not belong to the phage, namely NaCl clusters (figure 5.13-5.15). TEM images confirmed the presence of salt crystals on the NALDI plate, and on the phage. Thus the NaCl cluster peaks in the mass spectrum originate from grazing impacts on phage deposited on the NaCl crystals. A mass spectrum of only these impacts can be

Double Coincidence & One Anti-Coincidence

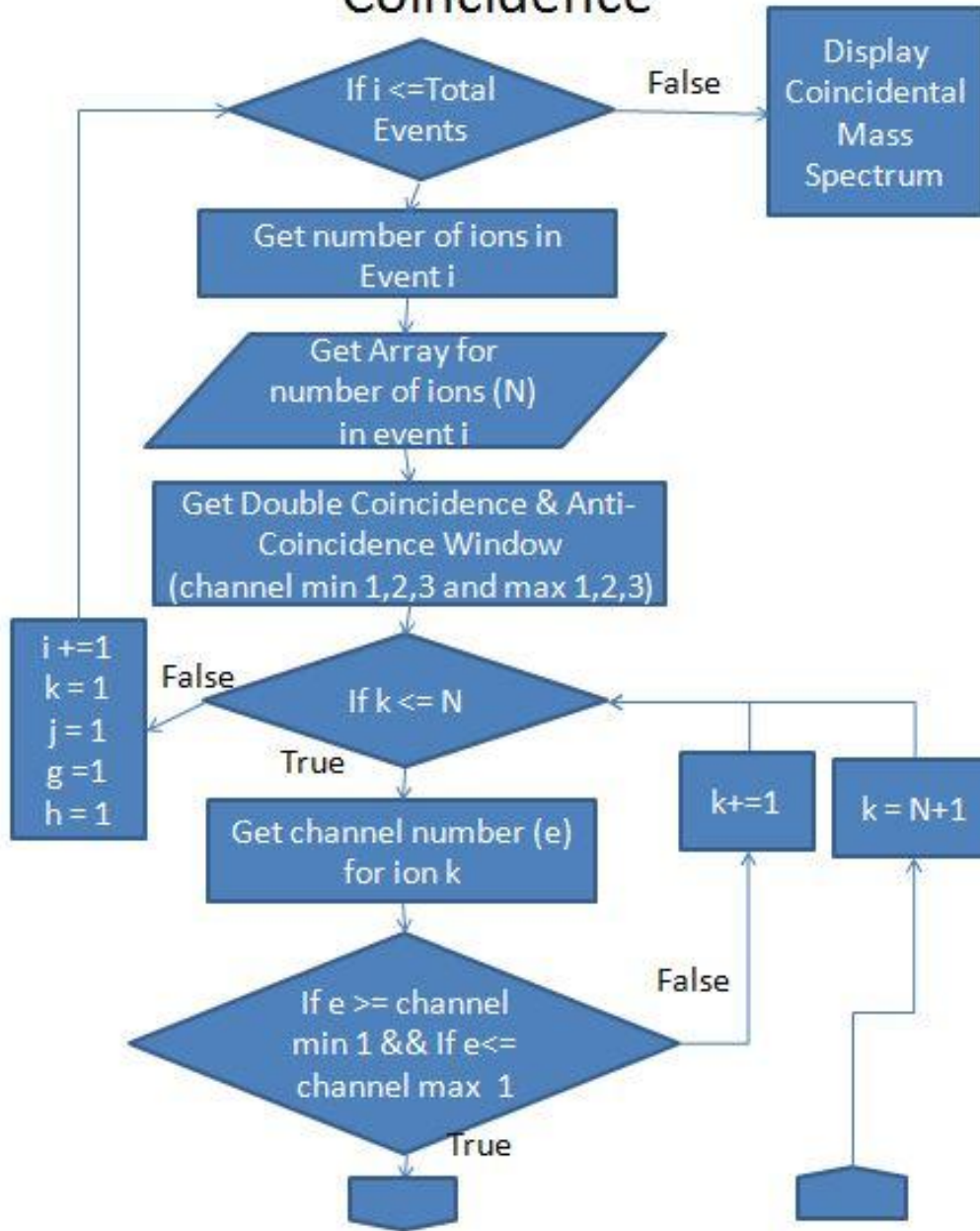


Figure 5.16 Double Coincidence One Ion Anti-Coincidence Logic Tree Part 1 of 3.

Logic tree for the double coincidence one ion anti-coincidence calculation part 1 of 3 (figures 5.16-5.18).

Double Coincidence & One Anti-Coincidence Continue

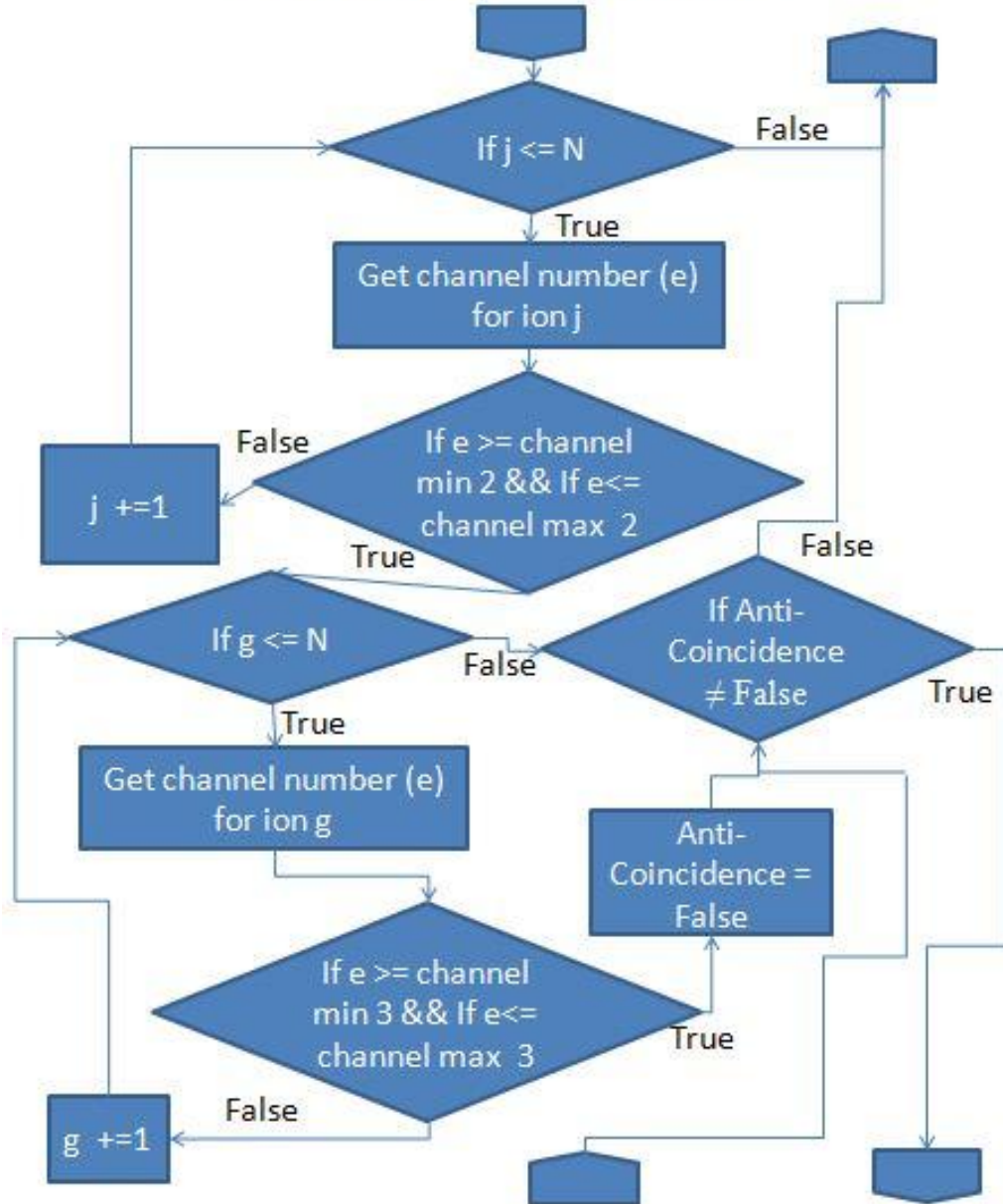


Figure 5.17 Double Coincidence One Ion Anti-Coincidence Logic Tree Part 2 of 3.

Logic tree for the double coincidence one ion anti-coincidence calculation part 2 of 3 (figures 5.16-5.18).

Double Coincidence & One Anti-Coincidence Continue

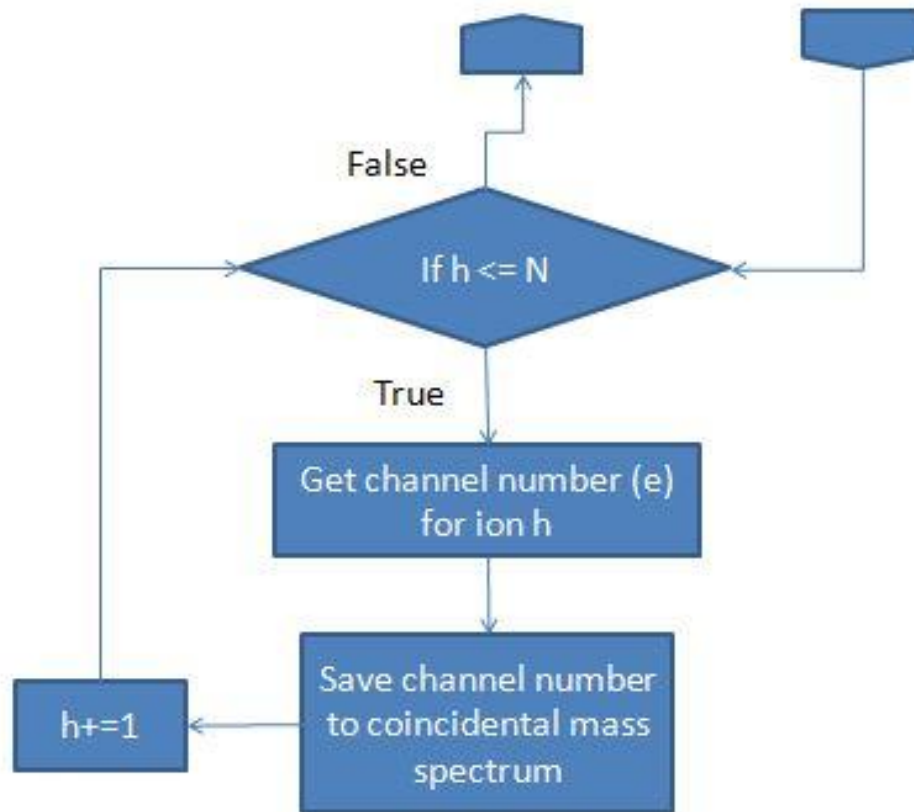


Figure 5.18 Double Coincidence One Ion Anti-Coincidence Logic Tree Part 3 of 3.

Logic tree for the double coincidence one ion anti-coincidence calculation part 3 of 3 (figures 5.16-5.18).

generated by placing a coincidence window on [Glutamic acid-H]⁻, a second coincidence window on NaCl₂⁻ and an anti-coincidence window on F⁻ (figure 5.19-5.20). In this case we get a refined mass spectrum from just the grazing impacts on phages covered by or in close proximity to salt crystals.

5.4 EIGHT ANDODE MASS RESOLUTION

A previous analysis program written by Rickman^[36], lacks the features which are needed for more advanced analysis, such as double coincidence, anti-coincidence and analysis of events with more than 50 ions in an event. A data processing scheme achieving these requirements is described below. Additionally, the method of coincidence analysis has been streamlined for faster execution on reduced random access memory.

A logic table can be found in figure 5.21-5.24. The data are loaded into the software in three loops, first the file is selected and the raw data are put into a one-dimensional array. This array will contain, sequentially, the data from each projectile impact (event), an example of this one-dimensional array can be found in table 5.1. A written description of the array follows, the channel number the ion was detected at paired to the anode it was detected on for as many ions that were detected in a single impact (up to 200 ions) will be listed. The end of an event is indicated by the end-of-collection time stamp. After the data are loaded the number of events is counted, corresponding to the number of end-of collection time stamps (32768). Additionally, the length of the acquisition is determined based on the largest channel number in the file.

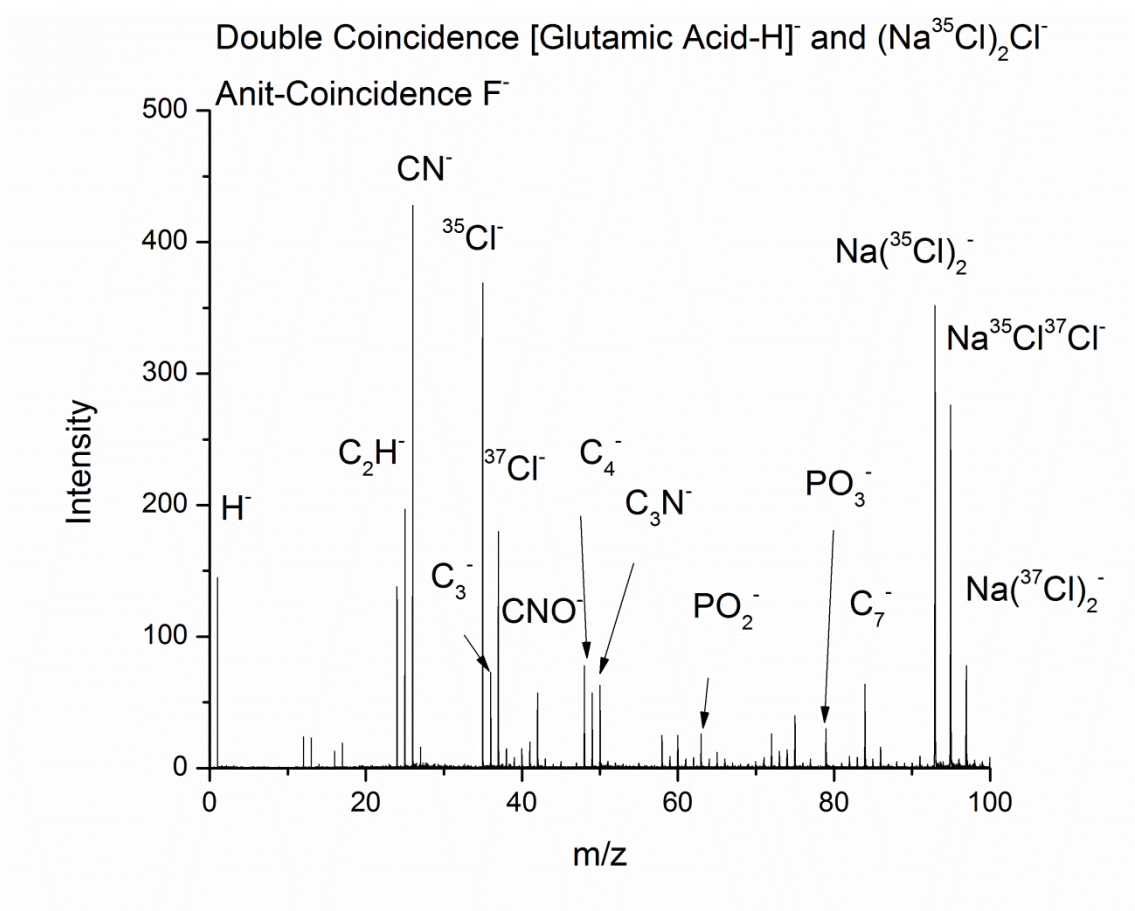


Figure 5.19 Mass Spectrum from Phage Deposited on NALDI Plate: Double Coincidence One-Ion Anti-Coincidence 0-100m/z. A double coincidence of [Glutamic acid-H]⁻, (NaCl)₂Cl⁻ and anti-coincidence F⁻.

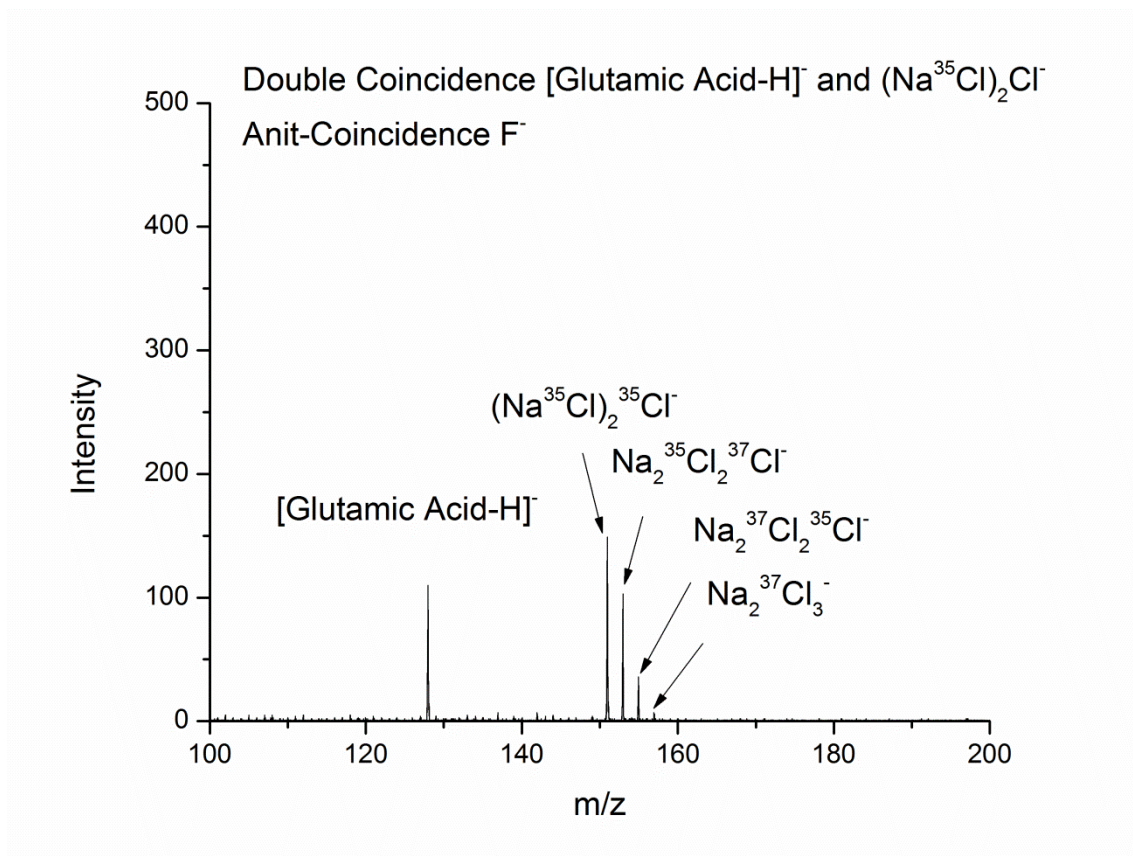


Figure 5.20 Mass Spectrum from Phage Deposited on NALDI Plate: Double Coincidence One-Ion Anti-Coincidence 100-200m/z. A double coincidence of [Glutamic acid-H]⁻, (NaCl)₂Cl⁻ and anti-coincidence F⁻.

Load Mass Spectrum

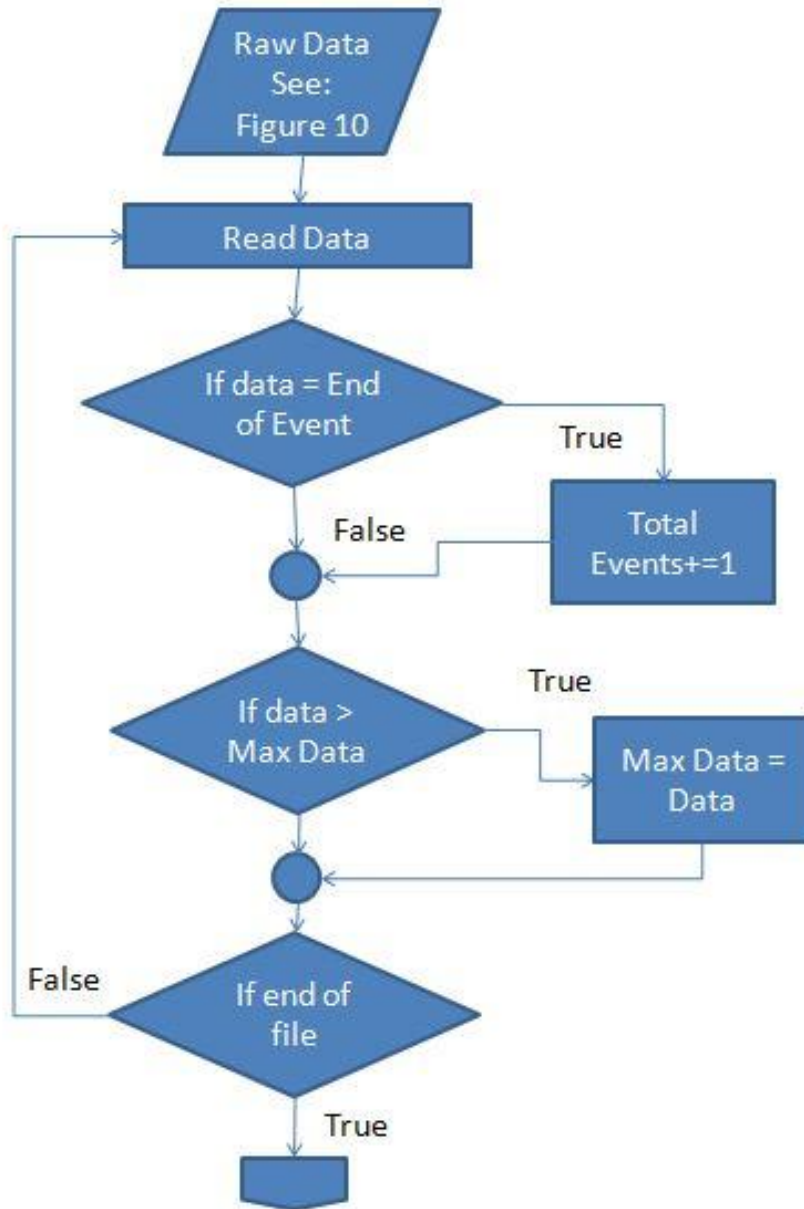


Figure 5.21 Load Mass Spectrum Logic Tree Part 1 of 4. Logic tree part 1 of 4 (figures 5.21-5.24) for loading mass spectra into the SAMPI program.

Load Mass Spectrum Continued

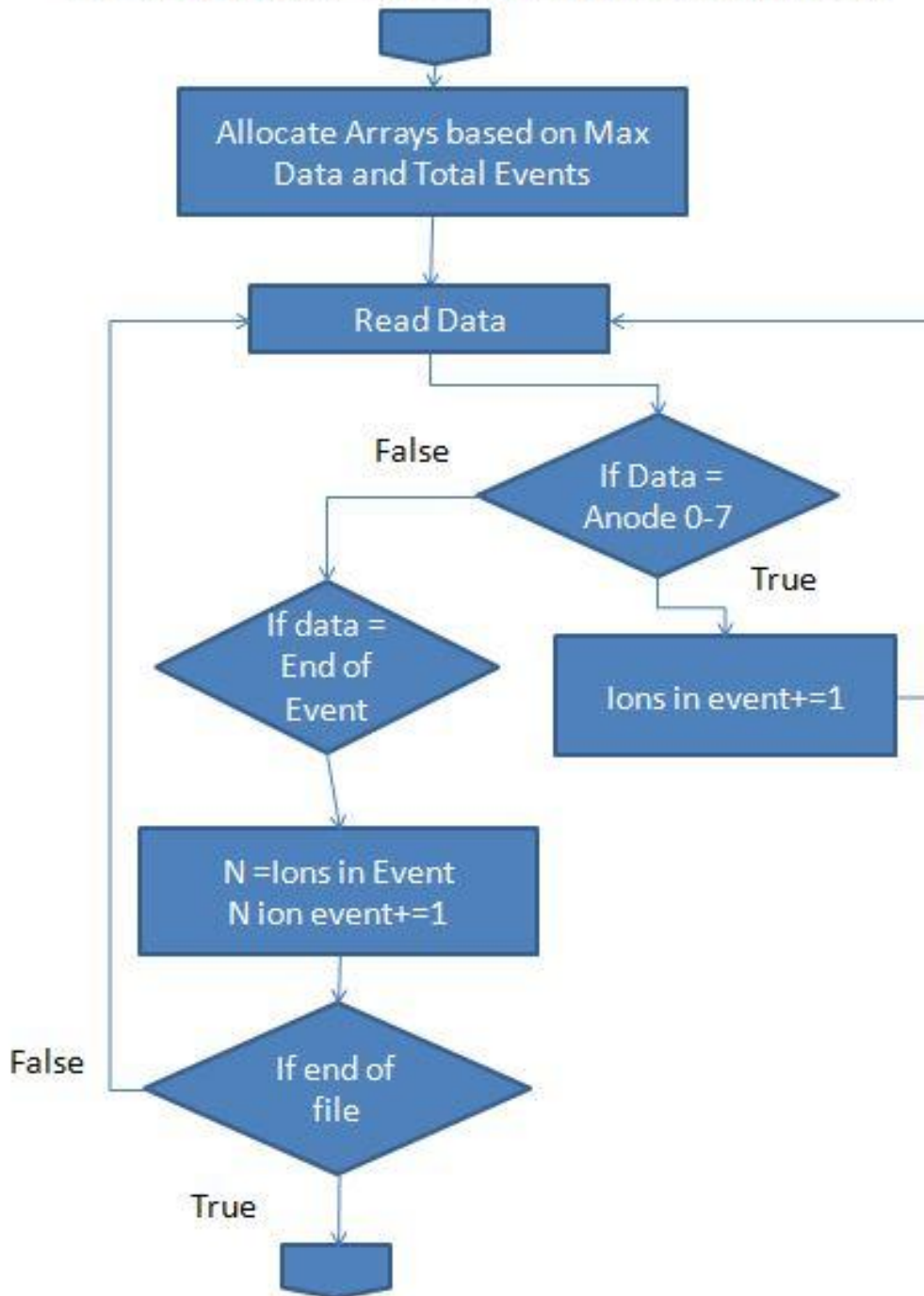


Figure 5.22 Load Mass Spectrum Logic Tree Part 2 of 4. Logic tree part 1 of 4 (figures 5.21-5.24) for loading mass spectra into the SAMPI program.

Load Mass Spectrum Continued

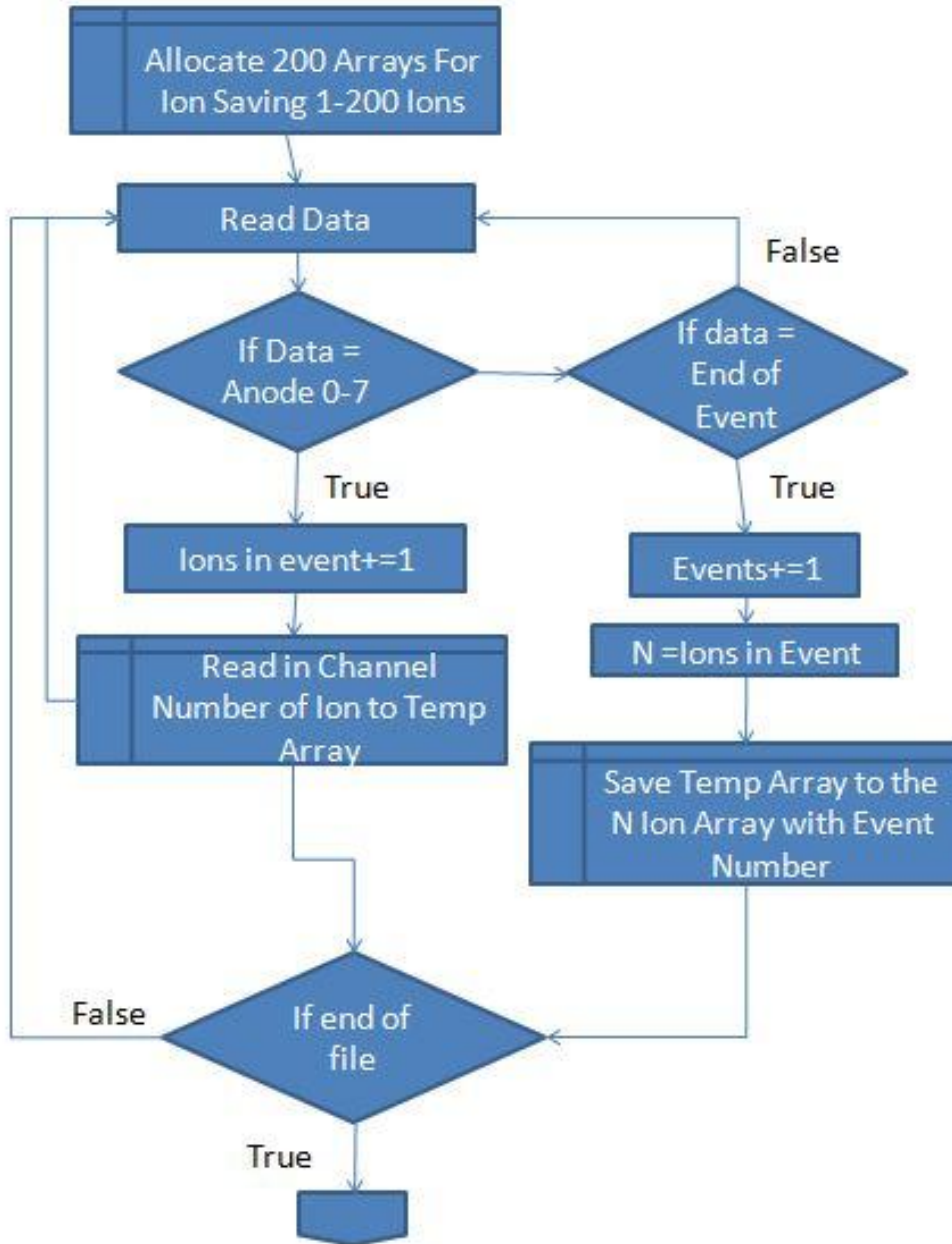


Figure 5.23 Load Mass Spectrum Logic Tree Part 3 of 4. Logic tree part 3 of 4 (figures 5.21-5.24) for loading mass spectra into the SAMPI program.

Load Mass Spectrum Continued

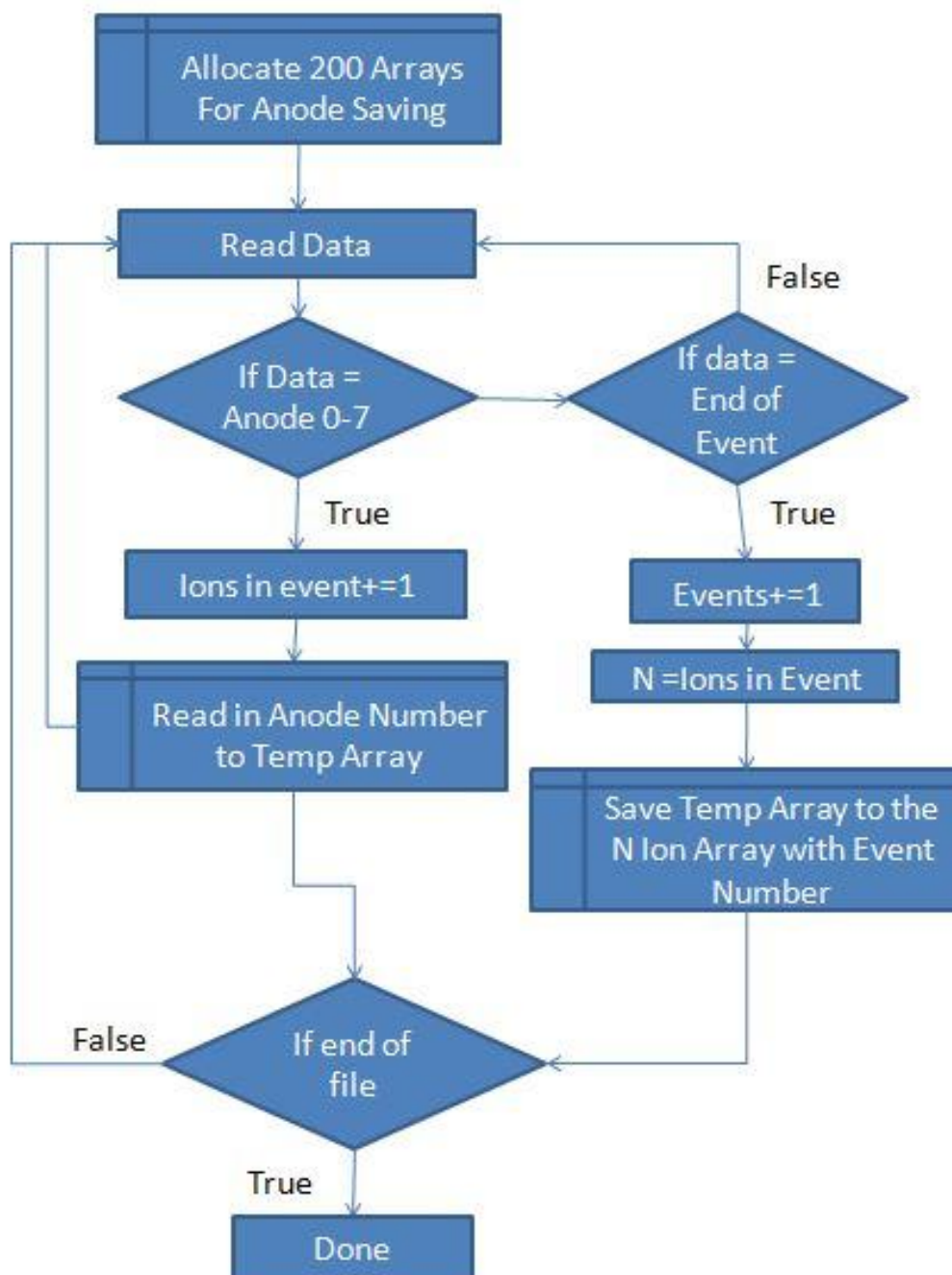


Figure 5.24 Load Mass Spectrum Logic Tree Part 4 of 4. Logic tree part 4 of 4 (figures 5.21-5.24) for loading mass spectra into the SAMPI program.

Table 5.1 Example 1-D Mass Spectrum Array. Example array from a mass spectrum, with channel number of ions detected, anode number and end of event marker.

0
11545
0
12985
0
14142
0
18755
0
22605
0
40586
32768
32768
32768
0
25710
32768
0
2858
0
24917
0
48200
32768
32768
0
14893
0
24565
0
24907
0
203320
32768
...

Mass spectra arrays are created based on the number of events, and the length of the acquisition.

The second load step is to count the number of secondary ions in each event. This can be displayed as a histogram corresponding to the ion multiplicity for a mass spectrum (figure 5.25). These numbers are used to allocate 200 dynamic arrays, one for each different number of detected secondary ions (1-200). This procedure ensures the least amount of memory is used for analysis. For example if there are 450 events with 24 ions detected, a 25x450 array is allocated.

The third step is to inspect each event and write the data into the corresponding array. Each time, the event number and each secondary ion's channel number are written into the array (example can be found in table 5.2). The last step is to create an identical set of 200 arrays that the channel numbers were written to, and instead of writing the channel numbers, the anode on which the ion was detected is written (table 5.3). The result is readily accessible data from which events can be selected and investigated a number of different ways see sections 5.2-5.3.

As mentioned previously, the expansion of analysis to 200 from 50 ions in a single event drastically increases the amount information available. Figure 5.26 shows the total ion distribution calculated using 50 ion limit. In figure 5.25 the total ion distribution, from the same mass spectrum, is calculated with the 200 ion limit. With a 50 ion limit the most prolific ion emission events are excluded, which are more likely to contain an ion of interest. Additionally, the number of zero ion events is significantly over estimated, because any event with greater than 50 ions is considered a null event.

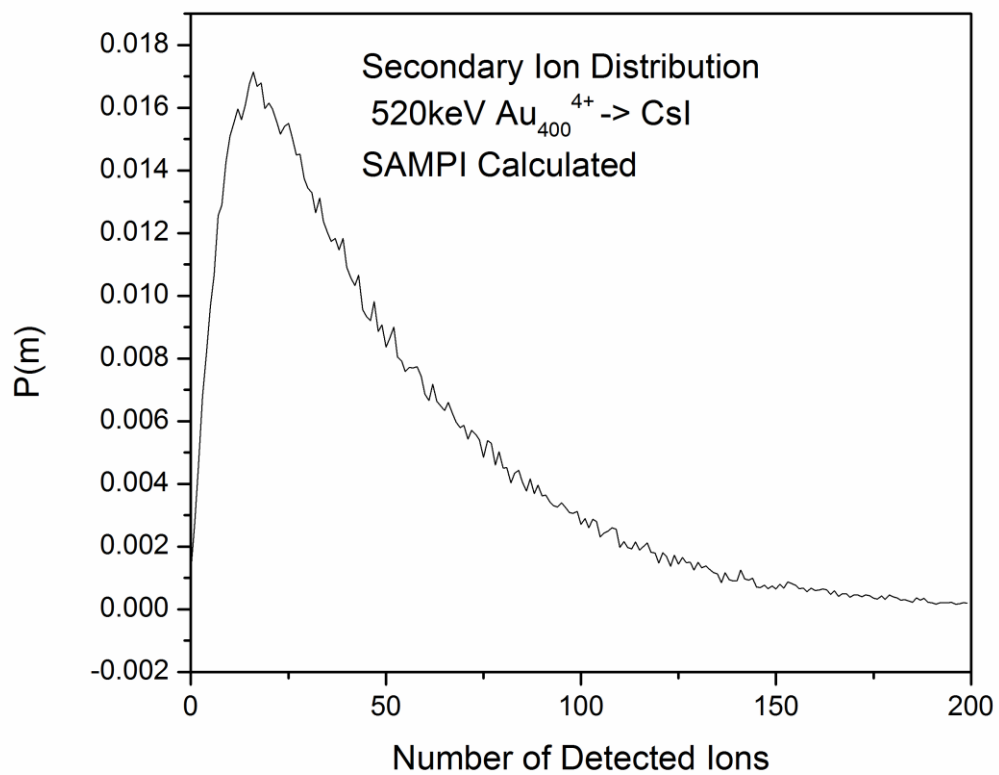


Figure 5.25 Total Ion Distribution for 200 Arrays. The total secondary ion distribution for Au₄₀₀⁴⁺ impacts on CsI calculated with the SAMPI software.

Table 5.2 14 Ion Array with Channel Numbers. The 14 Ion array, events containing exactly 14 ions, with corresponding event number and channel number for a selected group of events.

Event	lon 1	lon 2	lon 3	lon 4	lon 5	lon 6	lon 7	lon 8	lon 9	lon 10	lon 11	lon 12	lon 13	lon 14
121	2301	13095	21798	52566	56654	73370	75510	75920	76998	88260	93202	93903	101469	101464
251	24047	25504	30853	31866	31864	41338	47581	60777	105106	119321	119321	122951	122952	125717
485	6498	8337	8509	21313	65490	65942	69683	85730	88494	91411	100537	116854	122944	125676
866	873	2998	19412	35873	48438	67007	73519	97332	106916	109392	111397	114834	122292	122970
1040	3686	18135	35539	45796	49380	60336	74010	78516	94476	96926	114036	120220	120279	129492
1171	2596	3045	3921	3922	18310	20000	21587	25688	26050	27379	44721	58768	91159	94112
1458	6148	13606	17518	20495	25344	26076	39092	39384	52674	52653	95945	98989	119523	130301
1463	13604	16560	30128	30138	30122	30132	44907	52682	52667	52648	52657	53981	68088	102610
1740	16835	23305	38055	49029	53485	66834	69088	76314	87750	88626	93347	119968	124381	128077
1979	2249	19513	56559	56560	70812	75043	75191	81619	82601	91831	98212	103527	103528	105846
2096	27613	33497	53235	93597	102289	103036	104137	104137	111953	113356	128460	128489	129335	130572
2194	2210	29966	43172	46403	62812	62813	64086	71215	72182	75458	79188	79186	97465	108701
2693	5586	6789	7828	23263	33937	35196	46468	59299	79547	103046	112648	116132	119858	120254
2713	12999	27944	60234	73137	76791	81372	81387	81450	83479	91495	95656	102802	108617	129692
2758	12494	17057	39122	39118	48493	55188	59868	61618	61632	61646	62373	71973	88126	106848
2944	10407	12138	16589	27432	47777	47777	55252	58386	74780	76234	106449	108775	114022	124300
3302	6375	8932	17317	25574	45620	45620	53435	56202	60684	97395	106846	119194	122374	128522

Table 5.3 14 Ion Array with Anode Number. The 14 Ion array, events containing exactly 14 ions, with corresponding event number and anode number of each ion in a selected group of events.

Event	Ion 1	Ion 2	Ion 3	Ion 4	Ion 5	Ion 6	Ion 7	Ion 8	Ion 9	Ion 10	Ion 11	Ion 12	Ion 13	Ion 14
121	5	3	3	3	3	2	2	4	4	1	0	2	4	3
251	2	3	3	5	2	1	5	2	2	2	1	3	2	7
485	3	1	3	5	2	2	5	3	2	3	7	3	6	2
866	6	3	0	6	2	2	0	3	1	1	3	2	1	4
1040	2	2	7	1	3	3	3	4	3	2	3	2	0	2
1171	4	1	3	2	6	3	3	7	3	2	2	2	6	0
1458	7	6	5	1	4	7	3	2	7	4	5	2	4	2
1463	1	7	7	6	5	4	4	7	6	1	0	2	0	5
1740	1	1	2	2	5	3	2	1	2	6	3	1	3	3
1979	0	2	3	2	4	6	1	0	2	2	2	3	2	0
2096	1	0	5	1	2	3	2	1	2	3	3	2	3	3
2194	1	4	3	3	3	2	2	2	2	5	7	0	2	4
2693	4	2	3	2	1	1	4	4	2	3	7	6	3	0
2713	3	2	3	2	5	4	0	1	0	1	3	3	2	7
2758	3	1	5	4	2	6	5	6	5	4	5	4	3	2
2944	2	3	3	2	2	1	3	2	2	2	4	4	4	5
3302	3	6	1	2	4	3	2	4	2	2	2	1	4	1
3453	2	5	7	0	4	1	2	2	3	7	3	1	3	4

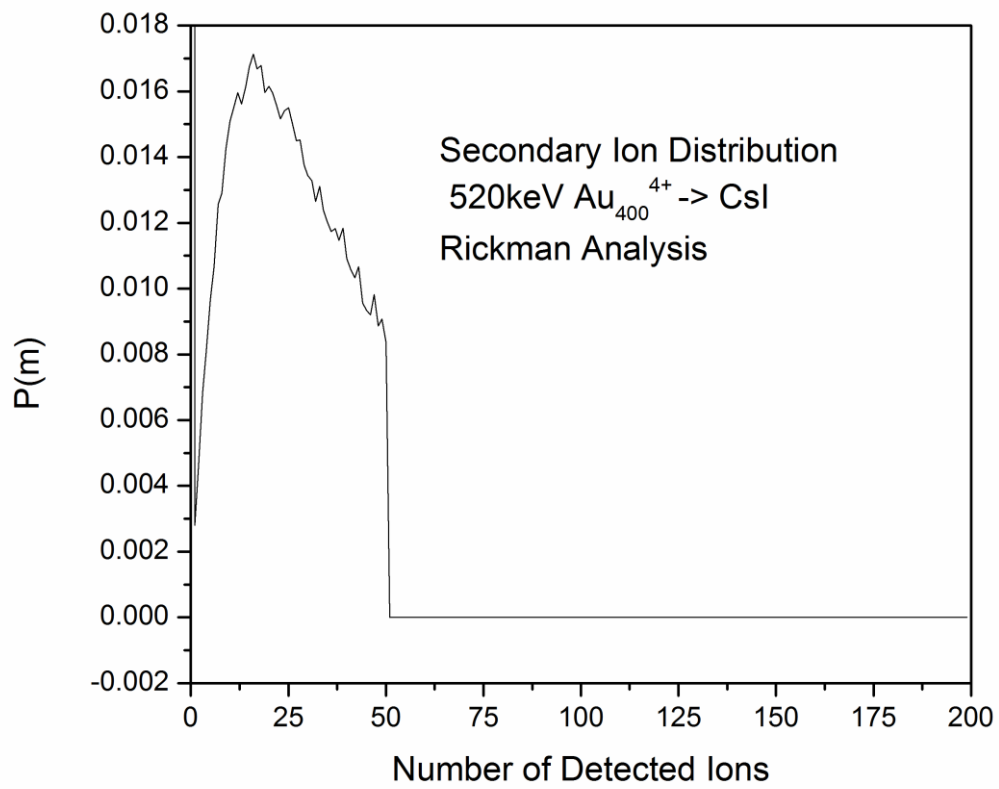


Figure 5.26 Total Ion Distribution for 50 Arrays. The total secondary ion distribution for Au₄₀₀⁴⁺ impacts on CsI calculated with the 50 ion limit.

By increasing the limit from 50 to 200, a more accurate and potentially more useful mass spectrum and total ion distribution is obtained.

The mass spectra data mentioned so far have abscissa in channel numbers. They can be converted to time-of-flight based on the time length of each channel, for the TDCs used in this study either 250 or 400ps per channel. A Time-of-flight spectrum can be changed to a mass spectrum knowing that each ion is given the same kinetic energy upon entering the field-free region of the time of flight mass spectrometer. Equation 5.2 gives the relationship between time of flight and the mass of the ion detected. The value measured is the difference between detection of an electron being detected and the ion being detected, as the electrons serve as the start of the time of flight measurement. In practice the equation is calculated using four known masses and creating a quadratic equation that fits those values for mass calibration. This approach is well suited for a detector equipped with a single anode. However, in order to detect multiple isobaric ions a multi-anode detector is required. Each anode will inevitably have a different time-of-flight, because each anode will have a different distance to the target (unless machined perfectly). Therefore, a quadratic equation for each anode is required for proper mass calibration. By using a different equation for each anode instead of a single equation for all anodes, the mass resolution can be improved by ~2X (see figure 5.27-29). Figure 5.27 shows the mass resolution full width half max, FWHM, for the uncorrected mass spectrum. The mass resolution for the uncorrected is 905 at m/z 26. Figure 5.28 shows the mass resolution, FWHM, for the corrected mass spectrum (1587 at m/z 26). The

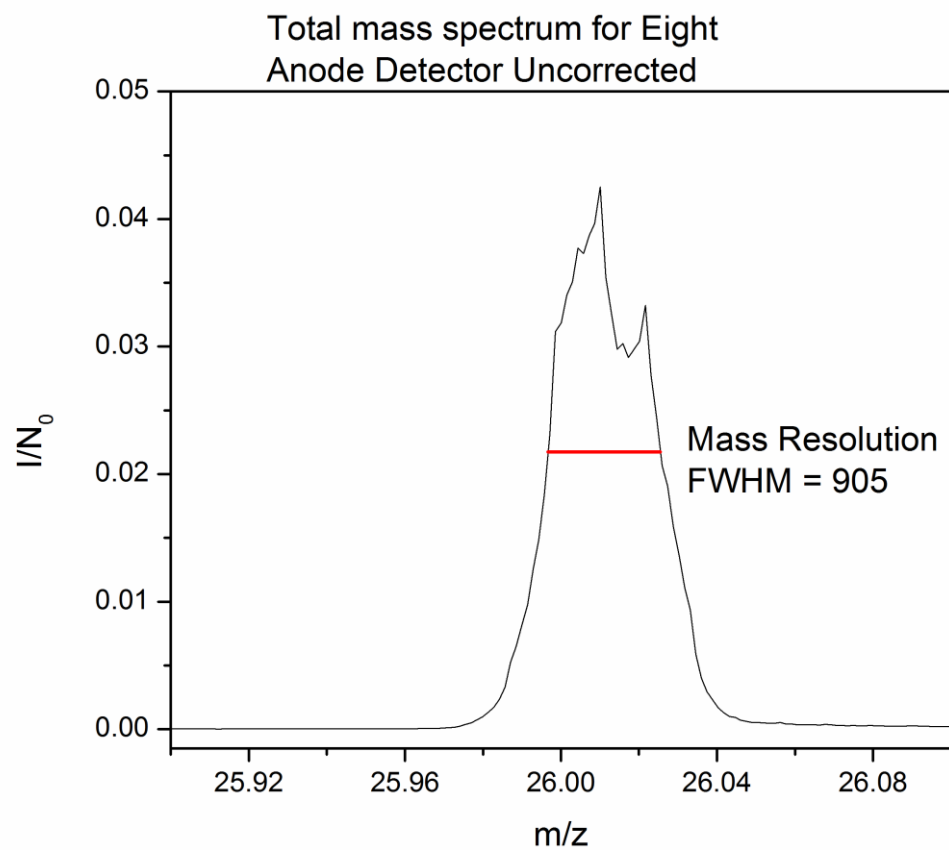


Figure 5.27 Uncorrected Mass Spectrum with Mass Resolution. The mass resolution at FWHM (905) for the uncorrected mass spectrum

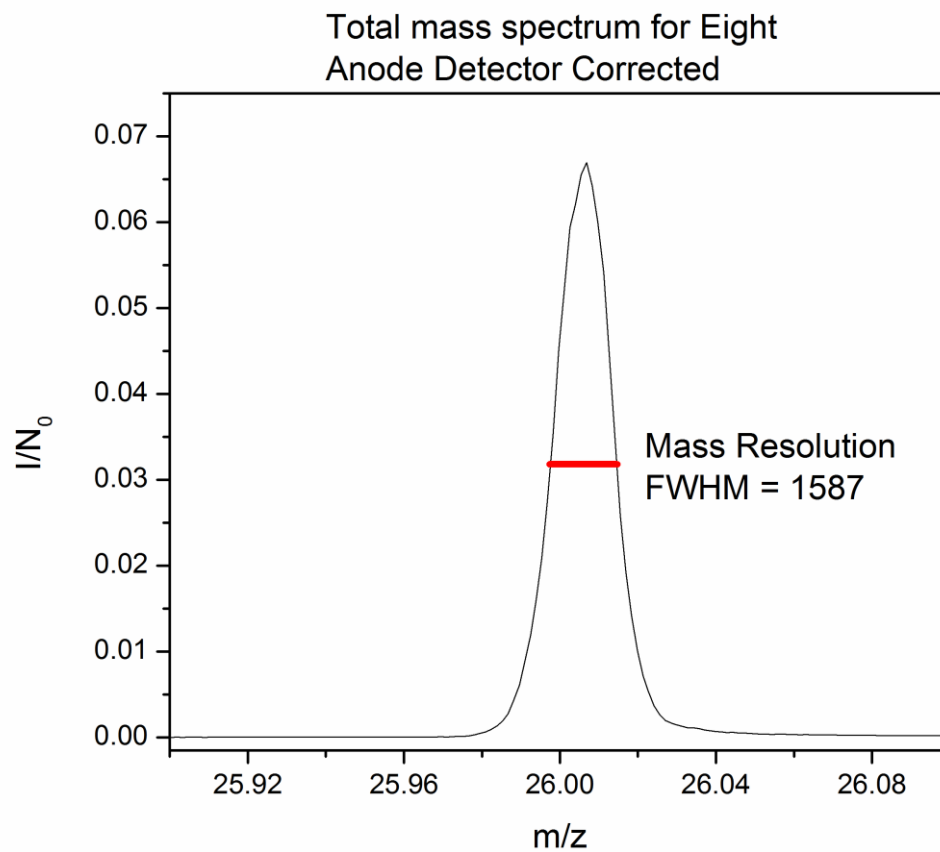


Figure 5.28 Corrected Mass Spectrum with Mass Resolution. The mass resolution at FWHM (1587) for the corrected mass spectrum

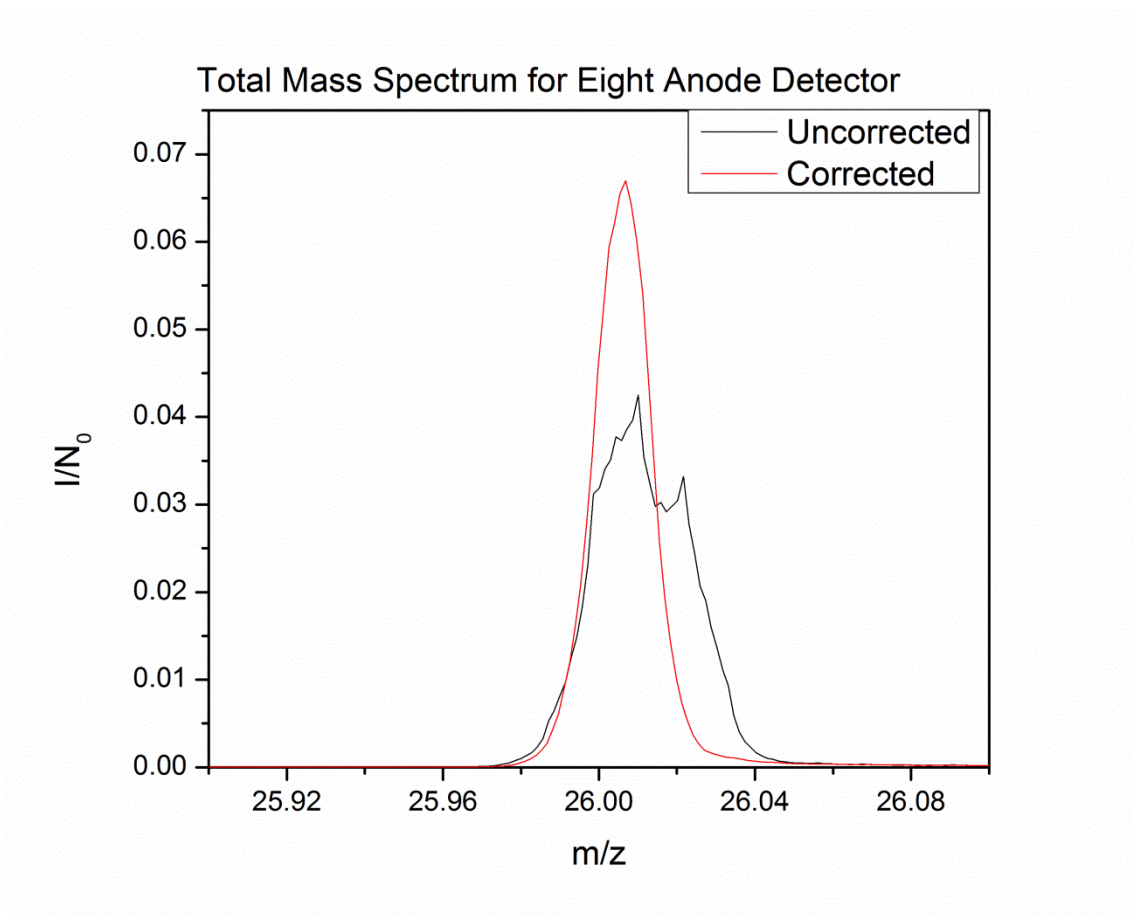


Figure 5.29 Overlay of Corrected and Uncorrected Mass Spectra. The mass resolution improvement and peak shape improvement can be seen

difference in peak shape and resolution improvement for the corrected mass spectrum compared to the uncorrected can be seen in figure 5.29. The procedure used, shifts the data such that all the mass spectra will overlay (see figure 5.30). The uncorrected data for each anode are shown in figure 5.31. There the differences in flight-times for each anode can clearly be seen. The shift is performed by selecting anode zero as the master and shifting all other anodes (1-7) to overlay with anode 0. In principle, any anode could act as the master and zero was chosen because it is loaded first.

$$\text{Equation 5.2 } \mathit{Mass} = \frac{2 * K_e * L^2}{T^2}, \text{ where } K_e \text{ is the kinetic energy of the ion, } L \text{ is}$$

the length of the field free region, and T is the measured time-of-flight.

5.5 ANODE DISTRIBUTION

A single ion polar calculation can display the distribution of an ion of interest on the eight anode detector. An example can be found in figure 5.32. The distribution of an ion of interest will depend on its average angular velocity and other instrument conditions. The angular distribution will be relative to the ion used to center the detector during data acquisition. This distribution can be a function of the mechanism generating the ion, the angle of bombardment, the size of the projectile, target topography and instrument effects.^[100] There have been previous measurements of the angular distribution of various ions with under Au₄₀₀ bombardment using a square 8x8 anode detection system.^[100] The ability to perform similar measurements with an eight anode detector with circular symmetry is described here.

Corrected mass spectra for eight anode detector

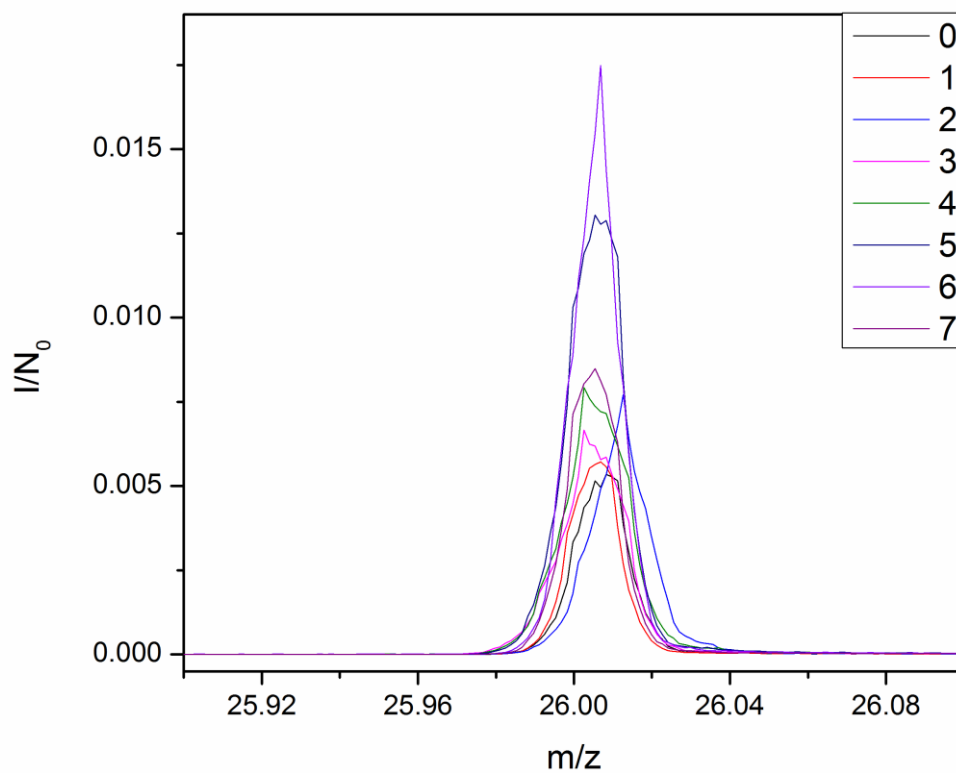


Figure 5.30 Overlay of Corrected Mass Spectra from Each Anode. The mass spectra at m/z 26 are shown for anodes 0-7.

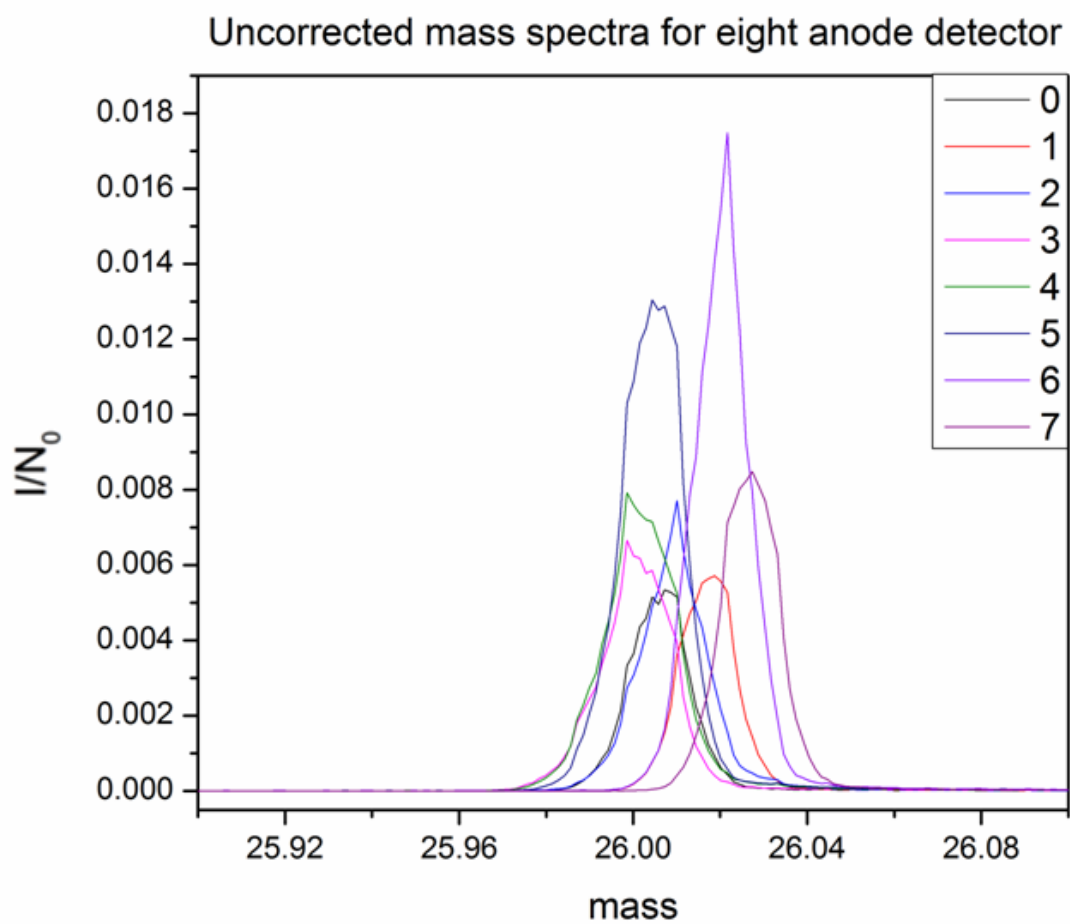


Figure 5.31 Overlay of Uncorrected Mass Spectra from Each Anode. The mass spectra at m/z 26 are shown for anodes 0-7.

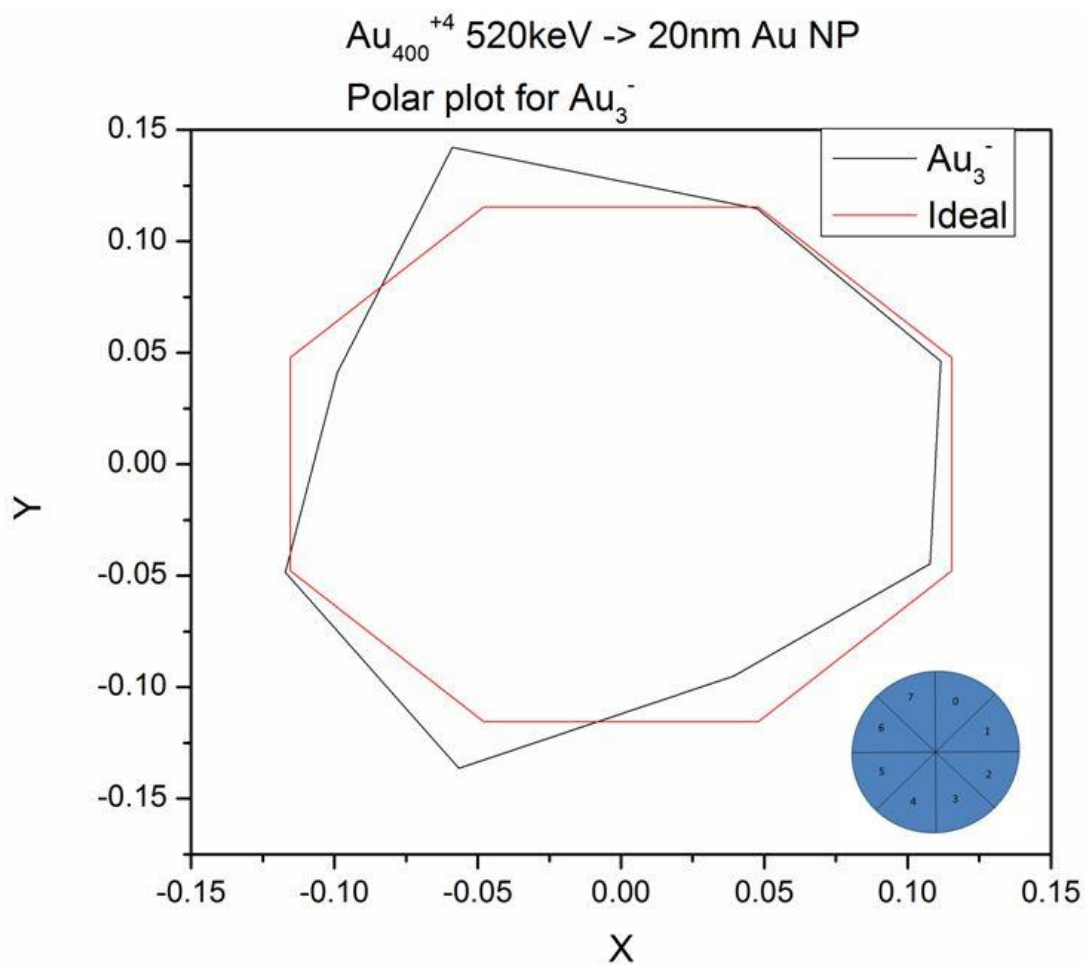


Figure 5.32 One Ion Polar Plot. Polar plot of Au_3^- (black) from impacts of Au_{400}^{+4} on 20nm Au NPs. The red plot is the ideal case, with 1/8 of the signal on each anode.

One Ion Polar Plot Calculation: The logic chart can be found in figure 5.33. From the main mass spectrum a single ion of interest is chosen. Firstly, a single event is examined for the ion of interest, if the ion is in the event the software identifies the anode where the ion of interest was detected. Each time the ion is found in the event (up to 8) the anode for that ion is recorded. This is repeated for all events in the mass spectrum. After all the events have been examined, the number of times the ion of interest was detected on each of the anodes is recorded. The data are plotted and compared to the “ideal” case where each anode has $1/8^{\text{th}}$ of the counts.

Ion Coincidence Polar Plot Calculation: The logic chart for this calculation can be found in figure 5.34-5.35. A brief written description of how the calculation is performed follows. From the main mass spectrum, two ions of interest are selected. With the first ion a coincidence calculation will be performed. The anode distribution will be calculated for the second ion, when it is in coincidence with the first ion. To calculate the anode distribution each event is examined to determine if the first ion was detected in the event. In the affirmative the event will be further examined to determine if the second ion was also detected in that event. If the second is in the event, then the software determines the anode on which the second ion was detected. If the second ion is detected more than once in the event the anode information for each time the ion is detected the anode is recorded. The examination is repeated for all events in the mass spectrum. After all events have been examined the number of times the second ion was detected on each anode, in coincidence with the first ion, is recorded. The data are

One Ion Anode Polar Plot

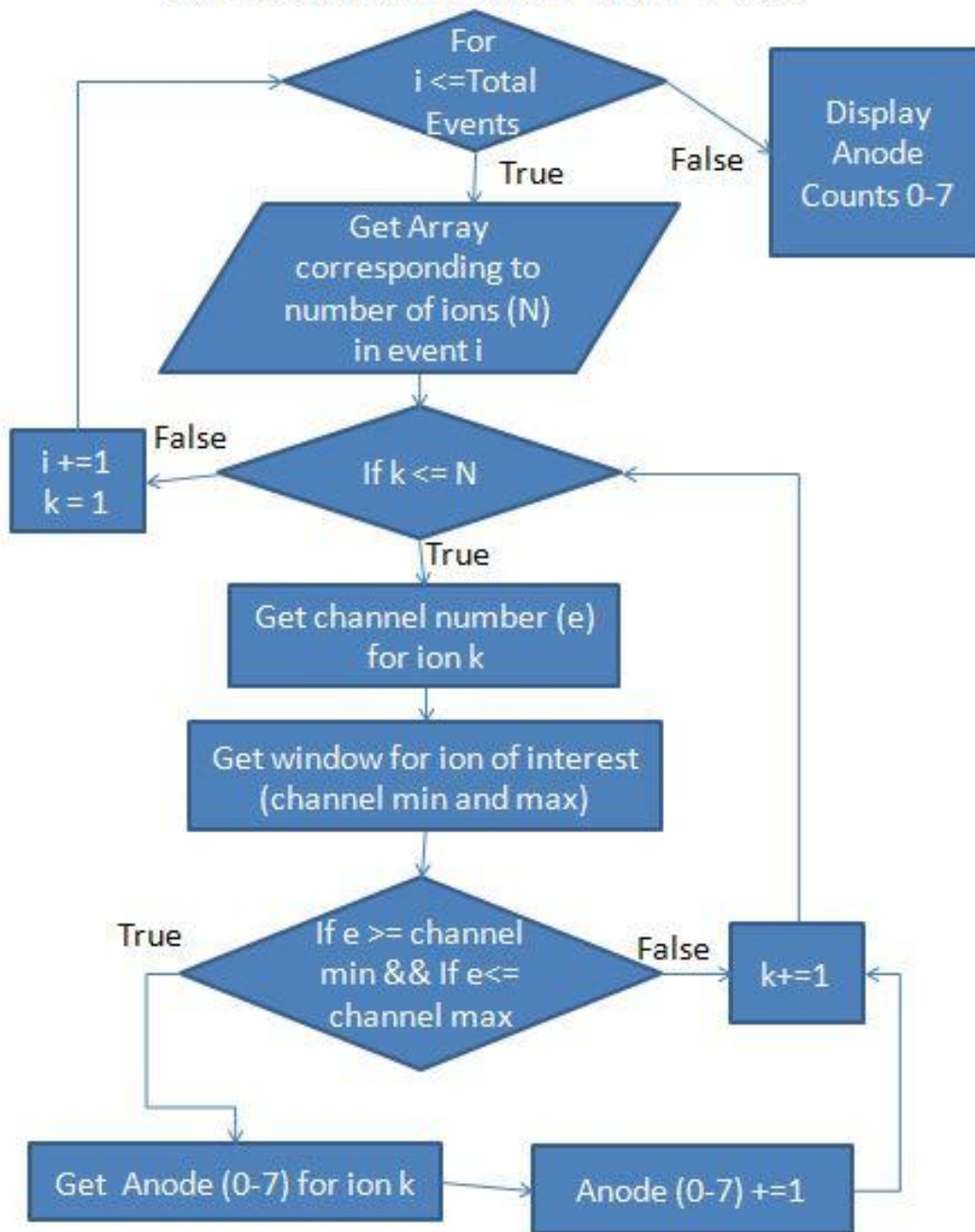


Figure 5.33 One Ion Polar Plot Logic Tree. Logic tree for one ion anode polar plot calculation.

Ion Coincidence Anode Polar Plot

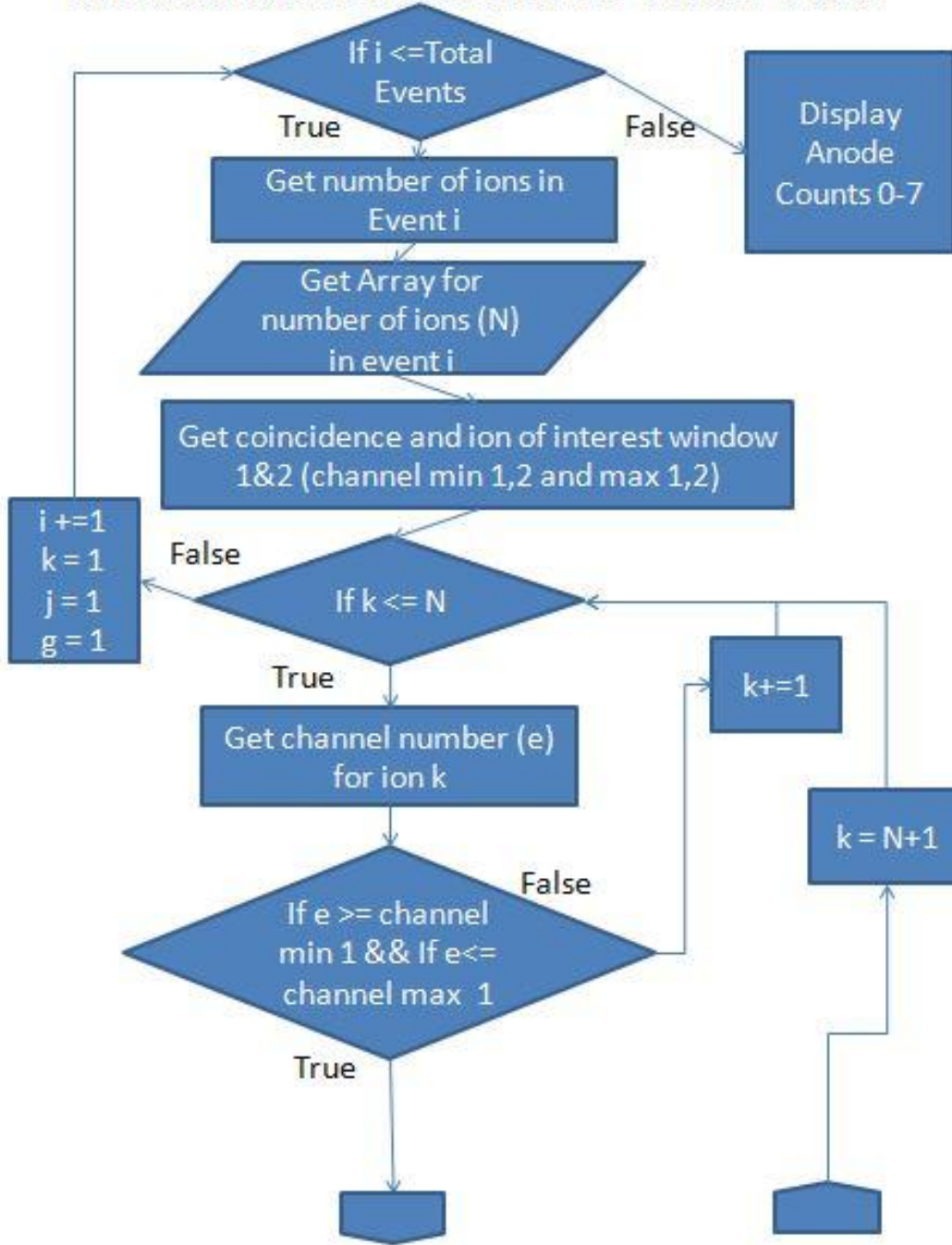


Figure 5.34 Ion Coincidence Anode Polar Plot Part 1 of 2. Logic tree for ion coincidence anode polar plot calculation part 1 of 2 (figures 5.34-5.35).

Ion Coincidence Anode Polar Plot

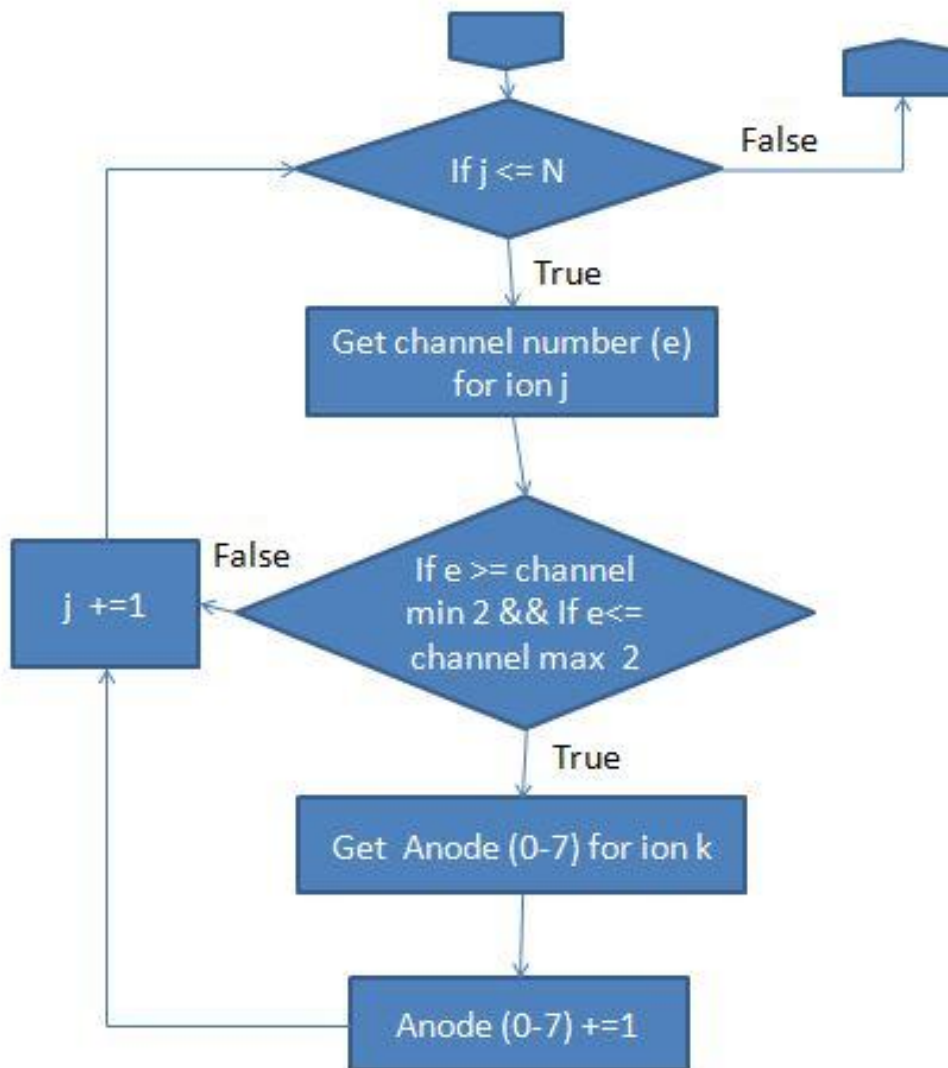


Figure 5.35 Ion Coincidence Anode Polar Plot Part 2 of 2. Logic tree for ion coincidence anode polar plot calculation part 2 of 2 (figures 5.34-5.35).

plotted in comparison to the “ideal” case, in which each anode has $1/8^{\text{th}}$ of the counts.

The polar plot calculation is a tool for understanding the angular distribution of ions generated from impacts on flat or structured surface of individual nano-particles. It allows also for separate isobaric ions which originate from different regions on a surface, as demonstrated in figures 5.36-5.38. In this example 20nm NPs have been deposited as a single layer on a silicon wafer.^[109] The sample was investigated using Au_{400}^{4+} at 520keV total impact energy.^[24] From this sample emission of Au_n^- ($n=1-7$) and $\text{Au}(\text{CN})_2^-$ are observed. The $\text{Au}(\text{CN})_2^-$ is the result of fragmentation- recombination of free Au atoms with synthesized CN^- .^[61, 110] The source of Au atoms can be the projectile or the Au NPs.^[54] To probe these two sources of Au atoms, and ultimately the type of impact (impacts on the NPs or impacts on the open Si) the coincidence methodology is used. Impacts on the NPs generate Au_n clusters $n \geq 3$, while impacts on the open Si have clusters $n \leq 2$ emitted. By placing a coincidence window on the Au_3^- ion, impacts on the Au NPs are selected. Alternatively, placing a coincidence window on SiO_3^- impacts on the open Si are selected. In both cases the emission of $\text{Au}(\text{CN})_2^-$ is observed. However, the radial distribution of $\text{Au}(\text{CN})_2^-$ is different for the two cases. A polar plot of all detected $\text{Au}(\text{CN})_2^-$ is shown in figure 5.36. In this case we see a mix of the two impact types. By placing a coincidence window on Au_3^- and then plotting the polar distribution of $\text{Au}(\text{CN})_2^-$ from those impacts (figure 5.37), a significantly different distribution compared to the total is observed. Instead of having a shift to the upper anodes (as in figure 5.36), the distribution is more centered on the detector. In contrast, by placing a

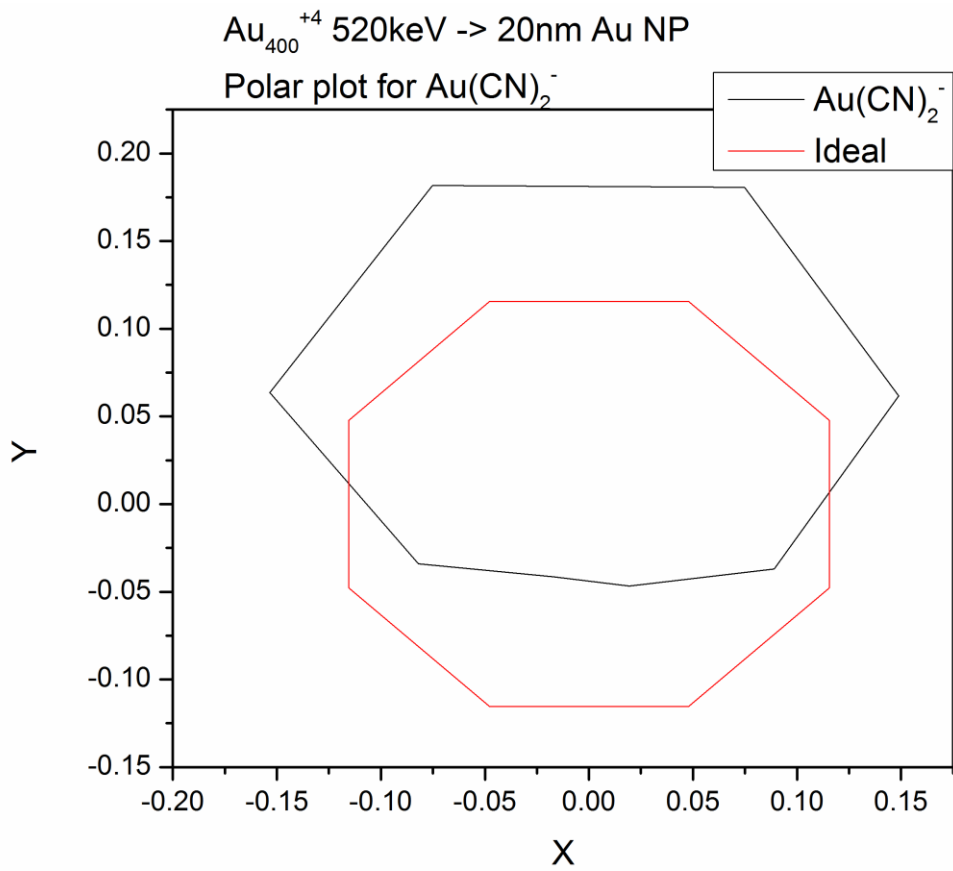


Figure 5.36 Polar Plot for $\text{Au}(\text{CN})_2^-$ from All Impacts.

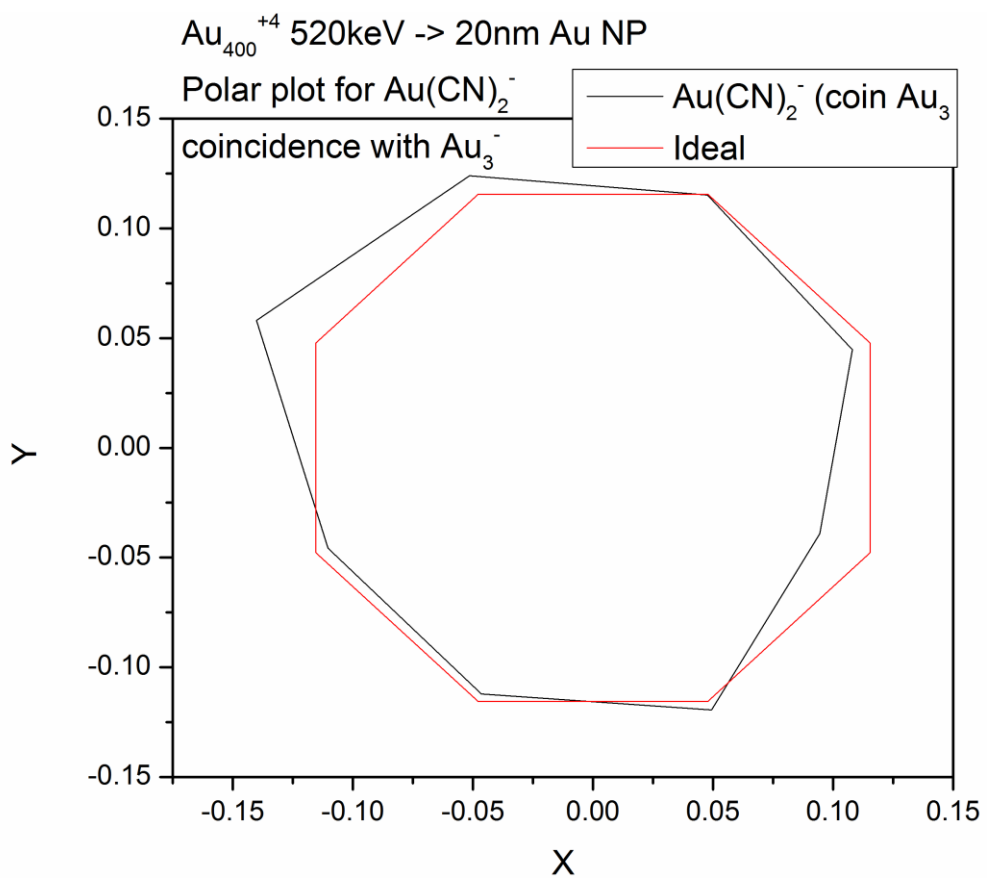


Figure 5.37 Polar Plot for $\text{Au}(\text{CN})_2^-$ in Coincidence with Au_3^- .

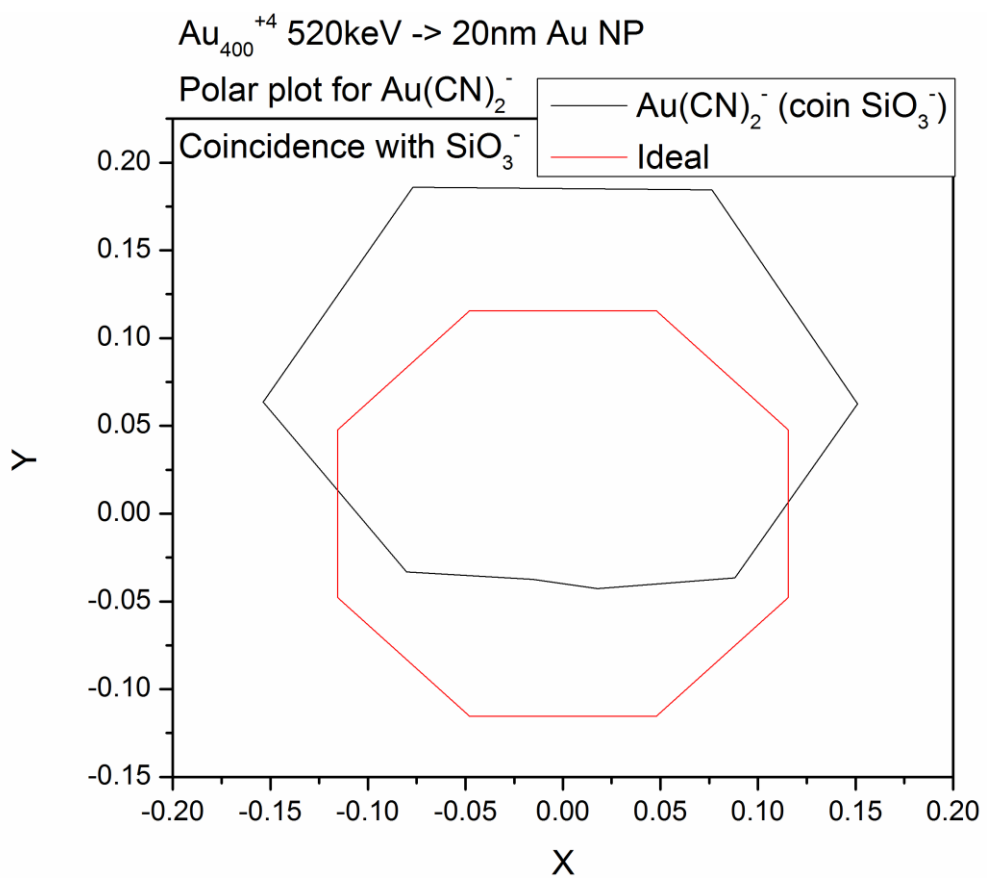


Figure 5.38 Polar Plot for $\text{Au}(\text{CN})_2^-$ in Coincidence with SiO_3^- .

coincidence window on SiO_3^- and plotting the polar distribution of $\text{Au}(\text{CN})_2^-$, the distribution resembles the total distribution for $\text{Au}(\text{CN})_2^-$. The ion coincidence polar plot calculation shows that different impact conditions (on NP or on Si wafer) have different polar distributions of $\text{Au}(\text{CN})_2^-$. The result is mass identification with enhanced accuracy.

6. CONCLUSIONS

The ability to localize individual projectile impacts with the emitted electrons via an electron emission microscope has been demonstrated. Using the most prolific events, ones which emit more than five electrons, and software collimation a resolution of 600nm was achieved. By collecting the SIs concurrently with the emitted electrons, ion selected maps and density plots can be generated. These maps show the distribution of a particular ion(s) on the surface. Detection of co-emitted SIs is a key advantage of the event-by-event methodology, as it enables the mapping of co-emitted species.

An issue at the outset of this work was the relationship between electron emission and ion emission. With the EEM we could study the number of emitted electrons based on the number and type of ion emitted. Our finding is that for flat homogeneous samples, the electron emission is independent of the type and number of emitted ions. This observation is key for the mapping experiment, because the process for localizing an ion(s) will be equivalent regardless of the ion chosen.

The electron emission from a series of nano-objects was also investigated. The observations were made on aluminum and gold nano-objects. The measured electron emission shows a size dependence. As the size of the nano-object decreases the measured electron emission decreases.

The study of electron emission from hyper-velocity C_{60} impacts provided some insight into its origin. A portion of the electrons measured is attributed to thermal electron emission. The temperatures calculated by molecular dynamic simulations, and

measurements on non-equilibrium systems make the production of thermal electrons from C_{60} impacts (15-50keV) plausible.

The development of custom analysis software has increased the amount of information which can be analyzed. The inclusion of the most prolific SI events (events with more than 50 ions emitted) in all coincidence calculations, increased the range of data available for analysis. The addition of new coincidental calculations, such as double coincidence, and one-ion coincidence one-ion anti-coincidence, has enabled the analysis of complex surfaces and size-restrictive nano-objects. Ion polar plots have added the ability to monitor the distribution of detected ions and can offer an additional tool to separate isobaric ions. A twofold improvement in mass resolution has been achieved by mass scaling each anode in a multi-anode detector setup.

Acquisition of data is a critical part of any experiment. The effort in data acquisition software included the development of real-time diagnostics for optimization of detectors, monitoring secondary ion yields, and calculating ion distributions.

Optimization and improvements to the primary ion source over the course of this study have resulted in the reliable production of C_{60}^{2+} and C_{60}^{3+} projectiles. As a result we report the first measurements of SI yields C_{60}^{3+} . For example, the secondary ion yield of [phenalyalamine-H]⁻ is 10.4% from impacts of 75keV C_{60}^{3+} compared to 6.0% from impacts of 50keV C_{60}^{2+} .

A large portion of the studies presented here represent the first measurements with an instrument in constant improvement. Further enhancement in hardware and

software can be imagined resulting in hardware with improved analytical capabilities. A few possible advances are outlined below.

As noted already, changes in the primary ion source have allowed the production of C_{60}^{3+} . Ionizing C_{60} by electron impact at 200eV has been shown to create charge states up to +7.^[111] A key requirement to generate higher charge states are electron currents greater than 200 μ A. By adding an additional Ta cathode, to the source described here, the current of electrons may be increased to a few hundred micro amperes. To obtain 1mA of current a different type of electron emitter may be required. Higher charge state C_{60} will result in increased SI and electron yields observed.^[112]

Custom written programs, such as those described here, have in inherent constraints due to the file format used which sets limits to the compatibility, and ultimately the usability of the software. All the software described in this document uses the TME© file structure. However, if a different file structure were to be used only the method of data input would need to be modified to accommodate the differences. In the current software, the data analysis is limited to events which generate 0-200 SIs, events which happen to produce more than 200 SIs cannot be analyzed. This is a consequence of the method of data input and analysis techniques used. Currently there are no events which generate more than 200 SIs in a single event. If the impact energy is increased by using a high charge state C_{60} , this may no longer be true. Additionally more analysis tools such as triple coincidence, and double coincidence polar plots could be developed to analyze some complex surfaces yet to be encountered.

In this document Au_{400}^{4+} is often mentioned as an effective projectile for SIMS studies, due to its large SI yields and specifically large yields for quasi-molecular ions. An EEM to localize impacts of Au_{400}^{4+} , will generate maps with more SI information. Additionally, the study of the emitted electrons from Au_{400}^{4+} impacts should be pursued. The first of such measurements have been performed and can be found in figure 6.1. The electron yield from 320keV Au_{400}^{4+} impacts on glycine were nearly double the electron yield as measured by impacts of 30keV C_{60} on glycine. Larger electron yields allow for a higher success rate for localizing the projectile, as there will be more impacts which generate, for example, more than five electrons in a single event. The additional electrons may allow for more restrictive localization parameters, such as decreasing the ROI for collimation or requiring more electrons for an impact cite to be assigned.

The characteristics (e.g. kinetic energy) of the electrons emitted by Au_{400} impacts to date are not known. It may be recalled that current theory cannot account for the observed electron emission. Further investigations focused on electron characteristics will advance our understanding of electron emission due to a collective effect(s).

Additionally, experiments on nano-objects will help establish the relationship between their size and electron emission. Investigations with nano-objects dispersed as a single layer may determine the volume of electron emission and the role of the substrate in electron emission.

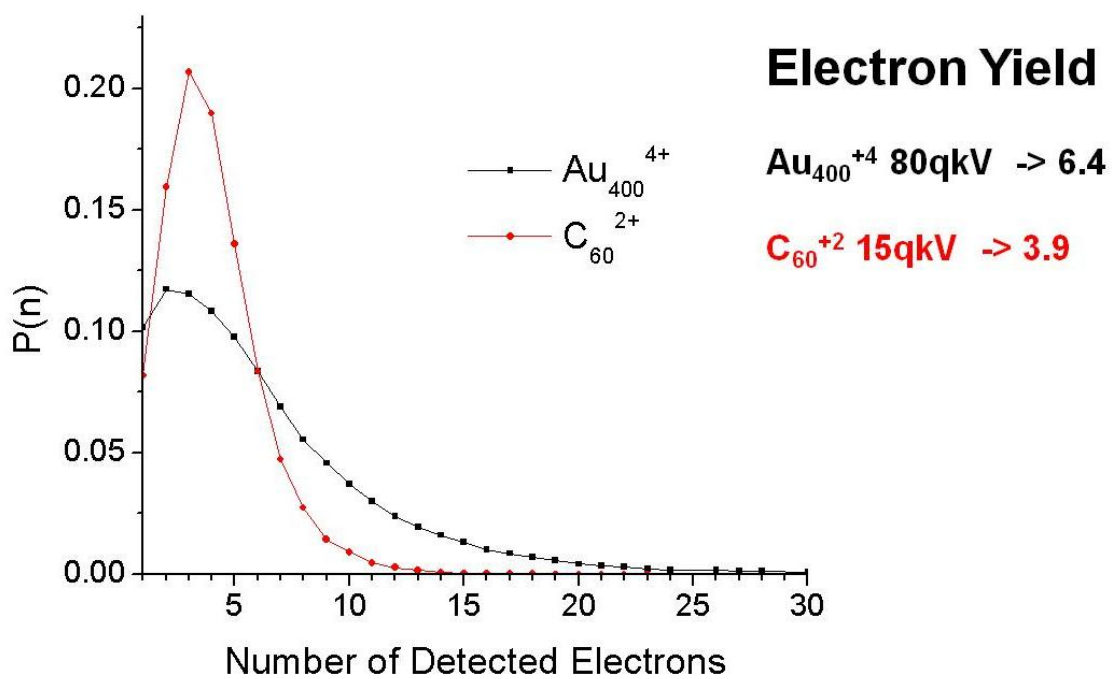


Figure 6.1 Measured Electron Distributions from Impacts of C_{60} and Au_{400} on Glycine. The measured electron distribution and yield for 30keV C_{60}^{2+} and 320keV Au_{400}^{4+} impacting a vapor deposited glycine target.

Returning to localization, the current resolution demonstrated here is competitive with alternate methods of mapping surfaces, and is better than the best reported resolution using C_{60} in the microprobe mode. Increasing the magnification of the EEM should result in improvements in resolution.^[46] Given the characteristics of the C_{60} source and other sources of large clusters, further improvements (reduction) in the beam size will be challenging. The ability to map below the probe size (beam or laser) shows the versatility of using an ion microscope or electron microscope to generate ion maps.^[113, 114]

As is noted in section 4.2, the C_{60} analysis beam often probes a surface unevenly. This uneven probing of a surface can give the illusion of a change in the amount of analyte across a region of the sample. Methods for normalizing such images, so that the relative concentration of an analyte on a surface can be determined should be developed. A proposed method of normalization of ion density plots is to divide the intensity in the ion density plot by the intensity in the total electron density plot.

All the experiments presented were carried out in negative ion mode. An obvious development is the addition of positive ion mass spectrometry. To perform event-by-event positive ion mass spectrometry, the ToF measurement can be based on the detection of H^+ .^[104] Nothing is known about the yield of H^+ under C_{60} bombardment. Experiments with Au_{400}^{4+} at 440keV have shown an average yield of $\sim 2H^+$ per impact, in the case of organic targets. The characteristics of H^+ (angle of emission, kinetic energy, radial velocity) are not known. With the preceding caveat, we suggest an evolution from the EEM to consider a Proton Emission Microscope, PEM.

Although proton transmission microscopes have been built, there is, to our knowledge, no description of the PEM in the literature.^[115]

REFERENCES

- [1] G. A. Somorjai, *Annual Review of Physical Chemistry* **1968**, *19*, 251.
- [2] U. Diebold, S.-C. Li, M. Schmid, *Annual Review of Physical Chemistry* **2010**, *61*, 129.
- [3] D. R. Rainer, D. W. Goodman, *J. Mol. Catal. A: Chem.* **1998**, *131*, 259.
- [4] J.-N. Audinot, A. Georgantzopoulou, J.-P. Piret, A. C. Gutleb, D. Dowsett, H. N. Migeon, L. Hoffmann, *Surface and Interface Analysis* **2012**, DOI: 10.1002/sia.5099.
- [5] M. L. Steinhauser, A. P. Bailey, S. E. Senyo, C. Guillermier, T. S. Perlstein, A. P. Gould, R. T. Lee, C. P. Lechene, *Nature* **2012**, *481*, 516.
- [6] D. F. Smith, E. W. Robinson, A. V. Tolmachev, R. M. A. Heeren, L. Paša-Tolić, *Analytical Chemistry* **2011**, *83*, 9552.
- [7] M. A. Robinson, D. J. Graham, D. G. Castner, *Analytical Chemistry* **2012**, *84*, 4880.
- [8] R. Ait-Belkacem, L. Sellami, C. Villard, E. DePauw, D. Calligaris, D. Lafitte, *Trends Biotechnol.* **2012**, *30*, 466.
- [9] F. Kollmer, W. Paul, M. Krehl, E. Niehuis, *Surface and Interface Analysis* **2012**, 10.1002/sia.5093.
- [10] S. Lozano-Perez, M. Schröder, T. Yamada, T. Terachi, C. A. English, C. R. M. Grovenor, *Applied Surface Science* **2008**, *255*, 1541.
- [11] P. Steffens, E. Niehuis, T. Friese, D. Greifendorf, A. Benninghoven, *Journal of Vacuum Science & Technology A: Vacuum, Surfaces, and Films* **1985**, *3*, 1322.
- [12] P. Sigmund, *Phys. Rev.* **1969**, *184*, 383.
- [13] P. Sigmund, *Nucl. Instrum. Methods Phys. Res., Sect. B* **1987**, *B27*, 1.
- [14] S. S. Wong, R. Stoll, F. W. Roellgen, *Z. Naturforsch., A* **1982**, *37A*, 718.
- [15] M. G. Blain, S. Della-Negra, H. Joret, Y. Le Beyec, E. A. Schweikert, *Physical Review Letters* **1989**, *63*, 1625.

- [16] S. Bouneau, A. Brunelle, S. Della-Negra, J. Depauw, D. Jacquet, B. Y. Le, M. Pautrat, M. Fallavier, J. C. Poizat, H. H. Andersen, *Phys. Rev. B: Condens. Matter Mater. Phys.* **2002**, *65*, 144106/1.
- [17] A. D. Appelhans, J. E. Delmore, *Analytical Chemistry* **1989**, *61*, 1087.
- [18] O. W. Hand, T. K. Majumdar, R. G. Cooks, *Int. J. Mass Spectrom. Ion Processes* **1990**, *97*, 35.
- [19] W. Szymczak, K. Wittmaack, *NATO ASI Ser., Ser. B* **1991**, *269*, 123.
- [20] R. D. Harris, S. M. J. Van, E. A. Schweikert, *Int. J. Mass Spectrom. Ion Processes* **1998**, *174*, 167.
- [21] R. D. Harris, W. S. Baker, S. M. J. Van, R. M. Crooks, E. A. Schweikert, *Rapid Commun. Mass Spectrom.* **1999**, *13*, 1374.
- [22] D. A. Brenes, B. J. Garrison, N. Winograd, Z. Postawa, A. Wucher, P. Blenkinsopp, *J. Phys. Chem. Lett.* **2011**, *2*, 2009.
- [23] E. A. Schweikert, M. J. van Stipdonk, R. D. Harris, *Rapid Communications in Mass Spectrometry* **1996**, *10*, 1987.
- [24] J. D. DeBord, Ph.D. Dissertation. Texas A&M University, College Station, TX, **2012**.
- [25] Z. Li, S. V. Verkhoturov, J. E. Locklear, E. A. Schweikert, *International Journal of Mass Spectrometry* **2008**, *269*, 112.
- [26] A. Carado, J. Kozole, M. Passarelli, N. Winograd, A. Loboda, J. Wingate, *Applied Surface Science* **2008**, *255*, 1610.
- [27] A. Novikov, M. Caroff, S. Della-Negra, J. Depauw, M. Fallavier, B. Y. Le, M. Pautrat, J. A. Schultz, A. Tempez, A. S. Woods, *Rapid Commun. Mass Spectrom.* **2005**, *19*, 1851.
- [28] R. D. Rickman, S. V. Verkhoturov, E. S. Parilis, E. A. Schweikert, *Physical Review Letters* **2004**, *92*.
- [29] E. J. Sternglass, *Physical Review* **1957**, *108*, 1.
- [30] R. J. Beuhler, L. Friedman, *Journal of Applied Physics* **1977**, *48*, 3928.
- [31] R. J. Beuhler, L. Friedman, *Nuclear Instruments and Methods* **1980**, *170*, 309.

- [32] F. Aumayr, G. Betz, T. D. Märk, P. Scheier, H. P. Winter, *International Journal of Mass Spectrometry and Ion Processes* **1998**, 174, 317.
- [33] W. S. Sanders, W. Nan, S. M. Bridges, B. M. Malone, Y. S. Dandass, F. M. McCarthy, B. Nanduri, M. L. Lawrence, S. C. Burgess, *BioMed Central* **2011**, 12, 115.
- [34] D. Mantini, F. Petrucci, D. Pieragostino, P. Del Boccio, P. Sacchetta, G. Candiano, G. M. Ghiggeri, A. Lugaresi, G. Federici, C. Di Ilio, A. Urbani, *Journal of Proteomics* **2010**, 73, 562.
- [35] O. Jardin-Mathé, D. Bonnel, J. Franck, M. Wisztorski, E. Macagno, I. Fournier, M. Salzet, *Journal of Proteomics* **2008**, 71, 332.
- [36] R. D. Rickman, Ph.D. Dissertation. Texas A&M University, College Station, TX, **2004**.
- [37] M. Dole, L. L. Mack, R. L. Hines, R. C. Mobley, L. D. Ferguson, M. B. Alice, *The Journal of Chemical Physics* **1968**, 49, 2240.
- [38] R. J. Beuhler, L. Friedman, *International Journal of Mass Spectrometry and Ion Physics* **1977**, 23, 81.
- [39] H. P. Winter, M. Vana, G. Betz, F. Aumayr, H. Drexel, P. Scheier, T. D. Märk, *Physical Review A* **1997**, 56, 3007.
- [40] K. Töglhofer, F. Aumayr, H. Kurz, H. Winter, P. Scheier, T. D. Märk, *Europhysics Letters* **1993**, 22, 597.
- [41] A. Brunelle, P. Chaurand, S. Della-Negra, Y. Le Beyec, E. Parilis, *Rapid Communications in Mass Spectrometry* **1997**, 11, 353.
- [42] P. W. Geno, R. D. Macfarlane, *International Journal of Mass Spectrometry and Ion Processes* **1989**, 92, 195.
- [43] M. Karas, F. Hillenkamp, *Analytical Chemistry* **1988**, 60, 2299.
- [44] R. J. Beuhler, *Journal of Applied Physics* **1983**, 54, 4118.
- [45] G. Westmacott, W. Ens, K. G. Standing, *Nuclear Instruments and Methods in Physics Research Section B: Beam Interactions with Materials and Atoms* **1996**, 108, 282.

- [46] S. V. Verkhoturov, M. J. Eller, R. D. Rickman, S. Della-Negra, E. A. Schweikert, *Journal of Physical Chemistry C* **2010**, *114*, 5637.
- [47] M. J. Eller, S. V. Verkhoturov, S. Della-Negra, E. A. Schweikert, *Journal of Physical Chemistry C* **2010**, *114*, 17191.
- [48] J. L. Wiza, *Nucl. Instrum. Methods* **1979**, *162*, 587.
- [49] S. Rajagopalachary, S. V. Verkhoturov, E. A. Schweikert, *Analytical Chemistry* **2009**, *81*, 1089.
- [50] P. Rudolf, F. Marchal, R. Sporcken, R. Caudano, T. dell'Orto, J. Almeida, A. Braem, F. Piuz, S. Sgobba, G. Paic, E. Nappi, A. Valentini, P. Sartori, C. Coluzza, *Nuclear Instruments and Methods in Physics Research Section A: Accelerators, Spectrometers, Detectors and Associated Equipment* **1997**, *387*, 163.
- [51] J. Almeida, F. Barbo, M. Bertolo, A. Bianco, A. Braem, S. Cerasari, C. Coluzza, T. dell'Orto, S. Fontana, G. Margaritondo, E. Nappi, G. Paic, F. Piuz, R. Sanjines, T. Scognetti, S. Sgobba, *Nuclear Instruments and Methods in Physics Research Section A: Accelerators, Spectrometers, Detectors and Associated Equipment* **1995**, *361*, 524.
- [52] V. Pinnick, S. Rajagopalachary, S. V. Verkhoturov, L. Kaledin, E. A. Schweikert, *Analytical Chemistry* **2008**, *80*, 9052.
- [53] S. Rajagopalachary, S. V. Verkhoturov, E. A. Schweikert, *Nano Letters* **2008**, *8*, 1076.
- [54] S. Rajagopalachary, S. V. Verkhoturov, E. A. Schweikert, *Surface and Interface Analysis* **2011**, *43*, 547.
- [55] M. J. Eller, S. V. Verkhoturov, S. Della-Negra, R. D. Rickman, E. A. Schweikert, *Surface and Interface Analysis* **2011**, *43*, 484.
- [56] B. J. Garrison, Z. Postawa, K. E. Ryan, J. C. Vickerman, R. P. Webb, N. Winograd, *Analytical Chemistry* **2009**, *81*, 2260.
- [57] A. Delcorte, B. J. Garrison, K. Hamraoui, *Analytical Chemistry* **2009**, *81*, 6676.
- [58] R. A. Baragiola, *Nucl. Instrum. Methods Phys. Res., Sect. B* **1993**, *B78*, 223.
- [59] S. V. Verkhoturov, M. J. Eller, S. Della-Negra, R. D. Rickman, J. E. Locklear, E. A. Schweikert, *Surface and Interface Analysis* **2011**, *43*, 49.

- [60] O. Restrepo, A. Prabhakaran, K. Hamraoui, N. Wehbe, S. Yunus, P. Bertrand, A. Delcorte, *Surf. Interface Anal.* **2010**, *42*, 1030.
- [61] C. Guillermier, S. Della Negra, R. D. Rickman, G. J. Hager, E. A. Schweikert, *International Journal of Mass Spectrometry* **2007**, *263*, 298.
- [62] M. A. Park, K. A. Gibson, L. Quinones, E. A. Schweikert, *Science* **1990**, *248*, 988.
- [63] L. J. Chen, S. S. Shah, J. Silangcruz, M. J. Eller, S. V. Verkhoturov, A. Revzin, E. A. Schweikert, *International Journal of Mass Spectrometry* **2011**, *303*, 97.
- [64] O. A. Restrepo, A. Prabhakaran, A. Delcorte, *Nuclear Instruments and Methods in Physics Research Section B: Beam Interactions with Materials and Atoms* **2011**, *269*, 1595.
- [65] O. A. Restrepo, A. Delcorte, *Surface and Interface Analysis* **2011**, *43*, 70.
- [66] S. Dushman, *Phys. Rev.* **1914**, *4*, 121.
- [67] I. Langmuir, *Phys. Rev.* **1914**, *2*, 450.
- [68] O. W. Richardson, *Philos. Mag.* **1912**, *23*, 594.
- [69] H. Kawano, N. Serizawa, A. Tanaka, Y. Zhu, *Applied Surface Science* **1999**, *146*, 101.
- [70] P. Odier, J. F. Baumard, D. Panis, A. M. Anthony, *Journal of Solid State Chemistry* **1975**, *12*, 324.
- [71] J. G. Simmons, H. A. Mar, *Physical Review B* **1973**, *8*, 3865.
- [72] A. T. Fromhold, Jr., E. L. Cook, III, *Physiol. Rev.* **1967**, *163*, 650.
- [73] A. V. Samartsev, A. Duvenbeck, A. Wucher, *Phys. Rev. B: Condens. Matter Mater. Phys.* **2005**, *72*, 115417/1.
- [74] C. Anders, E. M. Bringa, F. D. Fioretti, G. Ziegenhain, H. M. Urbassek, *Phys. Rev. B: Condens. Matter Mater. Phys.* **2012**, *85*, 235440/1.
- [75] R. Paruch, L. Rzeznik, M. F. Russo, B. J. Garrison, Z. Postawa, *The Journal of Physical Chemistry C* **2009**, *114*, 5532.

- [76] D. M. Riffe, X. Y. Wang, M. C. Downer, D. L. Fisher, T. Tajima, J. L. Erskine, R. M. More, *J. Opt. Soc. Am. B* **1993**, *10*, 1424.
- [77] W. Szymczak, K. Wittmaack, *Nuclear Instruments and Methods in Physics Research Section B: Beam Interactions with Materials and Atoms* **1994**, *88*, 149.
- [78] R. D. Harris, M. J. Van Stipdonk, E. A. Schweikert, *International Journal of Mass Spectrometry* **1998**, *174*, 167.
- [79] J. E. Locklear, C. Guillermier, S. V. Verkhoturov, E. A. Schweikert, *Applied Surface Science* **2006**, *252*, 6624.
- [80] J. H. Moore, Davis; Christopher C.; Coplan, Michael A., *Building scientific apparatus : a practical guide to design and construction*, **2003**.
- [81] N. Bourdos, F. Kollmer, A. Benninghoven, M. Sieber, H.-J. Galla, *Langmuir* **2000**, *16*, 1481.
- [82] A. Attout, S. Yunus, P. Bertrand, *Polymer Engineering & Science* **2008**, *48*, 1661.
- [83] C. Zhou, Q. Li, V. L. Chiang, L. A. Lucia, D. P. Griffis, *Analytical Chemistry* **2011**, *83*, 7020.
- [84] P. Sjövall, J. Lausmaa, B. Johansson, *Analytical Chemistry* **2004**, *76*, 4271.
- [85] J. S. Fletcher, N. P. Lockyer, J. C. Vickerman, *Mass Spectrometry Reviews* **2011**, *30*, 142.
- [86] L. A. Klerk, N. P. Lockyer, A. Kharchenko, L. MacAleese, P. Y. W. Dankers, J. C. Vickerman, R. M. A. Heeren, *Analytical Chemistry* **2010**, *82*, 801.
- [87] X. Llopart, R. Ballabriga, M. Campbell, L. Tlustos, W. Wong, *Nucl. Instrum. Methods Phys. Res., Sect. A* **2007**, *581*, 485.
- [88] B. L. Doyle, G. Vizkelethy, D. S. Walsh, B. Senftinger, M. Mellon, *Nuclear Instruments and Methods in Physics Research Section B: Beam Interactions with Materials and Atoms* **1999**, *158*, 6.
- [89] S. G. Ostrowski, C. T. Van Bell, N. Winograd, A. G. Ewing, *Science* **2004**, *305*, 71.
- [90] P. D. Piehowski, A. M. Davey, M. E. Kurczy, E. D. Sheets, N. Winograd, A. G. Ewing, M. L. Heien, *Analytical Chemistry* **2009**, *81*, 5593.

- [91] P. D. Piehowski, A. M. Davey, M. E. Kurczy, E. D. Sheets, N. Winograd, A. G. Ewing, M. L. Heien, *Analytical Chemistry* **2009**, *81*, 5593.
- [92] W. W. Webb, R. E. Thompson, D. R. Larson, *Biophysical Journal* **2002**, *82*, 2775.
- [93] T. Wirtz, Y. Fleming, M. Gerard, U. Gysin, T. Glatzel, E. Meyer, U. Wegmann, U. Maier, A. H. Odriozola, D. Uehli, *Review of Scientific Instruments* **2012**, *83*, 063702.
- [94] A. Pilate, F. Adams, *Analytica Chimica Acta* **1980**, *122*, 57.
- [95] M. Stoeckli, T. B. Farmer, R. M. Caprioli, *J. Am. Soc. Mass Spectrom.* **1999**, *10*, 67.
- [96] M. Stoeckli, P. Chaurand, D. E. Hallahan, R. M. Caprioli, *Nat. Med.* **2001**, *7*, 493.
- [97] R. A. Scheltema, A. Jankevics, R. C. Jansen, M. A. Swertz, R. Breitling, *Analytical Chemistry* **2011**, *83*, 2786.
- [98] P. J. Trim, M.-C. Djidja, T. Muharib, L. M. Cole, B. Flinders, V. A. Carolan, S. Francese, M. R. Clench, *J. Proteomics* **2012**, *75*, 4931.
- [99] R. D. Rickman, S. V. Verkhoturov, S. Balderas, N. Bestaoui, A. Clearfield, E. A. Schweikert, *Applied Surface Science* **2004**, *231-2*, 106.
- [100] S. Della-Negra, J. Depauw, C. Guillermier, E. A. Schweikert, *Surface and Interface Analysis* **2011**, *43*, 62.
- [101] R. D. Rickman, S. V. Verkhoturov, G. J. Hager, E. A. Schweikert, *International Journal of Mass Spectrometry* **2005**, *245*, 48.
- [102] R. J. Paruch, B. J. Garrison, Z. Postawa, *Analytical Chemistry* **2012**, *84*, 3010.
- [103] X. A. Conlan, J. S. Fletcher, N. P. Lockyer, J. C. Vickerman, *The Journal of Physical Chemistry C* **2009**, *114*, 5468.
- [104] J. D. DeBord, F. A. Fernandez-Lima, S. V. Verkhoturov, E. A. Schweikert, S. Della-Negra, *Surf. Interface Anal.*, DOI: 10.1002/sia.5009.
- [105] F. A. Fernandez-Lima, J. D. DeBord, E. A. Schweikert, S. Della-Negra, K. A. Kellersberger, M. Smotherman, *Surface and Interface Analysis* **2012**, DOI: 10.1002/sia.4901.

- [106] H. D. Flosadóttir, S. Denifl, F. Zappa, N. Wendt, A. Mauracher, A. Bacher, H. Jónsson, T. D. Märk, P. Scheier, O. Ingólfsson, *Angewandte Chemie International Edition* **2007**, *46*, 8057.
- [107] L. J. Chen, J. H. Seo, M. J. Eller, S. V. Verkhoturov, S. S. Shah, A. Revzin, E. A. Schweikert, *Analytical Chemistry* **2011**, *83*, 7173.
- [108] C. K. Liang, S. V. Verkhoturov, Y. Bisrat, S. Dikler, J. D. DeBord, F. A. Fernandez-Lima, E. A. Schweikert, S. Della-Negra, *Surface and Interface Analysis* **2012**, 10.1002/sia.5084.
- [109] L. Yang, M. P. Seah, E. H. Anstis, I. S. Gilmore, J. L. S. Lee, *The Journal of Physical Chemistry C* **2012**, *116*, 9311.
- [110] C. Guillermier, S. Della-Negra, E. A. Schweikert, A. Dunlop, G. Rizza, *Int. J. Mass Spectrom.* **2008**, *275*, 86.
- [111] P. Scheier, B. Duenser, R. Woergoetter, S. Matt, D. Muigg, G. Senn, T. D. Maerk, *Int. Rev. Phys. Chem.* **1996**, *15*, 93.
- [112] A. Brunelle, S. Della-Negra, C. Deprun, J. Depauw, P. Håkansson, D. Jacquet, Y. le Beyec, M. Pautrat, *International Journal of Mass Spectrometry and Ion Processes* **1997**, *164*, 193.
- [113] J. H. Jungmann, L. MacAleese, J. Visser, M. J. J. Vrakking, R. M. A. Heeren, *Analytical Chemistry* **2011**, *83*, 7888.
- [114] H. Hazama, H. Yoshimura, J. Aoki, H. Nagao, M. Toyoda, K. Masuda, K. Fujii, T. Tashima, Y. Naito, K. Awazu, *J. Biomed. Opt.* **2011**, *16*, 046007/1.
- [115] R. Levi-Setti, T. R. Fox, *Nucl. Instrum. Methods* **1980**, *168*, 139.

APPENDIX A

SOURCE SETUP AND SHUTDOWN

A description of setting up and shutting down the C₆₀ effusion source is found in this appendix.

To setup follow these steps:

1. Ensure that the ion source and analysis chamber have good vacuum, better than 6×10^{-6} torr, if this is not true, check the system for leaks.
2. Begin heating the C₆₀, by setting the voltage applied to the heater to +6V. The topward power supply has 2 independent voltages that can be applied, with current control. One for the heater, a second for the cathode.
3. Set the current to the cathode to 0.4A, this will stay at this voltage for ~1hour
4. After 15 minutes turn increase the heater voltage by 5V.
5. Continue increasing the voltage on the heater every 15min until it reads 27.5V. This will correspond to a temperature of ~600K.
6. After the heater has been brought to a maximum increase the current on the cathode to 1.5A.
7. Turn on the bias voltage for electrons to +150V.
8. Simultaneously turn on the bias voltage for the C₆₀ source (+15kV) and the extraction voltage (~11.4kV)
9. Turn on the potential on the primary ion lens (located on the source assembly)
10. Leave the source on for at least ~70min or until a measurable current is detected on the collimator.
11. Once the source is emitting well, the current on the cathode may be increased/decreased to get the desired beam intensity, keep the current below 1.6A.

To shutdown the source follow these steps:

1. Turn off the primary ion lens.
2. Simultaneously turn off the source bias (+15kV) and the extraction voltage (~11.4kV).
3. Reduce the bias voltage for electrons to 0V.
4. Decrease the voltage on the source heater to 0V.
5. Reduce the current on the cathode to 0.4A.
6. After 45min reduce the current on the cathode to 0A.

APPENDIX B

CAMERA SETUP

A description of setting up the camera is detailed in this appendix. This setup only pertains to a M3 camera produced by Integrated Design Tools.

First plug in the cooling fan, and then plug in the camera. If the trigger out and trigger in cables are not connected, connect them now. Also connect the Camera Link cables to the PC.

Start up the most recent Motion Studio software (currently version 2.10.04). After the software initializes, select Open Camera from the list of options. The M3 camera should show up, if not, ensure that the camera is powered on and properly connected through the camera link cable. Select the M3 camera and the software will load the camera. Now that the camera is loaded remove the lens cap (be sure to replace it at the end of the experiment). To initially check the camera set the frame rate to 6 frames per second, fps, and the exposure time to 166,666 μ s. To focus the lens follow the steps below.

To setup the focusing of the Schneider lens: The lens has two adjustments, one focusing lens, and one aperture. Ensure that the aperture is completely open. With the camera software in the play mode (constantly collecting images) and even lighting across the phosphor glass (from room lighting), begin adjusting the focus on the lens. Find a point on the glass (piece of dust or small defect) and get it into focus.

Now that the camera is completely focused and operating correctly, you can either tune the EEM or collect images.

When tuning the EEM collect images in play mode at 6fps, this will allow you to see how changes to EEM lenses, deflectors, etc. affects the image.

After the EEM is tuned now the camera needs to be setup to collect frames of individual impacts. First the beam of projectiles must be below 250 impacts per second. First, set the camera to the desired exposure time for collection (usually 1000 μ s) and set the frame rate to 300fps. Now set the camera triggering to external triggering (edge high triggering). Edge high will ensure the camera is initialized at the beginning of the pulse (discussed more in section 3.3). Once that is true, the camera must go through a background correction. Background correction is found under advanced tools in the Motion Studio software. The software will prompt you to replace the camera lens cover, do so. After all these steps the camera is ready to acquire, be sure to remove the lens cap. Take a few snaps and visually inspect the frames, ensuring that there is little or no noise on the frame, and the electrons are easy to see.

Now that the frames can be acquired correctly, the recording needs to be setup. Create a folder to save all of your images, usually with the date, name of sample, and projectile used. Click the record setup button, select your folder and set the number of frames to be acquired to 50, and the save to tiff, and acquire the frames. After, the 50 frames have been acquired, check them and ensure that they are of good quality. If there is an issue, check the previous steps and ensure that all settings are correct. Now that the record function is setup correctly, click record setup, and set the number of frames to 2000, the file type to uncompressed avi, select download and save frames, and insert the number of times to repeat the 2000 frame avi file.

APPENDIX C

HELP FILE

Definitions:

Hot keys- hot keys are short cuts that perform a task in the program without finding/clicking the button or drop down selection.

Time-of-Fight Spectrum- Is a x,y plot showing the time of arrival of every ion detected. These data are displayed in channels, i.e. divided into bins, usually 400ps or 250ps per channel.

Mass Spectrum – Is a x,y plot of with the number of detected ions at a particular mass to charge ratio, this type of plot is generated by converting the time of flight spectrum using a quadratic polynomial.

Coincidence mass spectrum – is a mass spectrum of all detected ions which were detected concurrently with a selected ion of interest

Drop Down Options:

File: Load 8 Anode TME, Load TME #1, Load TME #2, Save Mass Spectrum, Save SI Distribution, Save Monitor Ion, Reset, and Exit.

Calculate: Secondary Ion Distribution, Single Coincidence, Double Coincidence, Anode Coincidence, Ion Selected Distribution, Multi-molecular Ion Coincidence, Single Ion Coincidence & One Ion Anticoincidence, Monitor Yield, Double Ion Coincidence & One Ion Anticoincidence and One Ion Radar.

Options: Scroll Speed, Save XY Main, Save XY Coincidence, Show File Name, Multiple Mass Spectra, MS All Anodes, Show Total MS, Select Anode.

Mass Scale: Mass Scale 8 Anode TME, Mass Scale TME1 and Mass Scale TME2.

Help: Help File and About.

Explanation of drop down features: File

Load 8 Anode TME – Select a data set that uses an 8 anode detector and load it for analysis

Load TME1– Select a data set and load it for analysis

Load TME2 – Select a second data set and load it for analysis

Save Mass Spectrum – Creates a file which the data from the loaded mass spectrum is saved. The extension of the file is called .msa (mass spec array). The data are saved in a single column with the number of counts in each channel starting with channel 0. An option to save the total or coincidental mass spectrum is given.

Save SI Distribution – Creates a file which saves the secondary ion distribution, number of detected ions in each event as a histogram. The extension of the file is called .sid secondary ion distribution. An option to save the calculated total secondary ion distribution or ion specific secondary ion distribution is given.

Reset – Will free up the memory that has been allocated and will allow for a new mass spectrum to be loaded.

Exit – Returns to the home panel.

Explanation of drop down features: Calculate

Secondary Ion Distribution – Calculates the number of secondary ions in each event and displays it as a histogram.

Single Coincidence – Calculates a coincidental mass spectrum, which is a mass spectrum of all the ions which were detected in the same event (single impact) as an ion of interest. The ion of interest is chosen based on the values in X1 and X2 which defines the window where the ion of interest is located (in the mass spectrum).

Double Coincidence – Calculates a double coincidence mass spectrum, which is a mass spectrum of all the ions which were detected in the same event (single impact) as two different ions of interest. The ions of interest is chosen based on the values in X1, X2 for the first ion of interest in the mass spectrum, and X3, X4 for the second ion of interest.

Anode Coincidence – Calculates a double coincidental mass spectrum, and calculates the coincidental anode distribution of an ion of interest. The double coincidence is calculated based on the values in X1, X2 for the first ion of interest in the mass spectrum and X3, X4 for the second ion of interest. Then the coincidental anode distribution for second ion (X3, X4) of interest is calculated, this anode distribution is the distribution of the second ion in events where the first ion was also detected, thus logically different than the original anode distribution of the second ion.

Ion Selected Distribution – Calculates the number of secondary ions of interest, selected by the values in X1, X2, in each event and displays it as a histogram.

Multi-molecular Ion Coincidence – Calculates a coincidental mass spectrum where an ion of interest is detected two or more times in the same event and displays all ions

detected in those events. The ion of interest is selected based on the values in X1 and X2 which defines the window where the ion of interest is located.

Single Ion Coincidence & One Ion Anticoincidence – Calculates a coincidental mass spectrum where an ion of interest is detected and a second ion of interest is not detected and displays all ions detected in those events. The ion of interest is selected based on the values in X1 and X2 which defines window where the ion of interest is located and the second ion of interest is selected based on the values in X3 and X4.

Double Coincidence & One Ion Anticoincidence – Calculates a double coincidental mass spectrum where two ions of interest were detected and a third ion of interest is not detected and displays all ions detected in those events. The first ion of interest is selected based on the values in X1 and X2 which defines window where the ion of interest is located, the second ion of interest is selected based on the values in X3 and X4 and the third ion of interest is selected based on the values in X5 and X6.

Monitor Yield – Calculates the rate in which an ion of interest is detected during an experiment. This is done by counting the number of times an ion of interest, based on the values in X1 and X2, was detected in a user defined bin (number of events, e.g. 1000 events) and displaying it for the entire experiment (e.g. 1,000,000 events).

One Ion Anode Distribution – Calculates the distribution of an ion of interest on the anodes.

Explanation of drop down features: Options

Scroll Speed – Displays a panel which allows the speed that the scroll buttons will move through the mass spectrum to be set.

Save XY Main – Creates a file to save the areas of a selected peak from the main spectrum to. Each time this menu item is used the selected peaks size (beginning and end of peak), area and number of events is written to the file.

Save XY Coincidence – Creates a file to save the areas of a selected peak from the coincidence spectrum to. Each time this hot key is used the selected peaks size (beginning and end of peak), area and number of events is written to the file.

Show File Name – Displays the name and location of the loaded file (TME1 or 8 Anode TME).

Multiple Mass Spectra – Will display a second mass spectrum (if loaded) and allow for comparison of two mass spectra.

MS All Anodes – Displays an overlay of all 8 anodes in the main spectrum window.

Show Total MS – Displays the total mass spectrum in the main spectrum window.

Select Anode – Displays a panel which allows for the user to display any one of the anodes mass spectra (0-7), the total mass spectrum, either corrected or uncorrected due to the different ToF for each anode.

Explanation of drop down features: Mass Scale

Mass Scale 8 Anode TME – Calculates the mass scale for each anode based on the values given by the user (only for data collected using 8 anodes). To properly mass scale this way, the time of arrival (in channels) for four ions of known mass must be typed in into the corresponding box for each anode. It is extremely helpful to keep the Anode Selection panel open while doing this. After calculating the mass scale for each anode, the program calculates the shift for each anode (mass dependent) to overlay all anodes onto the mass scale given by anode 0. This procedure will allow for an improvement in mass scale by a factor of 2 or more, depending on how the system is tuned and how the instrument is setup the day the experiment. There is an option to save/load this mass scale, since this is a time consuming process.

Mass Scale TME1 – Calculates the mass scale for the total spectrum (TME1) based on the values given by the user. To properly mass scale this way the time of arrival (in channels) of four ions of interest must be typed in.

Mass Scale TME2 - Calculates the mass scale for the total spectrum (TME2) based on the values given by the user. To properly mass scale this way the time of arrival (in channels) of four ions of interest must be typed in

Explanation of drop down features: Help

Help File – Links to this document.

About – Displays version information and contact information.

Hot keys used in the program:

Enter – takes the area of a selected peak in the main mass spectrum and displays the number of counts and the yield

Enter + CTRL– takes the area of a selected peak in the coincidental mass spectrum and displays the number of counts and the yield

1 - Takes the X values from the blue and red cursors in the selected mass spectrum and puts the value in X1 and X2 boxes.

2 - Takes the X values from the blue and red cursors in the selected mass spectrum and puts the value in X3 and X4 boxes.

3 - Takes the X values from the blue and red cursors in the selected mass spectrum and puts the value in X5 and X6 boxes.

c - Takes the X,Y values from the green cursor in the selected mass spectrum and puts the value in Xa and Ya boxes.

s + CTRL – Creates a file to save the areas of a selected peaks from the main spectrum to. Each time this hot key is used the selected peaks size (beginning and end of peak), area and number of events is written to the file.

k + CTRL – Creates a file to save the areas of a selected peaks from the coincidence spectrum to. Each time this hot key is used the selected peaks size (beginning and end of peak), area and number of events is written to the file.

APPENDIX D

ACQUISITION CODE

```
#include <userint.h>
#include "test acq.h"
#include <ansi_c.h>
#include <utility.h>
#define B 2600
#define C 100000
#define D 500000
#define E 32000
#define F 1000
#define G 260
#include "h:\beta aquire files\test acq.h"
#include "h:\include\NIDAQEx.h"
#include <formatio.h>
#include <easyio.h>
#include <dataacq.h>
# include <cvirte.h>
# include <userint.h>
static int panelHandle;
char
proj_dir[MAX_PATHNAME_LEN],file_name[MAX_PATHNAME_LEN],file_Name[
MAX_PATHNAME_LEN];
char File_Name[MAX_PATHNAME_LEN],FILE_name[MAX_PATHNAME_LEN];
char WriteFileName[G], FileNameToWrite[G], PathName[G], name[G], prj_dir[260];
char Date[G], Time[G],Date2[G], Time2[G], operator[G], id[G], target[G], pidat[G],
sidat[G],
startdat[G], stop1dat[G],stop2dat[G], test_name[G],buf[B];
unsigned int size, chanmax;
unsigned int events, ch0, ch1, ch2, ch3, ch4, ch5, ch6, ch7= 0;
unsigned int totalEvents, nullEvents, bigEvents, lochan = 0;
unsigned int stop1Events, stop2Events, stop3Events, stop4Events, stop5Events = 0;
unsigned int stop6Events, stop7Events, stop8Events, stop9Events, stop10Events = 0;
unsigned int stop11Events, stop12Events, stop13Events, stop14Events, stop15Events =
0;
unsigned int stop16Events, stop17Events, stop18Events, stop19Events, stop20Events =
0;
unsigned int stop21Events, stop22Events, stop23Events, stop24Events, stop25Events =
0;
```

```

unsigned int stop26Events, stop27Events, stop28Events, stop29Events, stop30Events =
0;
unsigned int stop31Events, stop32Events, stop33Events, stop34Events, stop35Events =
0;
unsigned int stop36Events, stop37Events, stop38Events, stop39Events, stop40Events =
0;
unsigned int stop41Events, stop42Events, stop43Events, stop44Events, stop45Events =
0;
unsigned int stop46Events, stop47Events, stop48Events, stop49Events, stop50Events =
0;
double x1ref, y1ref, x2ref, y2ref, x1, y1, x2, y2, dd, ee = 0;
double ma, sm, slope, intercept, mse, ca = 0;
int mon, dat, yr, hr, mn, sc, r, Status;
int hit1, hit2, hit3, hit4, hit5, hit6, hit7, hit8, hit9, hit10 = 0;
int hit11, hit12, hit13, hit14, hit15, hit16, hit17, hit18, hit19, hit20 = 0;
int hit21, hit22, hit23, hit24, hit25, hit26, hit27, hit28, hit29, hit30 = 0;
int hit31, hit32, hit33, hit34, hit35, hit36, hit37, hit38, hit39, hit40 = 0;
int hit41, hit42, hit43, hit44, hit45, hit46, hit47, hit48, hit49, hit50 = 0;
int ea1, ea2, ea3, ea4, ea5, ea6, ea7, ea8, ea9, ea10, ea11, ea12, ea13, ea14, ea15, ea16,
ea17, ea18, ea19, ea20 = 0;
int ea21, ea22, ea23, ea24, ea25, ea26, ea27, ea28, ea29, ea30, ea31, ea32, ea33, ea34,
ea35,
ea36, ea37, ea38 = 0;
int ea39, ea40, ea41, ea42, ea43, ea44, ea45, ea46, ea47, ea48, ea49, ea50 = 0;
int response, response1, response2, pen, en, nHit, n = 0;
int ch0en, ch1en, ch2en, ch3en, ch4en, ch5en, ch6en, ch7en = 0;
int d, z, x, y, q, e, llm, ulm, det, shift, ed = 0;
unsigned int t1;
unsigned int tempD[2000] = {0};
unsigned int tempT[2000] = {0};
unsigned int *coinspec, *currTArray, *currDArray;
int *coinspec0, *coinspec1, *coinspec2, *coinspec3;
int *coinspec4, *coinspec5, *coinspec6, *coinspec7;
unsigned int MultArray[51] = {0};
unsigned int MultXArray[51] = {0};
unsigned int *currHist;
double *normArray;
double *Mass;
double MassCalibY[8], MassCalibX[8], MassCalib[8] = {0};
short statai;
short iStatus = 0;
short iRetVal = 0;
short iDevice = 1;
short iGroup = 1;

```

```

short iPort = 0;
short iDir = 0;
short iSignal = 1;
short iEdge = 0;
short iAckDelayTime = 1;
short iDBModeON = 1;
short iDBModeOFF = 0;
short iOldDataStop = 1;
short iPartialTransfer = 0;
short iHalfReady = 0;
unsigned long iLoopCount = 0;
unsigned long iHalfBufsToRead = C;
unsigned long ulAlignIndex = 0;
short iResource = 11;
short iIgnoreWarning = 1;
unsigned long lTimeout = 180;
short iYieldON = 1;
short iGroupSize = 2;
short iReqPol = 1;
short iAckPol = 1;
unsigned short *piBuffer;
unsigned short *piHalfBuffer;
unsigned short *Coinspec;
unsigned long ulCount = E;
unsigned long ulPtsTfr = (E/2);
unsigned long ulBufferSize = E;
static int WriteFileHandle;
int AcquireResponse, inputcount;
//int array[10000000];
int updatecount, t, eventsTME;
int *totalspec;
int *SpecAnode0;
int *SpecAnode1;
int *SpecAnode2;
int *SpecAnode3;
int *SpecAnode4;
int *SpecAnode5;
int *SpecAnode6;
int *SpecAnode7;
double
countanode0,countanode1,countanode2,countanode3,countanode4,countanode5,countanode6,countanode7, sum;
double anodedist[8];
double jj, Size, zz = 0;

```

```

double cc = 100.00;
int run=0;
int ll=0;
int start=0;
int ncollect,i;
int xx1, xx2, ioncount;
int ionDist[1000];
int maxchan=0;
int csel=65535;
unsigned short *array;
int currentspec, responseg;
int counts, X1,X2;
double yield;
int flagg=0;

```

```

int main (int argc, char *argv[])
{
    if (InitCVIRTE (0, argv, 0) == 0)
        return -1; /* out of memory */
    if ((panelHandle = LoadPanel (0, "test acq.uir", PANEL)) < 0)
        return -1;

    SetCtrlAttribute (panelHandle, PANEL_MSPEC, ATTR_VISIBLE, 1);
    SetCtrlAttribute (panelHandle, PANEL_SIDist, ATTR_VISIBLE, 0);
    DisplayPanel (panelHandle);
    RunUserInterface ();
    DiscardPanel (panelHandle);

    return 0;
}

/*****Array Allocation
Functions*****/
void histArray(int maxChannel){
array=(unsigned short *)calloc(maxChannel+1, sizeof (unsigned short));
}

void histpiBuffer(int maxChannel){
piBuffer=( unsigned short *)calloc(maxChannel, sizeof (unsigned short));
}

```

```

void histpiHalfBuffer(int maxChannel){
piHalfBuffer=( unsigned short *)calloc(maxChannel, sizeof (unsigned short));
}
void histCoinspec(int maxChannel){
Coinspec=( unsigned short *)calloc(maxChannel, sizeof (unsigned short));
}
void histtotalspec(int maxChannel){

    totalspec=(int *)calloc(maxChannel+1, sizeof (int));
}
void histSpecAnode0(int maxChannel){

    SpecAnode0=(int *)calloc(maxChannel+1, sizeof (int));
}
void histSpecAnode1(int maxChannel){

    SpecAnode1=(int *)calloc(maxChannel+1, sizeof (int));
}
void histSpecAnode2(int maxChannel){

    SpecAnode2=(int *)calloc(maxChannel+1, sizeof (int));
}
void histSpecAnode3(int maxChannel){

    SpecAnode3=(int *)calloc(maxChannel+1, sizeof (int));
}
void histSpecAnode4(int maxChannel){

    SpecAnode4=(int *)calloc(maxChannel+1, sizeof (int));
}
void histSpecAnode5(int maxChannel){

    SpecAnode5=(int *)calloc(maxChannel+1, sizeof (int));
}
void histSpecAnode6(int maxChannel){

    SpecAnode6=(int *)calloc(maxChannel+1, sizeof (int));
}
void histSpecAnode7(int maxChannel){

    SpecAnode7=(int *)calloc(maxChannel+1, sizeof (int));
}

```

```

void IonDist()
{
    eventsTME=0;
    currentspec=8;
    GetCtrlVal(panelHandle,PANEL_X1,&x1);
    GetCtrlVal(panelHandle,PANEL_X2,&x2);
    countanode0=0;
    countanode1=0;
    countanode2=0;
    countanode3=0;
    countanode4=0;
    countanode5=0;
    countanode6=0;
    countanode7=0;
    xx1 = ("%d", (double) x1);
    xx2 = ("%d", (double) x2);

    if(xx2==0)
    {
        xx1=0;
        xx2 = ("%d", (double) maxchan);
    }
    for(x=0;x<maxchan;x++)
    {
        totalspec[x] = 0;
        SpecAnode0[x] = 0;
        SpecAnode1[x] = 0;
        SpecAnode2[x] = 0;
        SpecAnode3[x] = 0;
        SpecAnode4[x] = 0;
        SpecAnode5[x] = 0;
        SpecAnode6[x] = 0;
        SpecAnode7[x] = 0;
    }
    for(z=2;z<=ll-1;z++)

    {
        //This algorithm creates the mass spectrum
        //from each channel (8 in all)
of the CTN-M4 which can
        z++;
        //be viewed during the acquisition.
        q=array[z]&61440;

```

```

switch (q)
{
    case 0:
        t1=array[z]&4095;
        z--;
        e=array[z]+(t1*65536);
        totalspec[e]+=1;
        if(e>=xx1&&e<=xx2)
        {
            countanode0 = countanode0+1;
        }
        SpecAnode0[e]+=1;
        z++;
        ch0+=1;
    break;
    case 4096:
        t1=array[z]&4095;
        z--;
        e=array[z]+(t1*65536);
        z++;
        ch1+=1;
        if(e>=xx1&&e<=xx2)
        {
            countanode1 = countanode1+1;
        }
        SpecAnode1[e]+=1;
        totalspec[e]+=1;
    break;
    case 8192:
        t1=array[z]&4095;
        z--;
        e=array[z]+(t1*65536);
        z++;
        ch2+=1;
        if(e>=xx1&&e<=xx2)
        {
            countanode2 = countanode2+1;
        }
        SpecAnode2[e]+=1;
        totalspec[e]+=1;
    break;
    case 12288:
        t1=array[z]&4095;

```

```

        z--;
        e=array[z]+(t1*65536);
        z++;
        ch3+=1;
        totalspec[e]+=1;
        SpecAnode3[e]+=1;
        if(e>=xx1&&e<=xx2)
        {
            countanode3 = countanode3+1;
        }
break;
case 16384:
    t1=array[z]&4095;
    z--;
    e=array[z]+(t1*65536);
    z++;
    ch4+=1;
    totalspec[e]+=1;
    SpecAnode4[e]+=1;

if(e>=xx1&&e<=xx2)
    {
countanode4 =
countanode4+1;
    }
break;
case 20480:
    t1=array[z]&4095;
    z--;
    e=array[z]+(t1*65536);
    z++;
    ch5+=1;
    totalspec[e]+=1;
    SpecAnode5[e]+=1;
    if(e>=xx1&&e<=xx2)
    {
        countanode5 = countanode5+1;
    }
break;
case 24576:
    t1=array[z]&4095;
    z--;
    e=array[z]+(t1*65536);
    z++;

```

```

countanode6+1;
countanode7+1;
countanode3 + countanode4 + countanode5 + countanode6 + countanode7;
if(sum == 0)
{
    sum = 1;
}
anodedist[0] = countanode0/sum;
anodedist[1] = countanode1/sum;
anodedist[2] = countanode2/sum;
anodedist[3] = countanode3/sum;

        ch6+=1;
        totalspec[e]+=1;
        SpecAnode6[e]+=1;
        if(e>=xx1&&e<=xx2)
        {
                countanode6 =
        }
        break;
        case 28672:
                t1=array[z]&4095;
                z--;
                e=array[z]+(t1*65536);
                z++;
                ch7+=1;
                totalspec[e]+=1;
                SpecAnode7[e]+=1;
                if(e>=xx1&&e<=xx2)
                {
                        countanode7 =
                }
        break;
        case 32768:
                eventsTME+=1;
                t1=array[z]&4095;
                z--;
                z++;
        break;
        break;
}
}
// Updatedisplay
sum = countanode0+ countanode1 + countanode2 +
countanode3 + countanode4 + countanode5 + countanode6 + countanode7;
if(sum == 0)
{
    sum = 1;
}
anodedist[0] = countanode0/sum;
anodedist[1] = countanode1/sum;
anodedist[2] = countanode2/sum;
anodedist[3] = countanode3/sum;

```

```

        anodedist[4] = countanode4/sum;
        anodedist[5] = countanode5/sum;
        anodedist[6] = countanode6/sum;
        anodedist[7] = countanode7/sum;

        //          SetCtrlVal(panelHandle, PANEL_Events, eventsTME);

        DeleteGraphPlot (panelHandle, PANEL_Anode, -1,
VAL_IMMEDIATE_DRAW);
        PlotY (panelHandle, PANEL_Anode, anodedist, 8,
VAL_DOUBLE, VAL_VERTICAL_BAR, VAL_NO_POINT, VAL_SOLID, 1,
VAL_RED);
    }

void UPDATEfile ()
{
    for(i=0;i<1999;i++)
    {
        ionDist[ioncount]=0;
    }
    GetFileSize(FILE_name, &size);
    Size=("%d",(int) size);
    jj=cc/100;
    zz=(Size/2)*jj;
    ll = RoundRealToNearestInteger (zz);
    histArray(size);
    run=0;
    eventsTME=0;
    for (i=0;i<size;i++)
    {
        array[i]=0;
    }
    FileToArray (FILE_name, array, VAL_UNSIGNED_SHORT_INTEGER, ll, 1,
VAL_GROUPS_TOGETHER,
                VAL_GROUPS_AS_COLUMNS, VAL_BINARY);

// starts here    mine
    for(d=0;d<=ll-1;d++)
    {
        d++;
        q=array[d]&61440;
        switch (q)
        {
            case 32768:

```

```

        events+=1;
        t1=array[d]&4095;
        d--;
        e=array[d]+(t1*csel);
        if(e>maxchan)
        {
            maxchan=e;
        }//iif(e>maxchan)
        d++;
        break;
    }//switch (q)
    }//for(d=0;d<=11-1;d++)
    histtotalspec(maxchan+100);
    histSpecAnode0(maxchan+100);
    histSpecAnode1(maxchan+100);
    histSpecAnode2(maxchan+100);
    histSpecAnode3(maxchan+100);
    histSpecAnode4(maxchan+100);
    histSpecAnode5(maxchan+100);
    histSpecAnode6(maxchan+100);
    histSpecAnode7(maxchan+100);
    for(i=0;i<maxchan+10;i++)
    {
        totalspec[i]=0;
        SpecAnode0[e]=0;
        SpecAnode1[e]=0;
        SpecAnode2[e]=0;
        SpecAnode3[e]=0;
        SpecAnode4[e]=0;
        SpecAnode5[e]=0;
        SpecAnode6[e]=0;
        SpecAnode7[e]=0;
    }
    for(z=2;z<=11;z++)

    {
        //      This algorithm creates the mass spectrum
        //from each channel (8 in all) of the CTN-M4 which can
        z++;
        //be viewed during the acquisition.
        q=array[z]&61440;
        switch (q)

        {

```

```

case 0:
    t1=array[z]&4095;
    z--;
    e=array[z]+(t1*65535);
    totalspec[e]+=1;
    SpecAnode0[e]+=1;
    ioncount+=1;
    z++;
    ch0+=1;

    countanode0 = countanode0+1;
break;
case 4096:
    t1=array[z]&4095;
    z--;
    e=array[z]+(t1*65535);
    z++;
    ch1+=1;
    ioncount+=1;
    SpecAnode1[e]+=1;
    totalspec[e]+=1;
    countanode1 = countanode1+1;
break;
case 8192:
    t1=array[z]&4095;
    z--;
    e=array[z]+(t1*65535);
    z++;
    ch2+=1;
    ioncount+=1;
    SpecAnode2[e]+=1;
    totalspec[e]+=1;
    countanode2 = countanode2+1;
break;
case 12288:
    t1=array[z]&4095;
    z--;
    e=array[z]+(t1*65535);
    z++;
    ch3+=1;
    ioncount+=1;
    totalspec[e]+=1;
    SpecAnode3[e]+=1;
    countanode3 = countanode3+1;

```

```

break;
case 16384:
    t1=array[z]&4095;
    z--;
    e=array[z]+(t1*65535);
    z++;
    ch4+=1;
    ioncount+=1;
    totalspec[e]+=1;
    SpecAnode4[e]+=1;
    countanode4 = countanode4+1;
break;
case 20480:
    t1=array[z]&4095;
    z--;
    e=array[z]+(t1*65535);
    z++;
    ch5+=1;
    ioncount+=1;
    totalspec[e]+=1;
    SpecAnode5[e]+=1;
    countanode5 = countanode5+1;

break;
case 24576:
    t1=array[z]&4095;
    z--;
    e=array[z]+(t1*65535);
    z++;
    ch6+=1;
    ioncount+=1;
    totalspec[e]+=1;
    SpecAnode6[e]+=1;
    countanode6 = countanode6+1;
break;
case 28672:
    t1=array[z]&4095;
    z--;
    e=array[z]+(t1*65535);
    z++;
    ch7+=1;
    ioncount+=1;
    totalspec[e]+=1;
    SpecAnode7[e]+=1;

```

```

countanode7 = countanode7+1;

break;
case 32768:
    eventsTME+=1;
    t1=array[z]&4095;
    z--;
    ionDist[ioncount]+=1;
    ioncount=0;

    z++;
break;

break;

}
}

// Updatedisplay
sum = countanode0+ countanode1 + countanode2 + countanode3 +
countanode4 + countanode5 + countanode6 + countanode7;
if(sum == 0)
{
    sum = 1;
}

anodedist[0] = countanode0/sum;
anodedist[1] = countanode1/sum;
anodedist[2] = countanode2/sum;
anodedist[3] = countanode3/sum;
anodedist[4] = countanode4/sum;
anodedist[5] = countanode5/sum;
anodedist[6] = countanode6/sum;
anodedist[7] = countanode7/sum;
SetCtrlVal(panelHandle, PANEL_Events, eventsTME);
DeleteGraphPlot (panelHandle, PANEL_Anode, -1,
VAL_IMMEDIATE_DRAW);
DeleteGraphPlot (panelHandle, PANEL_MSPEC, -1,
VAL_IMMEDIATE_DRAW);
PlotY (panelHandle, PANEL_MSPEC, totalspec, maxchan,
VAL_INTEGER, VAL_CONNECTED_POINTS, VAL_SIMPLE_DOT, VAL_SOLID,
1, VAL_BLACK);
currentspec=8;

```

```

        SetCtrlVal(panelHandle,PANEL_Running,0);
        GetCtrlVal(panelHandle,PANEL_X1,&x1);
        GetCtrlVal(panelHandle,PANEL_X2,&x2);
        xx1 = ("%d", (double) x1);
        xx2 = ("%d", (double) x2);
        if(xx2>0)
        {
            xx2 = ("%d", (double) maxchan);
            IonDist();
            run=1;
        }
        if(run==0)
        {
            PlotY (panelHandle, PANEL_Anode, anodedist, 8, VAL_DOUBLE,
VAL_VERTICAL_BAR, VAL_NO_POINT, VAL_SOLID, 1, VAL_RED);
        }
    }
}
/*****Program A
CTNM4*****/

void StartDataAcquireA()
{
    GetCtrlVal(panelHandle,PANEL_NCollect,&ncollect);
    sprintf(FILE_name, "%d.tme", start);
    events=0;
    iLoopCount=0;
    iSignal = 0;
    iGroupSize = 4;
    iReqPol = 0;
    iAckPol = 0;
    ulCount = (E/4);
    ulPtsTfr = (E/4);
    ulBufferSize = E;
    histpiBuffer(E);
    histpiHalfBuffer(E/4);
    iStatus = Timeout_Config(iDevice, lTimeout);
    iRetVal = NIDAQErrorHandler(iStatus,
"Timeout_Config",iIgnoreWarning);
    iStatus = DIG_Grp_Config(iDevice, iGroup, iGroupSize, iPort,iDir);
    iRetVal = NIDAQErrorHandler(iStatus,
"DIG_Grp_Config",iIgnoreWarning);
}

```

```

        iStatus = DIG_Grp_Mode(iDevice, iGroup, iSignal, iEdge,
iReqPol,iAckPol, iAckDelayTime);

        iRetVal = NIDAQErrorHandler(iStatus,
"DIG_Grp_Mode",iIgnoreWarning);
        iStatus = DIG_DB_Config(iDevice, iGroup, iDBModeON,
iOldDataStop,iPartialTransfer);
        iRetVal = NIDAQErrorHandler(iStatus,
"DIG_DB_Config",iIgnoreWarning);
        iStatus = Align_DMA_Buffer(iDevice, iResource, piBuffer,
ulCount,ulBufferSize, &ulAlignIndex);
        iRetVal = NIDAQErrorHandler(iStatus,
"Align_DMA_Buffer",iIgnoreWarning);
        iStatus = DIG_Block_In(iDevice, iGroup, piBuffer, ulCount);
        iRetVal = NIDAQErrorHandler(iStatus,
"DIG_Block_In",iIgnoreWarning);
        WriteToDigitalLine(1, "4", 1, 4, 1, 1);
        WriteToDigitalLine(1, "4", 1, 4, 1, 0);
        WriteToDigitalLine(1, "4", 3, 4, 1, 1);
        while ((iLoopCount < ncollect) && (iStatus == 0)) {
iStatus = DIG_DB_HalfReady(iDevice, iGroup, &iHalfReady);
if (iStatus >= 0) {
    if (iHalfReady == 1) {
        iStatus = DIG_DB_Transfer(iDevice, iGroup,
piHalfBuffer, ulPtsTfr);
        iRetVal =
NIDAQErrorHandler(iStatus,"DIG_DB_Transfer", iIgnoreWarning);
        ++iLoopCount;
        ++inputcount;
        ++updatecount;
        for(z=0;z<=(E/4)-1;z++){
            inputcount++;
            if((piHalfBuffer[z]&61440) == 32768){
                events+=1;
                if(events==ncollect)
                {
                    iLoopCount=ncollect+1000;
                }
            }
        }
    }
}
        ArrayToFile (FILE_name, piHalfBuffer,
VAL_UNSIGNED_SHORT_INTEGER, E/4, 1,

```

```

        VAL_GROUPS_TOGETHER,
VAL_GROUPS_AS_COLUMNS, VAL_CONST_WIDTH, 10,
        VAL_BINARY, VAL_APPEND);
    }
}
else {
    iRetVal = NIDAQErrorHandler(iStatus, "DIG_DB_HalfReady",
iIgnoreWarning);
    }//else
    iRetVal = NIDAQYield(iYieldON);
    }
    WriteToDigitalLine(1, "4", 3, 4, 1, 0);
    iStatus = DIG_Block_Clear(iDevice, iGroup);
    iStatus = DIG_DB_Config(iDevice, iGroup, iDBModeOFF,
iOldDataStop,iPartialTransfer);
    iStatus = DIG_Grp_Config(iDevice, iGroup, 0, 0, 0);
    iStatus = Timeout_Config(iDevice, -1);
//    short error = WriteToDigitalLine (short device, char portNumber[], short
line,short portWidth, long configure,unsigned long lineState);
//    MessagePopup ("CTN-M4", "Data Acquisition Complete");

    UPDATEfile();
} //void Program A

/*****Coincidence
Routine*****/
void convertData() {
    int x, y, z, q, w, v = 0;
    w=0;
//    GetCtrlVal (cnspecPnl, COINPNL_LOCHANUM, &lochan);
    for(x=0;x<=((nHit*n)-1);x++){
        for(y=0;y<=(n-1);y++) {
            tempT[y]=currTArray[x];
            tempD[y]=currDArray[x];
            x++;
        }
        if(tempT[n-1]>lochan){
            for(y=0;y<=(n-1);y++){
                if((tempD[y] == 32768) || (tempD[y] == 0)) {tempD[y] =
0;}
                if((tempD[y] == 33792) || (tempD[y] == 4096)) {tempD[y]
= 1;}
                if((tempD[y] == 34816) || (tempD[y] == 8192)) {tempD[y]
= 2;}
            }
        }
    }
}

```



```

currTArray[w]=d;
currDArray[w]=det;
w++;

    }//if

    }//for

    z=n;
    }//if
}//////////
}//for
x--;
}//for
}//void
void shiftData() {
    int x, y, z, q, w, v = 0;
    w=0;
    for(x=0;x<=((nHit*n)-1);x++){
        for(y=0;y<=(n-1);y++) {
            tempT[y]=currTArray[x];
            tempD[y]=currDArray[x];
            x++;
        }
        for(y=0;y<=(n-1);y++){
            if((tempD[y] == 32768) || (tempD[y] == 0)) {tempD[y] = 0;}
            if((tempD[y] == 33792) || (tempD[y] == 4096)) {tempD[y] = 1;}
            if((tempD[y] == 34816) || (tempD[y] == 8192)) {tempD[y] = 2;}
            if((tempD[y] == 35840) || (tempD[y] == 12288)){tempD[y] = 3;}
            if((tempD[y] == 36864) || (tempD[y] == 16384)){tempD[y] = 4;}
            if((tempD[y] == 37888) || (tempD[y] == 20480)){tempD[y] = 5;}
            if((tempD[y] == 38912) || (tempD[y] == 24576)){tempD[y] = 6;}
            if((tempD[y] == 39936) || (tempD[y] == 28672)){tempD[y] = 7;}
        }

        for(z=0;z<=(n-1);z++){
            if((tempT[z]<=ulm) &&(tempT[z]>=llm)&&tempD[z]==en){
                shift=tempT[z]-llm;
                for(q=0;q<=(n-1);q++){
                    det=tempD[q];
                    d=tempT[q]-shift;
                    if (d>0){
                        switch (det)

```

```

        {
            case 0 : coinspec0[d]+=1; break;
            case 1 : coinspec1[d]+=1; break;
            case 2 : coinspec2[d]+=1; break;
            case 3 : coinspec3[d]+=1; break;
            case 4 : coinspec4[d]+=1; break;
            case 5 : coinspec5[d]+=1; break;
            case 6 : coinspec6[d]+=1; break;
            case 7 : coinspec7[d]+=1; break;
        }
    } //switch
} //if
if(response1>0){
    currTArray[w]=d;
    currDArray[w]=det;
    w++;
}
} //for
z=n;
} //if

} //for
x--;
} //for
} //void
/*****Data Acquisition
Functions*****/
void CVICALLBACK MenuStartDataAcquireCB (int menuBar, int menuItem, void
*callbackData,
int panel)
{
//    DisplayPanel(expPnl);
}
int CVICALLBACK MenuStopACB (int panel, int control, int event,
void *callbackData, int eventData1, int eventData2)
{
    switch (event)
    {
        case EVENT_COMMIT:
            r = iLoopCount;
            iHalfBufsToRead = r;
            break;
    }
}
return 0;
}

```

```

int CVICALLBACK exitCB (int panel, int control, int event,
                        void *callbackData, int eventData1, int eventData2)
{
    switch (event)
    {
        case EVENT_COMMIT:
            QuitUserInterface (0);
            break;
    }
    return 0;
}
int CVICALLBACK StartCB (int panel, int control, int event,
                          void *callbackData, int eventData1, int eventData2)
{
    switch (event)
    {
        case EVENT_COMMIT:
            countanode0=0;
            countanode1=0;
            countanode2=0;
            countanode3=0;
            countanode4=0;
            countanode5=0;
            countanode6=0;
            countanode7=0;
            start+=1;
            SetCtrlVal(panelHandle,PANEL_Startcount,start);
            SetCtrlVal(panelHandle,PANEL_Running,1);
            // if(start==1)
            // {
            //     AcquireResponse = GenericMessagePopup ("Acquire on TDC",
            //                                         "TDC
            Type and Model",
            //                                         "M4",
            //                                         "M3-
            6",
            //                                         "M3-
            8", 0, 0, 0,
            //
            VAL_GENERIC_POPUP_BTN1,
            //
            VAL_GENERIC_POPUP_BTN1,
            //
            VAL_GENERIC_POPUP_NO_CTRL);

```

```

//      }
AcquireResponse=1;
    switch(AcquireResponse)
    {
        case 1:
            StartDataAcquireA();
            break;
    }
    break;
}
return 0;
}
int CVICALLBACK ZoominMSCB (int panel, int control, int event,
    void *callbackData, int eventData1, int eventData2)
{
    switch (event)
    {
        case EVENT_COMMIT:

            if(flagg==1)
            {
                GetGraphCursor (panelHandle, PANEL_SIDist, 1, &x1, &y1);
                GetGraphCursor (panelHandle, PANEL_SIDist, 2, &x2, &y2);
                if((x2>x1)&&(y2>y1))
                {
                    SetAxisScalingMode (panelHandle,
PANEL_SIDist, VAL_XAXIS, VAL_MANUAL, x1, x2);
                    SetAxisScalingMode (panelHandle,
PANEL_SIDist, VAL_LEFT_YAXIS, VAL_MANUAL, y1, y2);
                    SetGraphCursor (panelHandle, PANEL_SIDist, 1,
x1, y1);
                }
            }
            if(flagg==0)
            {
                GetGraphCursor (panelHandle, PANEL_MSPEC, 1, &x1, &y1);
                GetGraphCursor (panelHandle, PANEL_MSPEC, 2, &x2, &y2);
                if((x2>x1)&&(y2>y1))
                {
                    SetAxisScalingMode (panelHandle,
PANEL_MSPEC, VAL_XAXIS, VAL_MANUAL, x1, x2);
                    SetAxisScalingMode (panelHandle,
PANEL_MSPEC, VAL_LEFT_YAXIS, VAL_MANUAL, y1, y2);

```

```

1, x1, y1);
                                SetGraphCursor (panelHandle, PANEL_MSPEC,
                                }
                                }
                                break;

                                break;
                                }
                                return 0;
}
int CVICALLBACK ZoomoutMSCB (int panel, int control, int event,
                                void *callbackData, int eventData1, int eventData2)
{
    switch (event)
    {
        case EVENT_COMMIT:

            if(flagg==0)
            {
                SetAxisScalingMode (panelHandle, PANEL_MSPEC,
VAL_LEFT_YAXIS,
                VAL_AUTOSCALE, y1, y2);
                SetAxisScalingMode (panelHandle, PANEL_MSPEC,
VAL_XAXIS, VAL_AUTOSCALE,y1, y2);
            }
            if(flagg==1)
            {
                SetAxisScalingMode (panelHandle, PANEL_SIDist,
VAL_LEFT_YAXIS,
                                VAL_AUTOSCALE, y1,
y2);
                SetAxisScalingMode (panelHandle, PANEL_SIDist,
VAL_XAXIS, VAL_AUTOSCALE,
                                y1, y2);
            }

            break;
        }
        return 0;
}

```

```

int CVICALLBACK Dist_Ion_SelectedCB (int panel, int control, int event,
void *callbackData, int eventData1, int eventData2)
{
    switch (event)
    {
        case EVENT_COMMIT:
            for(i=0;i<1999;i++)
            {
                ionDist[ioncount]=0;
            }

            eventsTME=0;
            GetCtrlVal(panelHandle,PANEL_X1,&x1);
            GetCtrlVal(panelHandle,PANEL_X2,&x2);
            countanode0=0;
            countanode1=0;
            countanode2=0;
            countanode3=0;
            countanode4=0;
            countanode5=0;
            countanode6=0;
            countanode7=0;
            xx1 = ("%d", (double) x1);
            xx2 = ("%d", (double) x2);
            for(x=0;x<maxchan;x++)
            {
                totalspec[x] = 0;
                SpecAnode0[x] = 0;
                SpecAnode1[x] = 0;
                SpecAnode2[x] = 0;
                SpecAnode3[x] = 0;
                SpecAnode4[x] = 0;
                SpecAnode5[x] = 0;
                SpecAnode6[x] = 0;
                SpecAnode7[x] = 0;
            }

            for(z=2;z<=11-1;z++)

            {
                //This algorithm creates the mass spectrum

                //from each channel (8 in all) of the CTN-

```

M4 which can

```

z++;
//be viewed during the acquisition.
q=array[z]&61440;
switch (q)

{

    case 0:

        t1=array[z]&4095;
        z--;
        e=array[z]+(t1*65536);
        totalspec[e]+=1;
        if(e>=xx1&&e<=xx2)
        {
            ioncount+=1;
            countanode0 = countanode0+1;
        }
        SpecAnode0[e]+=1;
        z++;
        ch0+=1;
    break;
    case 4096:
        t1=array[z]&4095;
        z--;
        e=array[z]+(t1*65536);
        z++;
        ch1+=1;
        if(e>=xx1&&e<=xx2)
        {
            countanode1 = countanode1+1;
            ioncount+=1;
        }
        SpecAnode1[e]+=1;
        totalspec[e]+=1;
    break;
    case 8192:
        t1=array[z]&4095;
        z--;

        e=array[z]+(t1*65536);
        z++;
        ch2+=1;
        if(e>=xx1&&e<=xx2)

```

```

        {
        countanode2 = countanode2+1;
        ioncount+=1;
        }
        SpecAnode2[e]+=1;
        totalspec[e]+=1;
break;
case 12288:
        t1=array[z]&4095;
        z--;
        e=array[z]+(t1*65536);
        z++;
        ch3+=1;
        totalspec[e]+=1;
        SpecAnode3[e]+=1;
        if(e>=xx1&&e<=xx2)
        {
        countanode3 = countanode3+1;
        ioncount+=1;
        }

break;

case 16384:
        t1=array[z]&4095;
        z--;
        e=array[z]+(t1*65536);
        z++;
        ch4+=1;
        totalspec[e]+=1;
        SpecAnode4[e]+=1;

        if(e>=xx1&&e<=xx2)
        {
        ioncount+=1;
        countanode4 = countanode4+1;
        }
break;
case 20480:
        t1=array[z]&4095;
        z--;
        e=array[z]+(t1*65536);
        z++;

```

```

        ch5+=1;
        totalspec[e]+=1;
        SpecAnode5[e]+=1;
        if(e>=xx1&&e<=xx2)
        {
            ioncount+=1;
            countanode5 = countanode5+1;
        }
break;
case 24576:
    t1=array[z]&4095;
    z--;
    e=array[z]+(t1*65536);
    z++;
    ch6+=1;
    totalspec[e]+=1;
    SpecAnode6[e]+=1;
    if(e>=xx1&&e<=xx2)
    {
        ioncount+=1;
        countanode6 = countanode6+1;
    }
break;
case 28672:
    t1=array[z]&4095;
    z--;
    e=array[z]+(t1*65536);
    z++;
    ch7+=1;
    totalspec[e]+=1;
    SpecAnode7[e]+=1;
    if(e>=xx1&&e<=xx2)
    {
        ioncount+=1;
        countanode7 = countanode7+1;
    }
break;
case 32768:
    eventsTME+=1;
    t1=array[z]&4095;
    z--;
    ionDist[ioncount]+=1;
    ioncount=0;
    z++;

```

```

                break;
                break;
            }
        }
        // Updatedisplay
        sum = countanode0+ countanode1 + countanode2 +
countanode3 + countanode4 + countanode5 + countanode6 + countanode7;
        if(sum == 0)
        {
            sum = 1;
        }
        anodedist[0] = countanode0/sum;
        anodedist[1] = countanode1/sum;
        anodedist[2] = countanode2/sum;
        anodedist[3] = countanode3/sum;
        anodedist[4] = countanode4/sum;
        anodedist[5] = countanode5/sum;
        anodedist[6] = countanode6/sum;
        anodedist[7] = countanode7/sum;
        SetCtrlVal(panelHandle, PANEL_Events, eventsTME);
        DeleteGraphPlot (panelHandle, PANEL_Anode, -1,
VAL_IMMEDIATE_DRAW);
        PlotY (panelHandle, PANEL_Anode, anodedist, 8,
VAL_DOUBLE, VAL_VERTICAL_BAR, VAL_NO_POINT, VAL_SOLID, 1,
VAL_RED);
        currentspec=8;
        break;
    }
    return 0;
}
int CVICALLBACK Anode0CB (int panel, int control, int event,
void *callbackData, int eventData1, int eventData2)
{
    switch (event)
    {
        case EVENT_COMMIT:
            currentspec=0;

            DeleteGraphPlot (panelHandle, PANEL_MSPEC, -1,
VAL_IMMEDIATE_DRAW);
            PlotY (panelHandle, PANEL_MSPEC, SpecAnode0,
maxchan, VAL_INTEGER, VAL_CONNECTED_POINTS, VAL_SIMPLE_DOT,
VAL_SOLID, 1, VAL_BLACK);
            break;

```

```

    }
    return 0;
}
int CVICALLBACK Anode1CB (int panel, int control, int event,
    void *callbackData, int eventData1, int eventData2)
{
    switch (event)
    {
        case EVENT_COMMIT:
            currentspec=1;
            DeleteGraphPlot (panelHandle, PANEL_MSPEC, -1,
VAL_IMMEDIATE_DRAW);

                PlotY (panelHandle, PANEL_MSPEC, SpecAnode1,
maxchan, VAL_INTEGER, VAL_CONNECTED_POINTS, VAL_SIMPLE_DOT,
VAL_SOLID, 1, VAL_BLACK);

                break;
    }
    return 0;
}

int CVICALLBACK Anode2CB (int panel, int control, int event,
    void *callbackData, int eventData1, int eventData2)
{
    switch (event)
    {
        case EVENT_COMMIT:
            currentspec=2;
            DeleteGraphPlot (panelHandle, PANEL_MSPEC, -1,
VAL_IMMEDIATE_DRAW);

                PlotY (panelHandle, PANEL_MSPEC, SpecAnode2,
maxchan, VAL_INTEGER, VAL_CONNECTED_POINTS, VAL_SIMPLE_DOT,
VAL_SOLID, 1, VAL_BLACK);

                break;
    }
    return 0;
}

int CVICALLBACK Anode3CB (int panel, int control, int event,
    void *callbackData, int eventData1, int eventData2)
{
    switch (event)
    {

```

```

        case EVENT_COMMIT:
            currentspec=3;
            DeleteGraphPlot (panelHandle, PANEL_MSPEC, -1,
VAL_IMMEDIATE_DRAW);
            PlotY (panelHandle, PANEL_MSPEC, SpecAnode3,
maxchan, VAL_INTEGER, VAL_CONNECTED_POINTS, VAL_SIMPLE_DOT,
VAL_SOLID, 1, VAL_BLACK);

                break;
        }
    return 0;
}

int CVICALLBACK Anode4CB (int panel, int control, int event,
    void *callbackData, int eventData1, int eventData2)
{
    switch (event)
    {
        case EVENT_COMMIT:
            currentspec=4;
            DeleteGraphPlot (panelHandle, PANEL_MSPEC, -1,
VAL_IMMEDIATE_DRAW);

                PlotY (panelHandle, PANEL_MSPEC, SpecAnode4,
maxchan, VAL_INTEGER, VAL_CONNECTED_POINTS, VAL_SIMPLE_DOT,
VAL_SOLID, 1, VAL_BLACK);
                break;
        }
    return 0;
}

int CVICALLBACK Anode5CB (int panel, int control, int event,
    void *callbackData, int eventData1, int eventData2)
{
    switch (event)
    {
        case EVENT_COMMIT:
            currentspec=5;
            DeleteGraphPlot (panelHandle, PANEL_MSPEC, -1,
VAL_IMMEDIATE_DRAW);

                PlotY (panelHandle, PANEL_MSPEC, SpecAnode5,
maxchan, VAL_INTEGER, VAL_CONNECTED_POINTS, VAL_SIMPLE_DOT,
VAL_SOLID, 1, VAL_BLACK);
    }
}

```

```

        break;
    }
    return 0;
}

int CVICALLBACK Anode6CB (int panel, int control, int event,
    void *callbackData, int eventData1, int eventData2)
{
    switch (event)
    {
        case EVENT_COMMIT:
            currentspec=6;
            DeleteGraphPlot (panelHandle, PANEL_MSPEC, -1,
                VAL_IMMEDIATE_DRAW);

            PlotY (panelHandle, PANEL_MSPEC, SpecAnode6,
                maxchan, VAL_INTEGER, VAL_CONNECTED_POINTS, VAL_SIMPLE_DOT,
                VAL_SOLID, 1, VAL_BLACK);
            break;
    }
    return 0;
}

int CVICALLBACK Anode7CB (int panel, int control, int event,
    void *callbackData, int eventData1, int eventData2)
{
    switch (event)
    {
        case EVENT_COMMIT:
            currentspec=7;

            DeleteGraphPlot (panelHandle, PANEL_MSPEC, -1,
                VAL_IMMEDIATE_DRAW);
            PlotY (panelHandle, PANEL_MSPEC, SpecAnode7,
                maxchan, VAL_INTEGER, VAL_CONNECTED_POINTS, VAL_SIMPLE_DOT,
                VAL_SOLID, 1, VAL_BLACK);
            break;
    }
    return 0;
}

int CVICALLBACK setwindwoCB (int panel, int control, int event,
    void *callbackData, int eventData1, int eventData2)
{

```

```

switch (event)
{
    case EVENT_COMMIT:
        GetGraphCursor (panelHandle, PANEL_MSPEC, 1, &x1, &y1);
        GetGraphCursor (panelHandle, PANEL_MSPEC, 2, &x2, &y2);

        SetCtrlVal(panelHandle,PANEL_X1,x1);
        SetCtrlVal(panelHandle,PANEL_X2,x2);
        break;
}
return 0;
}

int CVICALLBACK totalmsCB (int panel, int control, int event,
    void *callbackData, int eventData1, int eventData2)
{
    switch (event)
    {
        case EVENT_COMMIT:
            currentspec=8;
            DeleteGraphPlot (panelHandle, PANEL_MSPEC, -1,
VAL_IMMEDIATE_DRAW);
            PlotY (panelHandle, PANEL_MSPEC, totalspec,
maxchan, VAL_INTEGER, VAL_CONNECTED_POINTS, VAL_SIMPLE_DOT,
VAL_SOLID, 1, VAL_BLACK);

            break;
    }
    return 0;
}

int CVICALLBACK peakarea (int panel, int control, int event,
    void *callbackData, int eventData1, int eventData2)
{
    switch (event)
    {
        case EVENT_COMMIT:
            GetGraphCursor (panelHandle, PANEL_MSPEC, 1, &x1, &y1);
            GetGraphCursor (panelHandle, PANEL_MSPEC, 2, &x2, &y2);

            counts=0;
            if(x2>x1)

```

```

        {
            for(x=x1;x<=x2;x++)
            {
                switch(currentspec)
                {
                    case 0:
counts+=SpecAnode0[x];break;
                    case 1:
counts+=SpecAnode1[x];break;
                    case 2:
counts+=SpecAnode2[x];break;
                    case 3:
counts+=SpecAnode3[x];break;
                    case 4:
counts+=SpecAnode4[x];break;
                    case 5:
counts+=SpecAnode5[x];break;
                    case 6:
counts+=SpecAnode6[x];break;
                    case 7:
counts+=SpecAnode7[x];break;
                    case 8: counts+=totalspec[x];break;
                }
            }

            ee=("%d",(int) eventsTME);
            dd=("%d",(int) counts);
            yield=dd/ee;
            RefreshGraph (panelHandle, PANEL_MSPEC);
            Fmt(buf,"Peak Area = %d", counts);
            SetCtrlVal (panelHandle, PANEL_yield, yield);
            responseg = PlotText (panelHandle,
PANEL_MSPEC, x2, y2, buf, VAL_APP_META_FONT,
                                VAL_DK_BLUE,
VAL_TRANSPARENT);
            DeleteGraphPlot (panelHandle, PANEL_MSPEC,
responseg,
VAL_DELAYED_DRAW);
            SetCtrlVal(panelHandle, PANEL_counts,counts);
        }

```

```

        break;
    }
    return 0;
}

int CVICALLBACK secondaryionCB (int panel, int control, int event,
    void *callbackData, int eventData1, int eventData2)
{
    switch (event)
    {
        case EVENT_COMMIT:
            flagg=1;
            SetCtrlAttribute (panelHandle, PANEL_SIDist, ATTR_VISIBLE,
1);
            SetCtrlAttribute (panelHandle, PANEL_MSPEC,
ATTR_VISIBLE, 0);
            PlotY (panelHandle, PANEL_SIDist, ionDist, 300,
VAL_INTEGER, VAL_VERTICAL_BAR, VAL_NO_POINT, VAL_SOLID, 1,
VAL_RED);
            break;
        }
    return 0;
}

int CVICALLBACK SiDistCB (int panel, int control, int event,
    void *callbackData, int eventData1, int eventData2)
{
    switch (event)
    {
        case EVENT_COMMIT:
            case EVENT_RIGHT_CLICK:
                RefreshGraph (panelHandle, PANEL_SIDist);
                GetGraphCursor (panelHandle, PANEL_SIDist, 3, &x1, &y1);
                X1 = RoundRealToNearestInteger (x1);
                X2=ionDist[X1];
                Fmt(buf,"k = %d , I = %d",X1, X2);
                responseg = PlotText (panelHandle, PANEL_SIDist, x1, y1, buf,
VAL_APP_META_FONT,
VAL_DK_BLUE, VAL_TRANSPARENT);

                DeleteGraphPlot (panelHandle, PANEL_SIDist, responseg,
VAL_DELAYED_DRAW);
            break;
    }
}

```

```

        case EVENT_RIGHT_DOUBLE_CLICK:
            DeleteGraphPlot (panelHandle, PANEL_SIDist, -1,
VAL_IMMEDIATE_DRAW);
            RefreshGraph (panelHandle, PANEL_SIDist);
            SetCtrlAttribute (panelHandle, PANEL_SIDist, ATTR_VISIBLE,
0);
            SetCtrlAttribute (panelHandle, PANEL_MSPEC,
ATTR_VISIBLE, 1);
            flagg=0;
            break;
            break;
        }
    return 0;
}

```